MANUAL OF FORECASTING ICE-FORMATION FOR RIVERS AND INLAND LAKES

by

L. G. Shulyakovskii

GLAVNOE UPRAVLENIE GIDROMETEOROLOGICHESKOI SLUZHBY PRI
SOVETE MINISTROV SSSR. TSENTRAL'NYI INSTITUT PROGNOZOV

Main Administration of the Hydrometeorological Service. Central Forecasting Institute

MANUAL OF HYDROLOGICAL FORECASTING
No. 4
(Rukovodstvo po gidrologicheskim prognozam)

Manual of Forecasting Ice-Formation for Rivers and Inland Lakes

(Prognozy ledovykh yavlenii na rekakh i vodokhranilishchakh)

Edited by L. G. Shulyakovskii

GIMIZ
Gidrometeorologicheskoe Izdatel'stvo
Leningrad 1963

Translated from Russian

Israel Program for Scientific Translations
Jerusalem 1966

TT 66-51016

Published Pursuant to an Agreement with
THE U.S. DEPARTMENT OF COMMERCE
and
THE NATIONAL SCIENCE FOUNDATION, WASHINGTON, D.C.

Copyright © [illegible]
Israel Program for Scientific Translations Ltd.
IPST Cat. No. [illegible]

Translated by IPST Staff
Edited by A. Wald

Printed in Jerusalem by S. Monson
Binding: Wiener Bindery Ltd., Jerusalem

Price: $6.00

Available from the
U.S. DEPARTMENT OF COMMERCE
Clearinghouse for Federal Scientific and Technical Information
Springfield, Va. 22151

AUBURN UNIVERSITY
RALPH BROWN DRAUGHON LIBRARY
AUBURN, ALABAMA 35830

Table of Contents

Preface . . . vii

Chapter I. FORECASTING THE APPEARANCE OF FLOATING ICE ON RIVERS . . . 1
- A. Conditions for the beginning of ice formation . . . 1
- B. Forecasting of ice phenomena using weather forecasts . . . 2
  - § 1. Calculation of the appearance of floating ice on rivers . . . 2
  - § 2. Determination of the parameters necessary to calculate the beginning of ice formation . . . 6
  - § 3. Calculating the appearance of floating ice on rivers . . . 23
  - § 4. Physico-statistical (empirical) relationships . . . 33
  - § 5. Forecasting the intensification and stoppage of the ice drift . . . [illegible]
- C. Forecasts with allowance for the characteristics of atmospheric processes (long-range forecasts) . . . 51
  - § 1. Method of forecasting ice appearance on the rivers of ETS using a qualitative evaluation of the atmospheric circulation . . . [illegible]
  - § 2. Forecasting on the basis of the uniformity of the prevailing atmospheric processes of the synoptic season . . . [illegible]
  - § 3. Forecasting ice appearance with allowance for the conditions of the formation of the Siberian anticyclone . . . [illegible]

Chapter II. FORECASTING THE BEGINNING OF A STABLE ICE COVER ON RIVERS . . . [illegible]
- A. Formation of an ice cover. Decisive factors . . . [illegible]
- B. Ice-cover forecasting using air temperature forecasts . . . [illegible]
  - § 1. Relationships for the calculation of the beginning of the stable ice period on a given river stretch . . . [illegible]
  - § 2. Calculation of the beginning of continuous ice cover from the relationships for a given river stretch . . . [illegible]
  - § 3. Some variants of the relationships for the calculation of the beginning of stable ice cover on a given river stretch . . . [illegible]
  - § 4. Calculation of the beginning of stable ice cover on a river stretch from general relationships . . . [illegible]
  - § 5. Forecasting the beginning of a stable ice cover at a given point and the resulting rise of the water stage . . . [illegible]
- C. Forecasting of the beginning of stable ice cover taking into account the development of atmospheric processes (long-range forecasting) . . . 91

Chapter III. FORECASTING THE CONDITIONS FOR THE APPEARANCE OF ICE AND THE FORMATION OF A STABLE ICE COVER ON LAKES AND STORAGE RESERVOIRS . . . 96
- A. Conditions for the beginning of ice formation and ice cover on lakes and storage reservoirs . . . 96

B. Forecasting based on calculation (using weather forecasts) 97
§ 1. Calculation formulas 97
§ 2. Determination of the quantities necessary for calculating the beginning of ice formation 99
§ 3. Method of calculating the initial water temperature 105
§ 4. Example of calculation of the beginning of stable ice cover on still water 108
§ 5. Example of the calculation of the beginning of stable ice on a river with a considerable stream flow 114
§ 6. Forecasts based on empirical relationships and use of the weather forecast 120
C. Forecasting methods using the characteristics of the atmosphere process (long-range forecasts) 129
Chapter IV. FORECASTING THE THICKNESS OF ICE COVER . 131
§ 1. Determining factors 131
§ 2. Calculations and forecasts using air temperature forecasts . 134
§ 3. Calculation and forecasting using the air temperature forecast in the absence of observation data 140
§ 4. Short-range forecasts without air temperature forecasts . . . 143
§ 5. Possibilities of long-range forecasting 145
Chapter V. FORECASTING ICE BREAKUP ON RIVERS 149
A. Conditions for ice breakup on rivers. Basic determining factors . . 149
B. Short-range forecasting 151
§ 1. Calculation of the heat input to the ice cover and to the snow cover in the river basin 151
§ 2. Forecasting the first ice-cover push 156
§ 3. Forecasting ice breakup 158
§ 4. Forecasting ice clearing (freeing) 172
C. Forecasts taking into account the development of the atmospheric processes (long-range forecasts) 172
§ 1. Forecasting based on the uniformity of the atmospheric processes during the spring synoptic season 175
§ 2. Forecasting based on allowance for the character of the rearrangement of the atmospheric processes from winter to spring 185
Chapter VI. FORECASTING OF ICE BREAKUP AND ICE CLEARING ON LAKES AND STORAGE RESERVOIRS 194
A. Ice breakup and ice clearing on lakes and storage reservoirs 194
B. Calculations of ice clearing using the weather forecast 196
§ 1. Calculation of ice clearing 196
§ 2. Example of ice-clearing calculations 204
§ 3. Forecasting the dates of beginning of ice drift and ice clearing from empirical relationships 210
C. Forecasting using the characteristics of the atmospheric processes (long-range forecasting) 215
Chapter VII. FORECASTING OF ICE JAMS AND RISE OF WATER STAGE DUE TO JAMMING 224
§ 1. Conditions for the formation of jams. Factors determining ice-jam stage rise 224
§ 2. Forecasting ice-jamming 226
§ 3. Forecasting the maximum water stage caused by ice jamming . 230
BIBLIOGRAPHY 235
EXPLANATORY LIST OF ABBREVIATIONS 241
APPENDIX 1 Values of e^{-x} 242
APPENDIX 2 Synoptic terms 243

PREFACE

The current issue is one of four issues of the Manual of Hydrological Forecasting, prepared by the Central Forecasting Institute. The first three issues dealt with the forecasting of the elements of the water regime of rivers. Issue 1 – short-range forecasting of water discharges and stages; Issue 2 – long-range forecasting of lowland-rivers runoff; Issue 3 – forecasting of runoff of mountain rivers.

This issue deals with the forecasting of ice phenomena on rivers and storage reservoirs. In individual problems lakes are considered together with water reservoirs.

Like the previous ones, this is a practical handbook for lecturers and students studying hydrological forecasting and may be used to solve other hydrological problems.

In accordance with the main purpose of this book, theoretical problems are considered here only to the extent to which this is necessary for the understanding and mastering of its content.

Both methods of forecasting and calculation, which can be directly used when preparing forecasts are given in the book. The ways for working out relationships by the methods described are indicated. Special attention is paid to methods which have been tested and used in practice. The accuracy of these methods satisfies the requirements of the Instructions of the Forecasting Service (Section 3, Part I, 1962). An account of some new suggestions and improvements which arose during the work on the Manual are also given.

The calculation and forecasting methods described in the book are illustrated by numerical examples and graphs. However, in the case of the simplest methods, whose use is clear, numerical calculation examples are not given.

The various forecasting methods have not been treated evenly; forecasting ice phenomena in mountain rivers has not been discussed.

The science of hydrological forecastings (with particular reference to ice phenomena) is still in the making. Therefore, every new result in this field obtained after publication of the Manual is likely to improve the forecasting methods.

Apart from books listed in the bibliography, the authors used the vast experience of the hydrologists working at the Hydrometeorological Forecasting Service of the USSR.

This Manual has been written by the following scientists: I. V. Balashova, S. N. Bulatov, N. F. Vinogradova, B. M. Ginzburg, V. V. Piotrovich, and L. G. Shulyakovskii, in joint cooperation with B. P. Konevodov, V. Ya. Amineva, G. A. Andrianova, V. M. Busurina, F. V. Dement'eva, N. D. Efremova, L. V. Kozhankova, L. D. Polezhaeva, K. N. Polyakova, T. P. Chekirda, G. V. Chistyakova and others.

Scientific editing has been carried out by L. G. Shulyakovskii.

Chapter I

FORECASTING THE APPEARANCE OF FLOATING ICE ON RIVERS

A. CONDITIONS FOR THE BEGINNING OF ICE FORMATION

Independently of whether surface or anchor ice prevails on the river stretch under consideration, ice formation begins on the river surface.

As is known, ice forms on water surface when the surface temperature reaches the temperature of water crystallization which for rivers and fresh-water bodies is practically 0°C.

It is also known that at the moment of ice formation on the surface, the temperature below the water surface is positive. It varies with rivers and water bodies. For one and the same river stretch, or in the same region of a water body, it varies slightly from year to year.

What are the conditions which control the temperature in the water body at the moment when ice forms on its surface?

The answer to this question can be obtained by examining the heat balance of the water surface.

Let the equation of the heat balance at the water surface be in the form

$$A+B=0. \tag{1.1}$$

where A is the heat flow between the water body and the water-air interface; when the water cools off it is the heat flux from the water body to the water-air interface; B is the heat flux (at the water surface) resulting from radiant heat exchange (R), evaporation, or condensation (LE), and heat exchange with the air (P), as well as from the specific heat inflow or outflow (per unit surface and unit time) connected with the occurrence of precipitation on the river surface (m)

$$B=R+LE+P+m. \tag{2.1}$$

The heat flow is assumed to be positive if directed to the water surface and negative if directed to the air.

The heat flow between the water body and the water-air interface may be represented as

$$A=\alpha(\vartheta-\vartheta_{s}), \tag{3.1}$$

where α is the coefficient of heat transfer from the water body to the water-air interface or the reverse (in other words the coefficient of heat exchange), ϑ is the averaged water temperature over the cross section or depth, ϑ_{s} is the temperature of the water surface

In this case the heat-balance equation (1.1) will assume the form

$$\alpha(\theta - \theta_{w.s}) + B = 0. \tag{4.1}$$

The temperature gradient and the value $\theta_{w.s}$ in a thin surface layer vary with B while equation (4.1) remains correct. When the surface temperature $\theta_{w.s}$ drops to freezing point, a further increase in B cannot be compensated for by a decrease in $\theta_{w.s}$ and by an increase in the temperature gradient. In this case ice formation begins on the surface.

Thus, ice forms on the surface of a river or a water body when the surface temperature drops to freezing point, and the heat release at the water surface exceeds the heat inflow from the water mass.

Taking $\theta_{w.s} = 0$ at the beginning of ice formation and denoting the values of α, θ and B for this moment by α_n, θ_n and B_n, respectively, we obtain with equation (4.1) the following condition for the beginning of ice formation:

$$\alpha_n\theta_n \leqslant -B_n, \tag{5.1}$$

or

$$\theta_n \leqslant -\frac{B_n}{\alpha_n}. \tag{6.1}$$

Inequality (6.1) shows that ice formation on water surface becomes possible when the water temperature averaged over cross section or depth is lower than, or equal to $-\frac{B_n}{\alpha_n}$.

B. FORECASTING OF ICE PHENOMENA USING WEATHER FORECASTS

Forecasts of the appearance of floating ice with a forewarning period of several days are based on the use of the air temperature forecast. In this case, the forewarning period of the appearance of ice represents the number of days for which it is possible to obtain a reliable forecast of the air temperature. As is shown in practice, the forewarning period is 4 to 5 days on the average.

The prediction of ice appearance using the air temperature forecast can be prepared: (a) by calculation, and (b) by empirical (physical and statistical) relationships.

For river stretches for which there are no long-term data of observations on ice phenomena empirical relationships cannot be obtained. The prediction of the time of ice appearance on rivers after the construction of dams and creation of storage reservoirs under conditions of backwater and runoff control, using relationships which were established for a given river stretch from observations on this stretch in years preceding the runoff control, is impossible. For such river stretches forecasts can be prepared only by calculation.

§ 1. Calculation of the appearance of floating ice on rivers

As was shown above, the condition for the beginning of ice formation on a particular water surface is (inequality (6.1))

$$\theta_n \leqslant -\frac{B_n}{\alpha_n}.$$

Thus, in order to determine the probability of the beginning of ice formation at a given moment, it is necessary to know for this moment: (a) water temperature averaged over the cross section or depth, θ_n; (b) the specific heat transfer of the water surface, B_n; and (c) the coefficient of heat transfer from the water to the water-air interface α_n.

The water temperature θ_n at the end of the n-th time interval can be represented as a function of its determining factors:

$$\theta_n = \theta_0 e^{-na} + \frac{\alpha k}{\alpha k + (\alpha + k)\gamma c\rho}\sum_{i=1}^{n}\left[\theta_i\left(e^{-(n-i)a} - e^{-(n-i+1)a}\right)\right] + \\ + \frac{\alpha d + (\alpha + k)q}{\alpha k + (\alpha + k)\gamma c\rho}\left(1 - e^{-na}\right), \tag{7.1}$$

where

$$a = \frac{[\alpha k + (\alpha + k)\gamma c\rho]\,t}{(\alpha + k)\,hc\rho},$$

$$q = q_b + q_\gamma + q_e,$$

where θ_0 is the initial water temperature, e is the base of the natural logarithms, n is the number of time intervals (number of days) from the beginning of the calculation (for the time for which θ_0 was taken), i is the serial number of the time interval (day) from the beginning of the calculation, α is the coefficient of transfer of heat from the water to the water-air interface or the reverse, k is the coefficient of heat exchange (see (18.1)), d is the specific heat exchange at an air temperature equal to the water-surface temperature, γ is the specific inflow of underground water, h is the average depth, c is the specific heat of the water, ρ is the density of water, t is the unit time (24 hours), θ_i is the mean air temperature during the i-th time interval (during the i-th day), q is the specific channel heat inflow, q_b is the specific heat inflow from the bed; q_γ is the specific heat inflow from the underground water; q_e is the specific heat inflow due to energy dissipation.

Inserting from (7.1) the value of θ_n into (6.1), the condition for the beginning of ice formation becomes

$$\theta_0 e^{-na} + \frac{\alpha k}{\alpha k + (\alpha + k)\gamma c\rho}\sum_{i=1}^{n}\left[\theta_i\left(e^{-(n-i)a} - e^{-(n-i+1)a}\right)\right] + \\ + \frac{\alpha d + (\alpha + k)q}{\alpha k + (\alpha + k)\gamma c\rho}\left(1 - e^{-na}\right) \leqslant -\frac{B_n}{\alpha_n}. \tag{8.1}$$

With inequality (8.1) it is possible to calculate the time of the beginning of ice formation (i.e., of the appearance of floating ice on the river).

If the air temperature is averaged over the whole period of calculation (during n time intervals or n days), the expression for θ_n will be

$$\theta_n = \theta_0 e^{-na} + \frac{\alpha k\bar{\theta} + \alpha d + (\alpha + k)q}{\alpha k + (\alpha + k)\gamma c\rho}\left(1 - e^{-na}\right), \tag{9.1}$$

instead of inequality (8.I) it is then possible to use

$$\theta_0 e^{-na} + \frac{\alpha k\bar{\theta} + \alpha d + (\alpha + k) q}{\alpha k + (\alpha + k)\gamma c\rho}(1 - e^{-na}) \leqslant -\frac{B_n}{\alpha_n}. \qquad (10.I)$$

where $\bar{\theta}$ is the mean air temperature during the period of calculation.

Usually during the period of calculation (several days before the beginning of ice formation) the water temperature in a small or medium-size river is considerably lower than the temperature of the underground water. In this case, since the share of the heat inflow from the underground water in the heat balance of the river is relatively small during the period under consideration, it is possible to use the following, simpler calculation formulas:

(a) when the air temperature is averaged over individual time intervals, usually over 24 hours,

$$\theta_0 e^{-na_1} + \sum_{i=1}^{n}\left[\theta_i\left(e^{-(n-i)a_1} - e^{-(n-i+1)a_1}\right)\right] +$$
$$+\left(\frac{d}{k} + \frac{\alpha + k}{\alpha k} q\right)(1 - e^{-na_1}) \leqslant -\frac{B_n}{\alpha_n}, \qquad (11.I)$$

where

$$a_1 = \frac{\alpha k}{(\alpha + k)hc\rho};$$

(b) when the air temperature is averaged over the whole calculation period,

$$\theta_0 e^{-na_1} + \left(\bar{\theta} + \frac{d}{k} + \frac{\alpha + k}{\alpha k} q\right)(1 - e^{-na_1}) \leqslant -\frac{B_n}{\alpha_n}. \qquad (12.I)$$

For rivers with a very low velocity the values of α are large compared with those of k. In such conditions the difference between $\frac{\alpha + k}{\alpha}$ and unity can be neglected. In this case the following formulas can be used instead of (11.I) and (12.I):

(a) when the air temperature is averaged over individual time intervals,

$$\theta_0 e^{-na_2} + \sum_{i=1}^{n}\left[\theta_i\left(e^{-(n-i)a_2} - e^{-(n-i+1)a_2}\right)\right] +$$
$$+\frac{d + q}{k}(1 - e^{-na_2}) \leqslant -\frac{B_n}{\alpha_n}, \qquad (13.I)$$

where

$$a_2 = \frac{k}{hc\rho};$$

(b) when the air temperature is averaged over the whole calculation period,

$$\theta_0 e^{-na_2} + \left(\bar{\theta} + \frac{d + q}{k}\right)(1 - e^{-na_2}) \leqslant -\frac{B_n}{\alpha_n}. \qquad (14.I)$$

For a mean stream velocity on the flow stretch exceeding 0,4 to 0.5 m/sec, the difference between $\frac{\alpha + k}{\alpha}$ and unity may be neglected during the calculation period. The mean flow velocity at hydrometric gaging sites is usually considerably lower than the mean flow velocity at the indicated stretch. For the above-given mean flow velocity at the given stretch, the mean flow velocity at the hydrometric gaging site should be about 0,3 m/sec on the average.

It is obvious that the beginning of ice formation on rivers can be calculated from (13.I) if two conditions are fulfilled: (a) the flow velocity is not too low and (b) the water temperature is not high during the calculation period compared with the temperature of the underground water. In order to use (14.I), a third condition must be fulfilled (c) — it must be possible to average the air temperature over the calculation period without large errors being introduced. The fulfilment of the last condition is also necessary for the use of formulas (10.I) and (12.I).

Check calculations showed that the accuracy of calculations when using (8.I), (11.I) and (13.I) is almost the same. In 90% of the cases the calculation error does not exceed ± 1 day and in 98% of the cases the error does not exceed ± 2 days. The accuracy of calculation by (10.I), (12.I) and (14.I) is also almost the same. On the other hand, the accuracy of calculations by using the latter inequalities is much lower than that obtained with the first three expressions (the probability that the errors will not exceed ± 1 and ± 2 days is 82 and 91% respectively). However, this accuracy is sufficient to use the calculation in short-range forecasting of ice appearance.

Equations (10.I), (12.I) and (14.I), in which the air temperature is averaged over the whole calculation period, may give rise to considerable errors when the air temperatures at the beginning and end of the calculation period considerably differ, particularly with positive air temperature at the beginning of the period.

Thus, at a mean flow velocity at the hydrometric gaging site higher than 0,3 m/sec calculations may be carried out using (14.I) if according to the weather forecast, there will be no considerable differences between the air temperatures at the beginning and end of the period of calculation (it is important that the air temperature is not positive at the beginning of the period). If, on the other hand, the weather forecast foresees a considerable difference between the air temperatures at the beginning and end of the calculation period (particularly if a positive temperature is predicted for the beginning of the period), it is recommended to use equation (13.I).

As was indicated above, for rivers with a very low flow velocity it is advisable to use (11.I) or (12.I), i. e., without any averaging or with averaging of the air temperature over the calculation period, taking into account its variation during the calculation period.

When the air temperature above the river is relatively high during a considerable part of the calculation period (usually at beginning), formula (8.I) or (10.I) may be used. Such cases are most likely when the calculation period is long (on a large river – more than 5 to 6 days).

In calculations for small rivers we may use the simpler formula (14.I).

The date for which the first checking of the probability of ice occurrence is made is chosen so as to minimize the amount of successive calculations made until a positive result is obtained. If the first calculation shows the probability of first ice occurrence at the chosen date, the probability of the beginning of ice formation in the preceding day should be checked, and so on until a negative result is obtained (ice formation impossible).

If, instead of calculating the time of appearance of floating ice at a given place, we have to determine the place of its appearance (the place of first ice formation) we use, instead of (12.I), the following expression

$$l_0 = -\frac{(\alpha + k)hvc\rho}{\alpha k}\ln\frac{-\frac{B_n}{\alpha_n} - \bar{\theta} - \frac{d}{k} - \frac{(\alpha + k)q}{\alpha k}}{\theta_0 - \bar{\theta} - \frac{d}{k} - \frac{(\alpha + k)q}{\alpha k}}, \qquad (12a.I)$$

and instead of (14.I)

$$l_0 = -\frac{hc\rho v}{k}\ln\frac{-\frac{B_0}{c_0}-\bar{\theta}-\frac{d+q}{k}}{\theta_0-\bar{T}-\frac{d+q}{k}}. \qquad (14a.I)$$

In these formulas, l_0 is the distance from the initial cross section [of the ice-free river] to the cross section where ice formation begins, v is the average flow velocity along river stretch l_0. The rest of the notations are as before. Calculation is carried out by successive approximation.

§ 2. Determination of the parameters necessary to calculate the beginning of ice formation

a) The initial water temperature (θ_0) is taken from one of the upstream gaging sites. This temperature is taken for a date, which precedes by time (nt), equal to the time of flow from the initial to the calculation gaging site, the date for which the possibility of ice appearance at the given gaging site has been calculated. We will use the term calculation gaging site for the gaging site for which the ice appearance is calculated.

If the particular river stretch has tributaries whose water discharge in the initial cross section is not less than 20 to 30% of the total discharge in the initial cross sections, θ_0 is determined as the weighted average (with respect to the discharges) of the water temperatures in the initial cross section of the main river and in the tributary cross sections which correspond with respect to the flow time.

b) The time of flow* (τ_c) from the initial to the calculation gaging site can be determined as follows. As a rule, from a series of years the corresponding water stage at the initial and calculation gaging sites are chosen and for each pair of stages the time of flow (in days) is found. Selection is made from the water stages in the summer-autumn period. The values thus obtained do not usually give a clear correlation with the water stages. Therefore, for each stage chosen, the average of the mean flow velocities, v, at the hydrometric gaging sites situated on the stretch is found as a function of the water stage, H, from the graphs relating the mean flow velocity to the water level, drawn separately for each hydrometric gaging site. Then, from all the thus found values of the time of flow, τ_c, and of the flow velocity, v, the mean values $\bar{\tau}_c$ and $\bar{v}$ are determined. From the graph $v=f(H)$ the mean flow velocity in the given calculation period (v) is determined. The time of flow for the given calculation is determined by

$$\tau_c = \frac{\bar{\tau}_c\bar{v}}{v}. \qquad (15.I)$$

c) Average depth. Cartographic data for rivers with depth data, sufficient for determining the average depth on the stretch, are not always available. In addition, the determination of the average depth of a river stretch hundreds of kilometers long using cartographic data, where data of depth measurements are represented in the form of isobaths, is most laborious.

The average depth of a river during a given calculation period nt (during the time of flow τ_c from the initial (inflow) to the calculation gaging site) can be determined from the following formula without using data of depth measurements on the stretch:

$$h = \frac{\bar{Q}\tau_c}{F}, \qquad (16.I)$$

where $\bar{Q}$ is the mean water discharge on the stretch during the calculation period, F is the water surface area on the stretch from the initial to the calculation gaging site (including the area of the river arms).

The value of $\bar{Q}$ can be determined as the arithmetic mean of the water discharge Q_1 during the first days after the start of flow from the initial gaging site on the first segment and of the water discharge Q_n during the last days of flow on the segment nearest to the calculation gaging site.

If on the river stretch between the initial and the calculation cross section there are large tributaries, taken into account in the determination of θ_0 (see (a)), then the discharge Q_1 should also include the discharges of tributaries at a distance from the calculation cross section corresponding to a time of flow τ_c, and the value of F should also include the area of the water surface of the tributaries on a stretch corresponding to the time of flow up to the calculation cross section.

For rivers whose water surface area varies considerably during the period under consideration, due to variations in the water level, the value of F should be determined from the graph $F=f(H)$. This graph can be obtained by determining the values of F for several heights H of the water stage.

d) The air temperature during each day is taken from observations at the meteorological station nearest to the given river stretch during the given day; if necessary, it is determined by interpolation between the temperatures at neighboring stations.

It may happen that the stretches of the largest tributaries taken into account in the calculation (see (a) and (c)) are located so far from the corresponding stretches of the main river, in terms of the time of flow, that the air temperature in the region of the tributary differs considerably from the air temperature in the region of the main river. In this case the air temperature during the corresponding days is taken as the weighted mean (with respect to the surface area) of meteorological data which characterize the stretches under consideration of the main river and of the tributaries.

e) Specific heat exchange, d, at an air temperature equal to the temperature of the water surface, and the coefficient, k, of heat exchange. The values of d and k are given by

$$d = Q + I_e' + LE' \qquad (17.I)$$

and

$$k = -\frac{(LE-LE')+P+(I_e-I_e')}{\theta_{ws}-\theta}, \qquad (18.I)$$

where Q is the flux of solar radiant heat absorbed by the water, LE is the evaporative heat current from the water surface, LE' is the same at an air temperature equal to the water surface temperature, I_e is the difference

---

* (Also known as time of concentration, lag time or time of travel.)

TABLE 3. Specific heat exchange at air temperature equal to the temperature θ of the water surface for mean wind velocity (kcal/cm² day)

Region I

φ°	15/IX	20/IX	25/IX	30/IX	5/X	10/X	15/X	20/X	25/X	31/X	5/XI	10/XI	15/XI	20/XI	25/XI	30/XI	5/XII	10/XII	15/XII	20/XII	25/XII
67	82	71	60	49	38	28	18	10	3	−5	−12	−18	−22	−25	−27	−28	−29	−30	−31	−31	−31
66	85	74	63	52	41	31	21	13	6	−2	−8	−15	−20	−22	−24	−26	−27	−28	−29	−29	−29
65	88	77	66	55	44	34	25	17	10	2	−5	−12	−17	−19	−21	−23	−24	−26	−27	−27	−27
64	92	81	70	59	48	39	29	21	14	6	−1	−8	−13	−16	−18	−20	−22	−23	−24	−24	−24
63	96	85	74	63	52	42	33	25	18	10	3	−4	−9	−12	−15	−17	−19	−21	−22	−22	−22
62	100	89	78	67	56	46	37	29	22	14	7	0	−5	−9	−12	−14	−16	−19	−20	−20	−20
61	104	93	82	71	60	50	41	33	26	18	11	4	−2	−6	−9	−12	−14	−16	−18	−18	−18
60	108	97	86	75	64	54	45	37	30	22	15	8	2	−2	−6	−9	−12	−14	−16	−16	−16
59	113	102	91	80	69	59	50	41	34	26	19	12	6	1	−3	−6	−9	−11	−13	−13	−13
58	117	106	95	84	73	63	54	46	38	30	23	16	10	5	1	−3	−6	−8	−10	−10	−10
57	121	110	99	88	77	67	58	50	42	34	27	20	14	9	4	0	−3	−6	−8	−9	−9
56	125	114	103	92	82	71	62	54	46	38	31	24	18	12	7	3	0	−3	−5	−6	−6
55	129	118	107	96	86	75	66	58	50	42	35	28	21	16	11	6	3	0	−3	−5	−5
54	133	122	111	100	90	79	70	62	54	46	39	32	25	19	14	9	6	2	−1	−2	−2

Region II

φ°	15/IX	20/IX	25/IX	30/IX	5/X	10/X	15/X	20/X	25/X	31/X	5/XI	10/XI	15/XI	20/XI	25/XI	30/XI	5/XII	10/XII	15/XII	20/XII	25/XII
64	95	82	69	56	43	31	21	12	4	−5	−12	−20	−26	−30	−33	−36	−38	−39	−40	−40	−40
63	99	86	73	60	48	36	26	16	8	−1	−8	−16	−23	−26	−30	−32	−35	−36	−37	−37	−37
62	104	91	78	65	53	41	30	21	12	3	−4	−12	−19	−22	−26	−29	−32	−33	−34	−35	−35
61	109	96	83	70	57	46	35	25	17	7	0	−8	−14	−18	−22	−25	−28	−30	−32	−32	−32
60	113	100	87	74	62	51	40	29	21	11	4	−4	−10	−15	−18	−21	−24	−26	−29	−30	−30
59	118	105	92	79	67	55	44	34	25	15	8	0	−7	−12	−15	−18	−21	−23	−26	−27	−27
58	122	109	96	83	71	59	48	38	29	19	12	4	−3	−8	−12	−14	−18	−21	−23	−24	−24
57	127	114	101	88	76	64	52	42	33	23	16	8	1	−4	−8	−11	−15	−18	−21	−22	−22
56	132	119	106	93	80	68	56	46	37	27	20	12	6	1	−4	−8	−12	−15	−18	−19	−19
55	136	123	110	97	85	73	61	50	41	31	24	16	9	4	−1	−5	−9	−12	−16	−17	−17
54	139	126	114	102	90	78	66	55	45	35	25	20	13	7	3	−2	−6	−9	−12	−14	−11
53	143	131	119	107	95	83	71	60	50	39	32	24	17	11	6	2	−2	−6	−9	−11	−11
52	148	136	124	112	100	88	76	65	55	41	36	28	21	15	10	5	1	−3	−7	−8	−8
51	153	141	129	117	105	93	81	70	60	49	40	32	25	19	14	9	5	0	−3	−4	−4
50	158	146	134	122	110	98	87	76	66	55	45	37	30	23	18	13	8	4	1	0	0
49	163	151	139	127	115	104	93	83	74	62	53	45	37	31	25	20	15	11	8	7	7
48	165	154	143	132	121	110	103	91	81	70	61	51	45	39	33	28	24	19	15	14	14
47	171	160	149	138	129	117	107	97	88	78	69	60	58	47	41	36	32	29	24	23	23
46	178	167	156	145	135	124	114	104	96	86	77	69	61	55	49	44	40	36	32	31	31

Region III

φ°	15/IX	20/IX	25/IX	30/IX	5/X	10/X	15/X	20/X	25/X	31/X	5/XI	10/XI	15/XI	20/XI	25/XI	30/XI	5/XII	10/XII	15/XII	20/XII	25/XII
67	78	64	50	36	22	10	−2	−12	−20	−30	−37	−44	−49	−52	−54	−56	−57	−59	−59	—	—
66	82	68	54	40	26	14	2	−8	−16	−26	−33	−41	−46	−49	−51	−53	−55	−56	−57	—	—
65	86	72	59	44	31	18	6	−4	−12	−22	−30	−38	−43	−47	−49	−51	−53	−54	−55	—	—
64	91	77	63	49	36	23	11	1	−8	−18	−25	−33	−39	−44	−46	−48	−50	−52	−53	—	—
63	96	82	68	54	41	28	16	6	−3	−13	−21	−29	−35	−40	−42	−45	−47	−49	−51	—	—
62	101	87	73	59	46	33	21	11	2	−8	−16	−24	−31	−35	−38	−42	−44	−47	−49	—	—
61	106	92	78	64	51	38	26	16	7	−3	−11	−20	−26	−31	−34	−38	−41	−44	−47	—	—
60	111	97	83	69	56	43	31	21	12	2	−6	−15	−21	−26	−30	−34	−38	−41	−45	—	—
59	116	102	89	74	61	48	36	26	17	7	−1	−10	−17	−22	−26	−30	−34	−38	−42	—	—
58	122	108	94	80	66	53	41	31	22	12	3	−5	−13	−18	−22	−26	−31	−35	−39	—	—
57	127	113	99	85	72	59	47	36	27	17	8	−1	−9	−14	−18	−22	−27	−32	−36	—	—
56	132	119	104	90	78	65	53	42	32	22	13	4	−4	−10	−14	−19	−23	−28	−33	—	—
55	138	124	110	96	83	70	59	47	37	27	18	9	0	−5	−10	−15	−20	−25	−30	—	—
54	143	129	115	101	89	76	64	52	43	32	22	13	5	−1	−6	−11	−16	−21	−27	−29	—
53	150	136	122	109	94	82	69	58	48	37	27	18	9	3	−2	−8	−13	−19	−23	−25	—
52	155	141	127	113	100	88	75	64	53	42	32	22	14	7	2	−4	−9	−14	−19	−21	—
51	160	146	132	118	106	94	81	70	59	47	37	27	18	11	5	0	−5	−11	−15	−16	—
50	163	150	137	124	112	100	87	75	64	52	42	32	22	15	9	4	−2	−7	−11	−12	−12
49	171	158	145	132	119	106	94	83	72	59	49	39	30	23	17	12	7	2	−2	−3	−3
48	179	166	153	140	128	115	103	91	80	67	58	48	39	32	26	20	16	11	7	6	6
47	189	176	161	150	137	124	112	100	89	76	67	57	48	41	35	30	25	20	16	15	15
46	198	185	172	159	146	133	121	109	98	86	76	65	58	51	45	39	34	30	25	24	24
45	207	194	181	168	155	142	130	118	107	94	85	76	67	60	54	49	44	39	34	33	33

TABLE [illegible]

φ°N	31/VIII	5/IX	10/IX	15/IX	20/IX	25/IX	30/IX	5/X	10/X	15/X	20/X	25/X	31/X	5/XI	10/XI	15/XI	20/XI	25/XI	30/XI
Region IV																			
70	72	57	44	32	21	11	2	−6	−14	−22	−27	−33	−39	−44	−49	−54	—	—	—
69	76	61	48	36	25	15	6	−2	−10	−18	−23	−30	−36	−42	−47	−53	—	—	—
68	79	65	52	40	29	19	10	2	−6	−14	−20	−27	−34	−40	−46	−51	—	—	—
67	83	69	56	44	34	24	15	6	−2	−10	−17	−24	−31	−38	−44	−50	—	—	—
66	86	72	60	48	38	28	19	10	2	−6	−13	−21	−29	−36	−43	−49	—	—	—
65	90	76	64	52	42	32	23	14	6	−2	−10	−18	−26	−34	−41	−48	—	—	—
64	94	81	69	57	46	37	28	19	11	2	−6	−13	−21	−29	−36	−43	—	—	—
63	98	85	73	61	51	41	32	24	15	7	−1	−9	−17	−25	−32	−38	—	—	—
62	103	90	78	66	55	46	37	28	20	11	3	−4	−12	−20	−27	−34	—	—	—
61	107	94	82	70	60	50	41	33	24	16	8	0	−8	−16	−23	−29	—	—	—
60	111	99	87	75	64	55	46	38	29	20	12	4	−3	−11	−18	−24	−29	−32	−35
59	116	104	91	79	68	59	50	42	33	24	16	8	1	−7	−14	−20	−25	−29	−32
58	121	108	96	84	72	63	54	46	37	29	21	12	5	−3	−10	−16	−22	−26	−29
57	125	113	100	88	77	68	59	50	42	33	25	17	8	1	−6	−13	−18	−22	−26
56	130	117	105	93	92	72	63	54	46	38	30	21	12	5	−2	−9	−15	−19	−23
55	135	121	109	97	66	76	67	58	50	42	34	26	16	9	2	−5	−11	−16	−20
Region V																			
70	72	55	38	24	11	0	−9	−17	−25	−33	−40	−47	−55	−62	−68	−74	—	—	—
69	76	59	43	29	16	4	−5	−14	−22	−30	−36	−44	−52	−60	−66	−73	—	—	—

φ°N	31/VIII	5/IX	10/IX	15/IX	20/IX	25/IX	30/IX	5/X	10/X	15/X	20/X	25/X	31/X	5/XI	10/XI	15/XI	20/XI	25/XI	30/XI
68	80	64	48	33	20	9	−1	−10	−18	−26	−33	−40	−50	−57	−64	−71	—	—	—
67	84	68	52	38	24	14	4	−6	−14	−22	−30	−38	−47	−54	−62	−70	—	—	—
66	88	72	57	42	30	18	8	−2	−10	−20	−28	−34	−44	−52	−60	−68	—	—	—
65	92	77	62	46	34	22	12	2	−7	−16	−24	−32	−42	−50	−58	−66	—	—	—
64	97	82	67	52	40	28	18	8	−1	−10	−18	−26	−36	−44	−52	−61	—	—	—
63	102	88	72	58	45	34	24	14	4	−4	−12	−22	−31	−40	−48	−55	—	—	—
62	108	93	78	63	50	39	28	19	10	1	−8	−16	−26	−34	−42	−50	—	—	—
61	113	98	83	69	56	44	34	24	16	6	−2	−10	−20	−28	−37	−44	—	—	—
60	118	104	88	75	62	50	40	30	21	12	4	−6	−15	−24	−32	−39	−45	−49	−53
59	123	108	94	80	67	56	45	35	26	16	8	0	−10	−20	−28	−35	−41	−45	−49
58	128	114	98	85	72	61	50	40	32	22	13	4	−6	−16	−24	−31	−37	−41	−46
57	133	118	103	89	77	66	56	46	37	27	18	9	−2	−11	−20	−27	−33	−38	−42
56	138	123	108	94	82	72	60	50	42	32	24	14	2	−6	−16	−23	−29	−34	−39
55	143	128	113	99	87	76	66	66	45	37	28	19	7	−2	−12	−19	−25	−30	−35
Region VI																			
70	98	78	59	41	26	12	0	−10	−20	−30	−38	−46	−54	−60	−66	−72	—	—	—
69	103	83	64	46	31	17	5	−5	−15	−25	−34	−42	−51	−58	−63	−70	—	—	—
68	108	88	70	52	36	22	10	−1	−11	−21	−30	−39	−48	−53	−61	−67	—	—	—
67	112	94	75	57	42	27	15	4	−6	−17	−27	−35	−45	−50	−58	−65	—	—	—
66	117	99	81	63	47	33	20	8	−2	−12	−23	−32	−42	−49	−56	−62	—	—	—
65	123	104	86	69	52	39	25	13	2	−8	−19	−28	−39	−46	−53	−60	—	—	—
64	129	110	92	75	59	45	32	20	8	−2	−13	−22	−33	−40	−47	−55	—	—	—
63	135	117	99	82	66	52	39	26	15	4	−7	−16	−27	−34	−42	−49	—	—	—
62	142	123	105	88	72	58	45	33	21	11	−1	−10	−20	−29	−36	−44	—	—	—
61	148	130	112	95	79	65	52	39	27	17	6	−4	−14	−23	−31	−38	—	—	—
60	154	136	118	102	85	72	59	46	34	23	12	2	−8	−17	−25	−33	—	—	—

TABLE 1a (continued)

φ, deg	31/VIII	5/IX	10/IX	15/IX	20/IX	25/IX	30/IX	5/X	10/X	15/X	20/X	25/X	31/X	5/XI	10/XI	15/XI	20/XI	25/XI	30/XI	5/XII	10/XII	15/XII
										Region VII												
60	142	124	106	89	73	58	43	30	17	4	−8	−19	−30	−40	−48	−57	−63	−69	−73	−77	−81	−85
59	148	130	112	95	79	64	49	36	23	10	−2	−13	−24	−34	−43	−57	−60	−64	−69	−73	−77	−81
58	155	137	119	102	86	71	56	43	29	17	5	−7	−19	−29	−37	−47	−55	−60	−65	−69	−73	−78
57	161	143	125	108	92	77	62	49	36	23	11	−2	−13	−23	−32	−42	−50	−55	−60	−65	−70	−74
56	168	150	132	115	99	84	69	56	42	30	17	6	−8	−18	−27	−37	−45	−51	−56	−61	−66	−71
55	174	156	138	121	105	90	75	62	48	36	23	12	−2	−12	−22	−32	−40	−46	−52	−57	−62	−67
54	181	163	145	128	112	97	82	69	55	43	30	18	4	−6	−16	−27	−35	−41	−47	−52	−57	−62
53	188	170	152	135	119	104	89	76	62	50	37	25	10	0	−10	−21	−29	−36	−42	−47	−52	−58
52	196	177	160	142	126	111	97	83	70	56	43	31	17	6	−5	−15	−24	−30	−36	−43	−48	−53
51	203	184	167	149	133	118	104	90	77	63	50	38	23	12	1	−10	−18	−25	−31	−38	−43	−49
50	210	191	174	156	140	125	111	97	84	70	57	44	29	18	7	−4	−13	−20	−26	−33	−38	−44
										Region VIII												
55	194	172	151	132	112	92	76	60	43	27	11	−2	−18	−29	−41	−52	−60	−66	−72	−78	−84	−93
54	202	181	160	141	121	101	85	68	52	35	19	6	−10	−22	−34	−46	−64	−60	−66	−73	−79	−85
53	211	190	169	149	129	109	94	77	60	44	28	14	−3	−15	−27	−39	−48	−54	−61	−67	−74	−80
52	219	198	177	158	138	118	102	85	69	52	35	22	5	−8	−21	−33	−42	−49	−55	−62	−68	−75
51	228	207	186	166	146	127	111	94	77	61	45	30	12	−1	−14	−26	−36	−43	−50	−56	−63	−70
50	236	216	195	175	155	136	120	102	86	69	53	38	20	6	−7	−20	−29	−37	−44	−51	−58	−65
49	248	227	206	186	166	147	130	113	97	80	64	49	32	18	6	−7	−16	−24	−31	−38	−45	−52
48	260	239	217	196	176	157	141	124	108	91	75	61	44	30	18	6	−3	−11	−18	−25	−32	−39
47	272	250	229	207	187	168	151	134	118	102	86	73	55	43	31	19	11	3	−5	−12	−19	−27
46	284	262	240	218	197	178	162	145	129	113	97	84	67	55	43	32	24	16	8	1	−6	−14
45	296	273	251	228	208	189	172	156	140	124	108	95	79	67	56	45	37	29	21	14	7	−1
44	304	282	261	239	220	201	185	169	154	138	123	110	94	82	71	60	53	44	36	29	22	14
43	313	292	272	251	232	214	198	182	167	152	137	125	109	97	86	76	68	60	52	45	38	30

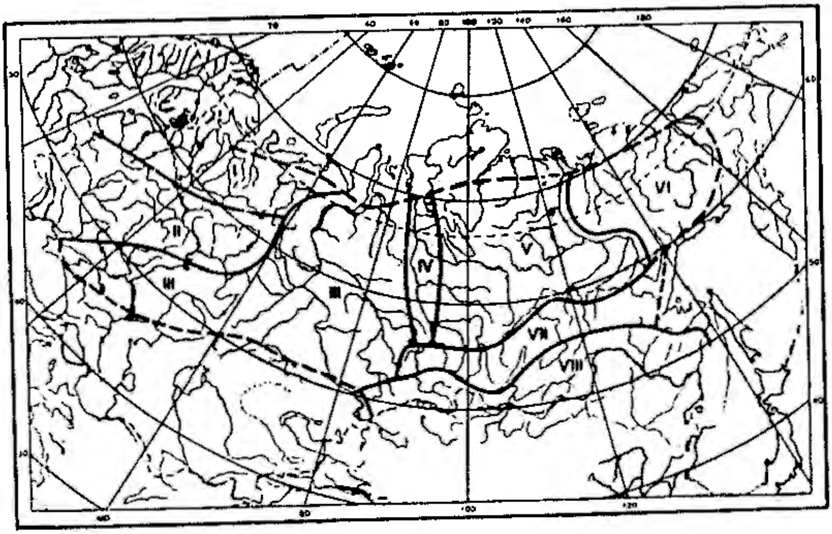

FIGURE [illegible]. Classification of the territory according to the magnitude of the parameter α

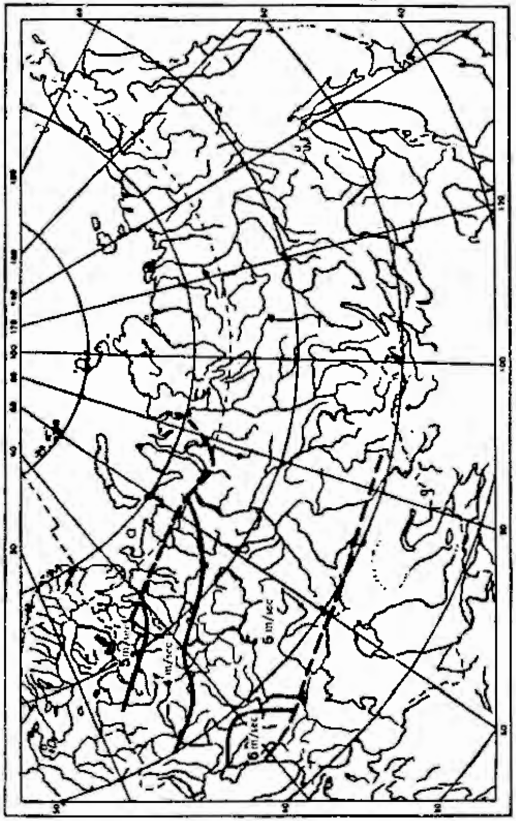

FIGURE 2. Values of the mean wind velocity of the autumn water-cooling period

between the radiant heat fluxes of the water surface and of the back radiation of the atmosphere (effective radiation), I_0' is the same at an air temperature equal to the water surface temperature, P is the specific heat exchange with the air (turbulent heat exchange with the air); θ_w is the temperature of the water surface, θ is the air temperature.

The value of d for the ETS,[*] West Siberia and North Kazakhstan (regions I–III, Figure 1) can be determined from Tables 1 and 2.

Table 1 gives values of d corresponding to the long-term mean wind velocity during the period under consideration in the given region (as well as to the mean values of the cloudiness and to the mean relation between air humidity and air temperature). Values of the mean wind velocity for the period of autumn water cooling are given for this territory in Figure 2.

TABLE 2. Corrections Δd for the deviation of the wind velocity from its mean value, cal/cm^2 day

Region in Figure 3	Deviation of the wind velocity from its mean value, m/sec												
	−6	−5	−4	−3	−2	−1	0	+1	+2	+3	+4	+5	+6
I	17	14	11	9	6	3	0	−3	−6	−9	−11	−14	−17
II	—	24	19	14	10	5	0	−5	−10	−14	−19	−24	—

Table 2 gives the corrections to the values of d for the deviation of the wind velocity from its mean value Δd. The corrections are given separately for two regions (Figure 3), which differ somewhat in the relation between air humidity and air temperature.

For the regions of East Siberia and the Far East shown in Figure 1 (regions IV–VIII) the values of d can be determined from Tables 1a and 2a. In Table 1a, as in Table 1, the values of d correspond to the long-term mean characteristics of the day and night cloudiness and to the mean relation between air temperature and air humidity in the given region in the period under consideration. However, in contrast to Table 1, the values of d in Table 1a are not given for the long-term mean wind velocity during the period under consideration, but for an arbitrary value of 3 m/sec, since the mean wind velocity gives, within the marked regions, a most diversified picture which is obviously connected with the topographical features of the territory under consideration. With the data of Tables 1a and 2a the value of d can be found for any wind velocity, including the long-term mean value of the water cooling period, which is determined in this case from observation data at the station for whose region the value of d is being found.

Suppose it is necessary to determine the value of d for 5 October for a point situated in region V at 57° lat. with a wind velocity of 6 m/sec. From Table 1a we find for d the value of 46 cal/cm^2 day. In the first row of Table 2a we find the correction value of −21 cal/cm^2 day. The required value of d will thus be $46 - 21 = 25$ cal/cm^2 day.

The values of the heat-exchange coefficient k for water bodies situated in regions I–III (Figure 1) can be determined from Table 3, where they are given for various values of the wind velocity and air temperature. The

[*] [Evropeiskaya territoriya SSSR = European Territory of the USSR.]

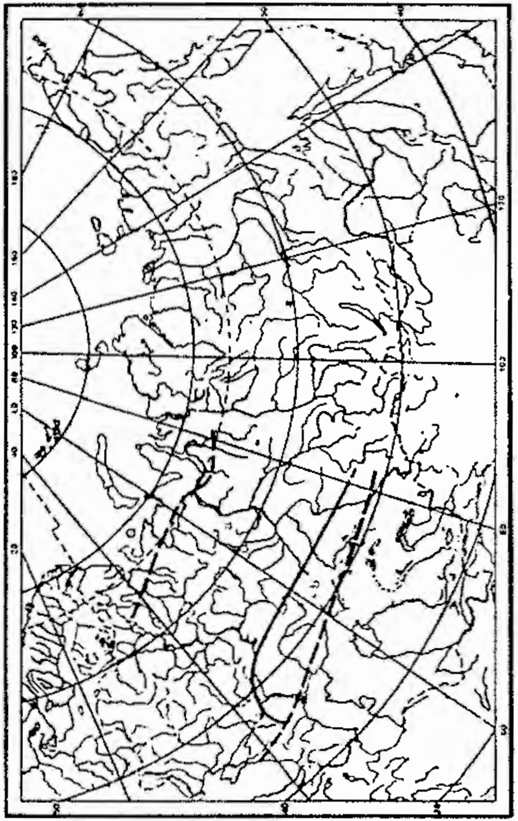

FIGURE 3. Classification of the territory according to the relation between air humidity and air temperature

[illegible]

[illegible]	0	1	2	3	4	5	6	7	8	9	10	11	12	13	14	15
IV—VI	21	14	7	0	—7	—14	—21	—28	—34	—41	—48	—55	—62	—69	—76	—83
VII—VIII	32	21	11	0	—11	—21	—32	—42	—52	—62	—73	—84	—94	—105	—116	—126

[illegible]

[illegible]	0	1	2	3	4	5	6	7	8	9	10
—20	15	19	23	25	32	36	40	44	48	52	56
—19	15	19	23	28	32	36	40	44	48	52	56
—18	15	19	23	28	32	36	40	44	48	52	56
—17	15	19	24	28	32	36	40	45	49	53	57
—16	15	19	24	28	32	36	40	45	49	53	57
—15	16	20	25	29	33	37	41	46	50	54	58
—14	16	20	25	29	33	37	41	46	50	54	58
—13	16	20	25	29	33	37	41	46	51	55	59
—12	16	20	25	29	34	38	42	47	51	55	60
—11	16	20	25	29	34	38	43	47	52	56	61
—10	17	21	26	30	35	39	44	48	53	57	62
—9	17	21	26	30	35	39	44	49	53	57	62
—8	17	21	26	30	35	40	45	49	54	58	63
—7	17	21	26	31	36	40	45	50	54	59	64
—6	17	21	26	31	36	41	45	51	55	60	65
—5	18	22	27	32	37	42	47	52	56	61	66
—4	18	22	27	32	37	42	47	52	57	62	67
—3	18	22	27	33	38	43	49	53	58	63	68
—2	18	22	27	33	38	43	49	54	60	64	69
—1	18	23	28	33	39	44	49	55	60	65	70
0	18	23	28	33	39	44	50	55	61	66	71
1	19	24	29	34	39	44	50	55	61	66	71
2	19	24	29	34	40	45	51	56	61	67	72
3	19	24	29	34	40	45	51	56	62	67	72
4	19	24	29	34	40	45	51	56	62	67	72
5	19	24	29	34	40	45	51	56	62	67	72
6	20	25	30	35	40	45	51	56	62	67	72
7	20	25	30	35	41	45	52	57	63	68	73
8	20	25	30	35	41	46	52	57	63	68	73
9	20	25	30	35	41	46	52	57	63	68	73
10	20	25	30	35	41	46	52	57	61	68	73

TABLE 3a. Heat-exchange coefficients k for regions IV–VIII (cal/cm² day degree)

Air temperature, °	Wind velocity, m/sec										
	0	1	2	3	4	5	6	7	8	9	10
−20	15	19	23	27	31	34	38	41	45	49	53
−19	15	19	23	27	31	34	38	41	45	49	53
−18	15	19	23	27	31	34	38	41	45	49	53
−17	15	19	23	27	31	34	38	42	46	50	54
−16	15	19	23	27	31	35	38	42	46	50	54
−15	15	19	23	27	31	35	39	43	47	51	55
−14	15	19	23	27	31	35	39	43	47	51	55
−13	15	19	23	27	31	35	39	43	47	51	55
−12	15	19	23	28	32	36	40	44	48	52	56
−11	15	19	23	28	32	35	40	44	48	52	56
−10	16	20	24	29	33	37	41	45	49	53	57
−9	16	20	24	29	33	37	41	45	49	53	57
−8	16	20	24	29	33	37	41	45	49	54	58
−7	16	20	24	29	33	38	42	46	50	54	58
−6	16	20	24	29	34	38	42	46	50	55	59
−5	17	21	25	30	34	38	43	47	51	56	60
−4	17	21	25	30	34	38	43	47	51	56	60
−3	17	21	25	30	35	39	43	48	52	57	61
−2	17	21	26	30	35	39	44	48	53	57	62
−1	17	21	26	30	35	40	44	49	54	58	63
0	17	22	27	31	36	41	45	50	55	59	64
1	18	22	27	31	36	41	45	50	55	60	65
2	18	22	27	32	37	42	46	51	56	61	66
3	18	23	28	32	37	42	47	52	57	62	67
4	18	23	28	33	38	43	48	53	58	63	68
5	18	23	28	33	38	44	49	54	59	64	69
6	19	24	29	34	39	44	49	54	59	64	70
7	19	24	30	35	40	45	50	55	60	65	71
8	19	25	30	35	40	46	51	56	61	66	72
9	19	25	30	35	40	46	51	56	62	67	73
10	19	25	30	35	41	46	52	57	62	68	73

TABLE 4. Total solar radiation Q' for a cloudless sky (cal/cm² day)

Month	Latitude, degrees					
	45	50	55	60	65	70
September	500	430	350	330	280	240
October	360	280	230	180	130	100
November	250	160	120	80	30	—
December	190	100	60	40	—	—

values of k given in this table are calculated for the mean cloudiness characteristics and for the mean relations between the air humidity and air temperature of the autumn water-cooling period before the onset of ice formation for low water temperatures. The variations in k with the water temperature within the indicated limits are here negligible.

For the regions IV–VIII the values of k are given in Table 3a. The values of k in this table are calculated like the values of Table 3. For low wind velocities the difference between the values of k for the two groups of regions (Table 3 and 3a) is negligible. For periods with a positive air temperature, in the case of a mean water temperature during the period higher than 4 to 5°, it is recommended to calculate the values of k from (18.1). The values of d can in this case be calculated by (17.1). The values of d and k can be calculated by equations (17.1) and (18.1) from the mean values of the cloudiness, air humidity and wind velocity for any particular time interval.

The magnitudes of the heat fluxes in equations (17.1) and (18.1) can be calculated by the formulas:

$$Q = Q'[1 - 0.14(N_t - N_l) - 0.67N_l](1 - r), \qquad (19.1)$$

$$I_e = -0.96\sigma T_w^4 + \sigma T_{200}^4[0.97N_l + 0.87(N_t - N_l) + A(1 - N_t)], \qquad (20.1)$$

$$I_e' = -\sigma T_{200}^4[0.96 - 0.97N_l - 0.87(N_t - N_l) - A(1 - N_t)], \qquad (21.1)$$

$$LE = 7.8(e_{200} - e_0)(1 + 0.72w_{200}) \text{ cal/cm}^2 \text{ day} \qquad (22.1)$$

$$LE' = 7.8(e'_{200} - e_0)(1 + 0.72w_{200}) \text{ cal/cm}^2 \text{ day}, \qquad (23.1)$$

$$P = 5.07(\theta_{200} - \theta_w)(1 + 0.72w_{200}) \text{ cal/cm}^2 \text{ day} \qquad (24.1)$$

In these formulas

Q' is the total solar radiation in a cloudless sky (Table 4),

N_t is the total cloudiness in fractions of unity,

N_l is the low-level cloudiness in fractions of unity,

r is the albedo of the water surface, it can be taken as a constant, equal to 0.10,

σ is the Stefan-Boltzmann constant, equal to $1.168 \cdot 10^{-7}$ cal/cm² day degree⁴,

θ_w is the temperature of the water surface,

θ_{200} is the air temperature at a height of 200 cm,

T_w is the absolute temperature of the water surface,

T_{200} is the absolute air temperature at a height of 200 cm,

A is a parameter characterizing the back radiation of the atmosphere in a cloudless sky (Table 5),

e_{200} is the pressure (millibars) of water vapor in the air at a height of 200 cm,

e_0 is the saturation pressure (millibars) of the water vapor at the temperature of the water surface,

e'_{200} is the pressure (millibars) of the water vapor in the air at a height of 200 cm for $\theta_{200} = \theta_w$,

w_{200} is the wind velocity (m/sec) at a height of 200 cm.

The values of σT^4 (σT_{200}^4 and σT_w^4) are determined from Table 6.

TABLE 5. Coefficient A as a function of air humidity

e_{200} mb	0.1	0.5	1.0	1.5	2.0	4.0	6.0	8.0	10.0
A . . .	0.46	0.62	0.68	0.71	0.73	0.77	0.80	0.82	0.83

TABLE 6. Values of σT^4 (cal/cm² day)

[illegible]	0.0	0.1	0.2	0.3	0.4	0.5	0.6	0.7	0.8	0.9
0	661	662	662	664	665	665	667	668	670	670
1	671	671	672	672	674	674	675	677	677	678
2	680	681	681	682	684	685	685	687	688	688
3	690	691	691	693	694	694	696	697	698	698
4	700	701	701	703	704	705	706	707	708	708
5	710	711	711	713	714	714	716	717	718	718
6	720	721	723	723	724	726	727	729	729	730
7	732	731	733	734	737	737	737	739	740	740
8	742	743	743	744	746	746	747	749	750	750
9	752	753	754	754	756	757	759	760	760	762
10	763	765	765	766	768	769	769	770	772	772
11	773	775	776	776	778	779	780	780	782	783
12	784	786	788	788	789	790	792	793	793	795
13	796	798	798	799	801	801	802	804	805	805
14	806	808	809	809	811	812	814	815	815	816
15	818	819	821	821	822	824	825	826	826	828
16	829	831	832	832	834	835	837	838	838	840
17	841	842	844	844	845	847	848	850	850	851
18	852	854	855	857	858	858	860	861	862	864
19	865	867	868	868	870	871	873	874	874	876
20	877	878	880	880	881	883	884	886	886	887
21	888	890	891	893	894	896	896	897	898	900
22	901	903	904	904	906	907	909	910	910	912
23	913	914	916	917	919	920	920	922	923	924
24	926	927	929	929	930	932	933	934	934	935
25	937	939	940	942	943	945	945	946	945	949

[illegible]	0.0	−0.1	−0.2	−0.3	−0.4	−0.5	−0.6	−0.7	−0.8	−0.9
0	661	660	660	658	657	657	655	654	654	652
−1	651	649	649	648	648	646	645	645	644	644
−2	642	641	641	639	638	636	636	635	634	634
−3	632	631	631	629	628	628	626	625	624	624
−4	622	621	621	619	619	617	616	616	615	615
−5	613	612	612	610	610	609	608	608	606	606
−6	605	603	603	602	602	600	599	599	598	598
−7	596	595	595	593	592	590	590	589	588	588

TABLE 6 (continued)

[illegible]	0.0	−0.1	−0.2	−0.3	−0.4	−0.5	−0.6	−0.7	−0.8	−0.9
−8	586	585	585	583	583	582	580	580	579	579
−9	577	576	575	574	574	573	572	572	570	570
−10	569	567	566	566	566	564	563	563	562	561
−11	560	559	559	558	557	556	555	554	554	553
−12	553	552	552	550	550	549	547	547	546	546
−13	544	543	543	541	541	540	538	538	537	537
−14	536	535	534	533	533	531	530	530	528	529
−15	527	526	525	524	521	523	521	521	520	520
−16	518	518	517	516	516	516	514	513	513	513
−17	511	510	510	508	508	507	505	505	504	504
−18	502	501	501	501	500	498	498	498	497	495
−19	496	495	494	492	492	492	491	490	490	490
−20	488	487	487	485	487	484	482	482	481	481
−21	479	478	478	475	477	475	475	475	474	472
−22	472	472	471	469	469	469	465	466	466	466
−23	465	464	464	464	462	461	461	461	459	458
−24	458	456	456	455	455	454	452	452	451	451
−25	449	449	445	448	448	446	446	445	445	444
−26	444	441	442	441	441	441	439	436	438	435
−27	436	435	435	435	433	432	432	432	430	429
−28	429	429	428	426	425	426	425	423	423	423
−29	422	420	420	420	419	418	418	418	416	415

f) The coefficient of heat transfer α from the water to air at the water-air interface. The heat transfer coefficient α is determined by the formula

$$\alpha = (1745v + 100w)c\rho \text{ cal/cm}^2 \text{ day degree}, \quad [illegible]$$

where v is the mean flow velocity (m/sec), w is the wind velocity at the altitude of the anemometer (m/sec), c is the specific heat of water, ρ is the density of water ($c\rho$ = 1 cal/cm³ degree).

When determining the coefficient α we take the average flow velocity during the period of calculation as the magnitude v. The latter is determined by dividing the length of the river from the portal to the calculation cross section by the corresponding time of flow.

When determining α_0 for the right-hand side of formulas [illegible] and (10.1) to (11.10) v is taken as the mean flow [illegible] cross section. The wind velocity w during a calm [illegible] at the given meteorological station is taken equal to 0.5 m/sec.

g) The approximate value of the specific heat influx q. [illegible] from the river bed, q [illegible] from the underground water q, [illegible] and [illegible] q, [illegible] written as $q = q + q_{.} + q_{.}$ To determine the value of q it is possible to use the data of Table 7, in which [illegible] values of q [illegible] for various values of the water depth, geographical latitude [illegible]

For the rivers of the ETS and of West Siberia, q_z can be taken equal to 30–45 cal/cm² day*, and the specific channel heat inflow q equal to 50–70 cal/cm² day

TABLE 7. Approximate values of the specific heat exchange q_b of the water with the water-body bed (cal/cm² · day)*

Month	Lat. (north)	Average depth of the water body, m				Month	Lat. (north)	Average depth of the water body, m			
		0–5	10	15	20			0–5	10	15	20
VII	40°	−22	−20	−17	−15	X	40°	28	25	22	18
	50	−24	−21	−19	−16		50	24	21	19	16
	60	−25	−22	−19	−17		60	23	20	18	15
	70	−27	−24	−21	−18		70	21	19	16	14
VIII	40°	−10	−9	−8	−7	XI	40°	31	27	25	21
	50	−9	−8	−7	−6		50	27	24	21	18
	60	−8	−7	−6	−5		60	24	21	19	16
	70	−8	−7	−6	−5		70	20	18	16	13
IX	40°	7	6	5	5	XII	40°	28	25	22	19
	50	9	8	7	6		50	21	19	16	14
	60	11	10	9	7		60	14	12	11	9
	70	13	12	10	9		70	9	8	7	6

* According to A. P. Braslavskii.

Values of γ for a number of rivers of the ETS were found to vary approximately from 3 to 7 cm/day

It is, of course, useful to correct, as much as possible, these values by data referring to the particular river stretch for which the time of ice appearance is calculated For mountain and foothill rivers with particular groundwater-flow conditions the above-given values, obtained for lowland rivers, cannot of course be recommended

In principle, in calculating the time of the beginning of ice formation on rivers of other regions it is necessary initially to investigate the values of q_z for these regions It should, however, be borne in mind that, for example, for the rivers of East Siberia some overestimation or underestimation of the values of q_z should not usually cause an additional error in determining the beginning of ice formation. The point is that the above values of q_z which are probable under these conditions are small compared with the values of the heat transfer through the open (free) surface, which are observed there in the period directly preceding the beginning of ice formation

The value of q_c can be calculated from

$$q_c = \frac{\rho v h i}{I}, \qquad (26.1)$$

where ρ is the water density, v is the mean flow velocity, h is the average flow depth, i is the slope of the water surface, I is the mechanical equivalent of heat, equal to 0.427 kgm/cal (42,700 gcm/cal)

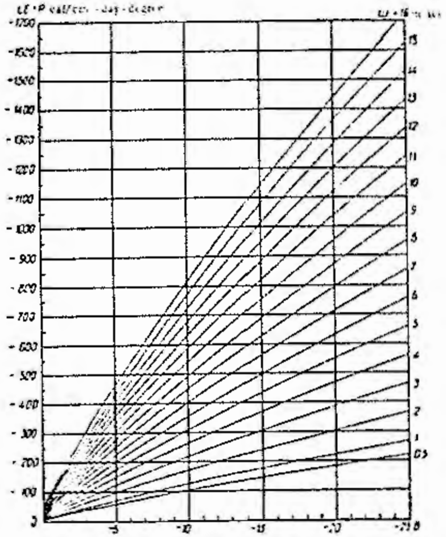

FIGURE 4. Nomograph for the determination of $LE+P$ [illegible] from evaporation and heat exchange with the air [illegible] water-surface temperature of 0°.

For the usual conditions of lowland rivers the magnitude of the heat inflow due to the dissipation of the stream flow energy is negligibly small However, in rivers with a high flow velocity, particularly for large depths and slopes, q_c is considerable.

When calculating the mean value of q_c for the flow path during the calculation period it is necessary to insert in (26.1) the mean values of v, h, i over the flow path during the calculation period

---

* [illegible] the lower limit were obtained for the Lower Volga and [illegible], values close to the upper limit, for the Upper Volga and for the Oka rivers. [illegible] methods of determining the values of q_z and of γ [illegible] Beginning of Freezing on Rivers, Lakes and Water Reservoirs), Chapter II, [illegible] Moscow. 1962.

Example of calculation of q_r. Suppose $v=100\,\text{cm/sec}$, $h=500\,\text{cm}$ and $i=0.00004$ have been determined. Substituting these values in (26.I) we obtain

$$q_r = \frac{1 \cdot 100 \cdot 86\,400 \cdot 500 \cdot 0.00004}{42\,700} = 4\ \text{cal/cm}^2\cdot\text{day}$$

b) The specific heat transfer B_n of the water surface is determined as the sum of the heat fluxes resulting from evaporation LE, turbulent exchange P and effective radiation I_e

$$B_n = LE + P + I_e. \qquad (27.I)$$

The water-surface temperature ϑ_w is taken in this case equal to 0°

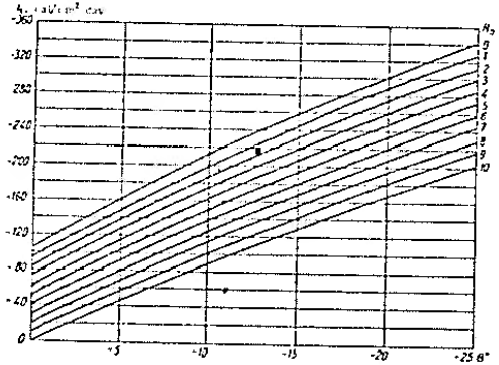

FIGURE 5. Nomogram for determining the effective radiation I_e for a water-surface temperature equal to 0°

The values of LE, P, I_e can be determined from Figures 4 and 5, or calculated by formulas (20.I), (22.I) and (24.I)

§ 3. Calculating the appearance of floating ice on rivers

Example 1. Let us calculate the date of first ice appearance (floating ice) on the Kama River at Sarapul in 1946 (before the creation of storage reservoirs on the Kama River)

We calculate using formula (11.I)

$$\vartheta_0 e^{-na_0} + \sum_{i=1}^{n} \left[\theta_i \left(e^{-(n-i)a_0} - e^{-(n-i+1)a_0}\right)\right] + \left(\frac{d}{k} + \frac{(a+k)q}{ak}\right)\left(1 - e^{-na_0}\right) \leqslant -\frac{B_n}{a_n},$$

where

$$a_0 = \frac{t_\tau k}{(a+k)hc\rho}.$$

As the initial gaging site we take the Perm' station situated 420 km upstream from Sarapul (Figure 6). The mean time of flow τ_c from Perm' to Sarapul is determined from the respective water stages; it is equal to 4.5 days (see § 2b)

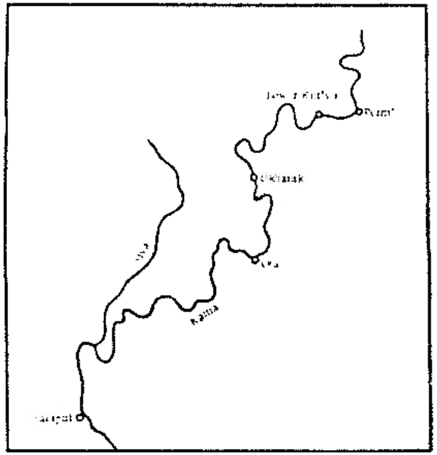

FIGURE 6. Map of the Kama River from Perm' to Sarapul (before the creation of the Votkinsk storage reservoir)

From the graphs $v=f(H)$ we determine the mean flow velocities v at the hydrometric sites of Perm', Lower Kur'ya, Osa and Sarapul,* corresponding to each water level used for the determination of $\overline{\tau}$. Next, we calculate the average of v from these values; we obtain $\overline{v} = 0.53\,\text{m/sec}$

The catchment area (watershed) increases from 168,000 km² at Perm' to 189,000 km² at Sarapul, i.e., by 12.5%. The largest tributary on the given stretch of the Kama River is the Siva River with a catchment area of 4860 km². This is only 2.6% of the catchment area at Sarapul and 23% of the total increase in the catchment area

For the calculation we use the actual data on the air temperature. The use of the forecast air temperature does not introduce essential changes in the calculation technique

---

* The mean flow velocities can also be determined from a single hydrometric site.

The air temperature dropped to negative values in the second ten-day period of October in 1946. At the meteorological stations situated along the river from Perm' to Sarapul the mean-diurnal air temperature had the following values (Table 8).

TABLE 8. Mean-diurnal air temperature, October 1946.

Meteorological station	Date									
	11	12	13	14	15	16	17	18	19	20
Perm'	−1.2	−0.2	3.2	−0.7	−2.0	−1.8	−0.4	−5.2	−5.2	−7.5
Okhansk	−1.0	0.2	3.4	−0.4	−1.4	−1.6	−0.1	−5.2	−4.8	−9.4
Osa	0.0	0.6	3.6	−0.6	−1.5	−1.6	0.7	−4.3	−4.7	−12.3
Sarapul	2.3	1.0	3.3	−0.8	−1.8	−1.6	0.4	−3.4	−4.1	−8.5

We begin with the calculation of the probability of ice appearance at Sarapul on 19 October. The mean flow velocity ($\overline{v}$) for the above-indicated gaging sites in the period of 1945 under consideration is 0.49 m/sec. By (15.1) we find for the time of flow τ_c

$$\tau_c = \frac{\overline{\tau}_c \cdot \overline{v}}{v} = 4.5\frac{0.53}{0.49} = 4.8 \text{ days}.$$

During the time of flow, the discharge increased from 990 m³/sec on 14 October at Perm' to 1200 m³/sec on 19 October at Sarapul. The increase in the discharge amounted to 21%. However, as can be judged from the nature of the growth of the catchment area, the increase in the discharge is not uniform. In this case, we calculate for the initial water temperature, water discharges and morphometric data only for the Kama River.

Since the water temperature is measured only at 8 and 20 hours, in the calculation by the usual mean-diurnal air temperatures θ_0 can be taken either from the evening observations on the day before the first days of the calculation or from the morning observations on the first days of the calculation. For higher accuracy, the mean air temperatures, calculated for 24-hour intervals from the hour of the water-temperature measurement may be calculated. But in calculating a forecast such an accuracy is not necessary.

We begin the calculation by checking the probability of floating ice appearing at Sarapul on the evening of 19 October.

In accordance with the time of flow, we take θ_0 from the measurement at 20 hours on 14 October at Perm' equal to 2.4°.

By (16.1)

$$h = \frac{\overline{Q} \cdot \tau_c}{F}$$

we determine the average depth h on the river stretch under consideration. We find the water discharge $\overline{Q}$ in this case as the average between the discharge at Sarapul (Yaromaska) on the assumed day of floating-ice appearance at Sarapul and of the discharge at Perm' (Lower Kur'ya), taken in accordance with the time of flow for 5 days earlier

$$\overline{Q} = \frac{990 + 1200}{2} = 1095 \text{ m}^3/\text{sec}$$

The area F of the river surface is found (from a master map) to be equal to $3067 \cdot 10^5$ m².

From (16.1)

$$h = \frac{1095 \cdot 4.8 \cdot 86\,400}{3067 \cdot 10^5} = 1.48 \text{ m}$$

The air temperature during the time of flow from Perm' to Sarapul is taken according to the data of one of the meteorological stations (see Table 8), in accordance with its location along the river. We round off the flow time to 5 days. We take: $\theta_1 = -2.0°$ (Perm'), $\theta_2 = -1.5°$ (Okhansk), $\theta_3 = 0.7°$ (Osa), $\theta_4 = -4.3°$ (Osa), $\theta_5 = -4.1°$ (Sarapul).

The average of these temperatures is −2.3°.

Let us determine the mean wind velocity on the Osa path during 15 to 19 October, taking the velocity during each day from the data of the same meteorological station as the temperature. We find it equal to 4.3 m/sec.

From Figure 1 we find that the Kama River for the stretch from Perm' to Sarapul corresponds to region II. From Table 1 the mean value of the parameter d for 15 to 19 October in region II at 56°28' lat. (Sarapul) to 58°01' lat. (Perm') we find equal to 47 cal/cm² day for the mean wind velocity during the period preceding the autumn ice formation. From Figure 2 we find that this mean wind velocity is 5 m/sec. The actual wind velocity on 15 to 19 October 1946 was 4.3 m/sec. In Table 2 we find the correction Δd for the deviation of the wind velocity from the mean value. From Figure 3 we find that the correction should be [illegible] for [illegible] of the table. We obtain for Δd the value of 2 cal/cm² day. Thus, the calculated value of d is taken equal to 47 cal/cm² day.

From Table 3 for an air temperature of −2.3 and a wind velocity of 4.3 m/sec we find for the heat-exchange coefficient k the value 406 cal/cm² day degree.

The heat-transfer coefficient α is calculated by formula (25.1)

$$\alpha = (1745v + 106w)c_p \text{ cal/cm}^2 \text{ day degree}$$

The mean flow velocity v [illegible] dividing the length of the river stretch [illegible] by the time of flow

$$v = \frac{421 \cdot 1000}{4.8 \cdot 86\,400} = 1.02 \text{ m/sec}$$

For this value [illegible] $w = 4.3$ m/sec [illegible] obtain $\alpha = 2230$ cal/cm² day degree.

For specific [illegible] q [illegible] of q indicated [illegible] 50–70 [illegible] of the [illegible] consideration the Kama [illegible] of underground water is observed. [illegible] of q [illegible] 50–70 cal/cm² d [illegible]

The value of α_s is [illegible] $v = f(H)$ the mean flow velocity at Sarapul [illegible] we find $v = 0.42$ m/sec [illegible] α_s = [illegible] at 20 hours on 19 [illegible] = 1263 cal/cm² day degree.

The value of B_s is determined by taking the sum of the heat transfer from evaporation LE, turbulent heat-exchange P and effective radiation I_e using the nomographs of Figures 4 and 5. For the values $\theta = -2.8°$, $w = 5$ m/sec and $N_0 = 4$ observed at 19 hours on 19 October at Sarapul we obtain $LE + P = -112$ cal/cm²·day, $I_e = -93$ cal/cm²·day and $B_s = -205$ cal/cm²·day.

Thus, we obtained the following values for the determination of the probability of floating ice appearing at Sarapul at 19 hours on 19 October: $\theta_0 = 2.4°$; $h = 1.48$ m; $\theta_1 = -2.0°$; $\theta_2 = -1.6°$; $\theta_3 = 0.7°$; $\theta_4 = -4.3°$; $\theta_5 = -4.1°$; $\alpha = 2250$ cal/cm²·day·degree; $k = 40$ cal/cm²·day·degree; $d = 49$ cal/cm²·day, $q = 70$ cal/cm²·day; $B_s = -205$ cal/cm²·day; $\alpha_s = 1263$ cal/cm²·day·degree.

$n = 5$ (rounded off number of days of flow).

Further we determine the value of a_0

$$a_0 = \frac{t\alpha k}{(\alpha + k)hc\rho} = \frac{1 \cdot 2250 \cdot 40}{(2250 + 40) \cdot 148 \cdot 1} = 0.266.$$

From the table of e^{-x} (Appendix 1) we find the values of e^{-a_0}, e^{-2a_0}, $e^{-3a_0}, \ldots, e^{-na_0}$, and calculate their differences, which appear in formula (11.1). The calculation results are given in Table 9.

TABLE 9

No. of day i	Date	$e^{-(n-i)a_0}$	$e^{-(n-i+1)a_0}$	$e^{-(n-i)a_0} - e^{-(n-i+1)a_0}$	θ_i	$\theta_i(e^{-(n-i)a_0} - e^{-(n-i+1)a_0})$
1	15 X	0.346	0.264	0.082	−2.0	−0.164
2	16 X	0.450	0.346	0.104	−1.6	−0.166
3	17 X	0.587	0.450	0.137	0.7	0.096
4	18 X	0.766	0.587	0.179	−4.3	−0.770
5	19 X	1.000	0.766	0.234	−4.1	−0.959
						$\sum_{i=1}^{5} = -1.963$

Substituting the numerical values in formula (11.1), we obtain:

on the left-hand side, the water temperature averaged over the cross section

$$2.4 \cdot 0.264 - 1.963 + \left(\frac{49}{40} + \frac{(2250 + 40) \cdot 70}{2250 \cdot 40}\right)(1 - 0.264) =$$
$$= 0.634 - 1.963 + 2.212 = 0.88 \approx 0.9°,$$

on the right-hand side, the water temperature, averaged over the cross section, at which ice formation on the surface is probable

$$-\frac{-205}{1263} = 0.16 \approx 0.2°.$$

The left-hand side of (11.1) is larger than the right-hand side. Consequently, ice formation cannot begin at 19 hours on 19 October.

We make a similar calculation of $-\frac{B_s}{\alpha_s}$ for 1 hours on 20 October. We obtain: $-\frac{B_s}{\alpha_s} = -\frac{-273}{786} = 0.35°$. In this case, too, the left-hand side of (11.1) is larger than the right-hand side. Consequently, also at 1 hours on 20 October ice formation cannot begin.

Let us calculate the probability of ice formation at 19 hours on 20 October.

The water temperature at Perm' on the evening of 15 October was 1.9°. We take $\theta_0 = 1.9°$. The average water discharge $\overline{Q} = 1100$ m³/sec. The time of flow is 4.8 days. The average depth is equal to 149 cm. The air temperature (Table 3): $\theta_1 = -1.8°$ (Perm'); $\theta_2 = -0.1°$ (Okhansk), $\theta_3 = -4.3°$ (Osa); $\theta_4 = -4.7°$ (Osa); $\theta_5 = -8.5°$ (Sarapul). The average of these temperatures is −3.9°. The mean wind velocity along the flow path during the calculation period we find equal to 3.2 m/sec. For d we find 50 cal/cm²·day (see Tables 1 and 2), $k = 33$ cal/cm²·day·degree (Table 2). For $v = 1.02$ m/sec and $w = 3.2$ m/sec, we find by formula (25.1), $\alpha = 2120$ cal/cm²·day·degree. For a_0 we find

$$a_0 = \frac{t\alpha k}{(\alpha + k)hc\rho} = \frac{1 \cdot 2120 \cdot 33}{(2170 + 33) \cdot 149 \cdot 1} = 0.218.$$

For the exponential functions and their differences we find the following values (Table 10).

TABLE 10

No. of day i	Date	$e^{-(n-i)a_0}$	$e^{-(n-i+1)a_0}$	$e^{-(n-i)a_0} - e^{-(n-i+1)a_0}$	θ_i	$\theta_i(e^{-(n-i)a_0} - e^{-(n-i+1)a_0})$
1	16 X	0.418	0.336	0.082	−1.8	−0.148
2	17 X	0.520	0.418	0.102	−0.1	−0.010
3	18 X	0.647	0.520	0.127	−4.3	−0.545
4	19 X	0.804	0.647	0.157	−4.7	−0.737
5	20 X	1.000	0.804	0.196	−8.5	−1.665
						$\sum_{i=1}^{5} = -3.105$

We repeat the calculation of $-\frac{B_s}{\alpha_s}$ for 19 hours of 20 October. The air temperature according to the data of the Sarapul meteorological station was −8.3° at 19 hours of 20 October during calm weather and total cloudiness corresponding to point 4 on the cloudiness scale.

For these data we obtain from Figures 4 and 5 $LE + P = -92$ cal/cm²·day, $I_e = -152$ cal/cm²·day, $B_s = -244$ cal/cm²·day. For $v = 0.42$ m/sec and $w = 0.5$ m/sec (during calm weather at the meteorological station we take for the wind velocity over the water surface, as indicated above, a value of 0.5 m/sec) we obtain formula (25.1)

$$\alpha = (1745v + 106w)c\rho$$

which yields $\alpha_s = 786$ cal/cm²·day·degree

Substituting the numerical values in formula (11.1), we obtain:
on the left-hand side

$$1.9\cdot 0.336-3.105+\left(\frac{50}{33}+\frac{(2120+33)\cdot 70}{2120\cdot 33}\right)(1-0.336)=$$

$$=0.639-3.105+2.440=-0.05^\circ,$$

on the right-hand side

$$-\frac{-244}{786}=0.31^\circ\approx 0.3^\circ.$$

The left-hand side of the inequality is smaller than the right-hand side, i.e., the water temperature on 20 October is lower than that at which, under the given conditions, the beginning of ice formation on the surface is probable.

Consequently, floating ice should appear on the Kama River at Sarapul on 20 October (the appearance of floating ice at Sarapul in 1946 was recorded on the 20 October).

Favorable conditions for the beginning of ice formation also existed on the morning of 20 October, when the air temperature dropped considerably (−13.2° at 7 hours), the total cloudiness decreased to point 1 and calm weather was observed. Calculation by inequality (11.1), using the mean air temperatures during 24-hour intervals beginning from 7 hours on 15 October, shows that a beginning of ice formation at 7 hours of 20 October was probable.

Example 2. Let us calculate the time of the beginning of ice formation on the Kama River at Sarapul in 1946 by (12.1)

$$\vartheta_0 e^{-na_0}+\left(\bar{\theta}+\frac{d}{k}+\frac{\alpha+k}{\alpha k}q\right)\left(1-e^{-na_0}\right)\leqslant-\frac{B_n}{\alpha_n},$$

where

$$a_0=\frac{f\alpha k}{(\alpha+k)hc\rho}.$$

Use is made in this calculation not of the daily air temperatures, but of the mean temperature $\bar{\theta}$ during the calculation period.

Suppose that for the given calculation period we know only the diurnal-mean air temperatures.

To determine the values of d, k, α, α_n we take the mean wind velocity for the given region in the period preceding the beginning of ice formation. From Figure 2 the mean wind velocity for the region under consideration is 5 m/sec.

Let us calculate the probability of the beginning of ice formation on 19 October.

The initial gaging station is taken, as in the previous example, at Perm'. We use the values determined in Example 1: $\tau=4.8$ days (rounded off to 5 days), $h=148$ cm, $v=1.02$ m/sec, $\vartheta_0=2.4^\circ$, $\bar{\theta}=-2.3^\circ$, $q=70$ cal/cm² day. From Table 1 with given mean wind velocity we find $d=47$ cal/cm² day. From Table 3 we find for k corresponding to a wind velocity of 5 m/sec and an air temperature of −2.3°, a value of 43 cal/cm² day·degree.

For the heat-transfer coefficients α we find, with $v=1.02$ m/sec and $w=5.0$ m/sec, by (25.1)

$$\alpha=(1745v+106w)c\rho$$

a value of 2310 cal/cm² day·degree.

We also find

$$a_0=\frac{f\alpha k}{(\alpha+k)hc\rho}=\frac{1\cdot 2310\cdot 43}{(2310+43)\cdot 148\cdot 1}=0.286$$

$$na_0=5\cdot 0.286=1.43,\quad e^{-na_0}=0.239.$$

With a flow velocity at Sarapul at the time under consideration equal to 0.42 m/sec and a wind velocity $w=5.0$ m/sec, (25.1) gives $\alpha_n=1260$ cal/cm²·day·degree.

The value of B_n is determined by means of the nomographs from Figures 4 and 5. The air temperature θ at Sarapul on 19 October is −4.1° (Table 3). We take $w=5$ m/sec (rated value), $N_0=9$ (rated value). We obtain: $LE+P=-148$ cal/cm² day, $I_e=-50$ cal/cm² day, $B_n=-148-50=$ $=-198$ cal/cm² day.

Substituting the values obtained in formula (12.1), we have
on the left-hand side

$$2.4\cdot 0.286+\left(-2.3+\frac{47}{43}+\frac{(2310+43)\cdot 70}{2310\cdot 43}\right)(1-0.286)=1.0^\circ.$$

on the right-hand side

$$-\frac{-198}{1260}=0.16^\circ\approx 0.2^\circ.$$

Thus, condition (12.1) is not satisfied, and ice formation should not begin on 19 October. (There was indeed no floating ice at Sarapul on 19 October.)

Let us repeat the calculation for 20 October.

From the measurement at 20 hours on 15 October at Perm' we take $\vartheta_0=1.9^\circ$. For the mean air temperature on the flow path during the days of 16 to 20 October (Table 8) we obtain −3.9°. From Table 1 we find the mean value for the calculation period of $d=47$ cal/cm² day and from Table 3 $k=42$ cal/cm² day·degree. As in the previous calculation, $\alpha=2310$ cal/cm² day·degree, $\alpha_n=1260$ cal/cm² day·degree, $h=149$ cm. We obtain

$$a_0=\frac{f\alpha k}{(\alpha+k)hc\rho}=0.277,\quad na_0=5\cdot 0.277=1.38,\quad e^{-na_0}=0.252$$

For these values we have
on the left-hand side of (12.1)

$$1.9\cdot 0.252+\left(-3.9+\frac{47}{42}+\frac{(1260+42)\cdot 70}{1260\cdot 42}\right)(1-0.252)=$$

$$=-0.31^\circ\approx-0.3^\circ.$$

The air temperature on 20 October at Sarapul was −8.5°. The wind velocity and the total cloudiness is taken equal to their rated values for the period of the beginning of ice formation (5 m/sec and point 9 on the scale).

From Figures 4 and 5 we find: $LE+P=-272$ cal/cm² day, $I_e=-90$ cal/cm² day, $B_n=-272-90=-362$ cal/cm² day. On the right-hand side we obtain

$$-\frac{-362}{1260}=0.3^\circ.$$

The right-hand side of the inequality is larger in this case than the left-hand side, condition (12.1) is thus satisfied. Consequently, ice formation should begin on 20 October (floating ice actually appeared on the Kama at Sarapul in 1946 precisely on 20 October).

The negative sign of the result of the left-hand side of the inequality [illegible] indicates, as in the other examples, supercooling of the water. It [illegible] that by the time for which the calculation is made some ice has [illegible].

Example 4. Let us calculate the time of the beginning of ice formation on the Kama at Sarapul in 1946 by (13.1)

$$\vartheta_0 e^{-n\alpha_1}+\sum_{i=1}^{n}\left[\vartheta_i\left(e^{-(n-i)\alpha_1}-e^{-(n-i+1)\alpha_1}\right)\right]+$$
$$+\frac{d+q}{k}\left(1-e^{-n\alpha_1}\right)\leqslant-\frac{B_n}{\alpha_n},$$

where

$$\alpha_1=\frac{tk}{hc\rho}.$$

First we calculate whether the beginning of ice formation in the evening of 19 October is probable.

The initial data for the calculation of the time of floating ice appearance are the same as in Example 1: $\vartheta_0=2.4°$, $\vartheta_1=-2.0°$, $\vartheta_2=-1.6°$, $\vartheta_3=0.7°$, $\vartheta_4=-4.3°$, $\vartheta_5=-4.1°$; $k=40$ cal/cm² day degree; $h=1.48$ m; $d=49$ cal/cm² day; $q=70$ cal/cm² day; $B_n=-205$ cal/cm² day; $\alpha_n=1263$ cal/cm² day degree; $n=5$ (the number of days); $\alpha_2=\frac{tk}{hc\rho}=\frac{1\cdot40}{148\cdot1}=0.270$.

From the table of e^{-x} (Appendix 1) we find the values of $e^{-\alpha_1}$, $e^{-2\alpha_1}$, …, $e^{-5\alpha_1}$ and calculate the quantities in formula (13.1). The calculation results are given in Table 11.

Table 11

[illegible]		$e^{-(n-i)\alpha_1}$	$e^{-(n-i+1)\alpha_1}$	$e^{-(n-i)\alpha_1}-e^{-(n-i+1)\alpha_1}$	ϑ_i	$\vartheta_i\left(e^{-(n-i)\alpha_1}-e^{-(n-i+1)\alpha_1}\right)$
1	15 X	0.340	0.259	0.081	−2.0	−0.162
2	16 X	0.445	0.340	0.105	−1.6	−0.168
3	17 X	0.583	0.445	0.138	0.7	0.095
4	18 X	0.763	0.583	0.180	−4.3	−0.775
5	19 X	1.000	0.763	0.237	−4.1	−0.972
						$\sum_{i=1}^{5}=-1.981$

Substituting the numerical values in (13.1) we obtain on the left-hand side

$$2.4\cdot0.259-1.98+\frac{49+70}{40}(1-0.259)=0.84°\approx0.8°,$$

on the right-hand side

$$-\frac{-205}{1263}=0.16°\approx0.2°.$$

The left-hand side is larger than the right-hand side. Consequently, ice formation cannot begin at 19 hours on 19 October.

Let us repeat the calculation of the probability of the beginning of ice formation on 20 October.

As in Example 1 (see above), from the measurements of [illegible] on 15 October at 19 hours we take $\vartheta_0=1.9°$, [illegible] $\overline{Q}=$[illegible] the time of [illegible] 4.4 days, the average depth $h=1.49$ m, $\vartheta_1=-1$[illegible], $\vartheta_2=-0.1°$ (Okhansk), $\vartheta_3=-4.3°$ (Osa), $\vartheta_4=-4.7°$ (Osa), $\vartheta_5=-5.5°$ [illegible]. The mean air temperature along the flow path during 16 to 20 October [illegible] we obtain equal to −3.5°. The mean wind velocity during 16 to 20 October [illegible] 3.2 m/sec, and $d=50$ cal/cm² day (Tables 1 and 2); $k=33$ cal/cm² day degree (Table 3).

Next, as in Example 1, the mean [illegible] to be 0.42 m/sec. The wind velocity at [illegible] we take as 0.5 m/sec. We obtain $\alpha_n=780$ [illegible], $B_n=-362$ cal/cm² day, and $\alpha_2=\frac{tk}{hc\rho}=\frac{1\cdot33}{149\cdot1}=0.222$.

For the exponential functions and their differences we obtain Table 12.

Table 12

No. of day	Date	$e^{-(n-i)\alpha_1}$	$e^{-(n-i+1)\alpha_1}$	$e^{-(n-i)\alpha_1}-e^{-(n-i+1)\alpha_1}$	ϑ_i	$\vartheta_i\left(e^{-(n-i)\alpha_1}-e^{-(n-i+1)\alpha_1}\right)$
1	16 X	0.412	0.330	0.082	−1.8	−0.148
2	17 X	0.514	0.412	0.102	−0.1	−0.010
3	18 X	0.641	0.514	0.127	−4.3	−0.546
4	19 X	0.801	0.641	0.160	−4.7	−0.753
5	20 X	1.000	0.801	0.199	−5.5	−1.690
						$\sum_{i=1}^{5}=-3.147$

Substituting the numerical values in (13.1) we obtain on the left-hand side

$$1.9\cdot0.330-3.147+\frac{50+70}{33}(1-0.330)=0.627-$$
$$-3.147+2.440=-0.08°\approx-0.1°,$$

on the right-hand side

$$-\frac{-362}{780}=0.46°\approx0.5°.$$

The left-hand side of the inequality is smaller than the right-hand side [illegible] the water temperature on 20 October [illegible] at which [illegible] under the given conditions, the beginning of [illegible] is probable. Consequently, [illegible] the [illegible] on 20 October. The appearance of floating ice at Sarapul in 1946 was recorded on 21 October.

Example 4. Let us calculate the time of the beginning of ice formation on the Kama River at Sarapul in 1946 using (14.I):

$$\theta_0 e^{-na_2} + \left(\bar{\theta} + \frac{d+q}{k}\right)\left(1 - e^{-na_2}\right) < -\frac{B_n}{\alpha_n},$$

where

$$a_2 = \frac{tk}{hc\rho}.$$

We calculate for 19 October.

As in Example 2, we assume that for the given period we only know the diurnal-mean air temperatures.

The data for calculations are (see Example 2): $\tau = 4.8$ days (rounded off to 5 days), $h = 148$ cm, $\theta_0 = 2.4$; $\bar{\theta} = -2.3°$; $d = 47$ cal/cm² day (for a normal wind velocity of 5 m/sec), k, corresponding to a wind velocity of 5 m/sec and an air temperature of −2.3°, is 43 cal/cm² day degree, $q = 70$ cal/cm² day.

For a flow velocity at Sarapul at the time under consideration equal to 0.42 m/sec and a wind velocity equal to 5.0 m/sec, we obtain $\alpha_n = 1260$ cal/cm² day degree.

For B_n (see Example 2) we obtain from Figures 4 and 5 −198 cal/cm² day, and for

$$a_2 = \frac{tk}{hc\rho} = \frac{1 \cdot 43}{148 \cdot 1} = 0.290,$$

$$na_2 = 5 \cdot 0.290 = 1.45, \quad e^{-na_2} = e^{-1.45} = 0.235.$$

Substituting the numerical values obtained in (14.I), we have on the left-hand side

$$2.4 \cdot 0.235 + \left(-2.3 + \frac{47+70}{43}\right)(1 - 0.235) = 0.89° \approx 0.9°,$$

on the right-hand side

$$-\frac{-198}{1260} = 0.16 \approx 0.2°.$$

Thus, condition (14.I) is not satisfied and ice formation should not begin on 19 October. Floating ice actually was not observed at Sarapul on 19 October.

Let us repeat the calculation for 20 October.

The data for the calculation (see Example 2).

From the measurement at 20 hours on 15 October at Perm' we take $\theta_0 = 1.9°$. The mean air temperature along the flow path during 16 to 20 October is −3.9°. From Table 1 we find a mean value (for the calculation period) of $d = 47$ cal/cm² day, and from Table 3 we obtain $k = 42$ cal/cm² day degree. As for the previous calculation $\alpha_n = 1260$ cal/cm² day degree, and $h = 149$ cm. We find

$$a_2 = \frac{tk}{hc\rho} = \frac{1 \cdot 42}{149 \cdot 1} = 0.282,$$

$$na_2 = 5 \cdot 0.282 = 1.41, \quad e^{-na_2} = e^{-1.41} = 0.244.$$

With these values we will obtain on the left-hand side of (14.I)

$$1.9 \cdot 0.244 + \left(-3.9 + \frac{47+70}{42}\right)(1 - 0.244) = $$
$$= 0.464 - 0.847 = -0.38° \approx -0.4°.$$

Next, as in Example 2, from an air temperature on 20 October at Sarapul equal to −8.5°, a wind velocity $w = 5$ m/sec and a total cloudiness $N_0 = 0$ points, we obtain from Figures 4 and 5: $LE + P = -272$ cal/cm² day, $I_e = -90$ cal/cm² day, $B_n = -272 - 90 = -362$ cal/cm² day.

On the right-hand side of (14.I) we have

$$-\frac{B_n}{\alpha_n} = -\frac{-362}{1260} = 0.29° \approx 0.3°.$$

In this case, the right-hand side of the inequality is larger than the left-hand side; condition (14.I) is satisfied. Consequently, ice formation should begin on 20 October (actually floating ice appeared on the Kama River at Sarapul in 1946 on 20 October).

Example 5. Let us calculate the time of the beginning of ice formation on the Don upstream of Khovanskii in 1948 using (11.1):

$$\theta_0 e^{-na_0} + \sum_{i=1}^{n} \left[\theta_i \left(e^{-(n-i)a_0} - e^{-(n-i+1)a_0}\right)\right] +$$
$$+ \left(\frac{d}{k} + \frac{\alpha + k}{\alpha k} q\right)\left(1 - e^{-na_0}\right) < -\frac{B_n}{\alpha_n},$$

where

$$a_0 = \frac{t\alpha k}{(\alpha + k)\, hc\rho}.$$

As the initial gaging site we take the Pavlovsk station, situated 358 km upstream from Khovanskii (Figure 7). The mean time of flow t_1 from Pavlovsk to Khovanskii we find (from the corresponding water stages) equal to 6.7 days (see § 2, b).

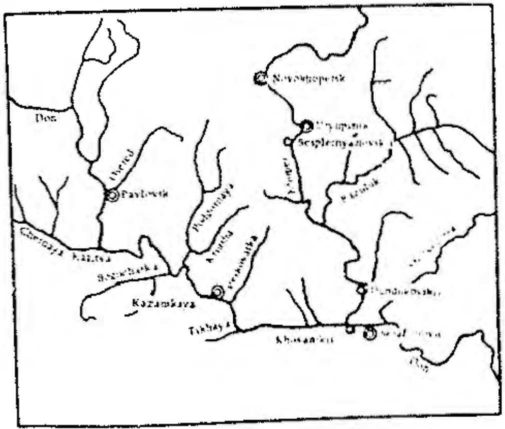

FIGURE 7. The Don River with tributaries on the Pavlovsk–Khovanskii reach

[illegible] the graphs $v=f(H)$ we determine the mean flow velocities v at [illegible] metric stations of Pavlovsk, Kazanskaya and Khovanskii, which [illegible] water stage used for the determination of $\overline{\tau}_1$. The average [illegible] of v is then $\overline{v}=0.23$ m/sec.

[illegible] area increases from 54,000 km² at Pavlovsk to 109,000 km² [illegible] by 102%. The largest tributary on the Don stretch [illegible] is the Khoper River with a catchment area of [illegible]. This amounts to 36.5% of the [illegible] area at Khovanskii and [illegible] of the total increase in the catchment area. The water discharge [illegible] Khoper River at a distance from the mouth corresponding to the time [illegible] the Don from Pavlovsk to the Khoper mouth amounted, in the [illegible] consideration, to about 20% of the total discharge in the [illegible].

[illegible] attention to [illegible] the water discharges of the main river and [illegible] the tributary, it is necessary [illegible] as indicated in § 2, [illegible] along with the characteristics of the main river, [illegible] characteristics of the tributary with its respective share.

[illegible] gauging site on the Khoper River we take the Novokhopersk [illegible]. The distance from it to the river mouth is 275 km and to the [illegible] on the Don, 397 km. The mean time of flow $\overline{\tau}$ [illegible] of Tretyakovskaya (45 km upstream from the [illegible]) [illegible]. The mean flow velocity found in the same [illegible] of the Don [illegible] 0.35 m/sec from [illegible] stations of Novokhopersk, Besplemyanovskii [illegible]. The mean time of flow from Novokhopersk to Khovanskii is [illegible].

[illegible] 24 November [illegible] 1949 [illegible] stations situated along the Don and Khoper River [illegible] [illegible] consideration [illegible].

[illegible]	18	19	20	21	22	23	24	25	26	27
[illegible]	1.4	0.6	2.7	1.5	2.7	3.0	−1.8	−2.8	−9.0	−7.8
[illegible]	1.0	0.7	2.6	2.0	2.6	3.4	−0.7	−2.6	−6.7	−6.7
[illegible]	1.3	0.3	2.0	1.4	1.4	3.8	0.8	−2.6	−8.4	−6.2
[illegible]	0.6	−0.2	1.4	0.9	1.8	2.2	−1.0	−3.1	−7.6	−8.9
[illegible]	1.2	0.4	1.5	1.4	2.1	2.9	−1.2	−3.3	—	—

[illegible] with the calculation of the probability of [illegible] on 25 November.

[illegible] flow velocity $\overline{v}$ for the period [illegible] 1949 [illegible] stations of Pavlovsk, Kazanskaya, Khovanskii on the Don [illegible].

From (15.1)

$$\tau_1=\frac{\overline{\tau}\,\overline{v}}{v}$$

[illegible] Novokhopersk [illegible]

The mean flow velocity on the Khoper River [illegible] Besplemyanovskii stations [illegible]

[illegible] $\overline{\tau}_1$ [illegible] 7.5 days.

[illegible] taken as 7.4 days [illegible] 7.3 and 7.5 days.

[illegible] θ_0 [illegible] at 20 hours [illegible]

$$\theta_0=\frac{0.5\cdot 96.0+0.7\cdot 24.2}{96.0+24.2}=0.54^\circ\approx 0.5^\circ.$$

[illegible]

$$h=\frac{\overline{Q}\tau}{F}$$

[illegible] h [illegible] $\overline{Q}$ [illegible] 24 [illegible] F [illegible]

$$h=\frac{\frac{56+24+175}{2}\cdot 7.4\cdot 86\,400}{(67.85+29.50)\cdot 10^{9}}=\frac{147.6\cdot 7.4\cdot 86\,400}{97.05\cdot 10^{9}}=0.97$$

[illegible]

19 November (meteorological stations Pavlovsk and Novokhopersk)

$$\theta_1 = \frac{0.6^\circ \cdot 876 + (-0.2^\circ) \cdot 500}{876 + 500} = 0.3^\circ.$$

20 November (Pavlovsk and Uryupinskaya)

$$\theta_2 = \frac{2.7^\circ \cdot 1060 + 1.8^\circ \cdot 339}{1060 + 339} = 2.5^\circ.$$

21 November (Pavlovsk and Uryupinskaya)

$$\theta_3 = \frac{1.8^\circ \cdot 683 + 1.4^\circ \cdot 370}{683 + 370} = 1.7^\circ.$$

22 November (Kazanskaya and Uryupinskaya)

$$\theta_4 = \frac{2.6^\circ \cdot 823 + 2.1^\circ \cdot 446}{823 + 446} = 2.4^\circ.$$

23 November $\theta_5 = 3.4^\circ$ (Kazanskaya)
24 November $\theta_6 = 0.8^\circ$ (Serafimovich)
25 November $\theta_7 = -2.6^\circ$ (Serafimovich)

The average of these temperatures is 1.2°.

Let us determine the mean wind velocity along the water flow path during 19 to 25 November; it is found to be 5.9 m/sec.

The Don River, from Pavlovsk to Khovanskii, and the Khoper River are situated in region III (see Figure 1). The mean value of d for 19 to 25 November at the latitude 50°27′ (Pavlovsk) – 49°35′ (Khovanskii), under normal wind velocity is 13 cal/cm² day (cf. Table 1). The correction for the deviation of the wind velocity from the normal value is, according to Table 2, −3 cal/cm² day. Thus, we take the working value of d as 10 cal/cm² day.

For an air temperature of +1.2° and a wind velocity of 5.9 m/sec, we find for the heat-exchange coefficient k, from Table 3, the value 50 cal/cm² day degree.

The value of the heat-transfer coefficient α is determined from (25.1)

$$\alpha = (1745v + 106w)c\rho \text{ cal/cm}^2 \text{ day degree}$$

The mean flow velocity v is found by dividing the river stretch under consideration by the time of flow

$$v = \frac{358 \cdot 1000}{7.4 \cdot 86400} = 0.56 \text{ m/sec}.$$

$$\alpha = (1745 \cdot 0.56 + 106 \cdot 5.9) \cdot 1 = 977 + 625 = 1602 \text{ cal/cm}^2 \text{ day degree}$$

The specific river-channel heat inflow q is taken equal to 60 cal/cm² day.

For a mean flow velocity at Khovanskii of 0.24 m/sec, determined from the graph of $v = f(H)$, a wind velocity $w = 9.0$ m/sec, from observations in Khovanskii at 19 hours on 25 November, we obtain by (25.1) $\alpha_n = 1373$ cal/cm² day degree.

The value of B_n, corresponding to the following values observed at the Serafimovich meteorological station at 19 hours on 25 November: $\theta = -4.0^\circ$, $w = 9$ m/sec and $N_0 = 10$, is determined from Figures 4 and 5.

We obtain: $LE + P = -260$ cal/cm² day, $I_e = -44$ cal/cm² day

$B_n = LE + P + I_e = -304$ cal/cm² day.

Thus, we have the following data for calculating whether the appearance of floating ice on 25 November is probable: $\theta_0 = 0.5^\circ$, $\theta_1 = 0.3^\circ$, $\theta_2 = 2.5^\circ$, $\theta_3 = 1.7^\circ$, $\theta_4 = 2.4^\circ$, $\theta_5 = 3.4^\circ$, $\theta_6 = 0.8^\circ$, $\theta_7 = -2.6^\circ$, $\alpha = 1602$ cal/cm² day degree, $k = 50$ cal/cm² day degree, $h = 97$ cm, $d = 10$ cal/cm² day, $q = 60$ cal/cm² day, $B_n = -304$ cal/cm² day, $\alpha_n = 1373$ cal/cm² day degree, $n = 7$.

We find for

$$a_0 = \frac{\tau\alpha k}{(\alpha + k)hc\rho} = \frac{1 \cdot 1602 \cdot 50}{(1602 + 50) \cdot 97 \cdot 1} = 0.500.$$

From Appendix 1 we find the values of $e^{-a_0}, e^{-2a_0}, \ldots, e^{-na_0}$ and calculate their differences which appear in (11.8). The results of the calculations are given in Table 14.

TABLE 14

[illegible]	[illegible]	$e^{-(n-i)a_0}$	$e^{-(n-i+1)a_0}$	$e^{-(n-i)a_0} - e^{-(n-i+1)a_0}$	θ_i	$\theta_i\,(e^{-(n-i)a_0} - e^{-(n-i+1)a_0})$
1	19 XI	0.050	0.030	0.020	0.3	0.006
2	20 XI	0.082	0.050	0.032	2.5	0.080
3	21 XI	0.135	0.082	0.053	1.7	0.090
4	22 XI	0.223	0.135	0.088	2.4	0.211
5	23 XI	0.368	0.223	0.145	3.4	0.493
6	24 XI	0.606	0.368	0.238	0.8	0.190
7	25 XI	1.000	0.606	0.394	−2.6	−1.023
						$\sum_{i=1}^{7} = 0.047$

Substituting the numerical values in (11.1), we obtain on the left-hand side, the water temperature:

$$0.5 \cdot 0.030 + 0.047 + \left(\frac{10}{50} + \frac{(1602 + 50) \cdot 60}{1602 \cdot 50}\right)(1 - 0.030) =$$

$$= 0.015 + 0.047 + 1.40 = 1.46^\circ \approx 1.5^\circ,$$

on the right-hand side, the water temperature at which ice formation on the surface is probable

$$-\frac{-304}{1373} = 0.22^\circ \approx 0.2^\circ.$$

The left-hand side of the inequality is larger than the right-hand side. Consequently, ice formation cannot begin at 19 hours on 25 November.

Let us repeat the calculation for 26 November.

The water temperature in Pavlovsk at 20 hours on 19 November was 0.5°, the water discharge 97.8 m³/sec; the water temperature in Novokhopersk at 20 hours on 19 November was 0.8°, the water discharge 24.2 m³/sec.

$$\theta_0 = \frac{0.5^\circ \cdot 97.8 + 0.8^\circ \cdot 24.2}{97.8 + 24.2} = 0.56^\circ \approx 0.6^\circ.$$

The discharge in Khovanskii on 26 November was [illegible] m³/sec. The average depth on the stretch is

$$h=\frac{\frac{97.8+21.2+149}{2}\cdot 7.4\cdot 86\,400}{(67.7+2950)\cdot 10^4}=0.89 \text{ m}$$

Let us determine the weighted average water temperatures [illegible] 20 November (Pavlovsk and Novokhopersk meteorological stations):

$$\theta_1=\frac{2.7°\cdot 876+1.4°\cdot 500}{876+500}=2.2°,$$

21 November (Pavlovsk and Uryupinskaya)

$$\theta_2=\frac{1.8°\cdot 1060+1.4°\cdot 339}{1060+339}=1.7°,$$

22 November (Pavlovsk and Uryupinskaya)

$$\theta_3=\frac{2.7°\cdot 883+2.1°\cdot 370}{883+370}=2.5°,$$

23 November (Kazanskaya and Uryupinskaya)

$$\theta_4=\frac{3.4°\cdot 823+2.9°\cdot 446}{823+446}=3.2°,$$

24 November $\theta_5=-0.7°$ (Kazanskaya),
25 November $\theta_6=-2.6°$ (Serafimovich),
26 November $\theta_7=-8.4°$ (Serafimovich).

The average value of these temperatures is −0.3°. The average wind velocity is 5.3 m/sec.

Next, proceeding as in the previous calculation, we find from Tables 1 and 2 $d=10$ cal/cm² day and from Table 3 $k=49$ cal/cm² day degree. For $v=0.5$ m/sec and $w=5.3$ m/sec we obtain by (25.1) $\alpha=1592$ cal/cm² day degree.

The value of q is taken equal to 60 cal/cm² day.

For the mean flow velocity at Khovanskii on 26 November we find from the graph $v=f(H)$ the value 0.25 m/sec. The wind velocity at 19 hours on 26 November is taken, on the basis of observations at the Serafimovich meteorological station, as 0.5 m/sec. From (25.1) we obtain for the coefficient α_n 489 cal/cm² day degree.

From the data of the Serafimovich meteorological station we have for 19 hours on 26 November $\theta=-7.[illegible]$, $N_0=10$, $w=0$ (we take $w=0.5$ m/sec). From Figures 4 and 5 we obtain $LE+P=-85$ cal/cm² day, $I_r=-70$ cal/cm² day, and $B_n=LE+P+I_r=-85-70=-155$ cal/cm² day.

Thus, we obtained the following data for the calculation of the probability of the beginning of ice formation on the Don River at Khovanskii at 19 hours on 26 November: $\theta_0=0.6°$, $\theta_1=2.2°$, $\theta_2=1.7°$, $\theta_3=2.5°$, $\theta_4=3.2°$, $\theta_5=-0.7°$, $\theta_6=-2.6°$, $\theta_7=-8.4°$, $\alpha=1592$ cal/cm² day degree, $k=49$ cal/cm² day degree, $d=10$ cal/cm² day, $h=89$ cm, $q=60$ cal/cm² day, $B_n=-155$ cal/cm² day, $\alpha_n=489$ cal/cm² day degree.

For a_0 we find

$$a_0=\frac{\tau\alpha k}{(\alpha+k)hc\rho}=\frac{1\cdot 1592\cdot 49}{(1592+49)\cdot 89\cdot 1}=0.535.$$

Then we obtain the values of the exponential functions and their differences (Table 15).

TABLE 15

No. of day i	Date	$e^{-(n-i)a_0}$	$e^{-(n-i+1)a_0}$	$e^{-(n-i)a_0}-e^{-(n-i+1)a_0}$	θ_i	$\theta_i(e^{-(n-i)a_0}-e^{-(n-i+1)a_0})$
1	20/XI	0.040	0.024	0.016	2.2	0.035
2	21/XI	0.069	0.040	0.029	1.7	0.049
3	22/XI	0.118	0.069	0.049	2.5	0.122
4	23/XI	0.200	0.118	0.082	3.2	0.262
5	24/XI	0.343	0.200	0.143	−0.7	−0.100
6	25/XI	0.586	0.343	0.243	−2.6	−0.631
7	26/XI	1.000	0.586	0.414	−8.4	−3.470
						$\sum_{i=1}^{7}=-3.733$

Substituting the numerical values in (31.1), we obtain on the left-hand side

$$0.6\cdot 0.024-3.733+\left(\frac{10}{49}+\frac{(1592+49)\cdot 60}{1592\cdot 49}\right)(1-0.024)=$$

$$=0.014-3.733+1.43=-2.29°\approx -2.3°,$$

on the right-hand side

$$-\frac{-155}{489}=0.32°\approx 0.3°.$$

The right-hand side is [illegible] than the left-hand side of the [illegible] condition (31.1) is thus [illegible] on 26 November floating ice [illegible] appeared on the Don River at Khovanskii on 26 November [illegible].

As in the other examples, the minus sign of the left-hand side [illegible] the result shows that by the time for which the [illegible] amount of ice has already formed.

§ 4. Physico-statistical (empirical) relationships

By physico-statistical (or empirical) relationships [illegible] relationships between the total heat transfer [illegible] necessary for the appearance of floating ice, and the [illegible] obtained statistically on the basis of [illegible] data [illegible] point or river stretch, or to a series of river stretches. The sum $\Sigma\theta_-$ of the mean diurnal negative air temperatures [illegible] approximate characteristic of [illegible].

Water temperature and river depth [illegible] the value of $\Sigma\theta_-$ [illegible] in time and over territory [illegible].

In Figure 8 [illegible] the dependence of the sum of the negative air temperatures $\Sigma\theta_-$, necessary for the appearance of [illegible] initial water temperature θ_0 and on the average river depth h on the day the ice appears

$$\sum \theta_- = f(\theta_0, h). \quad (28\ I)$$

Here, as in the methods described below, the initial water temperature is understood to be the water temperature when the air temperature takes on negative values. The sum $\Sigma\theta_-$ is found from the mean-diurnal values, and for θ_0 the water temperature a day before the mean-diurnal air temperature takes on negative values is taken.

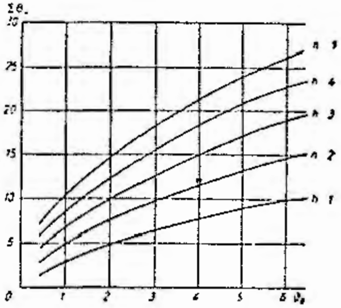

FIG. 8 I. Sum of the mean-diurnal negative air temperatures ($\Sigma\theta_-$), necessary for the appearance of floating ice, as a function of the initial water temperature θ_0 for various average river depths h, in m. (The graph was obtained on the basis of data for the Kama River before the creation of the storage reservoirs).

The graph is based on data referring to the Kama River at Bereznikov, Osa, and Okhansk (before the creation of the storage reservoirs).

If for a certain river stretch there is no physico-statistical (empirical) dependence for forecasting the appearance of ice, and it is impossible, for some reason, to calculate by the above-described methods, this graph is used. In this case, the initial conditions and the conditions of heat exchange and ice formation on the water flow path during the forewarning period of the forecast should not sharply differ from the respective conditions for the Kama River in its natural state. When using the graph, the following should be borne in mind: (1) the initial water temperature was taken for the point for which the calculation of the time of ice appearance is made, (2) the average depth was determined for a stretch 50 to 100 km long upstream from the point for which the calculation is made.

b) If the average depth of the river stretch (in the period of ice formation) varies relatively little, relationships of the following type are used:

$$\sum \theta_- = f(\theta_0). \quad (29\ I)$$

Mainly two types are used:

$$(\sum \theta_-)_{nec} = f(\theta_0), \quad (30\ I)$$

$$(\sum \theta_-)_{min} = f(\theta_0), \quad (31\ I)$$

where $(\Sigma\theta_-)_{nec}$ is the sum of the mean-diurnal negative air temperatures necessary for the appearance of floating ice for a given value of θ_0, $(\Sigma\theta_-)_{min}$ is the minimum $\Sigma\theta_-$ necessary for the appearance of floating ice for a given value of θ_0.

The relationship (30 I) can be obtained as follows.

From long-term observation data the annual data on the appearance of floating ice are chosen. Then from the mean-diurnal air temperatures at the nearest meteorological station for each case of ice appearance the date when the air temperature takes on negative values, directly preceding the appearance of floating ice, is determined. Next we calculate the values of $\Sigma\theta_-$ that include the air temperature on the day of ice appearance $\sum\limits_1^n \theta_-$ and the values of $\Sigma\theta_-$ that do not include the temperature of the day of ice appearance, $\sum\limits_1^{n-1} \theta_-$. From the observation data the values of θ_0 (the water temperature a day before the air temperature drops to below zero) are selected.

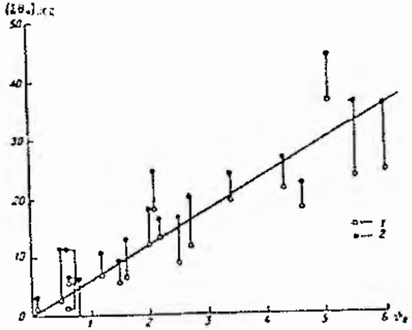

FIGURE 9 I. Sum $(\Sigma\theta_-)_{nec}$ of the mean-diurnal negative air temperatures, necessary for the appearance of floating ice, vs. the initial water temperature θ_0.

1 — $\Sigma\theta_-$ the temperature of the day of ice appearance is not included; 2 — $\Sigma\theta_-$ the temperature of the day of ice appearance is included.

With the values of θ_0 for the abscissa and of $\Sigma\theta_-$ for the ordinate we mark two points on the graph in Figure 9 I for each case of ice appearance, corresponding to the values of $\sum\limits_1^{n-1} \theta_-$ and $\sum\limits_1^{n} \theta_-$ for a given value of θ_0. The line showing the dependence of $(\Sigma\theta_-)_{avg}$ on θ_0 is drawn in such a way that below it lie the maximum number of points of $(\sum_{1}^{n-1}\theta_-, \theta_0)$ and above it the maximum number of points of $(\sum_{1}^{n}\theta_-, \theta_0)$.

Theoretical analysis shows that (30.I) should be expressed by a curve with its concave side to the θ_0-axis. In practice, however, it can be taken as a straight line.

The method of obtaining (31.I) differs from the above in that in this case only the points $(\sum_{1}^{n}\theta_-, \theta_0)$, i.e., the points corresponding to the sums of the negative air temperature which include the temperature of the day of appearance of floating ice, are plotted on the graph. Along the lower edge of the field of points (Figure 10) a straight line is drawn which gives $(\Sigma\theta_-)_{min}$, i.e., the minimum sum of negative mean-diurnal air temperatures necessary for the appearance of floating ice for a given value of θ_0.

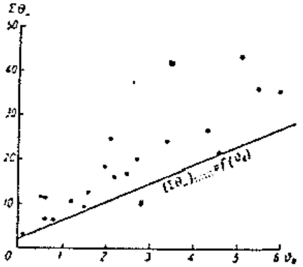

Figure 10. Minimum sum $(\Sigma\theta_-)_{min}$ of mean-diurnal negative air temperatures, necessary for the appearance of floating ice, vs. the initial water temperature θ_0

With regard to this relationship too, theoretically it should be expressed by a curve with its concave side away from the θ_0-axis, and the segment under consideration being, in practice, so close to a straight line that it may be taken as such.

The scatter of the points on the graph of relationship (31.I) is the result of mainly two reasons: (1) the excess air temperature on the day of the appearance of floating ice, amounting to a considerable part of $\Sigma\theta_-$ (actually, in many cases floating ice would appear on the same day at much higher air temperature than observed), and (2) the difference between the heat-exchange magnitudes corresponding to each degree of negative air temperature. It is thus obvious that the values of $(\Sigma\theta_-)_{min}$ determined from (31.I) correspond to the following two conditions:

1) the excess negative air temperature on the day of ice appearance has a minimum value;

2) the ratio of the heat transfer to the air temperature has maximum value.

From the relationship $(\Sigma\theta_-)_{min}=f(\theta_0)$, the value of $(\Sigma\theta_-)_{min}$ is determined for each case. From the air-temperature data, the date for the increment of this value is found. Then, for each case the number of days, a, is determined from the date of increment of $(\Sigma\theta_-)_{min}$ to the observed time of appearance of floating ice (in most cases a varies from zero to two days). The average of the number of days thus obtained, $\bar{a}$, is used in the calculation. When determining the date of appearance of floating ice from (31.I), the number $\bar{a}$, usually 1 day, is added to the date of increment of $(\Sigma\theta_-)_{min}$.

In deriving (31.I) it is recommended to mark, on the graph, the points of $(\sum_{1}^{n}\theta_-, \theta_0)$ also for those cases when, in periods with negative air temperature, floating ice did not appear. This makes it possible to refine the position of the relationship line.

Furthermore, in order to check the reliability of the obtained relationship for all the periods with negative air temperature in which floating ice did not appear, the calculation using the relationship must be checked to see if it really does not give the date of ice appearance. The same applies for (30.I).

Theoretically, $(\Sigma\theta_-)_{avg}$ and $(\Sigma\theta_-)_{min}$ should be equal to 0 for $\theta_0 = -\frac{B_n}{\alpha_n}$ (i.e., for θ_0 equal to the average water temperature over the cross section at the beginning of ice formation on the water surface, ref. Section 3). Since for rivers the value of $-\frac{B_n}{\alpha_n}$ amounts usually to only tenths or hundredths of a degree, the line of the relationship can be drawn from the origin of the coordinates.

Practically, however, the empirical relationships (30.I) and (31.I) give for $\theta_0=0$ some finite value of $\Sigma\theta_-$. This is so because 24 hours is taken as the unit time and, therefore, in calculating $\Sigma\theta_-$ it is actually assumed that, even when θ_0 exceeds only slightly the water temperature at which ice formation on its surface begins, not less than 24 hours is required for ice to appear.

The initial water temperature θ_0 should, in principle, be obtained by measurements in a cross section upstream from the point for which the forecast is being prepared, as is done in the calculation of ice appearance (see § 2). The distance from this point should in this case equal the length of the flow path during the period of calculation. The air temperature for the determination of $\Sigma\theta_-$ should, in principle, also be taken from different meteorological stations, the nearest to the flow path considered during each day of the calculation (forecast).

In practice, however, in most cases the value of θ_0 is measured at the point for which the forecast is being prepared. The values of $\Sigma\theta_-$ are usually determined from a single station, the nearest to the point for which the ice-appearance forecast is being prepared. For lowland rivers this is usually acceptable in the empirical relationships. This simplification is admissible because the variations in the differences between the actual values of $\Sigma\theta_-$, as well as of θ_0, determined by two methods for a time interval of several days, are usually not so large that a considerable decrease in the confidence limit of the permissible errors in the calculation [illegible] forecasting of the ice-appearance date would occur as a result of the [illegible] deviation.

If the water discharges (or depths) and the character of the variations [illegible] temperature do not differ considerably from the usual values for the given stretch in the period under consideration, the date of floating ice appearance is determined sufficiently accurately, by means of relationships of the type of (30 I) and (31 I). In such cases they can be used to prepare short-range forecasts. Of course, as is generally the case with empirical relationships, they can also be used if they are based on long-term observation data which reflect the regime on the given river stretch at the current time.

When using the relationships $\Sigma\theta_- = f(\theta_0, h)$ or $\Sigma\theta_- = f(\theta_0)$ it may be advisable in some cases, to introduce in the calculation the so-called critical air temperature for the beginning of ice formation. By this are understood the highest temperature at which ice formation can begin under given conditions (including the given water temperature). The introduction of the critical temperature into the calculation of a short-range forecast of ice appearance can increase the forecasting accuracy for rivers on which [illegible] starts at a relatively high water temperature and for which at the beginning of the ice formation only weak frosts are most frequently observed.

The critical air temperature for the beginning of ice formation on the water surface can be represented in the form

$$\theta_c = -\frac{\theta_w \alpha_w + LE' + I_e'}{k}, \qquad (32\ I)$$

where θ_w is the average cross-sectional water temperature at the beginning of ice formation, α_w is the coefficient of heat transfer from the water mass to the water-air interface for the same moment, LE' and I_e' are, respectively, the heat transfer by evaporation and the effective radiation at an air temperature equal to the water-surface temperature, k is the coefficient of heat exchange (see 5.2.6).

Equation (32 I) can be used to analyze the values of θ_c when a systematic [illegible] is made for a short-range forecast of ice appearance. Usually, [illegible] the value of θ_w precisely at the moment of ice appearance [illegible] observation data (it is known only at the standard observation hours). Therefore, along with the calculation of θ_c by equation (32 I), this value [illegible] determined empirically. It should be borne in mind that θ_c [illegible], as can be seen from (32 I).

[illegible] ice appearance we should use the values of θ_c taken from [illegible]. Direct determination of θ_c from (32 I) is [illegible] in this case. The difficulties are connected mainly with the fact that when preparing a forecast by means of empirical relationships the value of θ_w is unknown.

For forecasting the appearance of frazil ice on the Amu-Darya River the following equation is used

$$\sum_{n=2}^{n} \theta = -7.8^\circ - 0.0244x - c, \qquad (33\ I)$$

where $\sum_{n=2}^{n}\theta$ is the sum of the mean-diurnal air temperatures during three days before the appearance of frazil ice (during individual days of summation the air temperature may also be positive), x is the distance from the river mouth to the measuring point in km, c is a correction taken from Table 16, depending on the date.

TABLE 16. Values of c in formula (33 I)

Measuring point	[illegible]		[illegible]			[illegible]			[illegible]		
	2	3	1	2	3	1	2	3	1	2	3
[illegible]	2	2	1	0	−1	−2	−2	−2	−1	0	1
[illegible]	3	2	1	0	0	0	0	0	1	2	3

Equation (33 I) was obtained by generalizing the equations [illegible] individual points on the Amu-Darya River.

For example, for the measuring point at Chatly the equation has the form

$$\sum_{n=2}^{n} \theta = -13^\circ - c. \qquad (34\ I)$$

[illegible] The forewarning period of ice-appearance forecasts [illegible] air temperature forecast amounts to about 4–5 days [illegible]. This forewarning period is not always sufficient for [illegible]. However, [illegible] forecasts with a longer forewarning period, based [illegible] on the [illegible] forecast, may be unreliable.

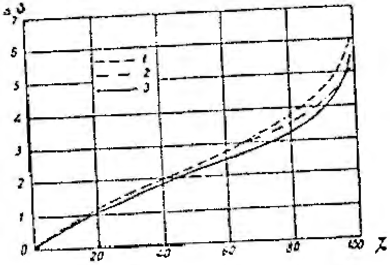

FIGURE 11. [illegible] Δθ

[illegible]

The forewarning period may be somewhat longer, approximately up to 10 days, in the case of forecasts in which not the expected [illegible]

[illegible] the phenomenon is given, but the date up to which the [illegible] phenomenon, in that case the appearance of floating [illegible] expected.

[illegible] it is possible to use the standard relationships $\Sigma\theta_- = f(\theta_0, h)$ or $\Sigma\theta_- = f(\theta_0)$. In this case, for a reliable forecast, we should [illegible] slightly lower expected air temperature.

[illegible] preparing such forecasts for large rivers it is possible to use [illegible] limit curves for the water-temperature drop during definite time intervals. Figure 11 gives confidence curves for the 10-day water temperature drop at several points on the Ob' and Irtysh rivers. By means of these curves it is possible to prepare forecasts of different degrees of confidence. The date up to which the appearance of floating ice is not expected is determined by

$$D = D_0 + \frac{10\theta_0}{\Delta\theta}, \qquad (35.1)$$

where D is the date up to which, with a given confidence limit, the appearance of [illegible] is not expected; D_0 is the date of preparation of the forecast; $\Delta\theta$ is the water temperature drop during a ten-day period with a [illegible]. With $\theta_0 < \Delta\theta$, it is not recommended to use (35.1).

[illegible] in order to dispense with the weather forecast, graphs [illegible] correlations are used to forecast the appearance of floating [illegible]

[illegible] date of [illegible] appearance and the date of the transition of the air [illegible] through 0°,

[illegible] the date of [illegible] appearance and the date of the water temperature [illegible] value,

[illegible] of the appearance, the date of transition of air temperature through 0°, and the date showing water temperature [illegible] day before.

[illegible] relationships do not guarantee sufficient reliability of [illegible]. This is due to the fact that they do not take into account [illegible] the temperature above and below 0° [illegible] to negative values, as well as the [illegible] temperature after the transition through 0°. Such relationships are [illegible] in regions or in periods with an irregular [illegible] temperature.

[illegible] the [illegible] and stoppage of [illegible]

[illegible] ice floats (floes) are formed and ice drifting [illegible] extent of ice cover on the given river, [illegible] three gradations: slight [illegible] floating ice covers [illegible] of the water surface of the river), medium ice drift (ice [illegible] 1/4 to 1/2 of the water surface) and almost complete ice drift ([illegible] than 1/2 of the water surface).

[illegible] drift [illegible] at a given gauging site depends on [illegible] the total heat [illegible] during the time from the appearance of floating ice until its [illegible] at the given gauging site; the [illegible] velocity of the river stream and its distribution over the corresponding river stretch; [illegible] velocity and river width between the ice edges on the stretch of the given gauging site.

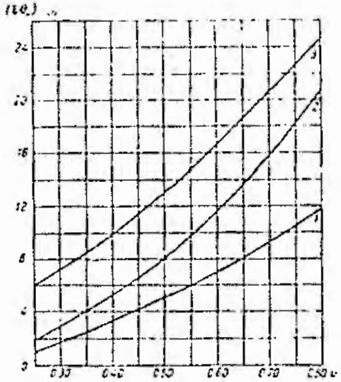

[illegible] $(\Sigma\theta_-)$ [illegible]

Figure 12 [illegible] $(\Sigma\theta_-)$ [illegible]

$(\Sigma\theta_-)$ [illegible]

[illegible]

The [illegible] $(\Sigma\theta_-)$ [illegible] $(\Sigma\theta_-) = f(\theta_0)$ [illegible]

Of the factors [illegible] given gauging site [illegible] transfer [illegible] total heat transfer [illegible] $(\Sigma\theta_-)$ [illegible] velocity [illegible] appearance. [illegible] the existence of [illegible] average [illegible] section of the gaging site and the flow velocities on the path of ice drift, (2) the fact that the graphs are based on observation data obtained at gaging sites of large lowland rivers for conditions, under which there exists a connection between the average current velocity and the river width (in particular, the river width between the shore ice).

From the graphs of Figure 12 it is possible to determine the time of the beginning of slight, medium or complete ice drift on deep reaches of lowland rivers which, by their morphological characteristics, correspond to the requirements imposed on the stretches of gaging sites.

When using these graphs to forecast the density of ice drift over a certain river stretch, including reaches of varying morphological characteristics (deep and shallow sections, bends, sections with branches, islands, etc.), we must allow for variation in the drifting capacity along the river and during the period of ice formation. It should also be borne in mind that of greatest practical interest as an obstacle to navigation is the highest density of ice drift at the given moment on parts of the given river stretch.

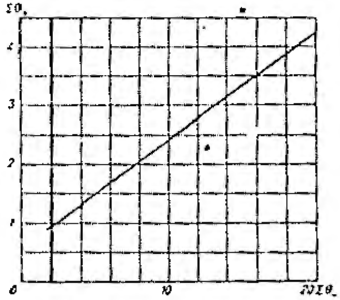

FIGURE 13. Variation in the sum ΣΘ+ of the mean diurnal air temperatures, necessary for the stoppage of a slight ice drift, with the sum ΣΘ− of the mean diurnal negative air temperatures from the day of floating-slush appearance.

The variation in the density of ice drift along the river, owing to the variation in the drifting capacity, is still not sufficiently studied.

Although gaging sites are usually provided on river stretches of large depth with relatively low current velocities (compared with the velocities on shallow sections), maximum density of ice drift within the given river stretch is not always observed on these sections. In a number of cases higher density of the ice drift is possible on individual sections of a stretch under consideration than on the given gaging site. This should be borne in mind when using graphs like those in Figure 12 in the preparation of a tentative forecast of the density of ice drift on some river stretch.

From the graph in Figure 13 it is possible to determine the possibility of the stoppage of a slight ice drift upon the onset of a melting period. In this case, the sum of the mean diurnal positive air temperatures, necessary to stop ice drift, is determined as a function of the sum of mean diurnal negative air temperatures, starting from the day of floating-slush appearance.

The graph is based on observation data for the Volga River measured on the stretch from the Rybinsk storage reservoir to the mouth of the Kama River. The graph can be used to forecast ice drift on medium and large rivers with similar heat exchange conditions.

C. FORECASTS WITH ALLOWANCE FOR THE CHARACTERISTICS OF ATMOSPHERIC PROCESSES (LONG-RANGE FORECASTS)

In order to work out methods for long-range forecasts of ice appearance, it is necessary to evaluate, with a long forewarning period, the date of autumn water cooling and its intensity. The course of water cooling depends, in the long run, on the development of atmospheric processes, on the frequency and intensity of the inrush of cold air or a cold wave. Forecasting of ice appearance would be most accurate if it were based on an early estimate of each cold wave. However, our present knowledge of the laws governing atmospheric processes only permits such estimates with a short forewarning period. It is possible to evaluate with a long forewarning period only the prevailing atmospheric processes and the mean averaged temperatures of the period in which the water cooling takes place and ice formation begins. These values determine in general the freezing time of rivers in each year. Thus, e.g., on the Severnaya Dvina, Kama rivers and on the rivers of West Siberia ice appears in the second half of October or in the first half of November. In the case of intensive cooling in October, the water cools down rapidly and usually ice begins to form already in this month. If the October coolings are of low intensity, ice formation is shifted to November, occurring at late dates. Thus, the time of ice appearance on these rivers is mainly determined by the character of the prevailing atmospheric processes and the resultant characteristic of air cooling in October connected with them.

Of course, the time of the arrival and the intensity of individual cold waves, particularly at the end of the period of water cooling, appreciably affect the dates of ice appearance.

It is clear from the above said that the working out of a method for long-range forecasting of ice formation should include:

a) an investigation of the peculiarities of the conditions of ice formation on the given body of water, clarification of the basic elements of the particular hydrological and meteorological regime, and of the possibility of allowing for the influence of hydrological factors in ice-range forecasting,

b) an analysis of the atmospheric processes that determine the inflow of cold air into the region of interest,

c) determination of the time dependence of atmospheric processes by means of which it is possible to evaluate the cooling intensity with a long forewarning period.

Long-range forecasting of ice phenomena takes into account the time dependence of atmospheric processes, as determined from investigations of the atmospheric circulation and from long-range weather forecasting.

In many cases of hydrological forecasts, satisfactory results are obtained by the use of even the most general regularities of this kind. For forecasting purposes it is possible to confine oneself to the use of [illegible] regularities of definite types of processes (in a definite time of the year) in a definite region, by using the integrated characteristics of the process [illegible].

The analysis of atmospheric processes and their development usually [illegible] qualitatively. However, for the method of hydrological forecasting [illegible] characterization is also necessary. A quantitative evaluation of the processes [illegible] introduces an element of subjectiveness into the [illegible] of the result expressed by a number (for example, the [illegible] days of processes of a definite type, etc.

[illegible] that in the practical application of forecasting [illegible] quantitative evaluation of atmospheric processes, the [illegible] of the forecasts is, as a rule, considerably lower than the [illegible] of the method calculated from the data of check forecasts [illegible].

[illegible] geographical regions the [illegible] are connected with [illegible] processes. The possibility of quantitative [illegible] evaluation of the development of these processes [illegible] long-range forecasting of ice appearance for the rivers [illegible] region [illegible] that the differences in the existing methods [illegible] of different fates, stem from the gradual expansion of [illegible] atmospheric processes, the [illegible] of the atmosphere, particularly its upper [illegible] of the corresponding observational data [illegible] for each stretch of the [illegible] long-range forecasting [illegible] according to [illegible] of the dates of the beginning of ice phenomena [illegible]

[illegible] the dates of the beginning of [illegible] development of atmospheric processes [illegible]. In fact, examining the map of the [illegible] of the dates of ice appearance (as well as [illegible] of the spring [illegible] of the same sign and even close [illegible] a large territory of a particular river basin. This [illegible] separate regions within each of which ice phenomena [illegible] dates which differ from the normal dates by the same [illegible].

[illegible] from the [illegible] is taken as a generalized [illegible] of the time of ice appearance (or of the [illegible] phenomena) on the rivers of a given region as a [illegible].

[illegible] of the dates of ice appearance on individual stretches of [illegible] characteristics depend on the size of the rivers [illegible], the development of [illegible] waves, as well as the annual deviations of the boundaries of the regions [illegible] atmospheric processes from the boundaries of the [illegible], for permanent recordings.

The accuracy of forecasts prepared [illegible] using forecasts of the generalized [illegible] method of background forecasting [illegible] expected accuracy. Therefore [illegible] are prepared by means of the method of [illegible] regional characteristic, check forecasts [illegible] the deviations from the [illegible] values resulting [illegible] are added (with respective sign) to the [illegible].

On the basis of check forecasts, the possibility [illegible] for a given river stretch by means of the method [illegible] determined, following the Official Rules of the Hydro[illegible] Service (Section 3, Part I).

It should be noted that the methods of [illegible] better results for [illegible] due to the fact that as a result of the [illegible] appearance of ice phenomena [illegible] cooling periods, which fact is not allowed for [illegible] forecasts.

[illegible] Method of forecasting ice appearance [illegible] the USSR using a qualitative evaluation of atmospheric circulation

Background forecasting of [illegible] G. R. Bregman and G. Ya. Vangengeim [illegible] presentation [illegible] classification proposed by Vangengeim [illegible] the initial state of [illegible].

Vangengeim [illegible] system (W), central [illegible]

Type W is characterized [illegible] and the southern regions of the USSR [illegible] Atlantic [illegible].

Type C [illegible] through North Scandinavia [illegible].

In type E there are [illegible] of the Siberian anticyclone [illegible] over the whole [illegible].

The type of [illegible] ranges.

For background forecasting [illegible] rivers the [illegible] type [illegible] derived for the summer-autumn and winter-spring periods from data on the prevailing types of circulation in each month. As the prevailing type of circulation in a given month it is agreed to consider that type whose frequency in the given month exceeds the mean long-term frequency for this month (the rated value). If two types have a positive deviation from the rated frequency value, there will be a combined (mixed) type of atmospheric circulation (for example W + C).

The appearance of ice on the rivers of the ETS depends on the relation between the intensity of heat transfer from the west (regions of the North Atlantic) and the inrush of cold air from the north and northeast (the Arctic Zone). The prevalence of any of these processes depends on the type of atmospheric circulation over the ETS. The state of the underlying surface of the region in which the air masses form and move is, in this connection, important.

The influence of the thermal state of the North Atlantic or of the Arctic Zone on the subsequent character of freezing (or ice break up) of rivers when western transport prevails is different than when the meridional or eastern circulation prevails.

The most intensive heat transfer from the Atlantic Ocean occurs in the northern part of the Gulf Stream. High water temperature in the northern part of the Gulf Stream in the summer-autumn months favors appearance of a stable positive air-temperature over these regions and a negative temperature over the ETS. Low water temperature in the northern part of the Gulf Stream gives rise to a reverse situation. In the summer-autumn period air masses passing over the North Atlantic are warmer or cooler than the underlying surface.

When forecasting ice appearance on rivers of the ETS, besides the atmospheric circulation, the heat exchange in the North Atlantic, expressed by the difference between the air and water temperatures during September, is also taken into account. In September a monsoon field which is characteristic of the cold time of the year sets in and the influence of the Atlantic on the weather of the ETS intensifies.

In order to characterize the thermal state of the Arctic Zone from where air masses surge into the ETS along normal and ultrapolar axes, data on the state of ice cover of the Barents Sea are used. The thermal state of this sea is very typical, in view of its geographical position, of the thermal state of all the seas of the western sector of the Arctic Zone and considerably affects (along with the influence of the Atlantic) the macrosynoptical processes over Europe and the air temperature over the ETS. However, the influence of the thermal state of the Barents Sea depends on the intensity of air mass transports from the Arctic Zone to the ETS, i. e., on the type of atmospheric circulation.

It is a fact that the air temperature over the ETS in the prewinter period is influenced by the heat accumulated during the summer in the surface water layer of the Barents Sea. An indirect characteristic of this heat accumulation is the variation in the extent of the ice cover over the sea during the April-September period. The ice cover of the Barents Sea is calculated from data on the position of the ice edge in the middle of April and September.

Details on the determination of the characteristics of the atmospheric circulation, as well as on the state of the surface of the Barents Sea and of the North Atlantic, are not given here.

Experience in the use of these forecasting methods over many years showed that although forecasts prepared by these methods were in general satisfactorily accurate, in a number of cases there were large errors, particularly for rivers of the south of the ETS. This is due mainly to the qualitative form of the evaluation of the atmospheric circulation. Such an evaluation is convenient and helpful in a number of cases for the analysis of the processes. However, its use in routine work often causes serious difficulties. In addition, the above characteristics of the atmospheric circulation do not always reflect the true development of the atmospheric processes. These shortcomings are of course characteristic also of other methods of visual evaluation of atmospheric processes, including the new standard schemes developed by Vangengeim (1952).

The observation data for the Atlantic and the Barents Sea are also not always sufficient to determine reliably the characteristics of the thermal state of the underlying surface.

For the forecasting of ice phenomena on the rivers of the Baltic Area and Byelorussia, methods were proposed using the new scheme of the atmopsheric processes developed by Vangengeim.

This scheme, used mainly for weather forecasting in the Arctic, differs from the former, briefly characterized above, mainly in the following. The same three circulation types are considered for the whole Northern Hemisphere by means of the H_{500} maps. The small amplitude and rapid displacement of high-altitude ridges and troughs is considered as the basic criterion of type W; in a number of cases this makes it impossible to relate some processes, which earlier were referred to the W type (for example, the Kara Sea and south Scandinavian surges), to type W. There are two versions of type E circulation. The first includes processes in which there are ultrapolar penetrations of anticyclones to the ETS or the branch (trail) of the Siberian anticyclone approaches. The second version is the existence of a high-altitude trough over the east Atlantic and a high-altitude ridge over the ETS. In this case heat is brought in to the ETS from the southwest, whereas cold surges are directed to West Siberia. These two opposing processes for the ETS are considered as variants of the same circulation type since they have some common features when considering the Northern Hemisphere as a whole, and in both cases there is a stable heat transfer to the western sector of the Arctic Zone. Incidentally, the former classification (of the forties) referred most of the second version of the type E to the type W.

In one of the forecasting methods proposed (for rivers of the Baltic areas the date of ice appearance is determined as a function of recurrence of the circulation type in September, as well as of the sign of the air temperature in September in the northeast Atlantic and in the western sector of the Arctic Zone.

In another method the dates of ice appearance are determined as a function of the sum of the air temperatures in September for three regions: the western sector of the Arctic Zone (the stations of Barentsburg, the Medvezhii isle, Tikhaya Bay, Cape Zhelaniya), the eastern Atlantic with the British Isles (the stations Westman, Lake Thorshavn (Torshavn), the town of Bergen, the town of Valencia), and the European continent (the stations Leningrad, Kiev, Warsaw, Stockholm). In cases of large sums of the air temperature in September, sharp variations in the atmospheric processes are observed in the following months. For these cases the sums of the temperature anomalies are multiplied by a coefficient less than unity (from 0.8 to 0.1). The values of the coefficient were obtained by trial and error from ten cases, depending on the frequency of type C circulation in September. The latter of course reduces the reliability of the forecasting method.

§ 2. Forecasting on the basis of the uniformity of the prevailing atmospheric processes of the synoptic season

The use of quantitative objective characteristics of atmospheric processes that cause the appearance of ice on rivers is extremely simple for long-range forecasts for rivers which freeze at the end of the synoptic season (autumn or prewinter period).

As is known, uniform atmospheric processes prevail throughout the synoptic season. This means that evaluating, for example, the direction of the leading current in the troposphere from maps of the beginning of the synoptic season, we may assume that this direction of current will also prevail during the whole season. The duration of the synoptic season varies usually from one and a half to two months and, therefore, by evaluating the "tendency of the season" from the processes at least of the first two natural synoptic periods of the season, it is possible to obtain an idea of the prevailing processes for one and one and a half months ahead.

The synoptic season of autumn begins on the average on 20 August and ends on 15 October, when it is replaced by the prewinter season which lasts on the average until 15 December. In individual years the beginning and end of the seasons deviate considerably from the mean dates.

For which rivers is it then possible to prepare freezing forecasts based on the uniformity of the processes of each of these seasons?

Firstly, for those rivers where early appearance of ice occurs already in the first half of October, i.e., at the end of the autumn season. There, if the atmospheric processes of the autumn cause intensive cooling, ice appears at earlier dates; if these processes cause the inflow of heat, the heat reserve of the rivers is not depleted; sometimes towards the end of autumn it even increases, and in the case of any further development of the processes ice may appear only later than at the mean dates. To these rivers belong those of the northern, and particularly northeastern, regions of the ETS, as well as most of the rivers of West Siberia.

Secondly, for rivers of the south of the ETS, where ice usually appears in the second half of November and in December, i.e., at the end of the prewinter season. In this case the freezing forecasts may be based on the characteristics of the atmospheric processes of the prewinter season. Let us consider some examples.

a) To forecast the freezing of rivers of the northern and particularly northeastern regions of the ETS, the direction of air-mass transport is taken as the principal characteristic of the atmospheric processes. During autumn, masses of cold Arctic air usually approach this region. The development of penetrations from the north and north-east therefore leads to intensive cooling and early freezing of rivers. When type C circulation is less pronounced and the leading current is directed from the northwest, air which has traversed a long path over the relatively warm waters of the North Atlantic arrives in this region. Therefore, cooling with this current direction prevailing (being normal for this time of the year), will be less intensive, and freezing will be close to the mean values. A stable western circulation and circulation from the south-west, give rise to a warm weather and late freezing of rivers.

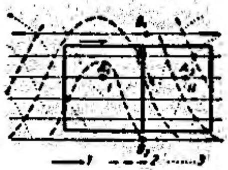

FIGURE 14. Scheme for the determination of the circulation indices

1—drawing of the isohypses on H_{500} maps in the case of a type W circulation; 2—drawing of the isohypses when the direction of the leading current to the rectangle II is from northwest; 3—drawing of the isohypses when the direction of the leading current to the rectangle II is from southwest

To evaluate the direction of the prevailing current, so-called index of meridionality is used. This is determined from H_{500} absolute isobaric surface contour maps. Two spherical rectangles, having a common side along the meridian (Figure 14), are marked out on the map. The first is situated to the west of the particular river basin, the second includes this basin. For each rectangle we calculate the average altitude of the 500 mb of the isobaric surface (average value of the geopotential) and substract the average altitude $\overline{H}_e$ for the eastern rectangle from the average altitude $\overline{H}_w$ for the western rectangle. This difference $I = \overline{H}_w - \overline{H}_e$ is taken as the index of meridionality. It can be seen from Figure 14 that if the prevailing current is directed from west to east, the value of I is close to zero. If it is directed from north or northwest, the index assumes positive values and if from south or from southwest negative values.

In particular, for a forecast of ice appearance on the rivers of the northeast of the ETS (Pechora, Mezen', Vychegda) the index is calculated from rectangles whose common side passes along 42° E. long., western boundary of the first rectangle along 36° W. long. and eastern boundary of the second rectangle along 105° E. long. The northern boundary of both rectangles passes along 78° N. lat., the southern boundary along 36° N. lat. On the whole, both rectangles cover the entire territory of the so-called natural European synoptical region. In the calculation we use data for the whole aerological reference network, plotted on maps of the Department of Long-Range Weather Forecasting of TsIP.*

The index is calculated for the time interval between the beginning of autumn synoptical season and 15 September. The latter date is chosen arbitrarily so as to ensure the necessary forewarning period of the forecast in cases of an early ice appearance (at the beginning of October); this forewarning range covers a period of 4 to 6 days (one natural synoptic period) so that it suffices even for the latest beginning of the autumn synoptical season (10 September).

The time of ice appearance on rivers is intimately connected with the values of the index I (Table 17). Figure 15 gives the graph of this

---

* When calculating the values of $\overline{H}_w$ and $\overline{H}_e$ and in general, the average values of the geopotential and atmospheric pressure for a given territory, it is better to determine these values from the isohypses (isobars) by measuring with a planimeter or by averaging the data over a grid of uniformly distributed points

[illegible] relationship [illegible] for all the [illegible] rivers [illegible] graph shows that despite this general relationship in some cases ice appearance markedly deviates from it. The reason for these deviations is the resulting direction

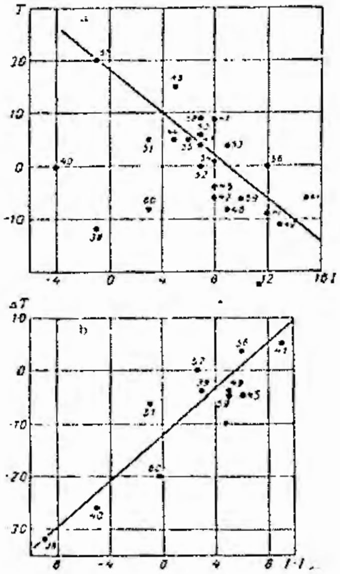

FIGURE [illegible]

[illegible] T [illegible] I [illegible] ΔT [illegible] the difference $I-I_{ct}$ [illegible] from H_{500} and H_{500}^{1000} maps.

[illegible] transport. High-altitude baric pressure formations (ridges and troughs) [illegible] determines the direction of the prevailing current, [illegible] their position corresponds to a definite [illegible] of the heat and [illegible]. When this correspondence is upset, the process is rearranged. The larger the noncorrespondence between the pressure and the temperature fields, the sharper is the rearrangement. For a

quantitative (indirect) evaluation of the point of the average air temperature in the troposphere we may use the H_{500}^{1000} relative isobaric surface-contour maps to calculate the index I_{ct} in the same sequence as the index I from the H_{500} maps. A comparison of these indices (Table 17) shows that in most cases a definite relationship is maintained between them. The deviations from this relation for values of I close to the average (I from +5 to +9 dkm) are small and do not significantly influence the subsequent development of the processes. With considerable anomalies of the air-transport direction (i.e., of the index I) this relationship between the indices becomes most important.

TABLE 17. Values of the meridionality [illegible]

Year	I	I_{ct}	Year	I	I_{ct}	Year	I	I_{ct}
1938	−1	8	1946	9	8	1954	8	3
1939	12	9	1947	8	3	1955	6	3
1940	−4	1	1948	5	−4	1956	12	6
1941	15	6	1949	13	8	1957	−1	−4
1942	8	2	1950	7	−5	1958	7	9
1943	7	3	1951	3	4	1959	10	4
1944	5	−4	1952	7	1	1960	3	4
1945	6	2	1953	9	5			

In order to take into account in the forecasting [illegible] for cases when the value of I was beyond the range of [illegible], the deviation of the actual ice-appearance dates from those determined from Figure 15a is related to the difference $I-I_{ct}$ (Figure 15b).

The forecast is prepared in the following sequence.

From the data of the H_{500} maps the value of the index I is calculated. If the value of I is within +5 and +9 dkm, the deviation T of the time of ice appearance on rivers from the rated value is determined from Figure 15a. If the value of I is beyond these limits, the value of I_{ct} is calculated from H_{500}^{1000} maps and the difference $I-I_{ct}$ is determined. From Figure 15a the value of T corresponding to the value of I is found, and from Figure 15b the correction ΔT corresponding to the difference $I-I_{ct}$ is determined. This correction should be added to the value T of the deviation from the rated value obtained from Figure 15a.

As an example, let us consider the preparation of forecasts for ice appearance in the years 1959 and 1960. The meridionality index I calculated from H_{500} maps for the period from 21 August to 15 September 1959 was 7 dkm, i.e., within the above-indicated limits (from +5 to +9 dkm). We therefore use in the forecast only the graph of Figure 15a. From it we obtain for $I = 7$ dkm a value of $T = +$[illegible] days for the deviation of the ice-appearance date from the rated value. Ice actually appeared on the rivers in this year [illegible] days later than expected.

In 1960 the synoptic [illegible] began on 31 August; the meridionality index according to H_{500} maps during the period from 31 August to 15 September was 3 dkm, i.e., considerably smaller than the mean value (it was beyond the limits of +5 to +9 dkm). It was, therefore, necessary [illegible] also the value of the index I_{ey} from H_{1000}^{500} relative isobaric surface-contour maps for the same period. This value was $I_{ey}=4$. The actual difference $I-I_{ey}$ was -1. From Figure 15a we find for $I=3$ [illegible] a deviation of +12 days of the ice-appearance dates from the rated value. From Figure 15b the correction to it for $I-I_{ey}=-1$ is −14 days, i.e., ice should appear 2 days earlier than expected. Ice actually appeared on the [illegible] in [illegible] 5 days earlier than the normal date.

The main shortcoming of this technique lies in the determination of the beginning of the autumn synoptical season, for which there are no sufficiently objective methods.

(b) A more objective and reliable evaluation of the atmospheric processes of the autumn synoptical season can be achieved by using the characteristics of the atmospheric processes for September, during which the processes of this season already prevail. It is obvious that the characteristics for September can be used for long-range forecasts of ice appearance on rivers, where ice appears not earlier than the mid-October. For these rivers, of course, the influence of the processes of the autumn season on freezing is smaller, particularly in cases of late ice appearance. Nevertheless, as shown in practice, it is sufficient in order to obtain a satisfactory forecast of ice appearance on the northern tributaries of the Upper Volga, on rivers of the northeastern regions of the ETS and on many rivers of West Siberia.

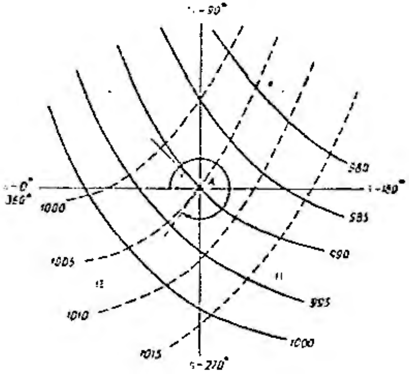

Fig. 16. Determination of the orientation angle of the isobars.

[illegible] first case; dashed lines — second case.

The forecasting techniques for each of these regions differ both in their details, due to the peculiarities of the physiographical conditions, and by the methods used for the quantitative characterization of the atmospheric processes. They are all based on the fact that the prevailing direction of [illegible] transport in September is allowed for.

To forecast ice appearance on the Sukhona River near the village of [illegible] Bor, for which the expected mean date of ice appearance is 4 November, the earliest date is 15 October and the latest date is 24 November, the direction of the air current is estimated by means of the mean monthly maps of the atmospheric pressure at sea level during September. The current direction on these maps approximately corresponds to the air transport direction in the troposphere in the same month. The direction of the current is estimated by the angle **α** between the isobars (along the current direction) and the parallel. The direction along the parallel from West to East is taken as zero direction. The direction of a current from the north has an angle **α** = 90°, a current from the south has an angle of 270°. Figure 16 shows examples of the determination of the prevailing air current direction.

First case. The low pressure is to the right of the reference point *A*, the high pressure to the left. To determine the orientation angle of the isobar, [illegible] the [illegible] of *A* [illegible] direction 90–270° is made to coincide with the longitude of the reference point. As we can see, the 590 mb isobar passes through *A*. [illegible] the angle between the horizontal axis and the [illegible]. The result is **α** = 45°.

Second case. The low pressure is to the left of the reference point [illegible], the high pressure to the right. In this case, the 1005 mb isobar passes through the point *A*. The angle **α** between the [illegible] and the horizontal axis is 310°.

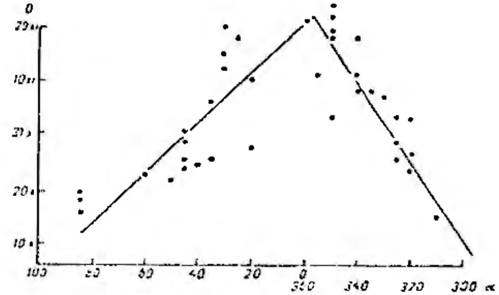

Fig. [illegible]. *D* [illegible] the angle **α** [illegible]

This method, of course, is not as objective as the calculation of the index *I*. [illegible] different persons determine the angle **α**. By the example given in Figure 17 a slight variation in the angle, for example, by 10°, gives a difference of 5–7 days in the ice appearance dates. [illegible] explained because it was then possible to [illegible] data of a long series of observations (maps of the mean pressure at sea level are available since 1891).

In the example given, a series of observations from 1921 is used, i.e., from the time of the opening of the Ivanov Bor gaging site. The values of the angle α, determined from the mean maps for September of these years, varied from 0 to 35° and from 310 to 360° (Table 18).

TABLE 18. Values of the inclination angle α of the isobars in September, used to forecast ice appearance on the Upper Volga catchment basin

Year	Angle α, degrees	Year	Angle α, degrees	Year	Angle α, degrees
1921	45	1937	350	1950	320
1922	35	1938	355	1951	45
1924	335	1939	50	1952	320
1925	325	1940	325	1953	45
1926	10	1941	85	1954	350
1927	320	1942	35	1955	325
1928	360	1943	330	1956	25
1929	350	1944	340	1957	340
1930	30	1945	85	1958	30
1931	30	1946	310	1959	5
1932	250	1947	20	1960	60
1935	350	1948	340		
1936	85	1949	20		

Figure 17 gives the relationship between the dates of ice appearance on the Sheksna River at Ivanov Bor and the value of the angle α during September. It can be seen, however, that in accordance with the abovesaid, for angles α close to 0° (western air current), i.e., in the presence of conditions for a late freezing of the rivers, the dependence is weaker. The mean square error for cases when the angle α varied from 0 to 30° and from 330 to 360° is 7.4 days, for all the remaining cases it is appreciably lower, equal to 5.1 days.

c) Another example of the use of the characteristic of the atmospheric processes prevailing in September as determined from data on the mean monthly atmospheric pressure is the method used in forecasting ice appearance on the rivers of the northwestern regions of the ETS.

The ice regime of the rivers of these regions is very complicated. Ice often appears several times on the rivers of the northwest of the ETS and there are even repeated periods of stable ice, the amplitude of the dates of ice appearance reaching there more than 60 days. However, in this case too it is possible to get an idea of the dates of ice appearance on the rivers from the processes developing in September.

The main characteristics, which determine the relation between the intensities of inflow of warm and cold air masses into a given region, are the prevailing direction of transport of air masses and the intensity of the western transport. They can be taken into account in two ways:

1. The degree of meridionality of the leading current is determined by means of H_{500} isobaric-surface contour maps on the basis of the same considerations as in the determination of the meridionality index (see subsection a); the estimate, however, is not made from the values of the geopotentials, averaged for a large territory, but from the difference in the geopotentials over two chosen characteristic stations (cf. Figure 14): A_1 – located to the west of the region under consideration (Klaipeda), A_2 – located slightly to the east of it (Vologda). The intensity of the western transport is estimated by the difference in the geopotentials along the meridian at two points: B_1 – to the south of the region under consideration (Warsaw), and B_2 – to the north of it (Murmansk). The sum of these two geopotential differences $C = (A_1 - A_2) + (B_1 - B_2)$ is taken as the general transport characteristic (Table 19). Large negative values correspond to a well-developed western transport, or to a western transport supplemented by transports from the southwest. The ice-appearance dates are determined as a function of C. Figure 18 gives an example of such a dependence for the Volkhov River catchment basin.

TABLE 19. [illegible]

Year	Pressure contrast in September K, mb	Year	Pressure contrast in September K, mb	Year	Pressure contrast in September K, mb	[illegible] C
1901	−8*	1920	−4*	1938	−10	−23
1902	+7	1921	6	1939	18	−10
1903	+3	1922	5	1940	−1*	−21
1904	−4*	1923	−8	1941	11	−16
1905	0*	1924	−11*	1942	−10*	−25
1906	6	1925	2*	1943	0	−21
1907	−3*	1926	−5*	1944	−12	−28
1908	−2*	1927	7	1945	11	−14
1909	3	1928	−4	1946	9	−14
1910	3	1929	−9	1947	−12*	−29
1911	−2*	1930	21	1948	−1	−23
1912	7	1931	4	1949	−4	−31
1913	0	1932	−4	1950	−6*	−20
1914	4	1933	−2	1951	0*	−22
1915	16	1934	−5*	1952	6	−21
1916	4	1935	7	1953	2*	−21
1917	−6*	1936	10	1954	−5*	−32
1918	1	1937	−10	1955	−15*	−21
1919	−11*			1956	4	−20
				1957	10	−15
				1958	11	−26
				1959	20	−6
				1960	1*	−13

[illegible] < [illegible] the North Atlantic.

2. In order to estimate the degree of meridionality from maps of the mean-monthly pressure at sea level the "contrast" (Table 19) is determined between the deviations Δp_E from the rated pressure above the center of the ETS (Kazan' meteorological station), and in the regions of coupled centers of atmospheric activity in the North Atlantic (Δp_A) (meteorological stations of Vik and Barentsburg) and in the zone of the Siberian anticyclone (Δp_C) (Peleduj meteorological station):

$$K = \Delta p_A - \Delta p_E - \Delta p_C.$$

A negative value of the contrast K shows the presence of an intensified heat transport from the southwest to the northwestern regions of the ETS in the case of delayed formation of the Siberian anticyclone whereas a positive contrast indicates a certain directionality of the air current from the northwest and a rapid formation of a cold center in Siberia. It should be noted that not only the conditions of the flow of warm or cold air directly to the basins under consideration during the autumn synoptic season are connected with the value of the contrast. A negative value is connected also with the prevalence in the Atlantic of winds contributing to the driving of warm water into the Norwegian and Barents seas, which increases the stability of the heat transport to the northwestern regions of the ETS not only during the autumn synoptic season, but also later. This factor therefore maintains its influence on the ice appearance, despite the fact that even the normal dates of this phenomenon, for example, on the Volkhov River and on the rivers of the Lake Il'men' basin fall in November and in late cases – in December.

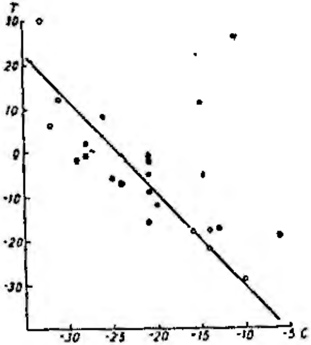

FIGURE 18. Deviations T of the time of ice appearance on the rivers of the Volkhov River catchment basin from the rated value as a function of the sum C of the latitudinal and longitudinal geopotential differences in September.

The influence of the intensity of the western transport is taken into account by singling out a number of cases when, for negative values of K, i.e., for a strong development of the Icelandian pressure minimum, the pressure in the region of the Azores is also below the rated value (or in the case of a very low pressure in the North Atlantic $\Delta p < -6$ mb, in the region of the Azores it was close to the rated value). In such a situation the western transport is weakened, a fact which brings about already in October a decrease in the negative contrast and, consequently, also an earlier ice appearance than in the case of the same value of K and a developed western transport.

As an example, we give in Figure 19a the dependence of the dates of ice appearance on the Volkhov River and on the rivers of the Lake Il'men' basin on the contrast of the mean pressure during September with allowance for the distribution of the pressure anomaly in the Atlantic. Figure 19b gives a similar dependence for the mean pressure contrast in October. It can be used to correct forecasts at the beginning of November.

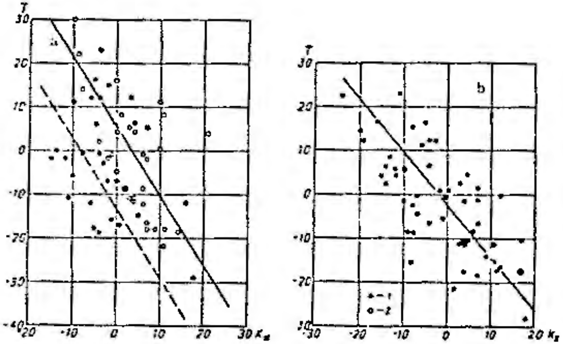

FIGURE 19. Deviations T of the time of ice appearance on the rivers of the Volkhov catchment basin from the rated value:

a – as a function of the contrast K_{SX} of the pressure anomaly in September, [illegible] reduced pressure in the region of the Azores [illegible] in September, [illegible]; b – as a function of the contrast K_X of the pressure anomaly in October.

d) As is shown in practice, and as follows from the essence of the technique, considerable errors arise in ice-appearance forecasts based on the use of the uniformity of the atmospheric processes prevailing during the autumnal synoptical season. This happens in cases when the pre-winter synoptical season following the autumn begins early and the character of the processes sharply differ from those of the autumn.

The uniformity of the atmospheric processes prevailing in the pre-winter synoptical season can be used to forecast ice appearance on the southern rivers of the ETS. On these rivers ice usually begins to form in the second half of November and only in rare early cases in the first ten-day period of November. The pre-winter synoptical season usually begins in the middle of October. Consequently, toward the end of October it is already possible to form an idea of the prevailing processes of the season and, accordingly, to forecast the freezing of the rivers with a sufficient forewarning period.

Considerable temperature drops, whose frequency and intensity determine the time of ice appearance on the rivers, are connected in the southern regions with the surges of anticyclones from the north, northwest or northeast. Any characterization of the development of these processes should take into account not only the direction of the surges, but also their intensity. Such a characterization can be obtained if the days on which the air temperature dropped and the pressure rose are found, and the values of the temperature drops during these dates are summed. The calculation and the use of this characteristic will be illustrated in the example of the method of forecasting ice appearance on the Lower Volga.*

For the main meteorological station of Saratov days are chosen when the mean-diurnal temperature was lower and the air pressure higher than the day before. For each of the days chosen the temperature drop below + 15° is determined, i.e., $\Delta\theta = 15° - \theta$, where $\Delta\theta$ is the temperature drop and θ is the mean-diurnal air temperature. This renders a unique characteristic of the magnitude of all the cooling periods, both those which led to the drop of the temperature below 0°, and those when it remained positive.

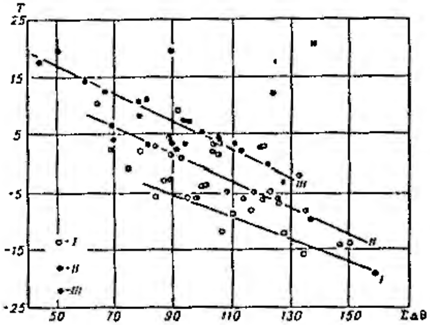

FIGURE 20. Deviations T of the time of ice appearance on the Lower Volga from the rated values as a function of the sum $\Sigma\Delta\theta$ of the temperature drops during October, taking into account the inversion of the sign of the pressure anomaly in Murmansk and Arkhangel'sk from September to October.

I—case of transition from a negative to a positive pressure anomaly at both points; III—case of transition from a positive to a negative pressure anomaly at both points or only in Arkhangel'sk; II—remaining cases.

Next, the sum $\Sigma\Delta\theta$ of the individual temperature drops during October is calculated. This quantity, called the sum of the temperature drops, is the characteristic of the degree of development of the processes under consideration. To make the calculation more objective, the sum of the temperature drops is calculated for the whole month of October, since the date of the beginning of the season, as was already mentioned, is determined from visual observations.

In October, along with new processes characteristic of the pre-winter period, those of the ending autumn season also have a certain influence. In forecasting it is therefore necessary to take into account the tendency and direction of the climatic transition from the autumn to the pre-winter period. Since for the appearance of ice on the southern rivers the development of surges of anticyclones in the northern regions of the ETS is of decisive importance, it is possible to form an idea of the processes from the variation in the pressure anomaly in these regions. If in September, the main month of autumn, the pressure anomaly in Murmansk and Arkhangel'sk is negative, and in October it is positive, the new season is characterized by an intensification of the northern surges. Consequently, an accelerated freezing of the rivers can be expected. An inverse order in the change of the pressure anomaly at both points, or even only in Arkhangel'sk with the sign of the anomaly maintained in Murmansk, points to an attenuation of the northern surges, which leads to delayed ice formation on the rivers.

Figure 20 shows the deviation of the time of ice appearance on the Lower Volga from the rated values as a function of the sum $\Sigma\Delta\theta$ of the temperature drops during October, taking into account the inversion of the sign of the pressure anomaly in the north of the ETS.

The total accuracy of forecasting with this dependence is characterized by the ratio $\frac{s}{\sigma} = 0,45$. It should be noted that forecasting is least accurate in cases of absence of a clearly-pronounced tendency of changes in the synoptical seasons (generalized in Figure 20 by the line II).

To increase the forewarning period of the forecast, it is possible to obtain a similar dependence when calculating $\Sigma\Delta\theta$ for the first 20 days of October. Its accuracy is, however, lower ($\frac{s}{\sigma} = 0,65$).

The most important forecasting errors in this case arise when, after a normal or warm pre-winter period, a warm winter begins at early dates. In such cases the appearance of ice may be delayed for a long period.

e) Methods, in which the mean air temperature during the autumnal synoptical season on days when centers of anticyclones pass over the territory of the given basin is used as the characteristic of the atmospheric processes, are similar to the methods described in this section. The reason for using this characteristic is that these anticyclones are formed in the same regions of the western sector of the Arctic and North Atlantic, from where subsequently also the air masses causing the freezing of rivers arrive. The air temperature during autumnal surges of anticyclones is therefore an index of the conditions of formation of such surges, and partially also of the conditions of their transformation on the path to the region under consideration.

This characteristic is determined as follows. For a given [river] basin a region for calculation is singled out which is somewhat larger than the area of the basin itself. For example, for rivers of the central ETS the calculation region includes the Volga and Ural basins. From composite-kinematic maps for the autumnal synoptic season days, when centers of anticyclones and pressure ridges were situated over the given region, are found. Then, the mean-diurnal air temperature for each of these dates is recorded from data of the main meteorological station. For rivers of the center, the Kazan' station is taken as a main (reference) station. Further, the air temperature is averaged over all the chosen days of passage of anticyclones (θ_a). The mean temperature during the days of passage of anticyclones can be determined for the whole autumnal synoptical season, or else the period of calculation can be limited to the day of issue of the forecast (for example, 1 or 10 October).

---

* The method, worked out for a generalized territorial characteristic of ice appearance on the Volga downstream from Kuibyshev before the creation of the Volga hydropower plants im. Lenin and im. XXII Congress of the Communist Party of the Soviet Union, is being used in recent years for stretches upstream and downstream of the Volgograd storage reservoir.

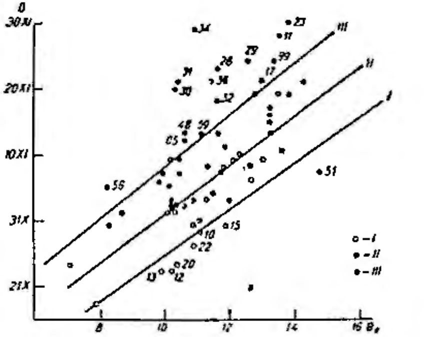

FIGURE 21. Date D of ice appearance on the Volga at the village of Prosek (Isada) as a function of the mean air temperature θ_a during days of passage of anticyclones, for various values of the coefficient k of the river storage (discharge) in September and of the water temperature ϑ at 1 October.

I—$k<0.8$, $\vartheta<4°$; II—$k<0.8$, $\vartheta>4°$, or $k\geq0.8$, $\vartheta<4°$; III—$k\geq0.8$, $\vartheta>4°$

The dependence of the dates of ice appearance on the value of θ_a is usually sufficiently accurate for the rivers of the northern half of the ETS, but not for other regions. In these calculations other variables are also taken into account. For example, to forecast ice appearance on the Volga downstream from the town of Gor'kii, the amount of water storage in the river and the water temperature are also taken into account. Figure 21 shows the dependence of the dates of ice appearance on the Volga at the village of Prosek (Isada) on the mean air temperature during the days of passage of anticyclones (θ_a). All the cases of ice appearance are classified into three groups according to the water storage of the river and the water temperature. The first group includes years when the coefficient k of the mean discharge of September was less than 0.8 and the water temperature toward 1 October was below 4°. In these cases ice appears relatively early. The third group includes cases of a large or medium water storage ($k\geqslant 0.8$) and late (after 1 October) transition of the water temperature through 4°. Under these conditions ice appearance is delayed. The second group includes all other cases.

The use of such dependences in routine practice gave positive results.

It should be noted that a shortcoming of this method of calculating the mean temperature during days of passage of anticyclones in the autumnal synoptical season is that the determination of the dates of the beginning and end of the season and of the positions of centers of anticyclones and ridges was not sufficiently accurate.

§ 3. Forecasting ice appearance with allowance for the conditions of the formation of the Siberian anticyclone

The beginning and development of autumnal atmospheric processes in Siberia and in the Far East and, consequently, also the beginning of ice formation on the rivers of this territory are mainly connected with the formation of the Siberian anticyclone and its principal ridges. The center of the Siberian anticyclone is usually situated in the region of Lake Baikal, its principal ridges are directed: one to the lower reaches of the Lena and Kolyma rivers, the second to the basin of the Amur River, the third to the lower reaches of the Ob' and Yenisei rivers. The Siberian anticyclone usually starts to form in August, in late cases – in September.

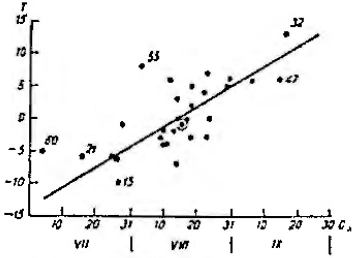

FIGURE 22. Deviation Γ of the time of ice appearance on the Upper Lena River from the rated value as a function of the date D_a of the appearance of stable anticyclonic formations in the region of Lake Baikal

Qualitative evaluation of the formation of the Siberian anticyclone has, for several years, successfully been used to forecast ice appearance on the rivers of the Amur basin. Since the dates of ice appearance on these rivers vary within narrow limits (20 to 25 days), it is sufficient for the forecasting to evaluate the general character of the (early or late) development of the Siberian anticyclone and its adjacent baric systems

Ice formation is early when the Siberian anticyclone begins to form as early as July; the cyclonic activity over Siberia weakens in the summer-autumn months, particularly over the northern regions and over northeastern China; the activity of the tropical maximums weakens and the surges of anticyclones from the north are intensified. An increased air pressure and a reduced air temperature over the north of Siberia are usually connected with these processes. Ice phenomena begin late if in July, August and the first half of September the Azores and Pacific Ocean maximums are situated mainly at a high altitude, and intensification of the anticyclonic activity over the Okhotsk, Japanese and Yellow seas is observed. In this case a low-pressure region is situated over Siberia, Mediterranean cyclones emerge on the north of West Siberia while cyclones pass through Central Asia to the Lena River. If in the summer-autumn months the features of one of these types of processes are not clearly pronounced, ice usually appears at dates close to the normal values. In routine practice for the preparation of a forecast, after determining the general river freezing characteristic, years are chosen when the development of atmospheric macroprocesses and the location of the main centers of the air pressure and temperature anomalies in July, August and September are closest to those observed in the current year. The expected dates of ice appearance on the rivers of the Amur basin in the current year are determined in accordance with how ice appeared on these rivers in reference (comparison) years.

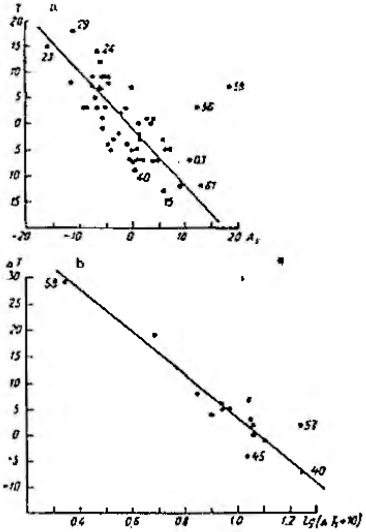

FIGURE 23. a–Deviation T of the time of ice appearance on the central Ob' from the rated value as a function of the variation A_1 in the total pressure anomaly in the West-Siberian ridge of the Siberian anticyclone from August to September; b–correction ΔT to the deviation of the time of ice appearance from the rated value, determined from the relationship between the value of a and the deviation ΔI_1 of the meridionality index from the rated value for cases when A_1 and ΔI_1 have opposite signs.

This forecasting method is of course imperfect, since it is based completely on a qualitative and therefore often subjective evaluation of the development of atmospheric processes.

Another method, closer to the quantitative methods, is used to forecast ice appearance on the Lena River.

If we take the appearance of stable anticyclonic formations in the region of Lake Baikal as a first indication of the beginning of the formation of the Siberian anticyclone, it is possible to trace a definite dependence of the dates of ice appearance on the Lena River on the dates when such baric formations appeared. An example of such a dependence is given in Figure 22. The use of this technique in practice is difficult due to the insufficient accuracy in the determination of the date of the beginning of the formation of the Siberian anticyclone. It is particularly difficult to determine this date in years when many alternations of cyclones and anticyclones occur in the Baikal region.

A more objective and discriminative evaluation of the formation of the Siberian anticyclone and its ridges can be obtained by using data on the variation of the pressure anomalies (deviations from the norm) and on the prevailing direction of the air-mass transport. In order to evaluate the formation of the ridges of the Siberian anticyclone, reference points were chosen in the direction of each of them: in the West Siberian ridge – Irkutsk, Yeniseisk and Surgut, in the Lena-Kolyma ridge – Irkutsk, Kirensk and Verkhoyansk, in the Far-Eastern ridge – Irkutsk, Chita and Khabarovsk. The sum $\Sigma\Delta p$ of the pressure anomalies for each group of points serves as the characteristic for the development of the respective ridge. A large positive pressure anomaly in August indicates an early beginning of the formation of the anticyclone. A considerable excess of the September over the August pressure anomaly characterizes a late formation of the anticyclone. Therefore, the variation $A = \Sigma\Delta p_{VIII} - \Sigma\Delta p_{IX}$ of the sum of the pressure anomalies from August to September for the above-indicated stations serves as the development characteristic of each ridge. The dependences of the dates of ice appearance in the central course of the Ob' River and in the upper course of the Lena River on the respective characteristics for the West Siberian A_1 and Lena-Kolyma A_2 ridges are given in Figures 23a and 24. These dependences are clearly defined, but in a number of cases there exist considerable deviations of the dates, obtained from the dependences, from the actual date. These deviations appear most sharply for the Ob' River. The reasons for this can be clarified by considering the direction of the air-mass transport.

The formation of the Siberian anticyclone and its ridges is connected with the advection of cold air, connected with meridional surges, from the north to the respective regions. The prevailing direction of air-mass transport, expressed by the meridionality index, is therefore an important factor, which should be taken into consideration when estimating the development of the East-Siberian maximum.

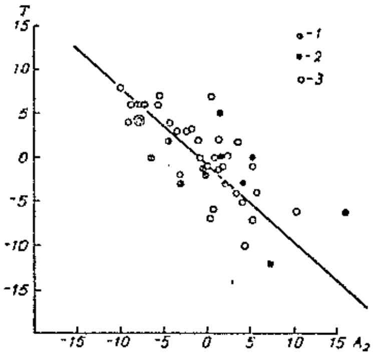

FIGURE 21. Deviation T of the time of ice appearance on the Upper Lena River from the rated value as a function of the variation A_2 of the total pressure anomaly in the Lena-Kolyma ridge of the Siberian anticyclone from August to September.

1 – $\Delta I_2 > 0$, $A_2 < 0$; 2 – $\Delta I_2 < 0$ with $A_2 > 0$; 3 – the signs of ΔI_2 and A_2 are the same.

The meridionality index I_1 for the region of the West-Siberian ridge is calculated as the difference between the average geopotentials of the 500 mb surface (H_{500}) over spherical rectangles within the following boundaries: (i) 105 and 60° E. long., 80 and 40° N. lat., (ii) 105 and 180° E. long., 80 and 40° N. lat.

For the region of the Lena-Kolyma ridge the index I_2 represents the difference between the average geopotentials over spherical rectangles within the following boundaries: (i) 90 and 120° E. long., 80 and 40° N. lat., (ii) 120 and 150° E. long., 80 and 40° N. lat. Considerable positive values of these indices in September represent the development of meridional surges from the north to the regions of the respective ridges; negative values of these indices show, on the contrary, the appearance of conditions for the transport of warm air masses from the southwest, causing a delay in the formation of these ridges (and, consequently, also a delay in the freezing of the rivers).

In a number of cases there exists a definite relationship between the values of the meridionality index I and the characteristics A of the air pressure variation (Table 20). With positive deviations ΔI of the value of I from the average (+2.3 dkm for the West-Siberian ridge and −1.0 dkm for the Lena-Kolyma ridge) we have positive values of A, and for negative deviations of the index I from the rated values the values of A are also negative. This relationship shows that the formation of the ridge of the Siberian anticyclone takes place during the given autumn season under more or less uniform conditions. If, for example, this process began early, thus pointing to a positive variation A of the pressure anomaly, then also in September favorable conditions are maintained for its further development, which is indicated by a positive deviation of the meridionality index I from its rated value.

TABLE 20. Starting data used in long-range forecasting of ice appearance on the Siberian rivers

Year	Variation of the pressure anomaly		Year	Variation of the pressure anomaly		Meridionality index in September	
	A_1	A_2		A_1	A_2	ΔI_1	ΔI_2
1901	5.0		1940	0.5	0.1	7.2	4.2
1902	6.5		1941	−5.6	−6.5	−0.1	0.8
1903	11.1		1942	−5.0	1.5	2.6	5.3
1904	−4.6		1943	0.4	−0.5	0.9	0.2
1905	−1.2		1944	−6.8	1.8	−0.4	−1.0
1906	−3.7		1945	−11.5	−7.4	1.1	2.5
1907	−3.9		1946	4.2	−8.2	3.8	1.5
1908	−0.6	1.5	1947	−0.2	—	−2.5	−4.8
1909	−0.4	5.4	1948	−1.3	−4.5	1.2	0.9
1910	1.2	1.3	1949	−7.1	−3.4	−6.5	−5.9
1911	−6.3	3.8	1950	−3.0	0.6	−1.4	1.7
1912	9.3	0.8	1951	−2.4	−9.2	1.5	2.9
1913	−9.4	0.0	1952	1.4	−3.1	3.5	2.4
1914	4.4	−2.0	1953	6.0	0.7	−0.6	2.5
1915	6.2	4.7	1954	−7.6	−9.8	1.6	−1.0
1916	−2.5	−7.9	1955	−5.5	−10.2	−0.3	−2.6
1917	1.4	−3.0	1956	12.6	4.4	−5.2	−4.6
1918	2.3	2.3	1957	−5.4	1.8	7.2	2.3
1919	−5.5	−0.9	1958	16.6	5.3	−7.8	−6.1
1920	1.5	−1.2	1959	3.6	1.7	−1.3	−1.0
1921	−4.7	10.7	1960	1.7	4.1	3.4	2.7
1922	−5.8	5.5	1961	13.2	15.8	−2.0	−2.8
1923	−16.1	6.3					
1924	−6.7	3.5					
1925	−6.1	−5.5					
1926	−7.6	−5.7					
1927	−8.6	2.5					
1928	7.2	−2.2					
1929	−11.4	−4.4					
1930	−4.6	−7.7					

However, such a uniformity is not always maintained. In a number of years (1956, 1958, 1959) with large positive values of A_1 and A_2 corresponding to an early beginning of the formation of both ridges, in September the conditions of their development were clearly unfavorable — the deviation of the indices I_1 and I_2 from the rated value in September was negative. This caused an interruption in the formation of the Siberian anticyclone and led to a delay in the appearance of ice on the rivers. The converse was also noted, for instance, in cases of a late or normal beginning of the formation of the ridges; favorable conditions for the development of this process existed in September, which led to an earlier ice appearance (1940, 1945 on the rivers of West Siberia and 1941, 1951, 1952 on the Lena River).

Therefore, in years when there are nonuniform conditions for the beginning and development of the ridges of the Siberian anticyclone, i.e., the signs of A and of ΔI (the deviation of the index I from the rated value are different*, it is necessary to take into account, along with the variation of the pressure, the meridionality index I. This is done by different methods, depending on the influence of the meridionality on the formation of the anticyclone and the appearance of ice. As was mentioned above, this influence is most important for the rivers of West Siberia. Therefore, we use an auxiliary relationship between the deviations, observed in these years, of the dates of ice appearance from the expected dates according to Figure 23a and the value of ΔI_1 which represents the deviations of the index I_1 from the rated value (Figure 23b). By means of this graph we determine the corrections to the dates of ice appearance expected according to the graph a and obtain the expected dates of ice appearance with allowance for both characteristics of the development of the atmospheric processes. Unfortunately, such corrections can be introduced in check forecasts only from data for the last 21 years for which there are aerological maps. It should, however, be emphasized that the most important deviations from the dependences $T = f(A)$ occurred in recent years.

The introduction of the corrections considerably increases the accuracy of the relationships for the last 22 years ($\frac{s}{\sigma}$ for the central Ob' River amounts to 0,53). To forecast ice appearance on the Lena River it is not necessary to derive auxiliary relationships, since the amplitude of the deviations of the actual dates from those determined from Figure 24 is relatively small. In this case it is possible to be confined to the selection and generalization of individual lines connecting groups of points which correspond to years when, for a negative value of A_z, the index I_2 had positive deviations from the rated values (1940, 1941, 1943, 1945, 1946, 1948, 1951, 1952), and to years when, for a positive value of A_z, the index I_2 had negative values (1944, 1956, 1958, 1959, 1961). The first group of points deviates from the central line toward early ice appearance, the second group toward late ice appearance. This corresponds to the above-considered physical meaning of the relation between the quantities A and I.

Allowing for both these characteristics of the atmospheric circulation the accuracy of the relationship may be increased. In the example given for the Upper Lena River $\frac{s}{\sigma}$ amounts to 0,66 for a r.m.s. error s less than three days.

Application of the described technique gives satisfactory results for rivers of the Ob' basin, for the central and, partially, for the lower course of the Yenisei River, and for the rivers of the Lena basin upstream from Yakutsk; somewhat less satisfactory results are obtained from the Amur and Irtysh river basins. In the Amur basin it is necessary to take into account the circulation conditions not only in the zone of the Siberian anticyclone, but also in adjacent regions of the Pacific Ocean. The freezing of rivers of the Irtysh basin is strongly affected by the atmospheric processes developing over the ETS and over Central Asia.

This technique is not perfect, even for such regions where good results are obtained. In particular, it does not take into account the influence of the intensity of the western air-mass transport which, in individual cases, causes an appreciable delay in the beginning of ice formation (for example, in 1953 on the Lena River).

---

* Or A close to 0 while ΔI has a large positive or negative value, as in the years 1940 and 1947.

Chapter II

FORECASTING THE BEGINNING OF A STABLE ICE COVER ON RIVERS

A. FORMATION OF AN ICE COVER. DECISIVE FACTORS

River freezing begins with the junction of individual bridges of floating ice in places favoring such phenomena, e.g., where the flow velocity decreases, where there are islands, where the river bed has bends, etc. The formation in such places of wide shore ice contributes to the formation of a continuous ice cover.

For the formation of a sufficiently wide ice shore and a sufficient amount of ice necessary for the appearance of ice cover in places of the river bed favorable for this, a definite amount of heat has to be transferred. This amount depends on the varying morphometric characteristics of the river bed and on the hydrological conditions on the given river stretch in the given period of ice formation.

Not always do stagnant ice blocks initiate the beginning of an ice bridge. In order for the ice blocks to freeze together and an ice bridge, indicating the formation of ice cover, to form, it is necessary that the ice blocks have sufficiently large dimensions and that the freezing together develops at the necessary rate. It is thus required that the air temperature in this period be sufficiently low (so that the heat transfer is sufficiently intensive).

The air temperature above which stable ice bridges do not form is called the critical temperature, θ_{cr}, which depends on the morphometric characteristics of the river bed and on the hydrological conditions at the time in the given river stretch.

Thus, for the beginning of a stable ice period on a river stretch, (i.e., for the formation of stable ice bridges) two conditions are necessary: (a) some heat transfer corresponding to the given conditions should occur, (b) the air temperature in the period when the first condition is fulfilled should not be higher than its critical value.

Ice blocks floating up to a formed bridge accumulate partially under the ice sheet and partially above the bridge, more or less rapidly freezing with it and with each other. Under the ice bridges and ice blocks frazil ice floating along the river accumulates.

Immediately after the formation of an ice bridge the upward advancement of the ice edge occurs mainly due to ice blocks situated on the section between neighboring ice bridges at the time of the formation of the lower one. The rate of propagation of the ice-cover edge obviously depends in this case on the density of the ice drift, the thickness of the ice blocks, the discharge of frazil ice and on the flow velocity. The total propagation of the ice-cover edge due to ice blocks existing on the section depends, in addition to the above, also on the length of the ice drift section at the time of the formation of the lower ice bridge.

Further propagation of the ice-cover edge is due to ice formation on the section between the ice bridges. The rate of propagation depends on the distance from the upper bridge, the rate of heat transfer and the flow velocity.

The upstream propagation of the ice-cover edge may extend over large areas in the upper stretches of rivers flowing from lakes, in river stretches downstream from hydroelectric stations and in cases of considerable water temperature gradients along the river, due to climatical conditions (for example, the Amu-Darya River), in the absence of an upper bridge.

In these cases the rate of upstream propagation depends on the following:

a) the distance from the lake or storage reservoir or from some constant cross section on the river,

b) the water temperature in the lake or storage reservoir or in some constant upstream cross section,

c) the rate of heat transfer,

d) the flow velocity.

A characteristic feature of ice cover formation on such stretches, as well as on stretches with high flow velocities, are ice shifts occurring during the formation of the ice cover when the air temperature or the flow velocity rise.

A stable ice period on a river stretch begins as the first stable ice bridges form. Knowing the time of formation of the first stable ice bridges is of practical importance, since from this time on a sharp change in the navigation conditions takes place. The technique of calculating and forecasting the beginning of stable ice period on a given river stretch is much more completely worked out at present than the technique of forecasting the formation of the ice cover at a specific point on the river.

B. ICE-COVER FORECASTING USING AIR TEMPERATURE FORECASTS

§ 1. Relationships for the calculation of the beginning of the stable ice period on a given river stretch

As indicated in the previous section, for the beginning of a stable ice period on a river stretch (for the formation of the first ice bridges) two conditions have to be fulfilled. First, there should be some heat transfer corresponding to the given conditions. Second, when the first condition is fulfilled, the air temperature should be not higher than the critical temperature θ_{cr}.

The sum of the mean-diurnal negative air temperatures from the day of the appearance of floating ice, $\Sigma\theta_-$, is usually taken as a relative characteristic of the heat transfer.

As mentioned previously, the necessary heat transfer, or the quantity $\Sigma\theta_-$, and the value θ_{cr} depend on the morphometric characteristics of the

river bed and on the hydrological conditions at the time in the given river stretch.

The morphometric and hydrological conditions are characterized by the water stage H at one of the gaging sites in the given stretch.

The time of the beginning of stable ice period on a river stretch is determined from long-time observation data for this stretch by the two relationships (using graphs):

$$(\Sigma\theta_-)_{cr} = f(H_{pr}) \qquad (1.II)$$

and

$$\theta_{cr} = f(H_{pr}), \qquad (2.II)$$

where H_{pr} is the water stage preceding the stable ice period; $(\Sigma\theta_-)_{cr}$ is the sum of the mean diurnal negative air temperatures necessary for (or rather approaching the necessary values) for ice cover formation (see subsection 5).

Below, a description is given of a technique for setting-up the working graphs and for calculating the beginning of the stable ice period.

a) Determination of the river-stretch boundaries. A river stretch should be more or less uniform. This means, firstly, that no large tributaries which might considerably increase the water discharge downstream from their inflow should exist on the stretch. Secondly, along the stretch the morphological and hydraulic characteristics of the river should be uniform.

The length of the river stretch should be such that its meteorological conditions can be approximately characterized by the data of a single meteorological station.

No less than two gaging sites (more are desirable) should be available on the stretch. In some cases, when it is known that the first ice bridges form every year directly downstream of a given site (or at its location), only one observation point is sufficient on the selected stretch.

b) Plotting the graph $(\Sigma\theta_-)_{cr} = f(H_{pr})$. For all cases of stable ice cover the dates of its beginning on the stretch are determined. For this date the earliest of all the dates of beginning of a stable ice period, as recorded on the stretch, is taken.

For each case, we determine the value of $\Sigma\theta_-$ from the day of the appearance of floating ice to the day of the beginning of the stable ice period, including the temperatures on the days of the beginning and end of this period (at the same meteorological station for all the cases).

For the water stage H_{pr} the minimum stage preceding stable ice period is taken. If a stage rise before the beginning of stable ice is caused by the travel of a flood along the river, the water stage on the day preceding the beginning of stable ice, or on the day preceding the increase in the rate of stage rise due to ice formation, is used for the calculation.

The value of H_{pr} is determined from one of the gaging sites of the river stretch.

The values of $\Sigma\theta_-$, increasing until the beginning of the junction of ice blocks, are unknown from observations. What are known are only the values of $\Sigma\theta_-$ accumulated toward the time when the stable ice period was recorded at a permanent observation point on the particular stretch. However, these values, in addition to those necessary for determining ice blocks junction, also contain a number of additional values of $\Sigma\theta_-$ (to $\Sigma\theta_-$

during the time from the beginning of ice junction to the moment when θ_{cr} was reached and the first stable ice bridges formed; (b) $\Sigma\theta_-$ during the time from the formation of the first stable ice bridges to the beginning of a stable ice period at least at one of the observation points; (c) the excess negative air temperature on the day of the beginning of the stable ice period.

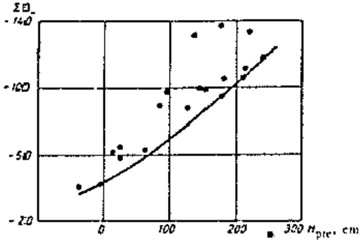

FIGURE 25. Sum of temperatures $(\Sigma\theta_-)_{min}$ necessary for the junction of ice blocks, as a function of the water stage H_{pre} preceding the stable ice period, using the magnitudes $(\Sigma\theta_-)$ for the period between beginning of freezing and onset of stable ice.

The graph in Figure 25 shows, in accordance with the values of H_{pre} (on the abscissa), the values of $\Sigma\theta_-$ from the day of ice appearance to the day of the beginning of a stable ice period. Since these values of $\Sigma\theta_-$ contain a number of the above-indicated additional parameters, the points $(\Sigma\theta_-, H_{pre})$ are scattered over a wide field.

In order to obtain from these data the sums of negative temperatures approaching those actually necessary for ice-block junction, the correlation line is drawn along the lower edge of the field of points, i.e., along the minimum values of $\Sigma\theta_-$, accumulated until the beginning of the stable ice period,

$$(\Sigma\theta_-)_{min} = f(H_{pre}).$$

c) Plotting the graph $\theta_{cr} = f(H_{pre})$. For each case of stable ice formation we determine from the graph $(\Sigma\theta_-)_{min} = f(H_{pre})$ the quantity $(\Sigma\theta_-)_{min}$. From the table of the mean-diurnal air temperatures the date of accumulation of $(\Sigma\theta_-)_{min}$ is found. Then, on a graph (Figure 26) with the water stage on the abscissa and the mean-diurnal air temperature θ_- on the ordinate, points corresponding to the water stage and to the values of θ_- of each day beginning from that at which $(\Sigma\theta_-)_{min}$ was reached are plotted. First we plot on the graph points for cases when $(\Sigma\theta_-)_{min}$ is reached on the day of the beginning of the stable ice period. Since the stable ice period begins in these cases on the day $(\Sigma\theta_-)_{min}$ is reached, it is clear that the air temperature of this day is equal to or lower than the critical value for the given conditions (for the given water level).

From these points we can obtain an approximate idea of the position of the correlation line $\theta_{cr} = f(H_{pre})$. Since these points correspond to air temperatures equal to or lower than the critical values, it is clear that the line of θ_{cr} cannot pass above the lower edge of the field of these points (the absolute values of the negative temperatures on the ordinate increase upwards from the origin of the coordinates).

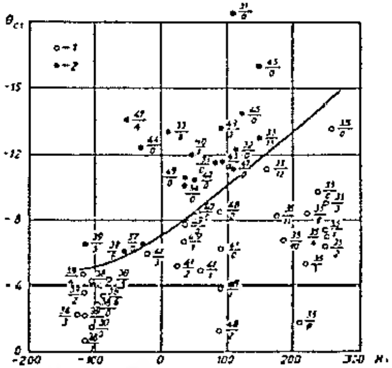

FIGURE 26. Relationship between the critical air temperature θ_{cr} and the water stage H on the day when this temperature has been [illegible] the stage preceding the stable ice period).

1—temperature is insufficient for the beginning of stable ice; [illegible] is sufficient for the beginning of stable ice. The [illegible] numerator—the year, in the denominator—the serial number [illegible] beginning from the day of accumulation [illegible] $(\Sigma\theta_-)_{min}$.

Next, for other cases of stable ice formation we plot on the graph the temperatures of each day in the period between the beginning of accumulation of $(\Sigma\theta_-)_{min}$ and the day whose temperature is equal to or lower than the critical value without passing, however, beyond the onset of stable ice period. There are instances when the day of the beginning of the stable ice period the temperature does not fall to the value given by the θ_{cr} line. This indicates that the first approximation line in this region is overrated and that the temperatures through which it has been drawn were lower than the critical values. In such cases the first approximation line is lowered so that the point corresponding to the day of the beginning of the stable ice period is situated on the line or above it. Completing the successive plotting on the graph of the points corresponding to the daily levels and temperatures during all the periods preceding the stable ice of all the cases analyzed, we correct the position of the correlation line in such a way that it passes in general at the same distance from the field points of temperatures that did not reach the critical values (below the line) or that exceeded the critical values (above the line).

§ 2 Calculation of the beginning of continuous ice cover from the relationships for a given river stretch

A short-range forecast of the beginning of continuous ice cover (stable ice period) on a river stretch from relationships for this stretch is prepared as follows.

1. The expected water stage for the date, for which the probability of ice blocking is calculated, is determined. This water stage is taken as H_{pre}. It is advisable to begin the calculation for a day when ice appearance is still improbable.

The forewarning period of the calculation, depending on the forewarning period of the air-temperature forecast used, is, as a rule, no longer than 5 to 6 days. Methods for forecasting water discharges and levels are described in "Rukovodstvo" (Manual), No. 1. A forecast of the water stages for the calculation of the beginning of stable ice with a forewarning period of about 5 days can usually be obtained by the simplest methods.

2. The quantity $(\Sigma\theta_-)_{min}$ is determined from the relationship $(\Sigma\theta_-)_{min} = f(H_{pre})$.

3. The value of $\Sigma\theta_-$, determined at the date for which the possibility of ice blocking is calculated, is determined from the data of the air temperature, during the period between the appearance of floating ice, and the day of preparation of the forecast of the beginning of stable ice and from the air temperature forecast for the next days.* The summation is carried out from the day of the appearance of floating ice, including this day. Since this calculation is made for an early date, the value of $\Sigma\theta_-$ is smaller than $(\Sigma\theta_-)_{min}$.

4. A similar calculation is made for the next day, and so on up to the day for which the value of $\Sigma\theta_-$ is found to be higher than (or equal to) the value of $(\Sigma\theta_-)_{min}$ determined from the water stage of this day. This is the day the value of $\Sigma\theta_-$ necessary for ice blocking is reached.

5. Beginning from the day $(\Sigma\theta_-)_{min}$ is reached, the temperature of each day is compared with the value of θ_{cr} corresponding to the level of the given day according to the function $\theta_{cr} = f(H_{pre})$. The first day whose temperature is equal to or lower than the respective θ_{cr} is taken as the day of onset of the critical air temperature.

6. The date of the onset of critical air temperature is taken as the date of the beginning of stable ice (formation of first stable ice bridges).

It should be borne in mind that, in accordance with the process of the ice-cover formation, the first stable ice bridges form earlier than the beginning of the stable ice period, determined from observations at gaging stations (see Section A).

7. If, in accordance with the assumed course of the air temperature, the critical temperature θ_{cr} occurs so much later than the accumulation of $(\Sigma\theta_-)_{min}$ that the forecasting of the beginning of stable ice, due to the limited forewarning period of the temperature forecast used, can be prepared only after the accumulation of $(\Sigma\theta_-)_{min}$, the date $(\Sigma\theta_-)_{min}$ reached is checked from actual data on the water stage and air temperature.

Check calculations (forecasts) differ from the above-described method only by the fact that all the values of the water stage and air temperature are taken from actual data.

Example of calculation of the beginning of stable ice (continuous ice cover). Let us calculate for a short-range forecast the date of the beginning of stable ice on a river stretch for which the working relationships are given in Figures 25 and 26.

Assume that floating ice appeared in this case on 19 November. The water stage on this date was 100 cm above the zero datum line at the gaging site used for plotting the stages in Figures 25 and 26.

Assume that water-stage and air-temperature forecasts for 5 days, from 20 to 24 November, are obtained (Table 21).

TABLE 21. Values of H, θ and $\Sigma\theta_-$ for the calculation of the beginning of stable ice by relationships ([illegible]) and ([illegible])

Date	19/XI	20/XI	21/XI	22/XI	23/XI	24/XI	25/XI	26/XI	27/XI	28/XI
Water stage, H	100	85	76	70	67	64	60	40	12	−9
Air temperature, θ	−12	−11	−6	−9	−6	−5	−3	−5	−3	−8
$\Sigma\theta_-$	−12	−23	−29	−38	−44	−49	−52	−57	—	—

From Figure 25 we find that for a stage of 100 cm (19 November) a value $(\Sigma\theta_-)_{min} = -70°$ is necessary for the beginning of stable ice, whereas on 19 November this temperature was only −12° (Table 21).

The water stage on 20 November was 85 cm. For this stage a value $(\Sigma\theta_-)_{min} = -65°$ is necessary for the beginning of stable ice, whereas on 20 November the actual temperature was only −23°.

A similar check is made for the next day up to 24 November. In these days, too, $\Sigma\theta_-$ is lower than $(\Sigma\theta_-)_{min}$ necessary for the beginning of stable ice for the water stages of the respective days.

On 20 November we obtain forecasts of the water stage and air temperatures for the period until 25 November inclusive (Table 21). (In this example we assume that the water-stage and air-temperature forecasts prepared on the previous days, are confirmed by the forecasts of the following days and that the forecasts of the water stage and air temperature are completely correct.)

For the beginning of a stable ice cover on 25 November with a water stage of 60 cm, a value $(\Sigma\theta_-)_{min} = -54°$ is required. However, on this day only −52° were recorded.

From the forecast for 22–26 November a lowering of the water stage on 26 November to 40 cm is expected. From Figure 25 we find that for this stage $(\Sigma\theta_-)_{min} = -53°$ is required. As follows from Table 21, this value is reached on 26 November.

Let us determine the date of the onset of the critical air temperature. From Figure 26 we find that for a stage of 40 cm a value $\theta_{cr} = -3°$ is necessary. But on 26 November (Table 21) a temperature of −5° is expected, i.e., higher than the critical value. For 27 November a level drop to 12 cm is expected, for which $\theta_{cr} = -$[illegible] But on 27 November only

−3° is expected. On 28 November a lowering of the water stage to −9 cm is expected. For this level $\theta_{cr} = -6°$. On 28 November −8°, i.e., a temperature lower than the critical, is expected.

Thus, we find that the beginning of a stable ice cover on the stretch (the formation of the first stable ice bridges) should be expected on 28 November

§ 3. Some variants of the relationships for the calculation of the beginning of stable ice cover on a given river stretch

a) For rivers with small variation in the water stage and, accordingly, a negligible variation in the mean flow velocity during the forewarning period of the forecast of the beginning of stable ice cover it is possible to use instead of the dependences of $(\Sigma\theta_-)_{min}$ and θ_{cr} on H_{pr} the relationships

$$(\Sigma\theta_-)_{min} = f(H_{fl}) \tag{3.II}$$

and

$$\theta_{cr} = f(H_{fl}), \tag{4.II}$$

where H_{fl} is the water stage on the day of the appearance of floating ice.

When preparing a forecast of the beginning of stable ice by means of these dependences, there is no need to obtain a forecast of the water stage.

The technique of plotting the graph of the dependence (3.II) in no way differs from the above-described technique of plotting the graph of the dependence (1.II). The difference consists only in that in the case considered here we take as the argument the water stage on the day of the appearance of floating ice, whereas when plotting the graph of the dependence (1.II) the water stage preceding stable ice is taken as the argument.

The technique of plotting the graph of the dependence (4.II) differs from the above-described for (2.II) only by the fact that the temperature of each day, beginning from the day at which $(\Sigma\theta_-)_{min}$ is reached, is not correlated here with the water stage of that day but with the stage on the day of the appearance of floating ice.

b) For small rivers it is expedient to take for the critical temperature not its mean diurnal values, but the diurnal minimums. Such a critical temperature is used, for example, to forecast the beginning of stable ice on the Seima and Oskola rivers.

c) For small rivers with a slow flow velocity, the value of $\Sigma\theta_-$ necessary for the beginning of stable ice, considered from the appearance of floating ice, is small. Therefore, if the forecast of the beginning of stable ice is prepared after the appearance of floating ice, its forewarning period may turn out to be too small. In order to increase the forewarning period for the forecast of the beginning of stable ice, up to a limit permissible by the forewarning period of a reliable air temperature forecast, it is possible to use the predicted date of ice appearance (see Chapter I).

If, in addition to these conditions, the long-term variations in the water stage during the ice formation period are small and the variations in the depths and mean flow velocities are negligible, it is possible not to introduce the water stage in the calculation and to determine the value of $(\Sigma\theta_-)_{min}$, necessary for the beginning of stable ice, as a function of the initial water temperature θ_0

$$(\Sigma\theta_-)_{min} = f(\theta_0), \tag{5.II}$$

bypassing the calculation of the date of ice appearance. In this case, as in the calculation of ice appearance, the water temperature on the eve of a day before the air temperature takes on negative values is taken as the initial water temperature.

The critical temperature θ_{cr} is assumed in such cases to be constant. The highest air temperature, at which the beginning of stable ice was observed on the given river stretch, is taken as θ_{cr}.

§ 4. Calculation of the beginning of stable ice cover on a river stretch from general relationships

In the absence of special relationships, obtained for a given river stretch from long-time observations on this stretch under conditions of the river regime existing at the present time, the beginning of stable ice on a stretch of a lowland river (the formation of the first stable ice bridges) can be calculated by means of the following formulas:

$$\Sigma\theta_- = -10.3v^{1.22}b^{0.33}, \tag{6.II}$$

$$\theta_{cr} = -0.65vb^{0.5}, \tag{7.II}$$

where $\Sigma\theta_-$ is the sum of the mean-diurnal negative air temperatures (beginning from the day of the appearance of floating ice) which is necessary for the beginning of stable ice (for the junction of ice blocks), θ_{cr} is the critical (mean-diurnal) air temperature necessary for the beginning of stable ice after the accumulation of $\Sigma\theta_-$ determined by (6.II); v is the mean flow velocity at the river cross section with the lowest flow velocity, in m/sec, b is the river width at this cross section, in m

If several gaging sites exist on the stretch, the value of v (as well as of b) can be determined at the gage with the lowest values of v. The determination is made from graphs of $v = f(H)$ and $b = f(H)$ for the ice-free period.

In the absence of the necessary gaging data, and also in cases when, from available topographic, morphometric or other data, it is obvious that in other cross sections on the stretch the flow velocities can be considerably lower than at the gaging sites, the values of v must be determined from the water discharge Q and the cross-section area F of the river at the place of lowest flow velocity

$$v = \frac{Q}{F}. \tag{8.II}$$

The time of the beginning of stable ice on a river calculated (forecast) by means of (6.II) and (7.II) is generally the same as the calculation from relationships for individual river stretches (§ 2).

To determine the values of $\Sigma\theta_-$ and θ_{cr} the nomographs (Figures 27 and 28), based on (6.II) and (7.II), can be used.

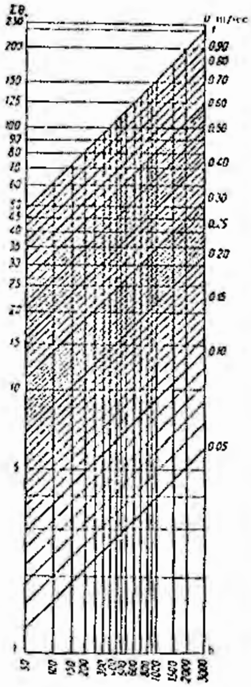

FIGURE 27. Nomograph for the determination of $\Sigma\Theta_-$, necessary for the beginning of a stable ice period (or the formation of the first stable ice bridges).

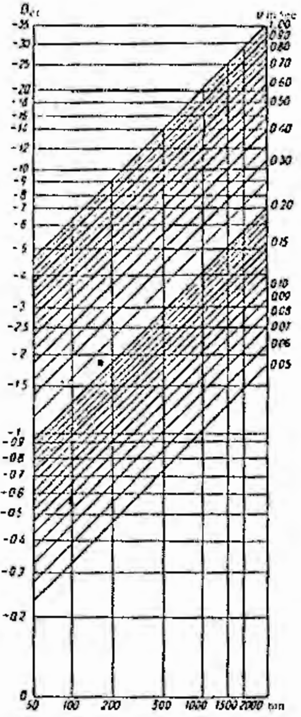

FIGURE 28. Nomograph for the determination of Θ_{cr}.

Calculation example. Let us calculate the beginning of the stable ice cover on the Kama River on the stretch between Bersut and Rybnaya Sloboda (from data for 1943) before the creation of the Kuibyshev storage reservoir.

From measurement data we find that of the gaging sites at which the water discharges were measured on this stretch the lowest flow velocities for the given water stages were recorded at the gage at the town of Chistopol'. The flow velocity and the river width will therefore be determined in the calculation from graphs of $v=f(H)$ and $b=f(H)$ based on measurement data for the town of Chistopol' (Figure 29).

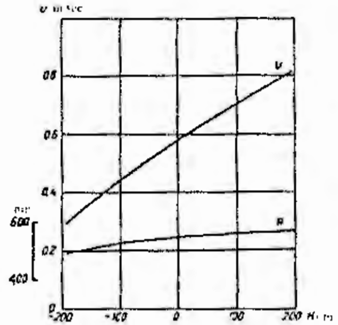

FIGURE 29. Graph of $v=f(H)$ and $b=f(H)$ according to measurement data from the Chistopol' station on the Kama River.

We establish that floating ice appeared on the stretch on 31 October.

In this example, considered here in order to clarify the calculation technique, we make use of actual data on the water stages and air temperature at the Chistopol' station (Table 22). In the case when use is made of

TABLE 22. Values of the water stage of the Kama River and mean diurnal air temperatures from data of the Chistopol' station for the period between ice appearance and the beginning of stable ice on the river stretch Bersut–Rybnaya Sloboda in 1943

Date	Water stage above the zero datum line, cm	Mean diurnal air temperature	$\Sigma\Theta_-$	Date	Water stage above the zero datum line, cm	Mean diurnal air temperature	$\Sigma\Theta_-$
October				8	45	−6.1	−35.9
29	166	−3.0	—	9	22	−9.5	−45.4
30	156	−8.4	—	10	−5	−4.2	−49.6
31	146	−6.7	−6.7	11	−54	−4.0	−53.6
November				12	−82	−4.4	−58.0
1	134	−7.2	−13.9	13	−108	−1.9	—
2	112	−3.8	−17.7	14	−125	−2.3	—
3	97	−0.8	−18.5	15	−122	−1.0	—
4	97	−3.2	−21.7	16	−109	−4.1	—
5	88	−3.7	−25.4	17	−95	−9.1	—
6	78	−0.8	−26.2	18	−54	−12.9	—
7	67	−3.6	−29.8	19	−60	−11.6	—

predicted water stages and air temperatures, the calculation technique remains the same.

The water stage on 31 October, on the day of the appearance of floating ice, was 146 cm (Table 22). From Figure 29 we obtain $v=0.76$ m/sec, $b=565$ m. From (6.II) or from the nomograph in Figure 27 we find that for these values of v and b a value $\Sigma\theta_-=-88°$ is necessary for the beginning of stable ice. But on 31 October, as followed from the data of Table 22, we have only −6.7°.

Since until 3 November there is no considerable lowering of the water stage, and on 3 November only −18.5° was recorded, the next calculation is made for 4 November.

On 4 November $H=97$ cm, $v=0.70$ m/sec, $b=560$ m. For the beginning of stable ice a value of $\Sigma\theta_-=-79°$ is necessary according to (6.II) or to Figure 27. But on 4 November (Table 22) only −22° was reached.

The next calculation is made for 9 November. $H=22$ cm, $v=0.61$ m/sec, $b=550$ m. A value of $\Sigma\theta_-=-65°$ is necessary. On 9 November, as follows from Table 22, only −45° is reached.

On 10 November a further drop of the water stage occurred. Let us repeat the calculation for this day. On 10 November $H=-5$ cm, $v=0.58$ m/sec, $b=550$ m. The necessary value of $\Sigma\theta_-$ is −62°, whereas the actual one is only −50°.

On 11 November $H=-54$ cm, $v=0.50$ m/sec, $b=540$ m. The necessary value is $\Sigma\theta_-=-52°$. As follows from Table 22, on this day $\Sigma\theta_-=-54°$.

Thus, the value of $\Sigma\theta_-$ necessary for the beginning of a stable ice period is reached on 11 November.

Let us determine the critical air temperature necessary for the beginning of a stable ice cover according to (7.II) or to Figure 28.

We begin the determination from 11 November — the day at which the necessary value $\Sigma\theta_-$ is reached for the beginning of stable ice.

On 11 November, $v=0.50$ m/sec, $b=540$ m. We find $\theta_{cr}=-7.6°$. But on 11 November the air temperature is equal to −4°. Consequently, stable ice cannot begin on 11 November.

On 12 November $H=-82$ cm, $v=0.46$ m/sec, $b=530$ m.

According to (7.II) or Figure 28, $\theta_{cr}=-6.8°$. The air temperature on 12 November is equal to −4°. Ice blocking could not occur.

Similar calculations are made for 13 and 14 November. The calculations show that the air temperatures on these days are higher than the values of θ_{cr} necessary for the beginning of stable ice, and therefore a stable ice cover could not start on these days.

From 15 November the water stage begins to rise. From observations at upstream gaging sites we find that the rise is not a result of a flood. We therefore make the calculation for the minimum water stage of −125 cm observed on 14 November. For this stage $v=0.40$ m/sec, $b=510$ m. We find $\theta_{cr}=-5.9°$. But on 15 November, $\theta=-1°$. Consequently, there should not be stable ice.

On 16 November the water stage continued to rise. Consequently, the necessary value of θ_{cr} remains equal to −5.9°. But the air temperature on 16 November is equal to only −4°, i.e., there should not be stable ice.

On 17 November, the rise of water stage continued. The necessary value of θ_{cr} remained equal to −5.9°. The air temperature on this day was equal to −9°, i.e., lower than the critical. We obtain the beginning of stable ice, i.e., the formation of the first stable ice bridges, on 17 November.

§ 5. Forecasting the beginning of a stable ice cover at a given point and the resulting rise of the water stage

Stable ice at any given gaging site begins owing to the upstream advance of the ice-cover edge. At some points a continuous ice cover begins as a result of the junction of ice bridges.

It is perfectly obvious that when the first stable ice bridge systematically forms at a given point, or directly below it, the beginning of stable ice at a given point can be calculated by the above described methods of calculation and forecasting of the beginning of stable ice cover on a river stretch.

After the formation of a stable ice bridge (cf. section A), the ice advances upstream mainly in the form of ice blocks existing by the time of formation of the bridge on the stretch between this bridge and the next upper one.

Further advance of the ice-cover edge is due to ice formation on the stretch between the bridges. The rate of advance is determined by the distance from the upper bridge, the intensity of heat transfer and the stream flow velocity. On the upper reaches of rivers issuing from lakes, on river stretches downstream from hydroelectric plants, and with considerable water-temperature gradients along the river, due to climatic conditions (for example, on the Amu-Darya River), the rate of advance of the ice edge depends on: (a) the distance from the lake or storage reservoir or from some constant cross section on the river; (b) the water temperature in the lake or storage reservoir, or in the indicated upper constant cross section; (c) the intensity of heat transfer; (d) the stream flow velocity.

In connection with investigations of ice-jam phenomena from data of observations on some rivers (Neva, Amu-Darya, and others) a technique for calculating and forecasting the movement of the ice-cover edge has been worked out, since these processes are closely interrelated.

In some investigations the rate of advance of the ice-cover edge on a given river stretch was related to the air temperature. Such investigations were carried out, in particular, for the Amu-Darya River.

In other cases, in particular, for the Neva River, observation data were used to investigate the influence of a large number of variables: air temperature and its fluctuations, flow velocity, inflow of ice from the lake.

However, empirical investigations have not reached the stage at which it is possible to recommend definite methods of setting-up relationships for forecasting the advance of the ice-cover edge and the formation of an ice cover at a given point.

For calculations of the upstream advance of the ice-cover edge the following formula has been proposed

$$l_{cd}=l_{in}+(l_{in}-l_0)\left(e^{\frac{(\theta_{cr}+c)\alpha}{L_{ic}\rho_i v h_c}}-1\right), \qquad (9.II)$$

where l_{cd} is the distance of the ice-cover edge from the initial river cross section (from a dam, an upper ice bridge or from some constant cross section on the river), at the given moment; l_{in} is the distance of the ice-cover edge from the initial cross section at some moment taken as the initial moment; l_0 is the distance from the initial cross section to the cross section at which ice formation begins; e is the base of the natural logarithm, B_{ic} is the resultant of the heat currents on the river surface when it is partially covered by ice; q is the specific channel heat inflow (see Part B, Chapter I, § 2); t is the unit time, n is the number of time units, L_{ic} is the ice-formation heat, ρ_{ic} is the ice density; h_{ic} is the thickness of the ice cover (together with slush ice), reduced to a density of 0.92, which is necessary for the upstream advance of the edge

It should be borne in mind that the edge advances when the sum $B_{ic}+q$ is negative. In this case the exponent in formula (9.II) is negative.

The value of l_e can be calculated from (12a.I) or (14a.I).

The value of h_{ic}, at which the edge advances, depends on the length of the ice-formation stretch, the flow velocity on this stretch and at the edge and on the heat-transfer intensity (i.e., on meteorological conditions). These variables also affect the amount of ice forming, the state of the ice formations (frazil ice, ice blocks, their dimensions) the strength of the ice blocks and the portion of ice drifting beneath the edge.

Thus, in order to calculate the advance of the edge by means of (9.II), it is necessary to know the dependence of h_{ic} on the above-indicated factors. This dependence, unfortunately, has not yet been investigated. Consequently, in design practice it is used to determine the value of h_{ic} as dependent on the flow velocity (in the absence of ice) by

$$h_{ic}=av, \tag{10.II}$$

where h_{ic} is given in m, and v in m/sec. On the strength of observation data for some rivers the coefficient a is taken in this case equal to 0.3–0.5

However, the determination of h_{ic} as dependent only on the flow velocity, in particular by (10.II), does not provide a calculation of the ice-edge advance with the accuracy necessary for the preparation of a forecast.

The rise of the water stage upon the beginning of a stable ice cover as a result of the advance of the ice-cover edge is mainly determined by the same factors as the rate of upward advance of the edge from an ice bridge. The water stage rises higher, the larger the amount of ice drifting below the edge when it advances a definite distance and the looser it piles up below the ice cover. The part of the ice going under the edge is larger, the smaller the dimensions of the submerged floating ice blocks, the larger the portion of frazil ice and the higher the flow velocity. The nature of the ice formations and the dimensions of the ice blocks depend on the heat transfer intensity, on the length of the ice-formation stretch and on the flow velocity

Thus, the height of the water-stage rise, with the onset of stable ice in a given place, generally depends on the intensity of heat transfer, the flow velocity and the length of the ice-formation stretch.

The height of the water-stage rise largely depends on the combination of the two characteristics the fluctuation in the flow velocity and in the heat-transfer intensity both along the river and with time. In addition to the fact that the amount of ice, drifting under the edge, and its structure largely depend on the combination of these characteristics, certain combinations of these characteristics may create conditions for the advance and retreat of the ice-cover edge During advances the amount of ice in the river bed considerably increases and accordingly the water stage additionally rises. In the tailwater of a hydroelectric plant the amount

of ice carried under the edge may be influenced by the variation in the water discharges incoming from the headwater section.

The rate of advance of the ice-cover edge and the height of the water stage rise on rivers issuing from lakes may be influenced by the inflow of ice from the lake, if floating ice on the lake at the river issue and the ice formation on the river are observed in periods corresponding to the time of river flow from the lake. In this case, the time of the formation of the ice cover in the lake region adjacent to the river outflow is important

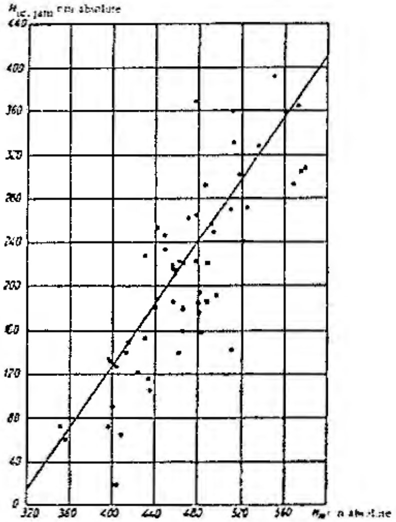

FIGURE 30. Variation of highest ice-jam water stages on the Neva River at the 5th hydroelectric station, $H_{ic.\,jam}$, with the mean levels of Lake Ladoga according to data from the Syas'skie Ryadki gaging site during November, H_{XI}

Large ice agglomerations, forming during the advance of the ice cover and causing sharp rises in the water stage, are called ice jams, sharp (high) rises — ice-jam rises, and the corresponding water stages — ice-jam stages.

The existing methods of forecasting the water-stage rise during the freezing of rivers (ice-jam rises or ice-jam stages) are based on setting up relationships between the water-stage rise or the height of the ice-jam stage and some of the indicated factors from data of long-time observations on the given river stretch. In this case, air temperature is usually introduced in the relationship instead of the heat transfer intensity, and the flow velocity is indirectly characterized by the water stage or discharge.

For rivers (or their upper stretches) whose runoff is regulated by large lakes it is possible to obtain satisfactory relationships between the maximum ice-jam water stage $H_{ic\ jam}$ and the mean water stage in the lake (or in the river at its outflow from the lake) in one of the preceding months (October, H_X, November, H_{XI}). Such relationships ensure a long forewarning period for long-range hydrological forecasts and accuracy required for long-range forecasts. The possibility of obtaining such relationships is based on the small rate of variation in the level of large lakes in the given period. Such relationships have been obtained for the Neva (Figure 30), as well as for the Angara rivers for the period preceding the construction of the hydroelectric plants on it.

For short-range forecasts which, in accordance with the shorter forewarning period, should be more accurate the dependence of the maximum ice-jam stage on the water stage or discharge alone does not give the necessary accuracy. Here, in addition to the water stage or discharge, the air temperature is introduced into the relationship. Figure 31 gives the dependence of the water-stage rise during the freezing of the Amu-Darya River at the Chatla gaging site, $H_{ic\ jam}$, on the mean air temperature in the freezing period θ_{fr}, and on the water discharge Q.

Similar dependences with the same or other characteristics of the air temperature of the freezing period have also been obtained for other rivers.

From observation data for the Angara River under natural conditions (before the construction of the hydroelectric plant) we also construct relationships between the water-stage rise during freezing and the air temperature amplitude during the period of frazil-ice movement, relationships of the water discharge with classification of all the cases into three groups according to the nature of the air-temperature fluctuations in the period of the frazil-ice movement and others.

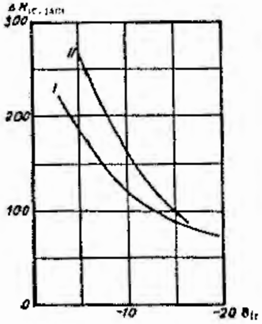

FIGURE 31. Ice-jam water-stage rise during the freezing of the Amu-Darya River, $\Delta H_{ic.\ jam}$, vs. the air temperature θ_{fr} for two values of the water discharge Q during the freezing period.

I – Q = 550 m³/sec; II – Q = 350 m³/sec.

It should be noted that the methods existing so far do not always yield relationships for short-range forecasting of the water-stage rise upon the advent of stable ice sufficiently accurate to comply with the requirements of the official Directions of the Service of Hydrological Forecasting. This is mainly due to the fact that in the existing technique the air temperature is taken into account only in an averaged or generalized form, and the flow velocity on the ice formation stretch only indirectly and in average values.

The way to improve the technique of short-range forecasting of ice-jam water-stage rises obviously consists in taking into account in detail all the dynamic and temperature conditions affecting ice formation and the ice-cover advance both in time and over the given river stretch.

The solution of the problem is, however, very difficult.

C. FORECASTING OF THE BEGINNING OF STABLE ICE COVER TAKING INTO ACCOUNT THE DEVELOPMENT OF ATMOSPHERIC PROCESSES (LONG-RANGE FORECASTING)

The time of the beginning of ice appearance and ice-cover formation can be determined for a long-range forecast as dependent on the character of the atmospheric processes to which this phenomenon is related.

If the duration of ice drift or its variation from year to year are small, the time of stable ice cover is determined by the same atmospheric processes as the time of ice appearance. If the duration of ice drift is long, other atmospheric processes (in particular the prevailing processes of the following synoptical season) begin to affect the dates of the beginning of stable ice cover.

The duration of ice drift depends on the ice-floating capacity of the river (in a given river stretch – on the amount of water in the given period in the given year) and on the cooling rate in the period of ice drift.

It is, therefore, expedient to begin to work out a technique of long-range forecasting of the beginning of stable ice cover by analyzing duration of and variation of ice drift. Useful in this connection is to consider the relationship between the dates of the beginning of stable ice cover and the dates of ice appearance.

Since, until recently, the dates on which navigation was stopped was determined from the date of ice appearance, and the number of river stretches where forecasts of the beginning of stable ice cover are necessary for planning works on the ice cover and on ice crossing is relatively small, the methods of long-range forecasting of the beginning of stable ice have not been developed much. This is partly due to the fact that when working out methods of forecasting the beginning of stable ice cover on rivers with a prolonged autumn ice drift, additional difficulties arise compared with the forecasting of ice appearance. The amplitude in the variation of the dates of stable ice is always considerably larger than that of the dates of ice appearance, and extremely early dates of these phenomena are usually close to each other. A forecast of the beginning of stable ice should, therefore, have on the average a longer forewarning period. In addition, the increase in the amplitude of the phenomenon complicates the use of such laws as the uniformity of the atmospheric processes prevailing during a synoptical season, since the probability increases for change of the season during the period from the issuing of the forecast and the occurrence of the phenomenon. In addition, the local features of each river stretch affect the time of the beginning of stable ice cover much more than the time of ice appearance.

Consequently, it is advisable to find out and evaluate relationships for the forecasting of the beginning of a stable ice cover on large and medium-size rivers for their individual stretches. To determine the boundaries of the stretches and the dates of the beginning of stable ice see Part B, § 1a.

For rivers with a short duration of ice drift, it is possible to obtain dependences of the dates of the beginning of stable ice on the same characteristics of the atmospheric processes which are used to forecast ice appearance. As an example we give the method of forecasting the beginning of stable ice on small rivers of the left-hand tributaries of the Upper Volga. The ice cover on these rivers forms, on the average, in the first half of November and sometimes, earlier — in the middle of October. Therefore, the time of the beginning of stable ice, as well as the time of ice appearance, can be determined in this case as dependent on the direction of the air current prevailing during the autumn season (see Chapter I, part C, § 2b).

For most large and medium-size rivers the dependences of the dates of the beginning of stable ice on the characteristics of the atmospheric processes which determine the dates of ice appearance can be used only to forecast the earliest date of the beginning of stable ice formation.

For some rivers there exist also special methods for the long-range forecasting of the beginning of stable ice. As an example we present the technique of forecasting the beginning of stable ice on the Lena River. An early beginning of stable ice on the Lena River is observed in the second half of October, a late beginning in the middle of November. First the lower reaches and the Markovo-Kiresnsk' stretch freeze, then the stable ice cover gradually extends over the whole river.

On the Lena River with its large flow velocity, a continuous ice cover can form only with a large amount of ice [bridges] and a low air temperature. The main condition for the freezing of the Lena is therefore the beginning of strong stable frosts. The latter is connected in these regions with the formation of the Lena-Kolymsk ridge of the Siberian anticyclone. It has been established that if in September a high-pressure region already forms in the northern regions of East Siberia and toward the end of the month an appreciable drop in the air temperature is observed in these regions, then an early onset of stable frosts and of a stable ice cover period can be expected.

Quantitatively the development of these processes is expressed by two indices. The first is determined from the mean H_{500} isobaric surface-contour maps for September. On these maps two (spherical) rectangles are prominent, of which the first (northern) is bounded by 60° and 160° E. long., 80° and 60° N. lat., and the second (southern) — by 80° and 150° E. long., 60° and 40° N. lat. In each of the rectangles the mean value of the geopotential is calculated (in the northern H_n, in the southern H_s), and then H_s is subtracted from H_n. The difference is designated by the index I_φ (always negative, Table 23). The value of I_φ is smaller, the earlier and more intensively the anticyclonic formations in the northern rectangle, causing stable coolings and early stable ice on the Lena River. Figure 32 shows the relationship between the dates of the beginning of stable ice on the Lena downstream from Kirenska up to Titim and the index I_φ. The dependence is fairly well pronounced. However, with the largest negative values of I_φ, observed in 1953 and 1959, stable ice began, instead of on the latest dates, even somewhat earlier than the mean date. This large deviation is a result of the fact that in September of these years a powerful anticyclone developed in the south of the region while the low pressure in the northern seas was due to a high-altitude cyclone. A stable inflow of heat

therefore did not occur and the further development of the anticyclone led to a comparatively early and strong cooling in October. It thus follows that the index I_φ is not a single-valued characteristic and, if it takes very large negative values, when preparing the forecast it is necessary to check whether a situation similar to that observed in September of 1953 and 1959 does not exist.

TABLE 23. The use of characteristics of the atmospheric circulation for long-range forecasting of the beginning of stable ice on the Lena River

Year	Circulation index I_φ	Temperature variation $\Delta\theta$	Year	Circulation index I_φ	Temperature variation $\Delta\theta$	Year	Circulation index I_φ	Temperature variation $\Delta\theta$
1901		−7.1	1930		−4.4	1949	−11	−3.3
1902		−6.5	1938	−9	—	1950	−8	−4.2
1903		−5.3	1939	−10	−4.4	1951	−11	−3.0
1916		−5.3	1940	−7	−4.4	1952	−7	−6.0
1918		−4.2	1941	−8	−1.9	1953	−21	−3.4
1920		−4.0	1942	−5	−3.8	1954	−10	−4.4
1921		−3.9	1943	−6	—	1955	−11	−2.5
1922		−6.5	1944	−7	−6.0	1956	−9	−4.0
1926		−4.3	1945	−14	−1.7	1957	−10	−2.0
1927		−2.2	1946	−10	−4.2	1958	−10	−2.0
1928		−5.2	1947	−12	−3.2	1959	−16	−4.8
1929		−5.0	1948	−10	−3.1	1960	−13	−3.4

Another, somewhat more reliable index of the beginning of the development of strong cooling periods in the Lena River basin is the air temperature drop in the northern regions toward the end of September.

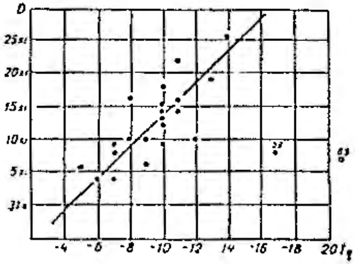

FIGURE 32. Dates D of the beginning of stable ice on the Lena stretch below the town Kirensk up to the mouth of the Vitim River as a function of the index I_φ of the atmospheric circulation.

The difference $\Delta\theta$ between the mean temperatures during the third ten-day period of September and during all this month, determined from observation data at two reference points, Verkhoyansk and Yakutsk, may serve as a characteristic of this temperature drop. The relationship between the dates of the beginning of stable ice on the same stretch of the Lena below Kirensk up to Vitim and the values of $\Delta\theta$ are given in Figure 33.

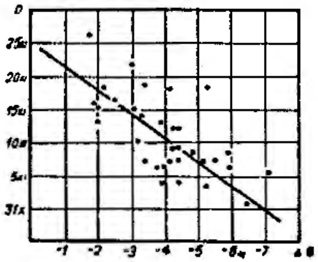

FIGURE 33. Dates D of the beginning of stable ice on the Lena River stretch downstream from the town of Kirensk up to the mouth of the Vitim River as a function of the difference $\Delta\theta$ between the mean temperatures at Verkhoyansk and Yakutsk during the third ten-day period of September and the whole month of September.

Such comparatively simple solutions to the problem of long-range forecasting of the beginning of stable-ice cover are possible for rivers of those regions in which interruptions and irregularities in the development of ice phenomena are rare.

The situation is far more complicated in regions characterized by a frequent alternation of heat and cold waves, which result in interruptions in the ice formation, repeated ice drifts and stable-ice periods. Such a development of ice formation is typical of the northwestern region of the USSR. However, large interruptions in the ice formation do not take place every year. Therefore, to forecast the beginning of stable-ice cover an early prediction of the following two elements becomes necessary: (1) the date of earliest appearance of ice cover on some rivers, or the date of its onset on most of the rivers of the region, and (2) its rate of advance, i.e., "rapidity." The rapidity of stable-ice advance is characterized by the number of days from the earliest to the latest beginning of its formation on one of the rivers of the region in the given year, i.e., the duration of the period during which stable ice spreads over all the rivers of the region. The mean duration of this period over 60 years of observations is 42 days, the least duration 7 days and the longest duration 106 days. In 30% of the cases a rapid spread (duration less than 20 days), and in 30% of the cases a slow spread (duration more than 50 days) of the stable ice was observed.

For an early prediction of the rapidity of river freezing in the northwest region based on the preceding atmospheric circulation, Vitel's' method is used. The amount of precipitation which fell in the basins of the Volkhov and Svir' rivers in September is used as an additional argument. The introduction of the precipitation indirectly takes into account the influence of the water storage of the given river on the formation of the ice cover.

The rapidity characteristics obtained from this dependence are used as one of the arguments in forecasting the beginning of stable ice.

The technique of forecasting the beginning of stable ice on rivers of the northwest is also based on the determination of the baric-circulational characteristics according to Vitel's' method. Such characteristics are determined for the prevailing deviations from the rated values on the rivers of the region.

It should be noted that the forecasting accuracy by this method in years with rapid river freezing is considerably higher than in years with slow freezing. For example, for the Msta River at the village of Devkino the ratio $\frac{s}{\sigma}$ for the whole series is 0,78, for cases of rapid freezing 0,67, and 0,90 for slow freezing. For the Pola River at the village of Kolesheva, $\frac{s}{\sigma}$ for the whole series is 0,77, for cases of rapid freezing 0,57, and 0,94 for slow freezing. The practical effectiveness of the forecasting for years with slow freezing is very low.

The above-described method has some shortcomings characteristic of all the forecasting methods based on Vitel's selection of baric-circulation characteristics. The principal drawback is the large number of forecasting indices, in the case of relatively short series, and unclear physical meaning of the relationship between the selected forecasting indices and the phenomenon under consideration.

Chapter III

FORECASTING THE CONDITIONS FOR THE APPEARANCE OF ICE AND THE FORMATION OF A STABLE ICE COVER ON LAKES AND STORAGE RESERVOIRS

A. CONDITIONS FOR THE BEGINNING OF ICE FORMATION AND ICE COVER ON LAKES AND STORAGE RESERVOIRS

The conditions for the beginning of ice formation on a water surface were considered in Chapter I, Part A. The condition for the beginning of ice formation can be represented by (5.1)

$$\alpha_n \vartheta_n \leqslant -B_n$$

or (6.1)

$$\vartheta_n \leqslant -\frac{B_n}{\alpha_n},$$

where ϑ_n, B_n and α_n are respectively the mean depth water temperature, the heat transfer of the water surface and the coefficient of heat transfer from the water depth to the water-air interface at the moment of the beginning of ice formation.

Inequality (5.1) implies that ice formation begins on the water surface when the surface temperature drops to the freezing temperature and the heat transfer of the water surface becomes larger than the heat inflow to it from the water depth.

Inequality (6.1) shows that ice formation on a water surface becomes possible when the cross-sectional or mean depth water temperature is lower than or equal to $\frac{B_n}{\alpha_n}$.

The condition for the beginning of ice formation on a water surface, represented by (5.1) or (6.1), is valid for lakes and storage reservoirs of any depth, if the water temperature ϑ_n is considered as the mean temperature in the mixing layer.

In the bank areas of natural water bodies the depths are usually smaller than in the main part of the water body. Although horizontal mixing of water masses takes place, ice formation in places of smaller depth, where the water cooling is faster, begins earlier.

If ice formation takes place in the presence of a weak wind, gradually, according to the general depth distribution, the water body, beginning from its banks (shores), is covered by an ice crust and a stable ice cover forms. It is obvious that in this case the beginning of ice formation on the main part of the water body also means the beginning of a stable ice period.

If ice formation in the shore zone (on shallow water) takes place in the presence of a sufficiently high wind velocity, floating ice forms there.

If an ice cover (shore ice) is formed in the shore zone before the wind is intensified, then on intensification of the wind it may be completely or partially destroyed. Floating ice, recorded at a gauging site, is usually the result of ice formation in a relatively shallow shore zone of the water body.

The role of this floating ice in the formation of stable ice depends on the direction and force of the wind in the subsequent period, the relationship between the water-body areas with different depths and, of course, on the subsequent intensity of heat transfer.

Floating ice forming at the shores may be transported by the wind to regions of the water body of larger depth, where ice formation at this time is still impossible. If the area of relatively large depth, to which ice is transported, is small compared with the area on which it is formed, then a stable ice period may begin due to the transported ice. This phenomenon usually occurs on storage reservoirs created in former river beds.

If, however, the area of relatively large depth, to which ice is transported, is large compared with the area on which it is formed, the ice transported usually does not produce stable ice. Stable ice appears there when ice formation on most parts of the given area becomes possible. Observation data show that stable ice begins usually on the same day when ice formation begins on most part of the water body, or of a fairly large part (zone) of it, of particular morphometric characteristics and uniform meteorological conditions. This is also confirmed by the results of numerous calculations.

Thus, both ice formation and stable ice may begin in different parts of a water body at different times. The variation in the flow velocities along the storage reservoir must be added to the general reasons for this fact (variations in depth and in meteorological conditions on storage reservoirs).

Conditions for the formation of an ice cover on storage reservoirs in the case when with the existing backwater a significant flow is maintained are somewhat different than in the absence of such a flow. The difference consists in that stream flow, as in rivers of natural conditions, hinders the formation of an ice cover. The beginning of ice formation in such cases does not imply, in practice, also the beginning of a stable ice cover as in the absence of considerable flow (in still water).

If, after the condition for the beginning of ice formation (6.1) is fulfilled, the heat inflow to the ice begins to exceed the heat transfer from the surface of the ice cover, the forming ice (ice cover) may thaw.

There are cases when a considerable intensification of the wind leads to breaking up of a thin ice cover already formed.

B. FORECASTING BASED ON CALCULATION (USING WEATHER FORECASTS)

§ 1. Calculation formulas

The time of the beginning of ice formation depends on the fulfillment of condition (6.1)

$$\vartheta_n \leqslant -\frac{B_n}{\alpha_n}$$

(see Part A of the present Chapter, as well as Chapter I, Part A).

In not too deep lakes and storage reservoirs a state close to homothermal is observed in the period preceding the beginning of ice formation. In this case the mean-depth water temperature (for the water body under consideration) is taken as ϑ_n.

Condition (6.I) is valid also for deep water bodies with temperature stratification. In this case, however, the temperature in the upper, mixing layer, should be taken as ϑ_n.

The mean water temperature ϑ_n for water bodies in which, in the period preceding the beginning of ice formation, a state close to homoisothermal is observed can be determined by the formula

$$\vartheta_n = \vartheta_0 e^{-n\alpha_0} + \left(\bar{\theta} + \frac{d}{k} + \frac{(\alpha + k)\,q}{\alpha k}\right)\left(1 - e^{-n\alpha_0}\right), \qquad (1.\mathrm{III})$$

where $\alpha_0 = \frac{t\alpha k}{(\alpha + k)\,hc\rho}$.

The time of the beginning of ice formation for these conditions can be determined by means of the inequality

$$\vartheta_0 e^{-n\alpha_0} + \left(\bar{\theta} + \frac{d}{k} + \frac{(\alpha + k)\,q}{\alpha k}\right)\left(1 - e^{-n\alpha_0}\right) \leqslant -\frac{B_n}{\alpha_n}, \qquad (2.\mathrm{III})$$

where ϑ_0 is the initial water temperature; e is the base of the natural logarithm; n is the number of time intervals (number of days) from the beginning of the calculation (from the time for which ϑ_0 is taken), t is the time unit (24 hours); α is the coefficient of heat transfer from the water mass to the water-air interface or in the opposite direction (the coefficient of heat transfer); k is the coefficient of heat exchange; h is the average depth; $c\rho$ is the specific heat per unit water volume; $\bar{\theta}$ is the mean air temperature during the period of calculation (during the time nt); d is the specific heat exchange at an air temperature equal to that of the water surface; q is the specific channel heat inflow.

In cases of sharp air-temperature fluctuations from the beginning to the end of the calculation period, the calculation by an inequality in which the air temperature is averaged not over the whole calculation period but over days, is more reliable

$$\vartheta_0 e^{-n\alpha_0} + \sum_{i=1}^{n} \left[\theta_i \left(e^{-(n-i)\alpha_0} - e^{-(n-i+1)\alpha_0}\right)\right] + \\ + \left(\frac{d}{k} + \frac{(\alpha + k)\,q}{\alpha k}\right)\left(1 - e^{-n\alpha_0}\right) \leqslant -\frac{B_n}{\alpha_n}, \qquad (3.\mathrm{III})$$

where i is the serial number of the day from the beginning of the calculation, θ_i is the mean air temperature during the i-th day.

If the mean flow velocity in the region of the given water body is less than 0.05 m/sec, the date of the beginning of ice formation, obtained by means of (2.III) or (3.III), is taken as the date of the beginning of stable ice cover.

If the mean flow velocity exceeds 0.05 m/sec, the date of the beginning of stable ice cover is determined by means of (6.II) and (7.II) (see Chapter II, Part B, § 4).

$$\sum \theta_- = -10.3 v^{1.22} b^{0.33},$$
$$\theta_{cr} = -0.65 v b^{0.5},$$

where $\Sigma\theta_-$ is the sum of the mean-diurnal negative air temperatures, counting from the date of the beginning of ice formation (including it) according to (2.III) or (3.III), θ_{cr} is the critical (mean-diurnal) air temperature necessary for the beginning of stable ice after the sum $\Sigma\theta_-$, is reached, using (6.II), v is the mean flow velocity in m/sec; b is the width of the water body in m.

It should be remembered that $\Sigma\theta_-$ is counted beginning from the calculated and not from the observed day of ice appearance. As indicated in Part A, the date of the appearance of floating ice, recorded at gaging sites, is usually the result of ice formation only in the shore zone of the water body

For rivers the time of the formation of the first stable ice bridges is calculated from (6.II) and (7.II). In this case, the lowest of the mean flow velocities for the given water stage on the given river stretch is taken as the calculation value of v; as the calculation value of b, the river width in the section with the lowest flow velocity is taken (Chapter II, § 5). Where obstructions create backwater, the variations in the depth and in the flow velocity along the stretch are smoothed out and the flow velocities and the time of advance of the ice cover from a bridge to a given place decreases. Therefore, in the case of a considerable backwater on the river area of storage reservoirs (forebay), it is possible by means of (6.II) and (7.II) to determine the date of the beginning of stable ice in any place, using the mean flow velocity in the cross section in this place. This, obviously, does not refer to stretches along which a considerable difference in the depths is maintained with the given flow velocities in places of comparatively small depth Such conditions may exist, in particular, in the headwater region of storage reservoirs closest to the zone of the upstream limit of the backwater level or, for example, when the backwater level covers a stretch full of rapids. In these cases the beginning of stable ice is calculated in the same way as for rivers in natural conditions (Chapter II, Part B, § 4).

§ 2. Determination of the quantities necessary for calculating the beginning of ice formation

a) Calculation water area. With considerable stream flows the length of the predicted stretch is determined from the forewarning period of the calculation or of the forecast and from the flow velocity

It should be borne in mind that when determining the flow velocity and the mean depth it is not necessary to use in the calculation the whole water area on this stretch. It is recommended to exclude the areas of shallow waters which are separated from the central part of the given river area of the storage reservoir by emerging, or even only by submerged bottom ridges.

If there is no considerable stream flow, when determining the boundaries of the water area necessary for the calculation we should use the fact that in different parts of large water bodies an ice cover may form at different times - in accordance with their different morphometric characteristics and meteorological conditions.

For the beginning of ice cover formation in each considered region of a lake or storage reservoir, and if observations are conducted from the shore, it is usual to consider the covering of the water area by an ice sheet (continuous or with polyniyas) within the visibility range from the observation point. The distance *s* from which the state of a lake (or storage reservoir) surface is observed under normal visibility varies approximately from 4 to 27 km for a height of the observation point from 1 to 50 m above the water-surface level.

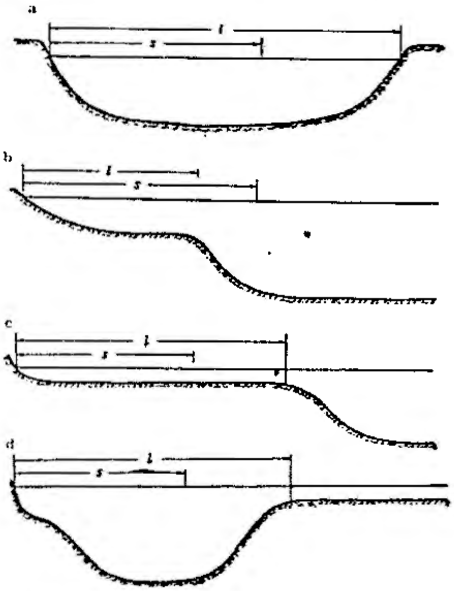

FIGURE 34. Diagram for determining the width *l* of the water area used in the calculation.

The width *l* of the water area used in the calculation can, however, be either larger or smaller than the distance *s*. The depth distribution over the water area should be taken into account (Figure 34).

If the depth of the water body varies as schematically shown in Figure 34a, the dimensions of the water area used in the calculation are limited only by the extent to which the meteorological conditions can be regarded as uniform over the area and along the dimensions of the water body (the width of the storage reservoir).

If the meteorological conditions can be regarded uniform over the whole width of the basin, then the whole water area (or the whole width of the water body can be used in the calculation.

If the depth varies, for example, as is shown in Figure 34b, c, d, the dimensions of the water area are determined by the nature of the depth variation over the area and, of course, by the extent to which the meteorological conditions can be considered uniform. In this case, variations in depth from the average value on the given water area, even if important but occurring on comparatively small stretches, do not have to be taken into account when determining the boundaries of the water area.

It should be borne in mind that in all cases sections which are separated from the main, decisive section of the water area under consideration by emerging or even only submerged ridges, should not be included in the water area used in the calculation if the depth sharply decreases over them.

b) Initial water temperature. Duration of the calculation period and forewarning period. The initial water temperature θ_0 is determined for a date that provides a sufficiently long forewarning period for the forecast of the beginning of ice formation or of the beginning of stable ice cover. The forewarning period of the beginning of ice formation and of the beginning of stable ice is determined by the forewarning period of the weather forecast used in the calculation, and does not exceed it. If in the period preceding the beginning of ice formation and the beginning of stable ice cover there occur considerable variations in the water inflow into the storage reservoir and in the discharge into the tailwater area, variations that have a considerable effect on the flow velocity in the reservoir, the forewarning period of the forecast cannot be larger than the period for which there is a forecast or where both inflow and discharge are controlled by man.

If the river flow velocity on the given reservoir stretch is lower than ~ 0.05 m/sec, the initial water temperature can be taken in the same region of the reservoir for which the calculation of the date of the beginning of stable ice is made. But even in the case of such low velocities, when determining the calculated value of θ_0 it is necessary to take into account the morphometric characteristics of the water body more upstream from the stretch under consideration. This is particularly important in cases when directly upstream from the stretch under consideration the reservoir has large areas where the depth considerably differs from that on the given stretch.

In the case of higher flow velocities the initial water temperature should be taken for a cross section situated upstream from the region for which the calculation of the date of the beginning of stable ice is being made by a distance equal to the path travelled by the stream during the forewarning period of the forecast.

If data of observation on the water temperature, characterizing the mean temperature in the given upstream cross section or in the corresponding region of the water body are available, the value of θ_0 is taken according to these data.

For considerable flow velocities in the initial cross section (approximately larger than 0.20 m/sec), the water temperature measured at a gaging site (if the measurement place satisfies the requirements imposed by the Instructions for Stations and Gaging Posts) can be taken as θ_0.

In cases of lower flow velocities it is not recommended to take θ_0 according to measurements at a single point of the site. In this case it is necessary to have measurement data along so-called profiles or at least at several points along the width of the initial cross section or on the water area under consideration.

If such measurements do not exist, the value of ϑ_0 can be calculated by the method described in § 3. It should, however, be remembered that one should strive to organize [routine] measurements of the water temperature. This considerably reduces the amount of calculations, a fact of great importance in preparing short-range forecasts.

The calculated forewarning period for the forecast of the time of the beginning of ice formation may exceed the actual forewarning period of the forecast. In this case, observed meteorological data are used for the period from the date of the beginning of the calculation (from the date for which ϑ_0 is taken) to the date of the preparation of the forecast.

Lengthening the period for which the calculation is carried out is desirable when the data of water-temperature measurement, according to which ϑ_0 is taken, are not sufficiently representative, or when ϑ_0 is determined by calculation.

The number of days of the calculation period can be determined from

$$n = -\frac{\ln\frac{\Delta\vartheta}{\Delta\vartheta_0}}{a_0}, \qquad (4.\text{III})$$

where $\Delta\vartheta$ is the permissible error in the calculation of the water temperature for the day of the beginning of ice formation (ϑ_a); $\Delta\vartheta_0$ is the typical error of the determination of ϑ_0; for a_0 (see (1.III)).

c) Time of flow (travel) from the initial to the calculation cross section. The calculated forewarning period for the forecast of the beginning of ice formation for a large stream flow, as indicated above, is equal to the time of flow τ_c from the initial to the calculation cross section.

For rivers the time of flow can be determined by the method of corresponding stages (Chapter I, Part B, § 2b).

For storage reservoirs the time of flow should be known in calculations of the beginning of ice formation in such river zones where considerable river flow is observed. However, under conditions of storage reservoirs in river stretches, the corresponding stages are insufficiently determined. Finding the time of flow from corresponding stages is impossible there.

The time of flow on such stretches can be determined from the mean velocities v_i in characteristic cross sections along the river stretch. The mean cross sectional velocities are determined, in the absence of data of direct measurements, by dividing the water discharge Q by the cross sectional area ω_i:

$$v_i = \frac{Q}{\omega_i}. \qquad (5.\text{III})$$

The magnitude of Q for the upstream (river) zones of storage reservoirs can be taken equal to the water discharge in the so-called inlet (upper) gaging site of the reservoir.

If considerable flow velocities are observed in the lower part of the reservoir, then there, in the absence of direct measurement data, the velocity v_i can be determined by dividing the water discharge through the hydroelectric station by the cross-section area under consideration.

The values of ω_i can be determined from the bathymetric chart of the reservoir for different water levels. The datum line in a given cross section, in the absence of a gaging site, can be determined by interpolation between neighboring sites or from backwater curves.

The time of flow from the initial to the calculation cross section for a given discharge and stage, is determined from

$$\tau_c = 2\sum_{i=1}^{N}\frac{l_i}{v_{i-1}+v_i} \qquad (6.\text{III})$$

or

$$\tau_c = \sum_{i=1}^{N}\tau_i, \qquad (6a.\text{III})$$

where N is the number of path segments between the indicated characteristic cross sections, l_i is the length of the i-th segment, τ_i is the time of flow along the i-th segment.

We then determine the time of flow along each path segment

$$\tau_i = \frac{2l_i}{v_{i-1}+v_i}.$$

With the values of τ_c, calculated from (6.III) for different discharges and stages, it is possible to obtain the relationship

$$\tau_c = f(Q, H), \qquad (7.\text{III})$$

where H is the river stage in the upstream area of the reservoir.

Figure 37a gives such a dependence for the time of flow from Cheboksary to Verkhnyi Uslon on the Kuibyshev storage reservoir (§ 5).

If a considerable part of the distance L from the initial to the calculating cross section is on an undammed stretch of the river or on a dammed stretch in which the particular channel-flow character is maintained, the time of flow for this stretch is determined, as for a river, from the corresponding stage.

The total time of flow τ_c is determined in this case as the sum of the time of flow along the river and of the time of flow along the reservoir.

d) Mean depth. The mean depth h of the water area used in the calculation is determined as a function of the stage H:

$$h = f(H). \qquad (8.\text{III})$$

In order to obtain the above relationship, the volume curve $V=f(H)$ and the area curve $F=f(H)$ are plotted for this water area.

The value of h in (8.III) is found from

$$h = \frac{V}{F}. \qquad (9.\text{III})$$

The value of h can also be determined by drawing cross sectional profiles in characteristic places of the water area used in the calculation (or of the stretch used in the calculation when there is stream flow).

If along the stretch involved in the calculation the mean depth varies considerably, the stretch should be divided into parts within which depth averaging cannot lead to an additional error in the calculation of the time of the beginning of ice formation. In practice, a stretch cannot be divided into parts if the total variation in the mean depth amounts to less than a factor of 1.5.

The mean depth on dammed-up river stretches in the case of small backwater is determined according to the indications given in Chapter I, Part B, § 2e.

e) The coefficient of heat input from the water mass to the water-air interface (coefficient of heat transfer α, coefficient of heat input α_n). The coefficient of heat transfer α is determined, as for rivers (Chapter I, Part B, § 2f), by (25.I)

$$\alpha = (1745v + 106w)c\rho \text{ cal/cm}^2\cdot\text{day}\cdot\text{degree},$$

where v is the mean flow velocity during the calculation period on the reservoir length used in the calculation, in m/sec; w is the mean wind velocity at the height of the vane during the calculation period in m/sec; c and ρ are the specific heat and density of water ($c\rho$ is taken equal to 1 cal/cm^3·degree).

The mean flow velocity v is determined by dividing the calculation length of the reservoir L by the time of flow τ_c (see subsection c):

$$v = \frac{L}{\tau_c}. \tag{10.III}$$

The coefficient of heat input α_n is also determined by formula (25.I). However, in this case, the flow velocity is taken at the closing (calculation) site (cross section) and the wind velocity in the same region at the time for which the probability of the beginning of ice formation is calculated. In the case of a calm, the wind velocity is assumed equal to 0.5 m/sec.

f) The parameters d and k. See Chapter I, Part B, § 2e.

g) The specific channel heat input ($q = q_b + q_u + q_e$). For lakes, as well as for storage reservoirs in periods when they are not discharged, it is possible, as a rule, to neglect the heat-exchange component q_u (the specific heat input from the groundwater) as well as the heat exchange component q_e (the specific heat input due to energy dissipation). The quantity q is therefore taken equal to the specific heat input from the river bottom q_b. Calculated values of q_b are given in Chapter I, Part B, § 2 (Table 6).

For the upstream (river) stretches of storage reservoirs when the backwater is comparatively small it is possible to take

$$q = q_b + mq_e, \tag{11.III}$$

where m is a factor smaller than unity, whose exact value has not been investigated. It can be taken approximately on the basis of a linear interpolation from unity, at the river at the end of the backwater area, to zero at the beginning of overflow (bank flow) up to the basic shores of the river valley.

For the values of q_e see Chapter I, Part B, § 2.

h) The specific heat transfer of the water surface to air, B_n. The magnitude of B_n is determined from (27.I) as the sum of the thermal currents of evaporation, LE, of exchange P and of effective radiation I_{eff} (at a water-surface temperature equal to 0°).

$$B_n = LE + P + I_{eff}.$$

The magnitudes of LE, P, I_{eff} can be determined from (20.I), (22.I) and (24.I) (see Chapter I, Part B, § 1).

The magnitude of B_n can be determined with sufficient accuracy also by means of nomographs (Figures 4 and 5) (see Chapter I, Part B, § 1).

In the case of a calm, the wind velocity is taken equal to 0.5 m/sec.

§ 3. Method of calculating the initial water temperature

In cases when there are no data of water-temperature measurements or when these measurements are conducted only at shore stations, the initial water temperature ϑ_0 appearing in (2.III) and (3.III) can be calculated by the methods described below.

If the daily air temperatures are used in the calculation, ϑ_0 can be calculated from

$$\vartheta_0 = \sum_{i=1}^{n_0}\left[\theta_i\left(e^{-(n_0-i)a_0} - e^{-(n_0-i+1)a_0}\right)\right] + \frac{d}{k} + \frac{(a+k)q_0}{ak}, \tag{12.III}$$

where n_0 is the number of days (preceding the date for which ϑ_0 is determined) whose air temperatures and other quantities are introduced in the calculation. For the rest of the notations see § 1.

In this case n_0 is determined from

$$n_0 = \frac{(a+k)hc\rho \lg \dfrac{\vartheta_0^* - \dfrac{d}{k} - \dfrac{(a+k)q}{ak}}{\Delta\vartheta_0}}{0.43ak}, \tag{13.III}$$

where ϑ_0^* is the water temperature at the beginning of the period n_0, which is used for finding ϑ_0; $\Delta\vartheta_0$ is the permissible error in the determination of ϑ_0.

Since the value of ϑ_0^* is unknown, a difficulty arises at determining n_0 by (13.III). This can be overcome by adopting an exaggerated value for ϑ_0^*. In this case, a somewhat exaggerated value is obtained also for the number n_0. The amount of calculations by (12.III) is consequently increased. But the calculation error $\Delta\vartheta_0$ is decreased. From the structure of formula (13.III) it follows that overestimation of n_0 due to overestimation of ϑ_0^* is comparatively small.

The calculation of ϑ_0 by (12.III) is laborious. A method for calculating ϑ_0 from the mean air temperature of some preceding period (of a length of n_0 days) is therefore recommended:

$$\vartheta_0 = \frac{\sum_1^{n_0}\theta}{n_0}. \tag{14.III}$$

The number n_0 in cases when the mean depth does not exceed 6 m is determined from

$$n_0 = -\frac{2d}{kh} - \frac{2(a+k)q_0}{akh} + \frac{2e^{-a_0}}{1-e^{-a_0}}. \tag{15.III}$$

Initially the value of n_0 is found to a first approximation from Figure 35. This makes it possible to determine the approximate values of the parameters involved in (15.III).

In cases of larger depths, the value of n_0 found from (15.III) is corrected (by trial and error) by the equation

$$\frac{d}{k}+\frac{(\alpha+k)\sigma_0}{\alpha k}+\left(\frac{n_0}{2}-\frac{e^{-\Delta_t}}{1-e^{-\Delta_t}}\right)t\delta+\Big[\vartheta_0'-\bar{\theta}-\frac{d}{k}-$$
$$-\frac{(\alpha+k)\sigma_0}{\alpha k}+\left(\frac{n_0}{2}+\frac{e^{-\Delta_t}}{1-e^{-\Delta_t}}\right)t\delta\Big]e^{-n_0\Delta_t}=0, \qquad (16.\mathrm{III})$$

where $\bar{\theta}=\frac{\sum_{1}^{n_0}\theta}{n_0}$.

In equations (15.III) and (16.III) δ is the air-temperature fluctuation during one day (degrees/day); in the case of a general drop of the air temperature δ is negative. For the rest of the notations see above, as well as § 1

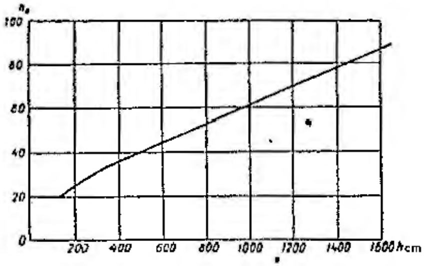

FIGURE 35. n_0 vs. the mean depth h.

δ is expressed by

$$\delta=\frac{\sum_{i=1}^{n_0}\left[\theta_i\left(e^{-(n_0-i)\Delta_t}-e^{-(n_0-i+1)\Delta_t}\right)\right]-\bar{\theta}\left(1-e^{-n_0\Delta_t}\right)}{\left[n_0-\frac{n_0}{2}\left(1-e^{-n_0\Delta_t}\right)-\frac{e^{-\Delta_t}\left(1-e^{-n_0\Delta_t}\right)}{1-e^{-\Delta_t}}\right]t}. \qquad (17.\mathrm{III})$$

However, with an accuracy sufficient for the calculation of ϑ_0, δ can be determined also more simply by drawing on a time graph of the mean-diurnal temperatures, a straight line of the general (averaged) air temperature variation (Figure 36).

The value of n_0 is corrected (by trial and error) by means of equation (16.III) as follows. The value of n_0, determined from (15.III), as well as the numerical values of all the remaining quantities involved in equation (16.III), are substituted in the latter equation. The values η obtained on the left-hand side of the equation in the general case differ from zero, and may assume positive or negative signs (in degrees). If a positive quantity is obtained, the number n_0 is underrated, whereas a negative quantity indicates that the number n_0 is overrated.

If a positive quantity is obtained, a value of n_0 larger by a unit is substituted in the equation and so on until the left-hand side of the equation becomes negative. The value of n_0 used in the calculation is that which gives in the left-hand side of equation (16.III) the least deviation from zero either positive or negative.

The procedure is similar when a negative quantity is obtained in the left-hand side of equation (16.III). But in this case smaller values of n_0 have to be substituted in the equation.

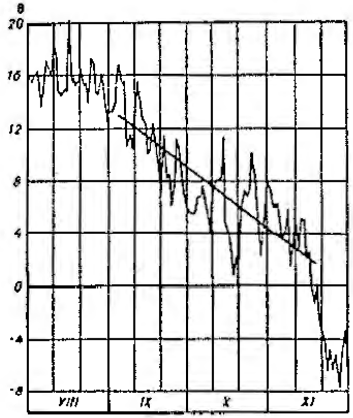

FIGURE 36. Mean-diurnal air temperature according to the Tunkoya meteorological station, 1954.

It should be borne in mind that since we assume an integral number of days, the left-hand side of the equation may vanish only in very rare cases of an appropriate combination of the values of the quantities involved in (16.III). In general, the left-hand side of the equation vanishes for a fractional value of n_0.

The correction of the value of n_0 (by trial and error) by equation (16.III) can be shortened when a value η = ± 0.20 – ± 0.30° is obtained. In this case, to obtain the required value of ϑ_0 the corresponding value of η should be added to the value of θ in the last calculation conducted with equation (16.III).

The value of ϑ_0 can also be determined from

$$\vartheta_0=\frac{\sum_{1}^{n_0'}\theta}{n_0'}+\frac{d}{k}+\frac{(\alpha+k)\sigma_0}{\alpha k}, \qquad (18.\mathrm{III})$$

where n_0' is smaller than n_0 for the same conditions. It is therefore expedient to use (18.III) when for some reasons it is desirable to shorten the period of averaging the air temperature. In particular, this formula can be used when the value of δ is determined graphically in cases when at the beginning of the period n_0t (in its early part) and for the rest of the period the nature of the general air-temperature fluctuation is different

The number n_0' is determined, in this case, to a first approximation by

$$n_0' = \frac{2e^{-a_0}}{1-e^{-a_0}}. \qquad (19.\text{III})$$

Then it is corrected by trial and error according to

$$\Delta\vartheta_0 = \left(\frac{n_0'}{2} - \frac{e^{-a_0}}{1-e^{-a_0}}\right)t\delta + \left[\vartheta_0^\circ - \bar{\theta} - \frac{d}{k} - \frac{(\alpha+k)q_b}{\alpha k} + \right.$$
$$\left. + \left(\frac{n_0'}{2} + \frac{e^{-a_0}}{1-e^{-a_0}}\right)t\delta\right]e^{-n_0' a_0}. \qquad (20.\text{III})$$

The value of n_0' is corrected until the value of $\Delta\vartheta_0$ is a minimum (see above concerning the correction of n_0 by trial and error according to (16.III)).

§ 4. Example of calculation of the beginning of stable ice cover on still water

Let us calculate the beginning of stable ice on Lake Chudskoe (Lake Peipus) in the Kodavere district in 1954.

We determine the boundaries of the section of the lake involved in the calculation for the given region according to the indications of § 2.

The meteorological data is taken from the nearest meteorological station Tiirikoya, situated 30 km to the north-northwest of Kodavere, on the lake shore.

The existence of measurement data for the water temperature is checked. We find that there are no data of measurements far from the shore, where the depths are characteristic of the given water area of the lake, and also that the water temperature measurements conducted at the gaging site on the shore cannot, in this case, characterize the mean water temperature of the given part of the lake. Therefore, the initial water temperature ϑ_0 is calculated.

When choosing the date for which the value of ϑ_0 will be calculated, the following instructions are taken into account (cf. § 2):

a) It is desirable to choose the date for which ϑ_0 is determined such that the air-temperature fluctuations up to this date do not complicate simple graphical determination of the mean rate of the general temperature drop (δ).

b) The date of ϑ_0 should be chosen so as to provide a sufficient forewarning period for the forecast and reduce, to some minimum, the error in the calculation of the water temperature for the assumed day of the beginning of stable ice cover, the error is due to the fact that ϑ_0 is calculated

From Figure 36 we find that on 16 November not only did a negative air temperature begin, but at about this time an abrupt change in the temperature curve occurred. Until 16 November the air temperature generally fell, though with considerable fluctuations; the mean rate of fall was considerably smaller than in the subsequent period.

On the strength of the above and in accordance with the course of the air temperature (Figure 36) we determine the value of ϑ_0 for 15 November.

The value of θ_0 (in accordance with (14.III)) is taken equal to the mean air temperature during some preceding period of n_0 days.

We determine the approximate value of n_0 from Figure 35.

The mean depth of the given part of the lake can be taken from the graph of $h = f(H)$ and is equal to about 920 cm (the water level in the lake in the given period varied within narrow limits).

For a depth of 920 cm we find $n_0 = 60$.

Let us calculate the value of n_0 from (15.III)

$$n_0 = -\frac{2d}{k\delta} - \frac{2(\alpha+k)q_b}{\alpha k\delta} + \frac{2e^{-a_0}}{1-e^{-a_0}},$$

where $a_0 = \frac{\alpha k t}{(\alpha+k)hc\rho}$.

The values of h, k, d, α, q_b and δ are determined for a period of 60 days from 17 September to 15 November.

For the mean depth h we find a value of 921 cm.

The mean air temperature $\bar{\theta}$ during the period from 17 September to 15 November is found to equal 6.2°. The wind velocity is taken equal to the mean value for the autumn cooling period (5 m/sec, Figure 2).

From Table 3 (for $\bar{\theta} = 6.2°$ and $w = 5$ m/sec) we find $k = 45$ cal/cm²·day·degree.

For the mean value of d during the calculation period we find, from Table 1 (region I) (for the geographical latitude and the date of the middle of the period – 17 October), the value 47 cal/cm²·day.

The value of the heat-transfer coefficient α is determined from (25.I)

$$\alpha = (1745v + 106w)c\rho.$$

For a wind velocity $w = 5$ m/sec (the rated value) and a flow velocity equal to zero, we obtain $\alpha = 530$ cal/cm²·day·degree. From Table 7 we find, on the average, for the calculation period $q_b = 18$ cal/cm²·day.

In order to determine the mean rate δ of the total air-temperature variation we draw, in Figure 36, the line of the total (averaged) temperature drop. We obtain $\delta = -0.15$ degree/day.

Let us calculate the values of a_0 and e^{-a_0} involved in (15.III)

$$a_0 = \frac{\alpha k t}{(\alpha+k)hc\rho} = \frac{530\cdot 45\cdot 1}{(530+45)\,921\cdot 1} = 0.045;$$

$$e^{-a_0} = e^{-0.045} = 0.956$$

(see Appendix 1).

Substituting the values found in (15.III), we obtain

$$n_0 = -\frac{2\cdot 47}{45\cdot 1\cdot(-0.15)} - \frac{2(530+45)18}{530\cdot 45(-0.15)} + \frac{2\cdot 0.956}{1-0.956} =$$
$$= 13.9 + 5.8 + 43.4 = 63.1.$$

Let us correct the value of n_0 by equation (16.III).

$$\frac{d}{k} + \frac{(\alpha+k)q_b}{\alpha k} + \left(\frac{n_0}{2} - \frac{e^{-a_0}}{1-e^{-a_0}}\right)t\delta +$$
$$+ \left[\vartheta_0^\circ - \bar{\theta} - \frac{d}{k} - \frac{(\alpha+k)q_b}{\alpha k} + \left(\frac{n_0}{2} + \frac{e^{-a_0}}{1-e^{-a_0}}\right)t\delta\right]e^{-n_0 a_0} = 0.$$

---

* If it is difficult to obtain the value of δ by a simple graphical construction, it should be calculated from (17.III).

We determine the values of the parameters for a period of 63 days (from 14 September to 15 November). From the tables and graphs indicated in the previous calculation we obtain: $h = 921$ cm, $\bar{\theta} = 6.4°$, $k = 45$ cal/cm²·day·degree, $d = 51$ cal/cm²·day, $\varphi_b = 18$ cal/cm²·day. The value of α remains as before, i.e., $\alpha = 530$ cal/cm²·day·degree. The value of $\dot{\theta}$ also remains as before (−0.15 degree/day).

The water temperature θ_0^* at the beginning of the considered period of 63 days, is taken approximately equal to the mean air temperature during a period of the same duration preceding the considered one, i.e., during 63 days from 13 July to 13 September. We obtain $\theta_0^* = 15.4°$.

We have

$$a_0 = \frac{\alpha k t}{(\alpha + k) h c \rho} = \frac{530 \cdot 45 \cdot 1}{(530 + 45) \cdot 921 \cdot 1} = 0.045;$$

$$e^{-a_0} = e^{-0.045} = 0.956, \quad e^{-na_0} = e^{-63 \cdot 0.045} = 0.058.$$

Substituting the values obtained in (16.III), we obtain

$$\frac{51}{45} + \frac{(530 + 45)\,18}{530 \cdot 45} + \left(\frac{63}{2} - \frac{0.956}{1 - 0.956}\right) \cdot 1 \cdot (-0.15) +$$
$$+ \left[15.4 - 6.4 - \frac{51}{45} - \frac{(530 + 45)\,18}{530 \cdot 45} + \right.$$
$$\left. + \left(\frac{63}{2} + \frac{0.956}{1 - 0.956}\right) \cdot 1 \cdot (-0.15)\right] 0.058 = 0.06°.$$

The fact that the result is not zero, but +0.06°, means that the mean air temperature during the 63 days (6.4°) gives a value of θ_0 underestimated by 0.06°. For such a small deviation from zero, further correction of n_0 is unnecessary. The value of θ_0 is obtained by adding the value of $\Delta\theta_0$ obtained from equation (16.III) to the mean air temperature during the 63 days. Rounding off to fractions of a degree, we have $\theta_0 = 6.4° + 0.06° = 6.5°$ (at the end of the day of the 15 November).

A negative mean-diurnal air temperature (according to the Tiirikoya meteorological station) began in 1954 on 16 November and was maintained until the beginning of December without sharp fluctuations (Table 24).

Bearing in mind that the most favorable conditions for the beginning of ice formation are low wind velocity and low cloudiness, we check the possibility for ice to form on 22 November (at 7 hours when the wind velocity was 1 m/sec, and cloudiness No. 1).

Since the calculation period is short (16–22 November) and fluctuations in the air temperature during this period are not sharp, we carry out the calculation by means of formula (2.III) in which the air temperature is averaged for the entire calculation period

$$\theta_0 e^{-na_0} + \left[\bar{\theta} + \frac{d}{k} + \frac{(\alpha + k)\varphi_b}{\alpha k}\right](1 - e^{-na_0}) < -\frac{B_n}{\alpha_n}.$$

The number n will be 6.3 (the calculation period nt from zero hours on 16 November to 7 hours on 22 November).

For the mean depth during the calculation period we obtain 941 cm from the graph $h = f(H)$.

The mean air temperature is $\bar{\theta} = -2.3°$, the mean wind velocity $w = 4.3$ m/sec (Table 24).

TABLE 24. Meteorological data according to the Tiirikoya station, 1954

Date	Air temperature					Wind velocity, m/sec					Degree of cloudiness			
	1 h.	7 h.	13 h.	19 h.	Mean	1 h.	7 h.	13 h.	19 h.	Mean	1 h.	7 h.	13 h.	19 h.
November														
14	2.0	−0.2	4.2	2.8	2.2	4	1	4	7	4.0	8	2	10	0
15	3.3	2.4	2.5	2.0	2.6	10	10	4	5	7.2	10	10	10	10
16	0.5	−1.2	0.7	−1.4	−0.4	5	4	3	2	3.5	10	10	0	6
17	−2.8	−2.9	0.4	0.6	−1.2	2	2	5	4	3.2	9	8	10	10
18	0.5	0.4	0.1	−0.9	0.0	2	3	3	5	3.2	10	10	10	10
19	−1.8	−2.4	−2.1	−4.5	−2.7	5	7	5	6	5.7	10	10	7	10
20	−3.3	−3.8	−4.1	−3.5	−3.7	6	7	6	5	6.0	10	10	10	10
21	−3.0	−2.0	−4.8	−6.9	−4.2	5	4	4	4	4.2	10	10	7	10
22	−4.4	−8.8	−6.0	−6.4	−6.4	5	1	1	2	2.2	10	1	10	10
23	−4.9	−6.5	−2.9	−4.5	−4.7	3	2	4	7	4.0	10	10	10	10
24	−4.3	−6.4	−6.3	−8.1	−6.3	7	7	10	12	9.0	10	10	10	10
25	−5.9	−5.7	−5.2	−3.6	−5.1	14	14	12	12	13.0	10	10	10	10
26	−5.0	−8.0	−7.4	−7.5	−7.0	12	10	12	10	11.0	10	1	2	0
27	−8.9	−9.8	−6.8	−4.7	−7.6	10	14	12	14	12.5	0	1	8	10
28	−3.9	−4.9	−6.1	−5.1	−5.0	12	12	12	14	12.5	10	10	10	10
29	−3.7	−3.0	−2.0	−4.6	−3.3	12	14	12	12	12.5	10	10	10	0
30	−6.0	−7.5	−7.1	−5.7	−6.6	12	12	10	10	11.0	0	0	1	10
December														
1	−5.1	−3.4	−4.7	−3.8	−4.2	12	12	12	12	12.0	10	7	10	10

From Table 3 we obtain $k = 40$ cal/cm²·day·degree; from Tables 1 and 2, $d = 6$ cal/cm²·day (region 1); from Table 7, $\varphi_b = 21$ cal/cm²·day. From (25.I)

$$\alpha = 106 \cdot 4.3 \cdot 1 = 456 \text{ cal/cm}^2\cdot\text{day}\cdot\text{degree}.$$

We obtain

$$na_0 = \frac{6.3 \cdot 456 \cdot 40 \cdot 1}{(456 + 40)\,941 \cdot 1} = 0.246;$$

$$e^{-na_0} = e^{-0.246} = 0.78.$$

Substituting the values obtained in the left-hand side of the inequality we obtain

$$6.5 \cdot 0.78 + \left[-2.3 + \frac{6}{40} + \frac{(456 + 40)\,21}{456 \cdot 40}\right](1 - 0.78) = 4.72°.$$

Let us determine the right-hand side of the equality, i.e., the value of $-\frac{B_n}{\alpha_n}$, for 7 hours on 22 November. The value of B_n is found from equation (11.III)

$$B_n = LE + P + I_{eff}$$

with the aid of Figures 4 and 5. We obtain: $LE + P = -115$ cal/cm² day (for $\theta = -8.8°$ and $w = 1$ m/sec, Table 24); $I_{eff} = -188$ cal/cm²·day (for $\theta = -8.8°$ and $N_0 = 1$, Table 24); $B_n = -115 - 188 = -303$ cal/cm²·day.

For $v=0$ and $w=1$ m/sec we obtain from (25.1) $\alpha_n=106\cdot 1\cdot 1=$ $=106$ cal/cm²·day·degree.

For the right-hand side of the equality we find

$$-\frac{B_n}{\alpha_n}=-\frac{-303}{106}=2.86°.$$

Thus, on the left-hand side of inequality (2.III), which gives the mean water temperature in the considered region of the lake, we obtain at 7 hours on 22 November 4.72°, and in the right-hand side, which gives the mean water temperature at which the beginning of ice formation on the surface is possible, we obtain 2.86°. The left-hand side is larger than the right-hand side. Consequently, on 22 November ice formation on the considered part of the lake is impossible.

In the next days (Table 24) cloudiness increased, the wind velocity rose and so did the air temperature. Therefore, since on 22 November the left-hand side of the inequality was larger than the right-hand side by almost 2°, we consider it inexpedient to predict the probability of the beginning of ice formation for a day earlier than 27 November.

Let us check the possibility of ice formation to begin at 1 hours on 27 November when, according to the meteorological data (Table 24), conditions are more favorable for the beginning of ice formation.

We calculate the left-hand side of inequality (2.III) for the end of the 26 November (the beginning of 27 November).

For the initial water temperature θ_0 we use the value obtained above for 7 hours on 22 November. The number n will in this case be equal to 4.7.

According to the data and methods indicated in the previous calculations we obtain $h=950$ cm, $\overline{\theta}=-6.0°$, $w=8.2$ m/sec, $\alpha=869$ cal/cm²·day·degree, $k=56$ cal/cm²·day·degree, $d=-10$ cal/cm²·day, $\varphi_b=21$ cal/cm²·day.

We obtain

$$n\alpha_0=\frac{4.7\cdot 869\cdot 56\cdot 1}{(869+56)\,950\cdot 1}=0.261,\quad e^{-n\alpha_0}=e^{-0.261}=0.77.$$

Substituting the values obtained in the left-hand side of inequality (2.III), we obtain

$$4.72\cdot 0.77+\left[-6.0+\frac{-10}{56}+\frac{(869+56)\,21}{869\cdot 56}\right](1-0.77)=2.29°.$$

Let us determine the right-hand side of the inequality, i.e., the value of $-\frac{B_n}{\alpha_n}$, for 1 hours on 27 November.

We determine the magnitude of B_n from equation (27.1)

$$B_n=LE+P+I_{eff}$$

with the aid of Figures 4 and 5. We obtain: $LE+P=-490$ cal/cm²·day (for $\theta=-8.9°$ and $w=10$ m/sec), $I_{eff}=-200$ cal/cm²·day (for $\theta=-8.9°$ and $N_0=0$, Table 24), $B_n=-490-200=-690$ cal/cm²·day.

For $v=0$ and $w=10$ m/sec we obtain from (25.1) $\alpha_n=1060$ cal/cm²·day·degree.

The value of the right-hand side of the inequality is, therefore, $-\frac{B_n}{\alpha_n}=$ $=-\frac{-690}{1060}=0.65°$.

The left-hand side of the inequality (2.29°) is larger than the right side. Consequently, ice formation also cannot begin at 1 hours on 27 November

From the meteorological data (Table 24) it can be concluded that ice formation will not begin in the nearest time either; the wind intensified and the cloudiness increased, and after 7 hours on 27 November the air temperature also rose.

This appearance of the clouds and a drop in the air temperature (with the wind velocity remaining high) began at the end of 29 November.

Let us check the probability for ice to form at 1 hours on 30 November. We calculate the left-hand side of the inequality (the mean water temperature) for the end of the 29 November.

For the initial water temperature (θ_0) we take the value obtained by calculation for the end of 26 November (2.29°). We have $n=3$.

From the respective graphs, tables and formulas (see above), for the period from 27 to 29 November we obtain: $h=950$ cm, $w=12.5$ m/sec, $\overline{\theta}=-5.3°$, $k=78$ cal/cm²·day·degree, $d=-25$ cal/cm²·day, $\varphi_b=18$ cal/cm²·day, $\alpha=1325$ cal/cm²·day·degree, $n\alpha_0=0.233$, $e^{-n\alpha_0}=0.79$.

For the left-hand side of the inequality we obtain

$$2.29\cdot 0.79+\left[-5.3+\frac{-25}{78}+\frac{(1325+78)\,18}{1325\cdot 78}\right](1-0.79)=0.69°.$$

We determine the right-hand side of the inequality from the meteorological data for 1 hours on 30 November (for $\theta=-6.0°$, $w=12$ m/sec and $N_0=0$). We obtain: from Figure 4 $LE+P=-415$ cal/cm²·day, from Figure 5, $I_{eff}=-172$ cal/cm²·day, $B_n=-415-172=-587$ cal/cm²·day. From (25.1) we find $\alpha_n=1272$ cal/cm²·day·degree. For the right-hand side of the inequality we obtain

$$-\frac{B_n}{\alpha_n}=-\frac{-587}{1272}=0.46°.$$

The left-hand side is larger than the right side of the inequality. Ice formation cannot begin at 1 hours on 30 November.

At 7 hours on 30 November a further drop in the air temperature was recorded. We repeat the calculation of the probability of ice to form at 7 hours. For the initial water temperature we take the value obtained by calculation for the end of 29 November (0.69°). The number n will be equal to 0.3. For the time interval from the beginning of the day to 7 hours on 30 November we obtain: $h=950$ cm, $\overline{\theta}=-6.8°$, $w=12$ m/sec, $k=74$ cal/cm²·day·degree, $d=-22$ cal/cm²·day, $\varphi_b=17$ cal/cm²·day, $\alpha=1272$ cal/cm²·day·degree, $n\alpha_0=0.021$, $e^{-n\alpha_0}=e^{-0.021}=0.98$.

For the left-hand side of the inequality we obtain

$$0.69\cdot 0.98+\left(-6.8+\frac{-22}{74}+\frac{(1272+74)\,17}{1272\cdot 74}\right)(1-0.98)=0.54°,$$

or, rounding off to tenths, 0.5°.

Let us determine the right-hand side of the inequality. From the data for 7 hours on 30 November ($\theta=-7.5°$, $w=12$ m/sec, $N_0=0$) we find $LE+P=-500$ cal/cm²·day (Figure 4), $I_{eff}=-188$ cal/cm²·day (Figure 5), $B_n=-500-188=-688$ cal/cm²·day, $\alpha_n=1272$ cal/cm²·day. We obtain

$$-\frac{B_n}{\alpha_n}=-\frac{-688}{1272}=0.54°,$$

or, rounding off to tenths, 0.5°.

The right-hand side is equal to the left-hand side of the inequality.* Thus, we see that ice may begin to form on the surface of the considered region of the Chudskoe Lake on 30 November. Since there is no stream flow there, an ice cover on this part of the lake should form on 30 November. According to observation data at the Kodavere gaging site an ice cover formed in 1954 on 30 November.

§ 5 Example of the calculation of the beginning of stable ice on a river with a considerable stream flow

Calculation of the time of the beginning of stable ice on the Kuibyshev storage reservoir at the Verkhnii Uslon. As initial cross section we take that at the Cheboksary gaging site, situated 133 km upstream from the Verkhnii Uslon.

Here a fairly high flow velocity is maintained, which amounts during NPL, depending on the water discharge, to about from 0.20 to 0.70 m/sec. The water temperature is measured at a steep shore, in a place with a depth characteristic of this part of the water reservoir. We assume that in these conditions the water temperature measured at the Cheboksary gaging site is so close to the mean in the cross section that taking it as the initial temperature (ϑ_0) does not introduce an additional error in the calculation of the time of the beginning of ice formation at the Verkhnii Uslon.

For the calculation, in addition to the initial water temperature and meteorological data, it is necessary to know the time of flow τ_c from the initial to the calculation cross section, the mean flow velocity v and the mean depth h on this part of the reservoir, the flow velocity v and the width b in the given cross section (at Verkhnii Uslon).

All these quantities depend on the backwater level H and on the water discharge Q, which varies here from year to year within wide limits. In order not to calculate these quantities in each calculation of the beginning of ice formation and the beginning of stable ice, the graphs $\tau_c = f(H, Q)$, $v = f(H, Q)$ and $h = f(H)$ for the stretch and $v = f(H, Q)$ and $b = f(H)$ for the calculation cross section are plotted.

To obtain these graphs on the Cheboksary–Verkhnii Uslon stretch of the reservoir 27 cross sectional profiles of characteristic cross sections (including the initial and calculation ones) were drawn.

For each cross section (ω_i) the values of h_i were calculated for several water levels, and for the same levels and several water discharges the values of v_i were calculated.

The time of flow τ_c for each of the indicated water discharges and levels was calculated from (6,III)

$$\tau_c = 2\sum_{i=1}^{N}\frac{l_i}{v_{i-1}+v_i}.$$

From the thus obtained values of τ_c the graph of τ_c vs. H was drawn for several values of Q (Figure 37a).

The mean flow velocity v for a given water level and discharge was determined as the quotient of the distance L between the initial and calculation cross sections to the flow time τ_c

$$v = \frac{L}{\tau_c}.$$

The values of v can be determined from Figure 37b.

The mean depths on the stretch were calculated for several water levels by*

$$h = \frac{\sum_{i=1}^{N}[l_i(h_{i-1}+h_i)]}{2L}.$$

The value of h can be determined from Figure 37c.

A number of values of the mean flow velocity in the cross section at Verkhnii Uslon for different water discharges and stages were obtained by dividing the water discharge by the respective cross sectional area. A graph was drawn on the basis of these data (Figure 37d), from which it is possible to find the mean flow velocity in the cross section at Verkhnii Uslon.

The values of b for the calculation of the beginning of stable ice are determined from Figure 37e.

Let us calculate the time of the beginning of ice formation and of the beginning of stable ice in 1960.

From Table 25 we find that favorable meteorological conditions for the beginning of ice formation existed on 25 October at 19 hours, when at an air temperature of −5.4° the wind velocity fell to zero, and cloudiness was of point 3.**

Let us check the possibility for ice to form at 19 hours on 25 October.

Let us determine the time of flow τ_c on the Cheboksary–Verkhnii Uslon stretch. In the period under consideration the water stage in the reservoir was close to 51.7 m, and the water discharges were close to 1700 m³/sec. From Figure 37a we find that for these values of H and Q the time of flow is τ_c = 10 days (rounded off to a whole number).

Let us correct the values of H and Q. We obtain a mean value of H during the 10 days from 16 to 25 October equal to 51.7 m. The value of Q at Cheboksary on 16 October was 1730 m³/sec. The values of H and Q remained unchanged. Consequently, the value of τ_c also remains 10 days.

The calculation period nt is equal to the time of flow τ_c (10 days).

We calculate the beginning of ice formation by means of inequality (2,III)†

$$\vartheta_0 e^{-\frac{nt a k}{(a+k)hc\rho}} + \left(\bar{\theta} + \frac{d}{k} + \frac{(a+k)q}{ak}\right)\left(1 - e^{-\frac{nt a k}{(a+k)hc\rho}}\right) \leqslant -\frac{B_n}{a_n}.$$

---

* A calculation for 30 November 13 hours gives 0.41° for the left-hand side and 0.54° for the right-hand side.

* Rigorously speaking, when determining the mean depth (for the calculation of the water temperature) the depths of individual segments should be weighted not with respect to their length l_i, but with respect to the corresponding time of flow τ_i. In this case the following formula should be used

$$h = \frac{\sum_{i=1}^{N}[(h_{i-1}+h_i)\tau_i]}{2\tau_c}.$$

Both formulas give very close results.

** [Both in Russian and American terminology full cloudiness refers to a sky completely covered by clouds (degree 1 on the American scale or 10 on the Russian scale). Thus we speak of cloudiness of 1 or 0.1–0.9 in the American terminology, and of cloudiness of 1 to 10 in Russian terminology.]

† In cases of sharp fluctuations in the air temperature from the beginning to the end of the calculation period, more reliable results are obtained by using (1,III) in which the air temperature is not averaged over the whole calculation period, but over days.

In accordance with the time of flow we take the initial water temperature from the measurement at 20 hours on 15 October at Cheboksary as $\theta_0 = 7.9°$ (the water temperature is measured at 8 hours and at 20 hours).

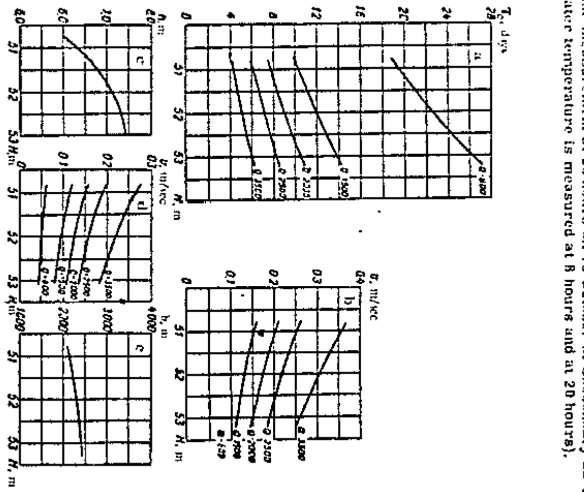

FIGURE 37. Graphs illustrating the calculation of the beginning of stable ice on the Kuibyshev storage reservoir at Verkhnii Uslon.

a—time of flow τ_c from Cheboksary to Verkhnii Uslon plotted against the stage H for several values of the water discharge Q in m³/sec; b—mean flow velocity v on the Cheboksary—Verkhnii Uslon stretch plotted against the stage H for several values of the water discharge Q in m³/sec; c—variation in mean depth h on the same stretch with the water stage H; d—mean flow velocity v at Verkhnii Uslon vs. the water stage H; e—reservoir width b at Verkhnii Uslon vs. the water stage H.

The meteorological data (air temperature and wind velocity) are taken from the Cheboksary and Kazan' meteorological stations in accordance with the time of flow (during the first three days according to Cheboksary, during the following three days the arithmetic means of the data according to Cheboksary and Kazan', during the last four days according to Kazan'). The thus calculated mean air temperature $\bar{\theta}$ from 16 to 25 October was −2.1°, and the mean wind velocity 5 m/sec.

TABLE 25. Meteorological data from the Kazan' meteorological station, 1960

Date	Air temperature, θ					Wind velocity w, m/sec				Cloudiness total/low level N_t/N_l			
	1	7	13	19	Mean diurnal value	1	7	13	19	1	7	13	19
October													
11	3.6	4.5	11.5	7.0	6.6	6	4	3	3	10/10	10/10	3/0	7/7
12	4.7	5.7	10.3	10.3	7.8	5	5	6	6	0/0	10/0	10/10	10/0
13	2.5	9.5	15.7	11.9	11.6	4	7	5	7	10/10	6/2	10/0	0/0
14	8.6	5.1	14.2	12.7	10.2	3	9	12	8	2/0	3/0	4/0	10/0
15	9.2	7.9	5.9	5.5	7.1	2	0	8	6	10/10	10/10	10/10	10/10
16	4.5	3.4	1.0	−1.4	1.9	8	7	8	8	10/10	10/10	10/10	10/6
17	−2.6	−4.8	0.6	2.0	−1.2	7	6	7	7	10/10	10/0	10/0	0/0
18	0.2	0.0	1.6	0.0	0.4	4	8	7	4	10/0	10/10	9/9	7/0
19	−3.8	−5.4	−1.9	−5.0	−4.0	2	3	5	3	0/0	8/0	6/0	0/0
20	−7.0	−8.3	−2.4	−4.4	−5.5	4	4	6	5	0/0	0/0	0/0	0/0
21	−4.8	−3.6	1.7	1.4	−1.4	8	9	7	10	0/0	8/4	10/10	10/10
22	0.4	1.0	1.7	0.4	0.9	7	6	8	6	10/10	10/10	10/10	9/9
23	−1.1	−1.8	−1.1	−2.1	−1.5	7	4	1	3	10/10	10/10	10/10	10/10
24	−2.5	−3.4	−3.4	−6.7	−4.0	4	4	7	4	10/10	10/10	10/10	0/0
25	−6.2	−5.6	−3.1	−5.4	−5.1	6	1	5	0	10/10	10/10	10/10	3/3
26	−4.2	−4.8	−1.8	−3.6	−4.6	2	0	3	3	10/10	10/10	9/8	10/10
27	−5.2	−4.7	−2.2	−3.0	−3.8	3	3	2	5	10/10	10/10	10/10	10/10
28	−4.2	−5.4	−3.1	−2.4	−3.8	9	8	4	3	10/10	10/10	10/10	10/10
29	−1.9	−1.4	−2.0	−4.6	−2.5	4	0	4	5	10/10	10/10	10/10	10/10
30	−5.3	−5.4	−4.5	−9.0	−6.0	5	5	4	2	10/10	10/10	3/3	8/0
31	−8.1	−4.2	0.2	1.3	−2.7	5	9	5	3	10/10	10/10	10/10	10/10
November													
1	−3.0	−5.2	−5.3	−5.3	−4.7	7	8	9	9	10/10	10/10	10/10	10/10
2	−9.0	−14.2	−12.3	−15.8	−12.8	7	3	3	0	10/0	2/0	1/0	0/0
3	−17.3	−17.6	−11.4	−14.0	−15.1	0	1	0	2	0/0	0/0	0/0	0/0
4	−17.6	−14.4	−7.1	−4.2	−10.8	1	3	5	6	9/0	10/0	10/0	10/0

The mean depth h on the stretch for a stage $H=51.7$ m (from Figure 37c) is equal to 6.90 m.

According to § 2g, we take for q (by interpolation between the values for the river part of the reservoir and for the reservoir itself) a value of 30 cal/cm²·day.

The mean value of d for the calculation period is found from Table 1 (Figure 1, region II) equal to 45 cal/cm²·day.

From Table 3 (for $\overline{\theta}=-2.1°$ and $w=5$ m/sec) we find $k=43$ cal/cm²·day·degree.

Let us determine the mean flow velocity on the stretch. From Figure 37b, for $H=51.7$ m and $Q=1700$ m³/sec we obtain $v=0.16$ m/sec. We determine the coefficient of heat transfer by (25.1).

$$\alpha=(1745\cdot 0.16+106.5)\cdot 1=810\ \text{cal/cm}^2\cdot\text{day}\cdot\text{degree}.$$

For the quantities na_0 and e^{-na_0} (according to Appendix 1) we obtain

$$na_0=\frac{10\cdot 810\cdot 43}{(810+43)\,690\cdot 1}=0.590;\quad e^{-na_0}=e^{-0.590}=0.554.$$

Substituting the values obtained in the left-hand side of inequality (12,III) we obtain

$$7.9\cdot 0.554+\left[-2.1+\frac{45}{43}+\frac{(810+43)\,30}{810\cdot 43}\right](1-0.554)=$$

$$=4.38+(-2.1+1.05+0.74)\,0.446=4.38-0.14=4.24°\approx 4.2°.$$

Let us calculate the value of the right-hand side of the inequality for 25 October 19 hours. The magnitude of B_n, equal to the sum of the rates of heat transfer by evaporation LE, turbulent exchange P, and effective radiation I_{eff}, is determined by means of the nomographs (Figures 4 and 5).

For the values observed at 19 hours on 25 October in Kazan' $\theta=-5.4°$, $w=0$ (for the reservoir we take $w=0.5$ m/sec), and $N_0=3$, we obtain $LE+P=-65$ cal/cm²·day, $I_{eff}=-130$ cal/cm²·day, $B_n=-65-130=-195$ cal/cm²·day.

The value of α_n is determined from (25.1). In this connection we find the flow velocity in the given cross section (on 25 October) from Figure 37d for $H=51.6$ m and $Q=1700$ m³/sec.

We obtain $v=0.12$ m/sec, $\alpha_n=(1745\cdot 0.12+106\cdot 0.5)\cdot 1=253$ cal/cm²·day·degree, $-\frac{B_n}{\alpha_n}=-\frac{-195}{253}=0.77°\approx 0.8°$.

The left-hand part of the inequality (4.2°) is considerably larger than the right-hand side (0.8°). Consequently, ice cannot form on 25 October.

From 26 to 29 October a relatively high air temperature prevailed with cloudiness of point 10 (Table 25). Since for 25 October the left-hand side of (12,III) is so much greater than the right-hand side, we assume that under the indicated meteorological conditions ice should not begin to form in the period from 26 to 29 October. More favorable conditions for the beginning of ice formation existed in the evening of 30 October, when by 19 hours the air temperature fell to −9° and the wind velocity to 2 m/sec; also there was no low-level cloudiness while the total cloudiness decreased to point 8.

Let us calculate the possibility for ice to form at 19 hours on 30 October from (12,III) similar to the calculation for the 25 October.

We obtain on the left-hand side 1.4° and on the right-hand side 0.6°. In this case, too, the left-hand side is larger than the right-hand side. Therefore, also on 30 October ice formation cannot begin.

We see from Table 25 that on 31 October (from 1 hours) the air temperature was positive at 13 hours and at 19 hours, the wind velocity rose, and low-level cloudiness developed (No. 10). On the next day, on 1 November, the air temperature was comparatively high (from −3 to −5.3°), the wind velocity rose to 7–9 m/sec and continuous low-level cloudiness was maintained.

We assume that under these conditions ice formation could not begin on 31 October and 1 November.

More favorable conditions for the beginning of ice formation existed at 1 hours on 2 November, when the air temperature fell to −9° and the cloudiness decreased to 10/0, although a relatively high wind velocity was maintained (7 m/sec).

Let us repeat the calculation of the possibility of the beginning of ice formation at 1 hours on 2 November.

From Figure 37a for $Q=1700$ m³/sec and $H=51.6$ m, we find $\tau_l=10$ days.

As the initial water temperature we take that measured at Cheboksary at 20 hours on 22 October, $\vartheta_0=3.1°$.

We determine the mean air temperature and the mean wind velocity during the period from 23 October to 1 November, as indicated above, from the data of the meteorological stations Cheboksary and Kazan'. We obtain $\overline{\theta}=-4.2°$, $w=4.2$ m/sec.

From Tables 1 and 2 we find $d=32+2=34$ cal/cm²·day.

For $\overline{\theta}=-4.2°$ and $w=4.2$ m/sec we have from Table 3, $k=38$ cal/cm²·day·degree.

For $v=0.16$ m/sec and $w=4.2$ m/sec we obtain from (25.1) for the heat-transfer coefficient α the value 724 cal/cm²·day·degree.

Substituting these values in the left-hand side of inequality (12,III) we obtain (the water temperature is taken for the end of 1 November*), $\vartheta_1\approx 0.8°$.

Let us calculate the right-hand side of the inequality (for 1 hours on 2 November from the data of the Kazan' meteorological station, Table 25). We determine the magnitudes of $LE+P$ and I_{eff} from the nomographs (Figures 4 and 5). For $\theta=-9.0°$, $N_0=10$ and $w=7$ m/sec we obtain $LE+P=-375$ cal/cm²·day, $I_{eff}=-80$ cal/cm²·day, $B_n=LE+P+I_{eff}=-455$ cal/cm²·day. Formula (25.1) gives for $v=0.12$ m/sec and $w=7$ m/sec, $\alpha_n=943$ cal/cm²·day·degree. We obtain, for the right-hand side of the inequality,

$$-\frac{B_n}{\alpha_n}=-\frac{-455}{943}=0.48°\approx 0.5°.$$

The left-hand side was 0.3° larger than the right-hand side of the inequality. Consequently, ice formation cannot begin at 1 hours on 2 November.

---

[*] Since there were no low-level clouds at the given observation hour, [illegible] the right-hand side of the inequality would not be larger than the left-hand side (0.8°) [illegible] were taken into account in the calculation. This can be checked by determining the magnitude of I_{eff} [illegible] There is no need for that in the given case, since even for $N_1=0$ the value $-\frac{B_n}{\alpha_n}$ is equal only to [illegible] ($I_{eff}=-225$ cal/cm²·day from the nomograph).

After 1 hours on 2 November a further decrease in the air temperature, in the wind velocity and in the cloudiness occurred. At 7 hours on 2 November $\theta=-14.$[illegible], $w=3$ m/sec, and $N=2/0$.

Let us check the possibility of ice formation beginning, according to the data, at 7 hours on 2 November. In this case we begin the calculation by determining the value of $-\frac{B_n}{\alpha_n}$.

By means of the nomographs (Figures 4 and 5) we obtain for the indicated meteorological data $LE+P=-295$ cal/cm²·day, $I_{eff}=-225$ cal/cm²·day, $B_n=-520$ cal/cm²·day.

For $v=0.12$ m/sec and $w=3$ m/sec, we have from (25.1) $\alpha_n=527$ cal/cm²·day·degree.

For the right-hand of the inequality we obtain $-\frac{-520}{527}=0.99^\circ\approx1.0^\circ$. The left-hand side of the inequality was smaller (0.8°) even at the end of 1 November. Since further heat transfer took place after this, it is clear that at 7 hours on 2 November the left-hand side of the inequality will be smaller than 0.8° and therefore it need not be calculated.

We thus obtain that ice formation on the Kuibyshev storage reservoir in the region of Verkhnii Uslon should begin in the morning of 2 November (rather, between 1 hours at night and 7 hours in the morning), which was indeed observed.

We calculate the date of the beginning of stable ice cover by means of (6.III)

$$\Sigma\theta_-=-10.3v^{1.22}b^{0.33}$$

and (7.III)

$$\theta_{cr}=-0.65vb^{0.5}.$$

For $H=51.3$ m and $Q=1770$ m³/sec (for 2 November) we obtain from Figure 37d a mean cross-sectional flow velocity at Verkhnyi Uslon $v=0.12$ m/sec and a reservoir width $b=2200$ m.

Substituting these values in (6.III) and (7.III), we obtain $\Sigma\theta_-=-16.4^\circ$, $\theta_{cr}=-3.7^\circ$.

From Table 25 we find that beginning from 2 November the sum $\Sigma\theta_-$ of mean diurnal negative air temperatures is recorded, reaches its recorded value on 3 November, and on 3 November the air temperature is below the critical θ_{cr}.

Thus, we have that a stable ice period should begin on the Kuibyshev storage reservoir in the region of Verkhnyi Uslon on 3 November, which indeed occurred.

§ 6. Forecasts based on empirical relationships and use of the weather forecast

When there are data of long-time observations on a given reservoir, the beginning of stable ice cover can be predicted by means of empirical relationships. For this purpose two graphs are plotted (Figure 38):

1) the relationship between the minimum sum of the mean diurnal negative air temperatures, necessary for the beginning of stable ice and the initial water temperature

$$(\Sigma\theta_-)_{min}=f(\theta_0); \qquad (21.III)$$

2) the relationship between the critical air temperature, necessary for the beginning of stable ice, and the wind velocity

$$\theta_{cr}=f(w). \qquad (22.III)$$

On the graph of relationship (21.III) the point $(\theta_0, \Sigma\theta_-)$ is plotted for each case of stable ice, the value of $\Sigma\theta_-$ being summed from the time when the air temperature passes through 0° to the beginning of stable ice (inclusive).

The dependence (22.III) is derived as follows.

For each case of stable ice cover the recorded date of $(\Sigma\theta_-)_{min}$, determined from (21.III), is found from the observation data of the nearest meteorological station (Figure 38a).

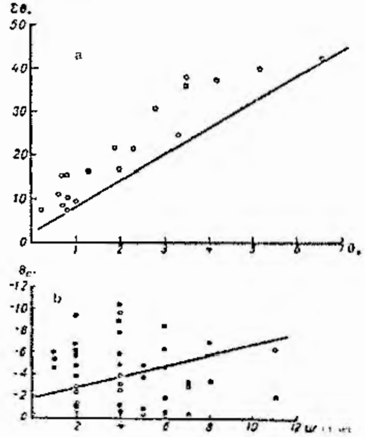

FIGURE 38. a) Minimum sum of [illegible] (passing through 0°) necessary for the beginning of stable ice on the Kuibyshev [illegible] water temperature a day before air temperature passes through 0°, θ_0; b) the relationship critical air temperature, θ_{cr}, necessary for the beginning of stable ice, is a function of the wind velocity w (according to the Kuibyshev meteorological station).

Then, for cases when stable ice began on the day on which $(\Sigma\theta_-)_{min}$ was recorded, we determine the air temperature and the wind velocity of this day and mark on the graph a point with the obtained coordinates (θ, w). These points are designated arbitrarily, showing that the air temperature at the given wind velocity is sufficient for the formation of an ice cover (in Figure 38b the black circles). Further, for all the remaining cases, [illegible] for cases when stable ice began not on the day $(\Sigma\theta_-)_{\min}$ was recorded but on one of the following days, the points (θ, w) are plotted on the graph according to the data for each day, beginning from the day $(\Sigma\theta_-)_{\min}$ was recorded and ending with the day of the beginning of stable ice (inclusive). Points corresponding to days when there was no stable ice are denoted differently (in Figure 38b the white circles). Next, on the graph a line is drawn which separates signs indicating that the air temperature at the given wind velocity is sufficient for the formation of a stable ice cover (in Figure 38b the black circles) from signs indicating that the air temperature is not sufficient for the beginning of stable ice (the white circles). In this way we obtain the line of the dependence (22.III)

$$\theta_{cr} = f(w).$$

The dependences (21.III) and (22.III) can be assumed linear.

A forecast of the beginning of stable ice by means of dependences (21.III) and (22.III) is prepared as follows.

From $(\Sigma\theta_-)_{\min} = f(\theta_0)$ we find the value of $(\Sigma\theta_-)_{\min}$ which corresponds to the water temperature observed on the day before the air temperature passes through 0°. Let us determine the date of the accumulation of this sum of negative temperatures. From the dependence $\theta_{cr} = f(w)$ we determine the air temperature necessary for the beginning of stable ice on the day $(\Sigma\theta_-)_{\min}$ is recorded.

If the mean-diurnal air temperature on this day according to the forecast is equal to or lower than the thus determined value of θ_{cr}, stable ice should be expected on the day $(\Sigma\theta_-)_{\min}$ is recorded.

If an air temperature higher than the critical is expected on this day, we determine θ_{cr} from the dependence $\theta_{cr} = f(w)$ for the next day and compare it with the air temperature expected for this day. We proceed thus until the day on which the expected air temperature is equal to or lower than θ_{cr} for this day.

Example of calculation. Let us determine the date of the beginning of stable ice on the Rybinsk storage reservoir in the Ves'egonsk district in 1954. We have the following data on the air temperature and wind velocity (according to the Kes'ma meteorological station)

TABLE 26. Mean-diurnal values of the air temperature θ and of the wind velocity w according to data of the meteorological station, November 1954

Date	14	15	16	17	18	19	20	21	22	23
θ, degrees	2.1	0.4	−1.8	−7.8	−6.0	−6.3	−6.1	−3.3	−4.7	−10.4
w, m/sec	5	2	2	1	0	5	11	8	5	1

As follows from the data of Table 26, the air temperature passed through 0° on 16 November. From the observation data on the water temperature we find that a day before, on 15 November, the water temperature was 3.5°. From Figure 38a we find for $\theta_0 = 3.5$ a value of $(\Sigma\theta_-)_{\min}$ equal to 23°.

From Table 26 we find that a sum of mean-diurnal negative temperatures of 23° is recorded on 20 November. On this day the wind velocity was 11 m/sec. From Figure 38b we find that for a wind velocity of 11 m/sec the air temperature for stable ice to begin should be lower than −7°. The actual air temperature on 20 November was −6.1°. Consequently, there should not be stable ice on 20 November. On the next day, 21 November, the wind velocity dropped to 8 m/sec. From Figure 38b we find that at this wind velocity stable ice can begin if the air temperature is not higher than −5.7°. But, as follows from Table 26, the air temperature on 21 November rose and was only −3.3°. Consequently, also on 21 November a stable ice cover could not form. On 22 November the wind velocity decreased to 5 m/sec and the air temperature dropped slightly to −4.7°. From Figure 38b we find that for $w = 5$ m/sec for stable ice to begin the air temperature should not be higher than −4.3°.

We thus obtain that stable ice on the Rybinsk storage reservoir in the Ves'egonsk district should begin on 22 November, which actually was the case.

C. FORECASTING METHODS USING THE CHARACTERISTICS OF THE ATMOSPHERIC PROCESSES (LONG-RANGE FORECASTS)

The ice cover on storage reservoirs forms in a definite sequence. First the shallow areas, which on lowland river reservoirs are very wide, freeze. Later deep-water regions, particularly near the dam of storage reservoirs, are covered with ice. In the stream part of the reservoir, near the end of the backwater zone, the flow velocity is low (compared with that in the river) and the depth is still small. Stable ice therefore begins there earlier than on deeper, downstream areas of the storage reservoir. If on the river upstream from this zone natural conditions are maintained, stable ice in the indicated stream part of the reservoir begins approximately at the same dates as when floating ice appears on the river, but usually considerably earlier than on that section of the river frozen before the creation of the reservoir. In this case, stable ice begins at earlier dates than before the creation of the reservoir also on the more upstream located area of the river, since the ice bridge forming at the end of the backwater zone hinders the drifting of ice. Thus, the ice bridge forming in the upstream part of the reservoir limits navigation along the reservoir.

Somewhat different is the nature of freezing of the upstream part of storage reservoirs situated in a power plant chain (cascade). The headwater of such a reservoir is situated in the tailwater of the more upstream located plant. Therefore, on it not only is there no ice drift from above but, on the contrary, the water discharged through the dam of the plant from the deep-water part of the upper water reservoir and arriving at this pool is relatively warmer. This delays the beginning of ice formation and the formation of a stable ice cover on the uppermost part of the reservoir.

For storage reservoirs, on which there exist stretches which freeze considerably earlier than the others and thus restrict navigation, in practice it is necessary, first of all, to work out a technique of forecasting the beginning of stable ice on these stretches.

It was mentioned above that the ice cover on reservoir stretches limiting navigation, which are situated at the end of the backwater zone, forms approximately at the same dates in which floating ice appeared on the respective river stretches. It is, therefore, possible to apply to the forecasting of the beginning of stable ice on these water reservoir stretches the principles of the technique worked out for forecasting appearance of ice on rivers. In this case, of course, the specific features of control of the autumn runoff and of the regime of the reservoir zones under consideration (streamflow, variation in inflow, etc.) should be taken into account.

The technique of long-range forecasting of ice phenomena is based on the use of long-time observation series, which make it possible to establish empirical relationships between the dates of ice phenomena and the characteristics of the atmospheric processes determining them. Most of the existing storage reservoirs have been created only recently, and the practical use of hydrological forecasts for the national economy requires preparation of forecasts for storage reservoirs from the very beginning of their existence and, consequently, the forecasting technique should be worked out before completion of the power plant project and the filling of the storage reservoirs. A long-time series of dates of the beginning of stable ice for a given storage reservoir is therefore obtained by calculation from the meteorological data for the past years. The technique of such calculations is described in Part B of the present chapter.

To work out this kind of method is simplest for reservoirs in which, toward the beginning of stable ice formation, the same water level is always maintained. Such, for example, is the regime of the reservoir of the Novosibirsk power plant. The water level in the reservoir in the period preceding the formation of a stable ice cover is maintained, independently of the inflow, at the normal pondage level (NPL) of 113.5 m. Precisely for this level, a long-time series of dates of the beginning of stable ice in the region of the village of Ordynskoe, where stable ice begins earlier than on other stretches, were calculated. The reservoir width there is about 2600 m, the flow velocity is 0.04–0.10 m/sec. In the calculations use was made of data on the water temperature and discharges of the Ob' River near the town of Barnaul and of meteorological data from observations at the meteorological stations Barnaul, Kamen' and Ordynskoe. The calculated days of stable ice are connected with the characteristics of the atmospheric processes, which determine the freezing of the rivers of West Siberia, i.e., with the difference A_1 between the sums of the pressure anomalies in August and September, calculated according to data from meteorological stations situated on the territory covered by the western ridge of the Siberian anticyclone (Irkutsk, Yeniseisk, Surgut) and with the deviation ΔI_1 from the rated value of the meridionality index in September, calculated from the data of H_{500} maps (Figure 39). These characteristics are considered in Chapter I, Part C, § 3.

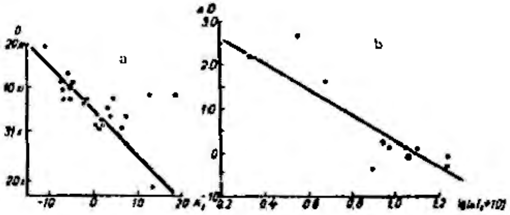

FIGURE 39. a—Relationship between the date D of the beginning of stable ice on the Novosibirsk water reservoir and the variation A_1 in the pressure anomaly in the western ridge of the Siberian anticyclone from August to September; b—corrections ΔD to the dates of the beginning of stable ice, obtained from Figure a, as a function of the deviation ΔI_1 from the norm of the meridionality index.

A more complicated picture is represented by the formation of stable ice in the stream part of the Kama storage reservoir. Navigation is usually limited there by the freezing of the river stretch in the Bereznikov district. The mean depth on this stretch is about 5 m, the flow velocity varies from 0.15 to 0.50 m/sec according to the variations in the water inflow to the reservoir.

On the broadened stretch upstream from the village of Chermoz the flow velocity drops to 0.04–0.01 m/sec. The time of the beginning of stable ice in the area of the village of Chermoz depends, therefore, only slightly on the flow velocity and, (besides the meteorological conditions) depends mainly on the reservoir depth. The latter may vary in autumn within wide limits, depending on the summer operation of the reservoir. Usually a NPL of 108.50 m is maintained, but in low-water years a reduction of the NPL to 106.00 m is still permissible. Calculations for a series of preceding years (1932) for both these pondage levels showed that in individual cases such a combination of conditions is possible, when stable ice first forms on the reservoir stretch of the river near Chermoz, and only then on the whole river stretch near Bereznikov.

The dependences of the calculated dates of stable ice on the characteristics of the atmospheric processes were established for the reservoir stretch of the river near Chermoz in two variants: for the pondage levels 108.50 and 106.00 m absolute; for the stretch near Bereznikov also in two variants: disregarding the inflow during freezing period and taking it into account.

The characteristics of the atmospheric processes, which cause the freezing of rivers of the northeastern regions of the ETS, are considered in Chapter I, Part C, § 2. These are the meridionality indices, determined from H_{500} and H^{500}_{1000} isobaric surface contour maps. As the basic relationship as well as for the forecasting of ice appearance on Pechora River, we took the dependence of the dates of the beginning of stable ice on the water reservoir on the index I. The form of this dependence for the stretch near Bereznikov is shown in Figure 40a. For the stretch near Chermoz it is, in general, similar.

The technique used for the Kama reservoir has a specific feature due to the more southern location of the Kama compared with the Pechora rivers; thus, the fact that the influence of a discrepancy between the fields of H_{500} and H^{500}_{1000} contours is manifested there only when the current has a very large meridional component $(-1 > I > +10)$. The number of such years in the existing series of observations is very small (1939, 1940, 1947, 1956) whereupon the graph of the corrections cannot be plotted. However, when the points of these years were plotted on the respective graph for the Pechora River (Figure 15b, Chapter I, Part C, § 2), it was found that they deviate only slightly from the dependence line. Therefore, as long as the number of years for plotting an independent graph of corrections for the Kama storage reservoir is still insufficient, the appropriate corrections can be introduced by means of the above-indicated graph for the Pechora River.

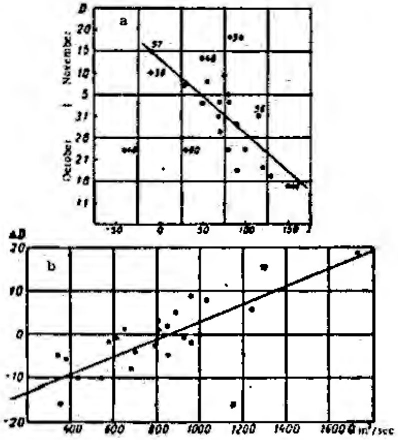

FIGURE 40. a—Relationship between the date D of the beginning of stable ice on the Kama storage reservoir at Bereznikov and the circulation index I in September; b—correction ΔD to the date of the beginning of stable ice, determined from a, as a function of the combined water discharge Q of the Kama River near Bondyug and of the Vishera River near Ryabinino.

Long-range forecasts by this method can be prepared as early as the middle of September. For the locality Bereznikov it is possible to correct the forecast by taking into account the water discharge which will pass there during ice formation. The influence of the magnitude of this discharge can be seen in Figure 40b, which gives the dependence of the difference between the actual dates of stable ice near Bereznikov and those expected by long-range forecasting on the sum of the water discharge of the Kama River near Bondyug and of the Vishera River near Ryabinino, i.e., on the inflow to the inflow site of the Kama storage reservoir. The introduction of discharge-dependent corrections by means of Figure 40b makes it possible to improve the forecasting accuracy noticeably. The r.m.s. error s decreases from 7.2 days to 4.5 days, and the ratio $\frac{s}{\sigma}$ decreases from 0.75 to 0.47. The time of flow from the indicated sites to the site of Bereznikov is 7 days. A short-range forecast of the discharge in these sites can be prepared with a forewarning period of about 8–10 days. Consequently, a more refined stable-ice forecast may have a forewarning period of about 15–17 days.

In both examples the estimates of the atmospheric processes were applied to the forecasting of ice appearance on the rivers of the same region where the storage reservoir is created.

There are, however, cases, when an independent technique for forecasting stable ice on a water reservoir is necessary. Let us consider such an example.

TABLE 27. Characteristics of the prevailing direction of transport of air masses in September, which are used to forecast the beginning of stable ice on the Tsimlyanskii storage reservoir

Year	Meridionality index I	Angle between the direction of the isobars and the parallel at the town of Kalach, α°	Year	Meridionality index I	Angle between the direction of the isobars and the parallel at the town of Kalach, α°
1938	−0.5	200	1950	−9.5	250
1939	−4.0	45	1951	−1.5	50
1940	−11.0	260	1952	−13.5	260
1941	−3.5	25	1953	−6.0	25
1942	−2.5	20	1954	−8.5	220
1943	−2.5	90	1955	−3.5	200
1944	−5.5	230	1956	0.0	30
1945	−2.5	50	1957	−11.5	340
1946	−5.5	10	1958	3.5	60
1947	0.0	180	1959	−3.0	35
1948	−3.5	15	1960	−4.5	25
1949	4.0	190			

For the Tsimlyanskii storage reservoir and for the Volga-Don canal the existing method of forecasting ice appearance on the lower Volga and on the Don River basin (see Chapter I, Part C, § 2), does not provide sufficient forewarning periods. Preparation of a forecast from data on the processes at the beginning of the synoptical prewinter season is possible not earlier than in the last ten-day period of October, whereas the formation of stable ice on the limiting stretch of the reservoir occurs, in early cases, already in the first ten-day period of November. Therefore, for the forecast to be issued in time it is necessary to investigate and estimate the development of the atmospheric processes from the autumn season to the prewinter season. A general solution of this problem involves large difficulties, but for the given region relatively simple laws governing the variation in the direction of transport of air masses have been found, on the basis of which satisfactory stable-ice forecasts can be prepared.

An estimate of the prevailing direction of transport is given by means of the above-described two characteristics: the meridionality index I, calculated from mean-monthly H_{500} absolute isobaric surface contour maps, and the angle α between the direction of the isobars and the parallel at the town of Kalach (Table 27). Taking into account the peculiarities of the high-altitude barometeric field for this region, in the calculation of the index I the values of the geopotential were averaged, for the western region, over the stations Riga, Minsk, Moscow, Kursk, Kiev and Vienna, and for the east, over the stations Orenburg, Kuibyshev, Khar'kov, Odessa, Rostov, Astrakhan and Sochi.

Both characteristics were determined for September and November. Comparison of the values of I for both months shows that they are most often uniform; however, a sharp variation in the index is observed in years when in September the current direction of air transport near the ground does not correspond to that prevailing in higher layers. It has also been established that the values of I and of α are interrelated, but the nature of this relationship is different in the case of a northern or of a northwestern direction of the isobars and in the case of a southwestern or southeastern direction.

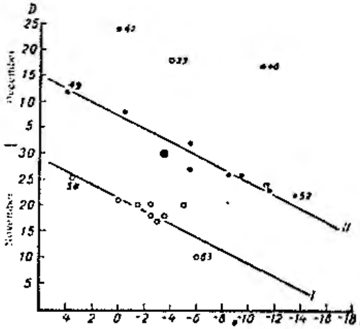

Figure 41. Date of the beginning of stable ice on the stretch between [illegible]–Skita of the [illegible] storage reservoir as a function of the [illegible] index I, and different values of the angle α between the direction of the isobars of the mean-monthly pressure in September and the respective parallel.

I—cases when $20° \leq \alpha \leq 110°$. II—cases when $\alpha < 20°$ or $\alpha > 110°$.

These data serve as the basis for the technique of forecasting the beginning of stable ice on the upper stretch of the reservoir, from the town of [illegible] to the village of Skita, which restricts navigation. The calculation of the dates of stable ice formation is made for the lower (32 m) and higher (34 m) pondage levels of the reservoir. The difference between the calculated dates for these two levels is relatively small. As an example we therefore give in Figure 41 one dependence (for the 34 m pondage level). The dates of stable ice cover are connected there with the value of the index I during September, all the cases being divided into two groups in accordance with the abovesaid on the relationship between I and α. One group includes cases when the air current near the ground penetrates from the north or northwest ($20° \leq \alpha \leq 110°$), the second group includes all the remaining cases. It is natural that when northern or northwestern penetrations prevail, formation of a stable ice cover begins for the same values of I earlier than in cases when other directions of transport of air masses prevail.

As mentioned, in the reservoir stretch which forms the downstream part of the preceding power plant of the cascade, stable ice usually begins much later than the day ice appeared on the corresponding river stretch before runoff control. Therefore, application of the principles of the technique worked out for forecasting ice appearance on a river to the forecasting of stable ice on such river reservoirs may not give positive results. In such cases, a special technique must be developed.

As an example we consider the technique of forecasting the beginning of stable ice on the Votkinsk storage reservoir. The Votkinsk reservoir is created by the backwater of the Votkinsk power plant upstream on the Kama River up to the dam of the more upstream located Kama plant. The reservoir width is relatively small — from 1 km in the upstream part to 10 km near the dam. In autumn the reservoir level is maintained close to the NPL, but the water discharges passing through the Kama and Votkinsk plants may vary within fairly wide limits — from 800 to 2200 m³/sec. In accordance with the discharge the flow velocities also vary, a fact having a considerable influence on the freezing of the reservoir. The reservoir can be separated into three parts: upper — from [illegible] to the town of Okhansk, middle — from the town of Okhansk to the town of Osa, and downstream – from the town of Osa to the Chaikovskii village. The flow velocities on the upper stretch for a mean depth of 6,3 m vary from 0,14 m/sec for the smallest discharge to 0,38 m/sec for the largest discharge. On the middle stretch, with a mean depth of 6–8 m, the flow velocities fall respectively to 0,05–0,13 m/sec. The mean depth of the lower part is 10 m, and the flow velocities do not exceed 0,08 m/sec even in the case of maximum discharges.

The most favorable conditions for the formation of a stable ice cover exist in the area of the town of Okhansk, where the flow velocities decrease appreciably (to 0,07–0,19 m/sec) and the mean depth is still not very large. Calculations of the dates of the beginning of stable ice near Okhansk, and in the region of the Nozhovka village (on the lower part of the reservoir) from meteorological data of past years were made in two variants: for the conditions of the minimum (800 m³/sec) and of the maximum (2200 m³/sec) water discharge through the hydroplant. Thus, the whole range of possible influence of the variations in the flow velocity on ice formation on the reservoir was covered. The initial water temperature during years since the commissioning of the Kama plant was taken in the calculation from observations in its tail-water area (the gaging site near Perm). The initial temperature for the preceding years was obtained by calculation for the part of the Kama storage reservoir near the dam.

The dates of the beginning of stable ice cover were calculated for the period from 1933 to 1961. The average date of the beginning of stable ice in the area of the town Okhansk is for a discharge of 800 m³/sec on 15 November, and for a discharge of 2200 m³/sec on 13 November, and for the area of the village of Nozhovka on 19 and 22 November, respectively.

Thus, the difference in the average dates for the beginning of stable ice along the reservoir, and for different water discharges through the hydroplant is small. The dates themselves are 11–17 days later than the average dates of ice appearance on the river under natural conditions (before construction of the dam).

The earliest dates of the beginning of stable ice on the reservoir are at the beginning of November, and the latest dates at the beginning of December

For forecasting, it is possible to use the uniformity of the atmospheric processes prevailing during the synoptical prewinter season. As shown in Chapter I, an idea of the character of these processes can be obtained from their development at the beginning of the season – in October.

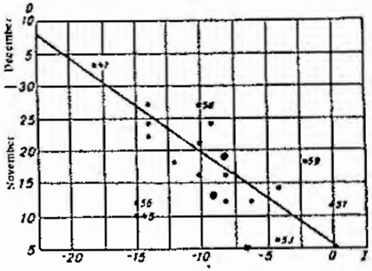

FIGURE 42. Date *D* of the beginning of stable ice on the Votkinsk storage reservoir in the area of the town Okhansk as a function of the meridionality index *I* during the first 20 days of October for a water discharge through the Kama power plant of 2200 m^3/sec

The meridionality index *I* is used as the characteristic of the atmospheric processes. Since, normally, in October and November the leading current in the troposphere is directed to the Kama River basin from the northwest, the regions for the determination of the index were chosen in the direction of this current: toward the northwest and the southeast of the Votkinsk storage reservoir. The first (northwestern) region is bounded by 40° and 55° E. long. and 76° and 60° N. lat., the second (southeastern region) by 55° and 80° E. long. and 62° and 48° N. lat. For each region the mean geopotential is averaged over the stations located within its boundaries. The geopotential is averaged over the first 20 days of October (to provide a sufficiently long forewarning period). The index *I* is obtained as the difference between the mean values of the geopotential in the first and the second regions.

The relationship between the dates of the beginning of stable ice on the Votkinsk reservoir in the area of Okhansk and the index *I* is given in Figure 42. The relationship is fairly accurate, but for some years (1945, 1956) considerable errors were noticed, which are due to the high rate of atmospheric cooling. It should be noted that a similar dependence was also found for the area of the village of Nozhovka. The accuracy of the relationship is somewhat higher for larger water discharges through the dam. This is due to the fact that, in this case, a larger total heat transfer is necessary for the formation of an ice cover and, consequently, the influence of the rate of individual cooling decreases.

Chapter IV

FORECASTING THE THICKNESS OF ICE COVER

§ 1. Determining factors

The thickness of the ice cover on rivers, lakes and storage reservoirs is determined by many meteorological elements, which affect the heat exchange between the surface of the ice or of the snow on the ice and the external space. The most important factors are: air temperature, wind velocity and cloudiness.

The thickness of the ice cover and its variation over the surface of a given water body also depend on: (a) the fact that the ice cover does not form simultaneously on the whole surface; (b) the conditions of its formation (ice piling and accumulation); (c) time and intensity of snowfall on the ice sheet and the transformation of the snow cover into ice; (d) formation of snow ice; (e) intensity of heat inflow from the water depth to the inner surface of the ice cover; (f) the formation of ice sheets. The factors listed vary strongly over the surface of rivers, lakes or storage reservoirs and over the given territory. Therefore, in each given moment the thickness of ice cover both on rivers and reservoirs, and within one part of a river or one reservoir, may considerably vary.

a) Nonsimultaneity of ice-cover formation. The ice cover forms earliest in the shallow area of rivers, lakes and reservoirs near the shore and in their stagnant zones. The degree of the delay in the formation of the ice cover in other zones of rivers and reservoirs as compared with shallow-water shore zones depends mainly on flow velocity depths (of reservoirs) and on the meteorological conditions (see Chapters II and III).

In general, the larger the variations in the meteorological conditions during the formation of the ice cover, the longer the period of ice movement on rivers; the deeper and wider the lake and reservoir, the more does the ice thickness vary over their surface.

During formation of an ice cover, in addition to large polynias, small stretches of ice-free water with dimensions varying from tens of centimeters to hundreds of meters usually remain. These small areas of pure water remaining among the ice usually freeze several hours after the junction of the ice blocks. This affects the distribution of the ice-cover thickness (on small areas at the beginning of the stable ice period) and is of practical importance.

b) Ice accumulation. Ice growth is slowest in places where there was pure water [and ice-free regions] and is most intensive in places where accumulations of ice material formed under the ice sheet and they essentially freeze together.

The increase in the rate of growth of the ice cover depends on the amount of ice contained per unit volume of the ice – water mixture.

It should be noted also that frazil and other types of ice, situated beneath the ice sheet, protect its inner surface from heat inflow from the water. For this reason the rate of growth of the ice cover in such places increases even more. At the same time, it should be borne in mind that in places of accumulation of ice the ice cover, as a rule, has an uneven outer surface. This unevenness contributes to snow accumulation, which delays the growth of the ice cover.

c) Snow cover on ice. The heat conductivity of snow is on the average one tenth of that of ice. Therefore, snow on an ice cover affects its growth considerably. The heat conductivity of snow is closely related to its density. Abel's well-known formula gives the following values

$$\lambda_{sn} = 0.0068\rho_{sn}^2, \qquad (1, IV)$$

where λ_{sn} is the heat conductivity of the snow cover, ρ_{sn} is its density.

From observations on some rivers and reservoirs the following formula has been obtained

$$\lambda_{sn} = 0.0090\rho_{sn}^2 + 0.00007. \qquad (2, IV)$$

Other formulas for determining the heat conductivity of the snow cover as a function of its density have also been proposed.

The height of the snow cover on the ice on a given river stretch is determined by the amount of snow, its compaction, wind snow drift, melting during periods of thawing, the transformation into snow ice and its rate of evaporation.

The density of the snow cover on ice depends on the nature of the precipitation (snow) and on the transformation of the snow due to wind, thaws and other factors.

A characteristic feature of the snow cover on ice is the sharp variation in its depth and density over the water area of rivers, lakes and reservoirs.

d) Formation of snow ice. Snow ice forms when water saturated with snow freezes on the surface of the ice sheet.

There is water in snow from melting during a thaw period, rains and mainly from the issue of water to the ice under the pressure of an excessive amount of snow on the ice and the capillary rise when the snow comes in contact with the water.

When the amount of water flowing into melting snow is in excess of the water-holding capacity of the snow, part of it percolates downward and accumulates on the ice cover, creating a layer of slob snow. In a subsequent cooling, the slob snow freezes and a layer of snow ice appears.

The thickest snow ice on water bodies forms as a result of the issue of water on the ice in the case of excess snow pressure Δp. The excess snow pressure is

$$\Delta p = \gamma_{sn} h_{sn} - (\gamma_w - \gamma_i) h_{ic}, \qquad (3, IV)$$

where h_{sn} is the depth of the snow on ice, γ_{sn}, γ_w and γ_i are, respectively, the specific weight of snow, water and ice, h_{ic} is the thickness of the ice cover.

The maximum depth of snow for various values of its density ρ_{sn} and the ice thickness for which water will not issue onto the ice (in the presence of openings in the ice) are given in Table 28.

TABLE 28. Maximum snow depth (cm) before water issues to the ice surface, for various values of ρ_{sn} g/cm³

Ice thickness, cm	ρ_{sn} = 0.10	ρ_{sn} = 0.20	ρ_{sn} = 0.30	ρ_{sn} = 0.40
10	9	4	3	2
20	18	9	6	4
30	27	14	9	7
40	36	18	12	9
50	45	22	15	11
60	54	27	18	14
70	63	32	21	16
80	72	36	24	18
90	81	40	27	20
100	90	45	30	22

Usually, in the middle of winter or later, the weight of the snow accumulated on the ice of reservoirs becomes larger than the buoyancy of the ice cover. From this moment water begins to seep out from cracks running through the ice and recent holes in the ice, saturating the lower snow layers. In the absence of cracks, holes or polynyas, water will stay for a long time under pressure and will not issue to the surface of the ice cover.

Above the slob snow a wet snow layer is observed, which forms due to capillary rise of the water. Its depth depends on the snow structure and varies from 2cm for firm snow to 5–6cm for fine-grained, loose snow. While freezing, this snow layer also forms snow ice, but less dense.

In the case of strong snowfalls, water may issue to the ice surface several times before the slob snow is completely frozen, and then several layers of snow with water remain in the ice cover.

The formation of snow ice causes a nonuniform increase in the ice cover thickness and at the same time a sharp decrease in the depth of snow on ice.

e) Heat input to the inner surface of the ice cover. The heat input from the depth of water to the inner surface of the ice cover on rivers in winter is due to dissipation of the kinetic energy of the water, to the arrival of heat from the bottom of the water body and from groundwater, and to heating of the water under the ice by solar radiation. During periods of thawing and in spring the inflow of snow-melt water also contributes to heat input.

The thickness of the ice cover on storage reservoirs and lakes also depends on the same heat sources except for the first.

The heat due to energy dissipation of the stream flow considerably affects the thickness of the ice cover in mountain rivers and on stretches of low-land rivers having rapids.

The heat arriving from the bottom of the water body reduces ice growth on rivers on the average by 10cm during the winter. On reservoir stretches with small flow velocity the heat flow from the bed reduces the ice thickness by 5–8 cm during the winter. In constricted sections of reservoirs, where the flow velocity rises, the heat flow to the ice from deeper layers sharply increases. In this case heat on ice melting comes not only by the heat flow from the nearest section of the bottom, but also from the heat accumulated in the water in the upper wide zone of smaller flow velocity. Therefore, relatively thin ice and polynias are observed in constricted areas of reservoirs.

The rise of groundwater to reservoirs is usually concentrated in individual stretches. In a number of cases the heat of the groundwater is the cause of the thin ice and polynias on some river stretches. On lakes and storage reservoirs its role is noticeable only in the shore zone.

The penetration of solar radiation through the ice cover into water layers below the ice affects the ice cover at its inner surface only in the absence of snow on the ice and of snow ice, and this mainly at the end of the winter owing to the intensive solar radiation in this period.

§ 2. Calculations and forecasts using air temperature forecasts

Forecasts of the ice-cover thickness in the case of thin ice, mainly for the beginning of the stable ice period, are based on the use of the air temperature forecasts. In accordance with the possibilities of obtaining a reliable forecast of the air temperature, the forewarning period of such forecasts is equal to several days (up to 5 or 6).

In the absence of snow ice and conditions for its formation (Table 28) during the calculation period (i.e., during the forewarning period of the forecast), as well as of ice accumulations under the ice cover, and if it is possible to neglect the heat input from lower water layers, the thickness of the ice cover can be calculated from

$$h_{ic}=-\frac{\lambda_{ic}}{\lambda_{sn}}h_{sn}+\sqrt{\left(h_{ic0}+\frac{\lambda_{ic}}{\lambda_{sn}}h_{sn}\right)^2+\frac{2\lambda_{ic}}{L_{ic}\rho_{ic}}86\,400\sum\theta_{su}},\qquad(4.\text{IV})$$

where h_{ic0} is the initial ice thickness; h_{sn} is the thickness of the snow on ice; λ_{ic}, λ_{sn} are, respectively, the heat conductivity of ice and of snow; L_{ic} is the ice-formation heat; ρ_{ic} is the ice density; θ_{s} is the temperature of the snow surface (or of the ice surface in the absence of snow); $\Sigma\theta_{su}$ is the sum of the mean-diurnal temperatures of the snow surface from the day for which the value of h_{ic0} is taken to the day for which h_{ic} is calculated.

The heat conductivity of snow is determined from its density (§ 1). The surface temperature θ_{su} is determined from the air temperature by means of Figures 43 and 44.

In the case of thin ice and small snow depth on the ice, considerable heat input from the water to the surface of the ice or of the snow on ice can exist thus making them warmer than the air. As the ice becomes thicker and the snow depth increases, the temperature of the snow (ice) surface approaches air temperature and in particular periods (at night in calm clear weather) may be lower than the air temperature.

To pass from the air temperature over the reservoir to the temperature of the snow (ice) surface in the case of small equivalent thickness

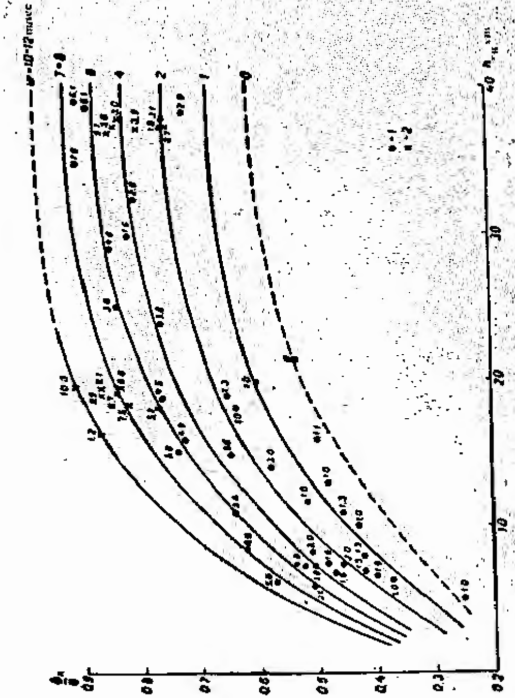

FIGURE 43. Ratio of the temperature θ_{sn} of the snow (ice) cover surface to the temperature θ of the air in the case of small equivalent ice thickness h_{eq} for different wind velocities w (m/sec).

1 – Volga at Polyana Fomino; 2 – Rybinsk storage reservoir. In the Rybinsk reservoir the numbers at the points give the wind velocity (m/sec) at a height of 2 m above the ice.

($h_i \leqslant 10$ cm), use is made of the dependence given in Figure 43, and in the case of a large h_{eq} that given in Figure 44 is used.

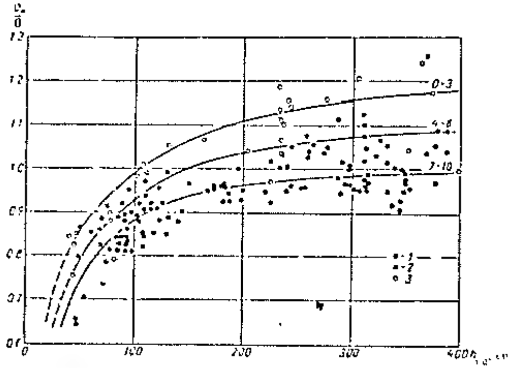

Figure 44. [illegible] of the temperature θ_{sn} of the snow surface to the air temperature θ at [illegible] in the case of large values of the equivalent ice thickness h_{eq} for different [illegible] degrees.

[illegible] 7-10; 2—between 4-6; [illegible] 0-3.

If the possible ice growth during a given time interval is small compared with h_{eq}, the ice growth Δh_i under the above-indicated conditions and in the absence of snow on the ice can also be calculated by

$$\Delta h_i = \frac{6.2\,\Sigma\theta_-}{h_i}, \qquad (5.\text{IV})$$

and, in the presence of snow on the ice, by

$$\Delta h_i = \frac{6.2\,\Sigma\theta_-}{h_{eq}}, \qquad (5a.\text{IV})$$

where h_{eq} is the ice thickness which is equivalent in terms of heat conductivity to the given ice thickness h_i and to the snow depth h_{sn} (and density) [illegible]; h_{eq} is determined from

$$h_{eq} = h_i + \frac{\lambda_i}{\lambda_{sn}} h_{sn}, \qquad (6.\text{IV})$$

the remaining designations are as before.

In the presence of ice accumulations, (5a.IV) has the form

$$\Delta h_i = \frac{6.2\,\Sigma\theta_-}{h_i\left(1 - \frac{\rho_f}{\rho_i}\right)}, \qquad (7.\text{IV})$$

where ρ_f is the density of the frazil ice (ice accumulations) or the ice mass per unit volume of the ice – water mixture.

It should, however, be borne in mind that (7.IV) has not been verified in practical calculations.

Example of forecasting ice thickness. Calculation by means of (7.IV).

The following quantities are known: $h_i = 30$ cm, $h_{sn} = 15$ cm, $\rho = 0.17$ g/cm^3, $\rho_f = 0.35$ g/cm^3.

The expected sum of negative mean diurnal air temperatures for six days in advance is $\Sigma\theta_- = -70$.

Let us estimate the possibility of the [illegible] of water on the ice and of the formation of snow ice in the above conditions, and [illegible] the possibility of using (7.IV).

From (3.IV) we find for $h_i = 30$ cm, $h_{sn} = 15$ cm, $\rho_{sn} = 0.17$ g/cm^3, $\rho_w = 1$ g/cm^3 and $\rho_i = 0.92$ g/cm^3 the excess snow pressure Δp will be equal to zero. Therefore, no snow ice will be formed.

Let us determine the equivalent ice thickness by (6.IV):

$$h_{eq} = h_i + \frac{\lambda_i}{\lambda_{sn}} h_{sn}.$$

We take λ_i equal to 0.0053 cal/cm · sec · degree [illegible] λ_{sn} we obtain from (2.IV) for a snow density $\rho_{sn} = 0.17$ g/cm^3 a value of 0.00033 cal/cm · sec · degree. Next we find

$$h_{eq} = 30 + \frac{0.0053}{0.00033}\,15 = 271 \text{ cm}.$$

From Figure 44 for $h_{eq} = 271$ cm and [illegible] 7-10 we find for the ratio of the surface temperature of the [illegible] to the air temperature a value of 0.98. We obtain $\Sigma\theta_{sn} = -70 \cdot 0.98 = -69$.

Substituting these values in (7.IV), we obtain [illegible] ice increment in the ice thickness

$$\Delta h = \frac{6.2 \cdot 69}{271\left(1 - \frac{0.35}{0.92}\right)} = 2.5 \text{ cm}.$$

Thus, the expected ice thickness will be

30 cm + 2.5 cm = 32.5 cm ≈ 32 cm.

Let us assume that under the same conditions [illegible] frazil ice accumulations beneath the ice cover, and the heat input from the water amounts to 10 cal/cm² · day.

In this case the ice increment is calculated in two stages.

First, by (7.IV) or (5a.IV) we find the increment when there is no heat input from the water (and no ice accumulations):

$$\Delta h = \frac{6.2 \cdot 69}{271} = 1.6 \text{ cm}.$$

Next, we determine the [illegible] heat input from the water. During 6 days the heat input is $\Sigma q_w = 10 \cdot 6 = 60$ [illegible]

The ice loss is

$$\frac{\Sigma q_w}{L_i \rho} = \frac{60}{80 \cdot 0.92} = 0.8 \text{ cm}$$

Thus, the increment in the ice thickness in this case amounts to only 1.6 cm − 0.8 cm = 0.8 cm. The expected ice thickness is 30.8 ≈ 31 cm.

These theoretical formulas, as indicated above, are not general expressions and can only be used with special observation data on hand.

For this reason empirical formulas and relationships are often used in calculations of ice cover thickness.

Bydin's formula is fairly widely used

$$h_{ic} = 2\sqrt{\sum \theta_{-}}, \qquad (8.IV)$$

where h_{ic} is the ice thickness in cm, $\Sigma\theta_{-}$ is the sum of the mean diurnal negative air temperatures from the beginning of the stable ice period to the dates for which calculations are made. This formula corresponds to the average conditions of presence of snow on the ice, ice accumulations under the ice cover, heat input from deeper water layers – mainly for the northwest of the ETS. It is sometimes used, however, also for other regions.

In the formula

$$h_{ic} = \left[90\pi_{ic}^{2} + 9\pi_{ic}(2.6 - a_0) + a_0\right]\sqrt{\sum \theta_{-}}, \qquad (9.IV)$$

where

$$a_0 = \frac{6h_{sn} + 52}{5h_{sn} + 20},$$

the ice thickness depends not only on the sum $\Sigma\theta_{-}$ of the mean diurnal negative air temperatures, but also on the depth h_{sn} of the snow on the ice and on the indirect characteristic π_{ic} of ice accumulations beneath the ice cover *.

The thickness of the ice cover in the absence of snow and ice accumulations under it can be calculated by the following formulas:

in the case of overcast weather and weak wind

$$h_{ic} = \left(\sum \theta_{-}\right)^{0.63}, \qquad (10.IV)$$

in the case of cloudless weather with a moderate wind intensity

$$h_{ic} = \left(\sum \theta_{-}\right)^{0.64}, \qquad (11.IV)$$

in the case of large ice thickness, under the conditions prevailing in Siberia,

$$h_{ic} = 1.25\left(\sum \theta_{-}\right)^{0.58}, \qquad (12.IV)$$

where $\Sigma\theta_{-}$ is the sum of the mean diurnal negative air temperatures and h_{ic} is the ice thickness in cm.

In general, however, it is recommended to derive the dependence $h_{ic} = f(\Sigma\theta_{-})$ from the observation data for each water body (or group of similar water bodies).

The dependence $h_{ic} = f(\Sigma\theta_{-})$ can also be obtained for conditions when snow exists on the ice. Such a dependence for approximate calculations of the average thickness of the ice cover on reservoirs is given in Figure 45. The dependence was obtained from data on ice-cover cross-cut profiles.

---

* For more details see Bulatov, S.N. Vliyanie zimnei vodnosti na ledovyi rezhim i vskrytie rek (Influence of the Winter Water Yield on the Ice Regime and on the Ice Breakup on Rivers). — Trudy TsIP, No. 60, 1957.

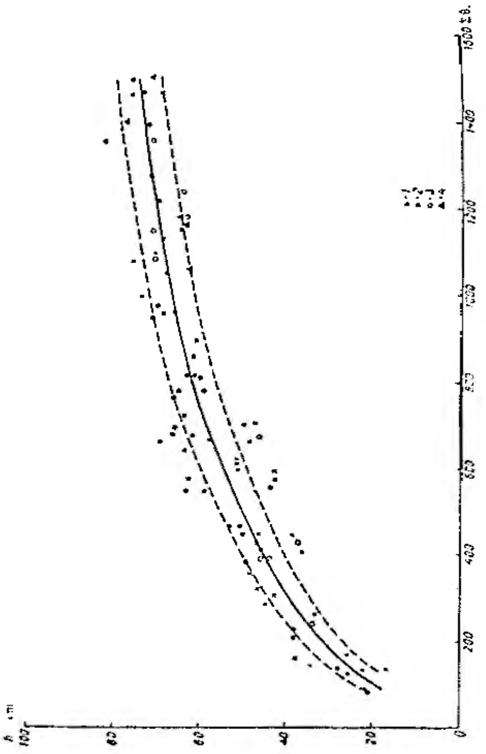

[illegible] h [illegible] ΣΘ [illegible] temperatures from the beginning [illegible]

[illegible]

An idea of the maximum ice thickness, determined by the numbers of ice blocks which appeared at the beginning of the ice drift and were preserved until the stable ice period, can be obtained if the sum of the mean diurnal negative air temperatures in the formulas or on the graphs for the determination of h_i are taken from the day of the beginning of ice drift. However, there are few such ice blocks on a river. Most ice blocks exist only during an ice drift of 1–3 days.

If more upstream on the river stable ice forms earlier (by Δt days) than on the given (lower) stretch, and in this case the following condition is satisfied

$$\Delta t > \tau,$$

where τ is the duration of motion of ice blocks from the upstream stable ice edge to the given downstream stretch, then at this stretch ice blocks freeze together during a time interval equal to their time of motion from the upstream stable ice. Therefore, to calculate the maximum thickness of these ice blocks, the sum of the air temperatures should be determined during the time of drift of the ice blocks from the upstream stable ice edge to downstream stretches. If, however, $\Delta t \leqslant \tau$ the air temperatures necessary to find the maximum ice thickness are calculated from the beginning of ice drift, which was observed (or expected) before the beginning of stable ice cover on the upstream stretch.* This is so because some ice-block accretions on the given stretch will start to form at the beginning of ice drift and will have a corresponding thickness.

If a stable ice cover on the given stretch forms earlier than anywhere more upstream on the river, the temperatures are summed from the beginning of the ice drift. The maximum ice thickness is calculated from the sum of temperatures found from the day after the observed or expected date of stable ice.

5.3. Calculation and forecasting using the air temperature forecast in the absence of observation data

In cold periods at the beginning of the winter, frequent in Siberia and in the north of the E.T.S., the thickness of the ice cover on water bodies can be calculated from data on the air temperature and precipitation at meteorological stations. In this case the role of ice accumulations under the ice cover and of the heat input from the water, which vary sharply along the length and width of a river, is not taken into account. The snow density is assumed constant and is determined from general consideration. Thus, such a calculation essentially gives for rivers only the relative growth and thickness of the ice.

Results of such a calculation with data on the ice thickness available for a number of points on the stretch during past years can, in particular, be used to determine the mean and extreme values of the ice thickness on the stretch.

---

* [illegible] calculated for past years [illegible] with meteorological data [illegible] the extreme [illegible]

[illegible]

Date	[illegible] $\theta°$	[illegible]	Time interval	[illegible] $\Sigma\theta_-$	[illegible] h_s, cm	$\frac{\theta_{i-1}+\theta_i}{2} = \bar{\theta}_i$, cm	[illegible]	h_{i} = [illegible]	[illegible] Δh, cm	[illegible] h_i, cm
1	2	3	4	5	6	7	8	9	10	11
November										
10	−23.9									
11	−22.[illegible]									
12	−21.4	0.3	10—12/XI	−45.9	0.9	0.015	5.9	8.9	9.2	12.2
13	−23.1	0.3								
14	−25.6									
15	−25.9	0.1	12—15/XI	−74.1	1.3	0.11	14.3	26.5	8.2	20.4
16	−29.4									
17	−23.3		15—17/XI	−54.4	1.3	0.13	17.1	37.5	5.0	25.4
18	−17.4	0.5								
19	−16.0	0.6								
20	−17.8	0.5	17—20/XI	−54.0	2.9	0.21	27.5	52.9	4.1	29.5
21	−13.5	0.7								
22	−13.4	0.1								
23	−15.2	1.0	20—21/XI	−43.7	4.7	0.35	50.0	79.5	2.7	32.2
24	−19.1	0.3								
25	−22.9	0.5	23—25/XI	−38.2	5.5	0.51	66.8	99.0	2.1	34.3
26	−10.4	0.6								
27	−17.6	1.3	25—27/XI	−30.6	7.4	0.64	84.0	118	1.5	35.8
28	−32.4	0.0								
29	−32.2	0.3								
30	−26.1	1.4	27—30/XI	−86.4	9.1	0.82	107	143	3.8	39.6

In order to calculate the ice thickness, data on the mean-diurnal air temperatures and on the daily precipitation from data of a main meteorological station are necessary; for the forewarning period of the forecast it is sufficient to know the expected sum of negative air temperatures.

In the example given (Table 29) the calculation is made using (10.IV). This, however, does not imply that this formula is preferred.

We divide the whole period from the day of the beginning of stable ice cover to the day of issuing the forecast, into separate intervals during which, according to the meteorological data, the depth of the snow cover on the ice and the ice thickness will vary only slightly. Therefore, at the beginning of the stable ice cover, when ice grows intensively and a snow cover forms on the ice, the length of these time intervals should not exceed 3–4 days. All days with a snowfall larger than 1.5 mm/day are taken as the beginning of a new time interval.

The ice thickness is found by calculating the increment Δh_{ic} for each time interval.

Table 29 gives an example of calculation of the ice thickness on the Yenisei River at the gaging site near Podkamennaya Tunguska at the beginning of the stable ice period.

From the observation data of the station a table is compiled of the daily data of air temperature and precipitation (Table 29, columns 2 and 3). Then, the calculation period is divided into the suitable time intervals (column 4). The sums $\Delta\Sigma\theta_-$ of the mean-diurnal negative air temperatures for each time interval (column 5) and the depth s_i of solid precipitation, expressed in depth of equivalent water (mm), from the beginning of the stable ice period until the end of each time interval (column 6),* are calculated. The mean of the values of s_i for the end of the given and the previous time intervals $\frac{s_{i-1}+s_i}{2}=\bar{s}_i$ (column 7) are determined. Heat conductivity of ice is taken as $\lambda_{ic}=0.0053$ cal/cm² sec degree, and density of the snow cover on the ice as 0.15 g/cm³. Let us calculate the heat conductivity λ_{sn} of the snow cover on the ice; in this example we use (2.IV), which gives $\lambda_{sn}=0.00027$ cal/cm sec degree.

We find the value of $\frac{\lambda_{ic}}{\lambda_{sn}}\cdot\frac{\bar{s}_i}{\rho_{sn}}$ (column 8). We calculate the value of h_{eq} (column 9) by (6.IV), represented in the form

$$h_{eq\,i}=h_{ic\,i-1}+\frac{\lambda_{ic}}{\lambda_{sn}}\frac{\bar{s}_i}{\rho_{sn}},$$

where $h_{ic\,i-1}$ is the ice thickness at the end of the preceding time interval.

From

$$\Delta h_{ic}=0.65(\Sigma\theta_-)h_{eq}^{-0.54}$$

we find the values of Δh_{ic} (column 10) which correspond to the values of $\Delta\Sigma\theta_-$ and h_{eq} for the given time interval. Adding the value of Δh_{ic}, obtained for the first time interval, to the value of h_{ic} at the beginning of the stable ice period (in our example h_{ic} at the beginning of the stable ice period is taken as 3 cm), we obtain the thickness h_{ic} for the end of the first time interval. Adding the value of Δh_{ic}, obtained for the second time interval, to the value of h_{ic} for the end of the first interval, we obtain h_{ic} for the end of the second time interval, and so on (column 11).

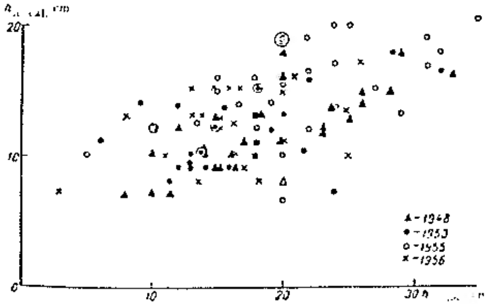

FIG. 46. [illegible] between observed $h_{ic\,obs}$ and calculated $h_{ic\,cal}$ [illegible] the Northern Dvina

Figure 46 presents a comparison of the thicknesses of the ice cover on the Northern Dvina River during 4 years (1948, 1953, 1955 and 1956) calculated by the method described above and actually observed at the gaging sites.

As we see, the calculated ice thicknesses are in general considerably smaller than the actual ones. The reason for this is, apparently, mainly the fact that ice growth took place in the presence of [illegible] under the ice cover. The scatter of the points on the graph is considerable. Smaller ice thickness evidently corresponds to areas frozen later than the polynyas and to places of large snow accumulation, [illegible] snow thickness was used in the calculation.

These graphs permit the determination of maximum and minimum ice thicknesses, which are possible on a given river with the corresponding quantities, i.e., for morphometric and hydraulic conditions that are characteristic of the stretches of the gaging sites.

It should be borne in mind that the relationships between the ice cover thickness and the sum of the negative air temperatures of the type $h_{ic}=f(\Sigma\theta_-)$, give a lower accuracy.

5.4 Short-range forecasts without air temperature forecasts

A forecast of the ice thickness on some rivers and reservoirs situated in regions with a comparatively stable winter (Siberia and Far East) [illegible]

---

* [illegible] at the meteorological station is not measured at the end of a period of 24 hours, but usually in the [illegible] half of the day. Therefore, for the convenience of comparing the calculated values with [illegible] the middle of the day was [illegible]. [illegible] the temperatures of the extreme days of the time interval were included in $\Delta\Sigma\theta_-$ with a coefficient of 0.5. In s_i (column 6) the depth of precipitation at the last [illegible] days of the time interval was included.

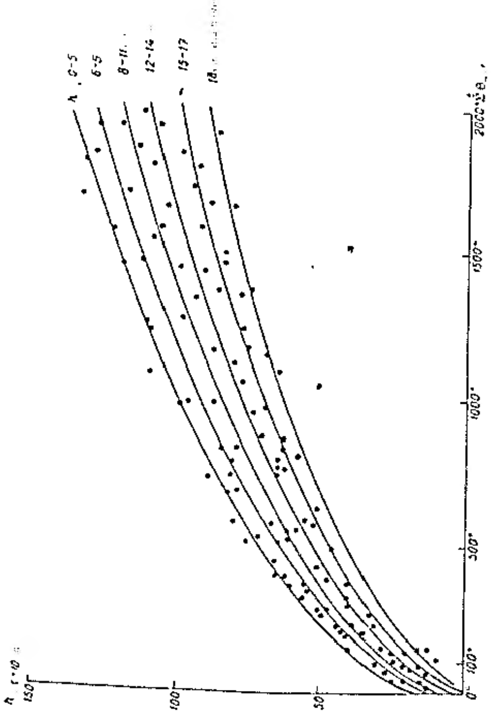

FIGURE 47. Relationship between ice thickness $h_{i,t+10}$ on the [illegible] River [illegible] and the sum $\sum_1^t \theta_{-,t}$ of the mean-daily negative air temperatures for various depths of the snow on the ice $h_{s,t}$.

be prepared without using air-temperature forecast (and in the absence of current data on the ice thickness).

The forecasting relationship is found from data of long-time observations of the ice thickness at a station and has the form

$$h_{i,t+m} = f\left(\sum^t \theta_-, h_{s,t}\right), \qquad (13.IV)$$

where $h_{i,t+m}$ is the ice thickness m days ahead (expected) of the date t of the preparation of the forecast, $\sum^t \theta_-$ is the sum of the mean daily negative air temperatures, calculated from the date of the air temperature transition through 0° to negative values or from the date of stable ice until the day of the issuing of the forecast, $h_{s,t}$ is the snow depth at the date t at a standard meteorological station or on the ice. The use of the snow depth on the ice of the reservoir instead of the snow depth at a meteorological station improves the accuracy of forecasting relationships.

The use of the snow depth at meteorological stations is possible only for reservoirs which freeze soon after the air temperature takes on negative values in autumn and under conditions when thaw periods are rare and the snow cover is stable.

As an example we give the relationship for the [illegible] River near the gaging site of Ust'-Ozery (Figure 47). The value of m is taken here equal to 10 days.

Example of preparation of a forecast. On the day of the issue of the forecast (30 November) the sum of the mean-daily negative air temperatures, after taking on negative values, was −270°, the snow depth at the meteorological station was 14 cm. For 10 December, according to Figure 47, an ice thickness of 27 cm is expected.

For small, freezing rivers such relationships of sufficient accuracy are usually not obtained, since the thickness of the ice cover there depends considerably, besides other factors, on the formation of [illegible] and the intensity of this process. In addition, such relationships are upset the moment ice reaches the river bottom. For large rivers such as the Yenisei, Lena, Angara and Kolyma, such relationships are [illegible] not obtained. This is due to the fact that stable ice forms on large rivers with passage of ice material.

5.5. Possibilities of long-range forecasting

We give here [illegible] of some possible [illegible] of long-range forecasting of the ice cover thickness [illegible] forecasts.

For lakes and storage reservoirs located in the [illegible] part of the European [illegible] catchment [illegible] is observed between the thickness of the ice cover on 1 December and the date of formation of a stable ice cover. [illegible] the thicker will be the ice on 1 December.

Figure 4[illegible] gives the relationship between the [illegible] cover on the Rybinsk reservoir towards 1 December and the mean date of stable ice according to the data from the stations Cherepovets, Mologa, [illegible] Rozhnovskii bridge, Breitovo, Myaksa, Koprino, Gavrilov [illegible], Volodarskoe [illegible].

From the data of a single gaging station such correlations are less accurate. A forecast by this method can be issued on the day stable ice forms on the reservoir. The forewarning period of the forecast therefore depends on the time of the beginning of stable ice. In the case of early stable ice the period may be more than a month.

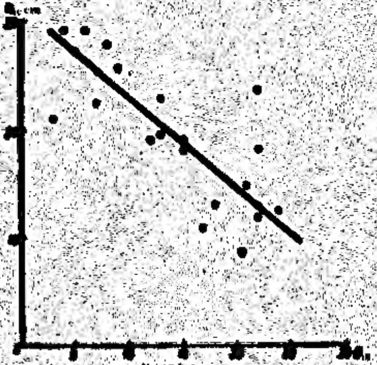

FIGURE 48. Mean ice thickness on the [illegible] reservoir on 1 December, [illegible], as a function of the date of the beginning of stable ice, [illegible].

The first time after formation of a stable ice cover on water reservoirs its growth depends particularly on the depth of snow on it. This fact can be used to forecast ice thickness on water bodies of Siberia, where the winter is stable and the main snowfalls are observed at the beginning of it until formation of the strong Siberian anticyclone.

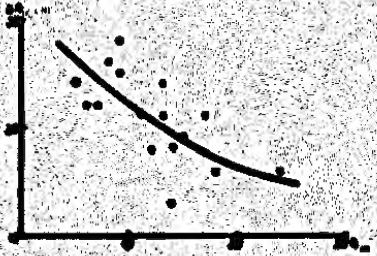

FIGURE 49. Mean ice-cover growth on the Lena River (the Ust'-Kut–Vitim stretch) during December, [illegible], as a function of the mean snow depth of ice snow on 1 December, [illegible].

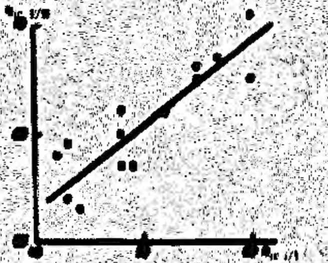

FIGURE 50. Mean ice thickness on 1 February ([illegible] I/II) as a function of ice thickness on 1 January ([illegible] I/I) on the Lena River (the Ust'-Kut–Vitim stretch).

Figure 49 gives the relationship between the ice-cover growth averaged over several stations on the Lena River during December and the mean depth of ice snow on 1 December as measured over the stretch from Ust'-Kut to Vitim (the stations of Ust'-Kut, Markovo, Kirensk, Ichera, Parshino and Vitim).

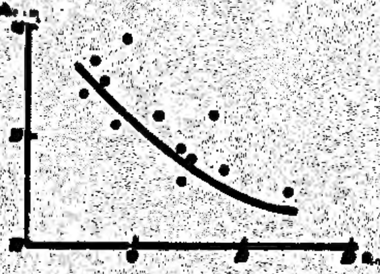

FIGURE 51. Mean ice-cover growth during December and January, [illegible], on the Lena (Ust'-Kut–Vitim stretch), as a function of the mean depth of snow on the ice, on 1 December, [illegible].

This relationship is less pronounced further east due to the fact that considerable snowfall occurs also during December and, in addition, the December air temperature in the east varies more sharply in different years.

On Siberian water bodies in some periods of the winter the thickness of the ice cover increases at a fairly constant rate. This makes it possible, in a number of cases, to determine the future thickness of the ice cover from its relationship with the ice thickness at the date of the issue of the forecast.

Figure 50 gives the relationship between the ice thickness on 1 February and the ice thickness on 1 January for the Lena River on the Ust'-Kut–Vitim stretch. The values of the ice thickness averaged over the stations on this stretch of the Lena River are taken.

For individual stations on the Lena such relationships are much less accurate. The reasons for this were indicated above.

Similar relationships for rivers and lakes of West Siberia are also less accurate due to the fact that the winter there is not so stable as in more eastern regions.

All the above said shows that the ice thickness on Siberian water bodies in February depends mainly on the conditions of ice growth in November and December, since in January the ice cover increases at a fairly constant rate.

Thus, a forecasting relationship between the ice growth during December and January (during the two months) and the depth of the snow on the ice at the beginning of December can be obtained. Such a relationship for the Lena River on the stretch between Ust'-Kut and Vitim is given in Figure 51.

At a specific point of a reservoir, owing to the large variations in ice-cover thickness over the water surface, the values thus obtained may considerably differ from the values obtained by the relationships given above.

Chapter V

FORECASTING ICE BREAKUP ON RIVERS

A. CONDITIONS FOR ICE BREAKUP ON RIVERS. BASIC DETERMINING FACTORS

Ice cover drift and ice breakup on a river (the beginning of ice drift) are usually the result of two processes: (1) melting of the ice cover, reduction of its thickness and strength and (2) increase in the water discharge and accordingly in the flow velocities and rise of the water stage as a result of snow melting in the particular river basin (sometimes also enhanced by rains).

Not always is ice breakup the result of an increase in the discharge and stage, but almost always, even on large rivers flowing to the north, ice breakup is preceded by the melting of the ice cover.

On partially freezing rivers the destruction of the ice cover, when the water stage rises, begins with the formation of cracks and the separation of the ice from the river banks or from the shore ice. Cracks in the ice cover form in this case not only along the banks, but also across the river and at various angles to the banks. This is due to the nonuniform thickness and strength of the ice cover and to the nonuniform strength with which it is attached to the banks. As the water discharge further increases, the ice cover continues to rise and ice flanges form. At the same time the melting of the snow on the ice and of the ice cover itself continues. The strength of the ice decreases, mainly due to the penetration of solar radiation. The ice cover also melts and is washed out owing to the flow of water around it. If the ice on tributaries breaks up earlier, the integrity of the ice cover is often upset.

When the rising water stage reaches a certain limit corresponding to the nature of the river bed on the given stretch, to the thickness and state of the ice cover, an ice push occurs. In pushes the ice cover breaks into separate fields, mainly along the crack lines, as well as in places of water holes and in other places, where the ice cover is weaker. In places of islands, in bed constrictions, on sharp turns, or on shallows the ice cover breaks up and accumulates against the shores. If the resistance of the shores or of the lower-lying ice cover is sufficient, the drift of the ice fields stops after a more or less intensive piling up and jamming. Further inflow of water and increase in the flow velocity, as well as melting and decrease in the ice strength, cause renewal of the pushes. This may be repeated many times until full ice drift sets in.

Irrespective of how the ice breakup takes place, with or without a flood, it begins when the flow velocity of the water under the ice for a given state of the ice cover is sufficient to overcome the resistance of the shore [illegible] of the shore ice, and to cause the breakup and drift of the ice cover downstream.

Pushes and breakup of ice on a river are determined by: (a) the state of the ice cover before the beginning of melting, (b) the input of heat to the ice cover and, in particular, of radiant heat, (c) the stream force, (d) the resistance of the shores to ice drift.

It can, in general, be considered that the total heat flow per unit outer surface of the ice cover, necessary for pushing the ice $\overset{p}{\Sigma} q_0$ or for ice breakup $\overset{b}{\Sigma} q_0$ is mainly determined by: (i) the mean thickness h_{ic} of the ice cover on the river stretch before the beginning of melting, (ii) the depth h_{sn} of the snow cover on the ice before the beginning of melting, (iii) the morphological characteristics Φ of the bed, (iv) the mean flow velocity v of the water in the bed towards the moment of the push or breakup of the ice, (v) the water stage H_0, the rise ΔH in the water stage and (vi) the total heat input, $\overset{p}{\Sigma} q_b$ or $\overset{b}{\Sigma} q_b$, per unit inner surface of the ice cover from the beginning of melting. The morphological characteristics of the bed, in particular, determine to a large extent the variation in the thickness of the ice cover on the given river stretch and the development of ice breakup. For given shapes of a river bed, the width of the ice flanges depends on H_0 and ΔH.

Thus, it can be assumed that

$$\overset{b}{\Sigma} q_0 = f\left(h_{ic}, h_{sn}\Phi, v, H_0, \Delta H, \overset{b}{\Sigma} q_b\right). \qquad (1.V)$$

In methods of forecasting local ice breakup on nonregulated rivers, the relationship (1.V) may be simplified

$$\overset{b}{\Sigma} q_0 = f(\overset{*}{h}_{ic}, \Delta H). \qquad (2.V)$$

Such a simplification of local relationships is possible since:

1. the usual measurements of the depth of snow cover on the ice are insufficiently conclusive due to the nonuniform distribution of the snow cover. The introduction, into the calculation, of the depth of the snow cover on the ice therefore does not usually improve the relationship for forecasting ice breakup;

2. the variations from year to year in the initial water stage H_0 are relatively small. The variations in the mean flow velocities depend on the value of ΔH. For the same value of ΔH, the variations in the width of the ice flanges and in the width of the ice cover, which has not adhered to the shores and to the bottom, are accordingly small;

3. the possible variations from year to year (during the melting period) in the intensity of heat input to the inner surface of the ice cover do not considerably influence the variations in the time of ice breakup.

The proportion between the effect of heat and stream force (as well as of the stage rise) on the ice cover is different for different rivers and years. Thus, in the large Siberian rivers, particularly in their middle and lower course, ice breaks up mainly due to high water. The high-water wave on these rivers is a result of the snow melting in the upstream, southern part of the river basin. Consequently, the time of ice breakup on these rivers is mainly determined by the time of the beginning and the intensity of the snow melting in the upstream part of the river basins. In the lower reaches of the Dnieper, Don and Volga the ice cover is destroyed mainly due to heat. Ice breakup on rivers issuing from lakes, e.g., the Neva, Svir', Volkhov, also occurs without any rise in the stage. The time of ice breakup on these rivers is determined by the time of the beginning of ice melting and the relation between the amount of heat necessary to melt the ice and the rate of heat input to it. However, ice breakup on most of the rivers is a result of the joint effect of the stage rise and of the thermal destruction of the ice, since the melting of the ice cover and of the snow cover in the given river basin usually begins almost simultaneously. It should be noted that in some years, depending on the direction of motion of the warming front, the main role may be played sometimes by the first and sometimes by the second of the above ice breakup factors. A characteristic example may be the Western Dvina (Daugava). If warm air masses move to its basin from the west, the ice is destroyed in the middle and lower course and only in the upper reaches ice breakup is due to the rise in the water stage. If warm air is transported to the upper reaches of the river from the southeast, the comparatively strong ice cover breaks up due to the high-water wave travelling downstream.

However, no matter the form of ice breakup on rivers, its cause is the input of heat to the ice and snow cover in the given river basin. Owing to the differences in the geographical location of rivers, direction of their flow, and in the orography and dimensions of their basins, in some cases the direct effect of heat on the ice cover and in other cases the melting caused in the basin and the formation of high water are of decisive importance.

B. SHORT-RANGE FORECASTING

§ 1. Calculation of the heat input to the ice cover and to the snow cover in the river basin

In the existing methods of forecasting ice breakup on rivers the heat input to the ice cover and to the snow cover in the river basin is allowed for either by introducing the characteristics of the air temperature, at which the melting of the snow and ice cover takes place, or by calculating the heat exchange from the meteorological data.

As the air temperature characteristic, we usually adopt the mean-diurnal positive temperature (during 13 hours) or the excess of the mean-diurnal temperature over some negative value of it, at which melting begins. The sums and the mean values of these temperatures during the melting periods are introduced into the calculation. In some methods the dates of the melting periods are introduced as an additional characteristic of the melting intensity.

The heat exchange can be calculated by means of the methods and formulas existing for the calculation of the components of the heat balance (see Handbook, No. 1, as well as Chapter VI of the present book).

The calculation of the heat exchange by means of nomographs, an example of which is shown in Figure 52, is widely used to forecast ice breakup.

With the aid of such a nomograph the heat exchange per unit (cm²) outer surface of the ice cover during daytime is determined for a given date and mean daytime air temperature. The heat exchange during the night is not introduced in the calculations. The values of the heat exchange obtained from the nomograph are taken as the specific daily amounts of heat exchange, q_0 cal/cm²·day. They consist of the specific amounts of radiant-heat input Q, the effective radiation I_{eff}, the turbulent heat exchange P, and the heat exchange by condensation or evaporation LE

$$q_0 = Q + I_{eff} + P + LE. \qquad (3.V)$$

With data for the calculation period available only for the mean-diurnal air temperature, when determining the value of q_0 from the nomograph it is possible to use the graph showing the relationship between the mean daytime temperature and the mean-diurnal temperature, obtained from data of observations in melting periods (of other years).

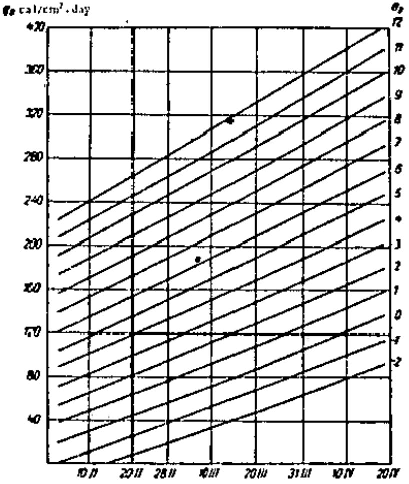

FIGURE 52. Nomograph for the determination of the specific heat exchange q_0 from the date and the mean-daytime air temperature θ_D for the district of Dnepropetrovsk.

When plotting the nomograph, the resulting amounts of heat exchange q_0 are calculated for the 15th of each month. The heat-exchange components Q, I_{eff}, P and LE can be calculated by means of the formulas used in the calculation of snow melting (see Manual, No. 1, and Chapter VI of the present book). In this case the values of I_{eff}, P, and LE, obtained by these formulas, should be multiplied by the length of the day expressed as a fraction of 24 hours k_d. The albedo, assumed constant for the melting period, is taken as its mean value of 0.50. The cloudiness and the mean-daytime wind velocity are assumed constant and equal to the mean-daytime values during the melting period obtained from the observation data at the meteorological stations of the particular region. The mean daytime vapor pressure of the air is determined from the graph that relates it to the mean daytime air temperature.

Such a nomograph was initially proposed and used for the calculation of snow melting. Calculation of the total snow melting by means of this nomograph gives values sufficiently close to the real figures.

As to the melting of the ice cover, in view of the peculiarities of this process compared with the melting of the snow cover, it cannot be affirmed that the use of such a nomograph gives results close to the real figures. In addition, on rivers considerable melting of the ice cover also occurs at the inner surface of the cover due to heat input from deeper layers of water. The latter possibility is not taken directly into account in forecasting methods of ice breakup. Therefore, independently of the accuracy of the calculation of the melting due to heat exchange through the outer surface, the heat sums obtained by means of the nomographs described should, apparently, be considered as relative characteristics of the ice cover melting.

Experience shows that allowance for the heat exchange only during daytime in the empirical relationships for the forecasting of the ice breakup on rivers nevertheless gives better results than an allowance for the heat exchange during the whole day (24 hours). These heat sums should also be considered as relative characteristics when considering the melting of the ice cover on lakes and storage reservoirs (Chapter VI) in the absence of a snow cover on the surrounding terrain. This is due to the fact that under these conditions considerable variations in wind velocity, air temperature and air humidity may take place over the surface of the ice cover.

Example of plotting the nomograph. Let us plot the nomograph from the data of the Dnepropetrovsk meteorological station. We calculate the heat-exchange components Q, I_{eff}, P, LE (cal/cm²·day) from

$$Q = 0.50Q'(1 - 0.47N_l - 0.20N_t), \qquad (4.V)$$

where Q' is the sum of maximum possible solar radiation, determined from Table 30; N_l is the low-level (daytime) cloudiness, expressed as a fraction of unity, and is determined from $N_l = \frac{N_{l,7} + 2N_{l,13} + N_{l,19}}{4}$.* N_t is the total (daytime) cloudiness, expressed in the ten-point scale, and is determined from $N_t = \frac{N_{t,7} + 2N_{t,13} + N_{t,19}}{4}$ (the albedo in formula (4.V) is taken equal to 0.50);

$$I_{eff} = k_d\left[-661 + \sigma T_a^4(0.76 + 0.11N_l + 0.10N_t)\right], \qquad (5.V)$$

where k_d is the length of the day expressed as a fraction of 24 hours determined from Table 31, σT_a^4 is the black-body radiation determined from the air temperature θ at the meteorological station (from Chapter I, Table 6).**

$$LE + P = k_d(7.02 + 3.84v)(\theta + 1.54e - 9.4),$$

---

* The indices 7, 13 and 19 denote the hours of observation.

** The values of I_{eff} can also be determined by means of Chapter VI, Figure [illegible].

where w is the mean daytime wind velocity at the meteorological station as measured at the height of the anemometer in m/sec $\left(w = \frac{w_I + 2w_{II} + w_{III}}{4}\right)$, θ is the mean daytime air temperature, and e is the mean-daytime vapor pressure of the air (mb) at the meteorological station at a height of 2 m

TABLE 30. Maximum possible density of total (direct plus scattered) solar radiation Q' on the 15th of the month, cal/cm²·day

Latitude, degrees	I	II	III	IV	V
40	325	415	550	680	—
45	210	320	460	610	—
50	115	220	390	570	660
55	72	170	330	510	675
60	50	130	296	475	645
65	—	65	240	446	647
70	—	58	200	445	650

We calculate the parameters for the middle of each month (in the present case February, March and April) for each whole degree of the mean daytime air temperature from −2° to +12°.

TABLE 31. Day (time) length expressed as a fraction of 24 hours (k_d) on the 15th of the month

Month	Latitude, degrees						
	40	45	50	55	60	65	70
I	0.40	0.38	0.36	0.32	0.28	—	—
II	0.45	0.44	0.42	0.40	0.35	0.35	—
III	0.50	0.49	0.49	0.49	0.49	0.49	0.49
IV	0.55	0.56	0.57	0.59	0.61	0.63	0.65
V	—	—	0.64	0.67	0.71	0.78	0.86

Let us start by finding the values of q_0 for 15 February

From long-time observation data at the Dnepropetrovsk meteorological station we find for the mean daytime values of the low-level and total cloudiness and of the wind velocity during melting days in February $N_l = 0.55$, $N_t = 0.73$, $w = 4.5$ m/sec. We use the observation data for the same days to plot a graph relating the mean daytime pressure of the water vapor of the air to the mean daytime air temperature.

Let us determine the value of Q. By means of Table 30 we obtain that the maximum possible flux of solar radiation for the latitude 48° on 15 February is 250 cal/cm²·day. Formula (4.V) gives for $N_l = 0.55$ and $N_t = 0.73$, $Q = 75$ cal/cm²·day. Since solar radiation is independent of air temperature, we write the same value obtained for Q in the columns of each air temperature (Table 32).

From (5.V) we determine the value of I_{eff} for each air-temperature value from −2 to +12°. For the middle of February at a latitude of 48° we find, from Table 31, $k_d = 0.43$. We find the values of σT_a^4 for each value of the air temperature from Table 6 (Chapter I). For example, for an air temperature $\theta = 2°$ we obtain, from Table 6, $\sigma T_a^4 = 680$ cal/cm²·day. Calculating with formula (5.V) for $N_l = 0.55$ and $N_t = 0.73$, we obtain the values of I_{eff} given in Table 32.

TABLE 32. Table for use in plotting the [illegible] in Figure [illegible]

Heat-exchange components, cal/cm²·day	Mean daytime air temperature, θ														
	−2	−1	0	1	2	3	4	5	6	7	8	9	10	11	12
Q	75	75	75	75	75	75	75	75	75	75	75	75	75	75	75
I_{eff}	−37	−34	−30	−26	−23	−19	−15	−12	−7	−3	1	5	9	13	16
$LE + P$	−37	−24	−9	5	19	33	47	61	74	88	102	116	130	144	158
q_0	1	17	36	54	71	89	107	124	142	160	178	196	214	232	249

From (6.V) we calculate the values of $LE + P$. The water pressure of the air is obtained from the graph $e = f(\theta)$, based on the observation data from the Dnepropetrovsk meteorological station (the graph is not given here). For $k_d = 0.43$ and a wind velocity (at the height of the anemometer) of 4.5 m/sec we obtain from (6.V) the values of $LE + P$ given in Table 32.

Summing for each air temperature the values of Q, I_{eff}, and $LE + P$, we obtain the values of q_0 (Table 32).

The calculation of q_0 for the middle of the next month (in our example for 15 March and 15 April) is similar.

The values of q_0 are plotted on a graph whose abscissa marks the date and ordinate the specific heat exchange q_0. The points obtained for each value of the air temperature are connected by a straight line (Figure 52).

§ 3. Forecasting the first ice-cover push

In practice, forecasting of two elements of the ice push are usually required: the date of its beginning and the water stage at which it occurs.

At present we still do not always have long-time regular observations of the water stage at the moment of ice push. When working out a forecasting method one has, in most cases, to operate with the water stages observed at the standard observation hours which, no doubt, lowers the accuracy of the method.

If the ice breakup develops during a rise in the water stage, the stage H_p at which the ice push occurs is determined mainly by the highest position of the ice cover during the winter, i.e., by the maximum winter stage H_w. Therefore, the following relationship is used in the technique of forecasting ice push which takes place during a rise in the water stage

$$H_p = f(H_m).$$

Figure 53 gives the dependence of the water stage in the first ice push on the highest stage during the stable ice period for the Lena River at Solyanka. This dependence can be used for:

1) long-range forecasting of the minimum (a) and of the most probable (b) water stage in the first ice push,

2) short-range forecasting of the date of ice push.

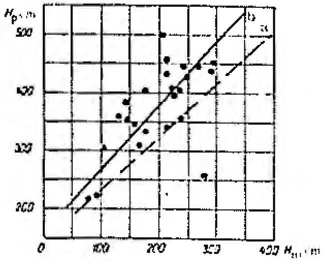

FIGURE 53. Water stage H_p during ice push on the Lena River at Solyanka as a function of the maximum winter stage H_m.

Having determined from the line b the most probable stage, it is possible to calculate the date of its beginning.

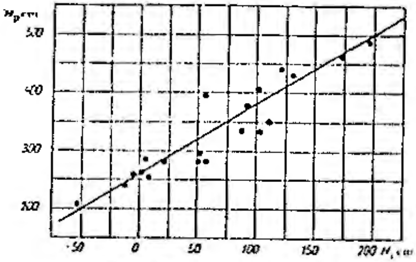

FIGURE 54. Water stage during the first ice push on the Lena River at Krestovskaya, H_p, as a function of the mean water stage during the first 5 days of the stable ice period, H_m.

Similar relationships can also be obtained for the forecast of the ice push on a river stretch. In these cases, the earliest ice push on the river stretch and the corresponding stage at a reference gaging site are determined.

The water stage at the first ice push can also be determined from its relationship with the water stage at the beginning of the stable ice period. This stage characterizes the freezing conditions and to some extent determines the ice breakup on the river.

Figure 54 gives the dependence of the stage during ice push on the Lena River at Krestovskaya on the mean stage during the first 5 days of the stable ice period.

On rivers where ice push is preceded by significant heat input, this should be taken into account in short-range forecasting of the date and stage of ice push. The input characteristics may be the sum of the positive air temperatures, the amount of heat which arrived at the ice cover [illegible]

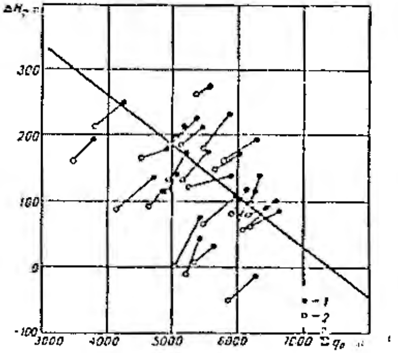

FIGURE 55. Relationship between the rise ΔH_p of the [illegible] on the Amur River at Komsomol'sk [illegible] above the maximum winter stage and the total heat input $\sum^{p} q_0$ on the day of [illegible].

1 — ΔH and $\sum q_0$ on the day of ice push, 2 — ΔH and $\sum q_0$ on the preceding day.

As an example we give the technique of forecasting the ice push on the Amur River at Komsomol'sk (Figure 55). In this case the date of the beginning of ice push is determined from the relationship between the total heat input $\sum^{p} q$ and the rise in the water stage ΔH_p over the maximum winter stage on the day of ice push

$$\Delta H_p = f\left(\sum^{p} q\right).$$

---

* [illegible] of [illegible] water discharges and stages are described in the Manual, No. 1.

The value of $\overset{2}{\Sigma q}$ is determined by means of a nomograph similar to that described in § 2 and based on the data from the Komsomol'sk meteorological station. The water stage is determined from the stage-rise tendency during the preceding period, with a forewarning period of up to 5 days.

For a more correct drawing of the relationship line, the points $(\Delta H, \Sigma q)$ are plotted on the graph (Figure 55) for two days: the day of ice push and the preceding day.

§ 3 Forecasting ice breakup

The ice cover on most rivers flowing from south to north (Ob', Irtysh, Yenisei, Northern Dvina, etc.) breaks up mainly due to the high water formed in the upstream part of the river basin.

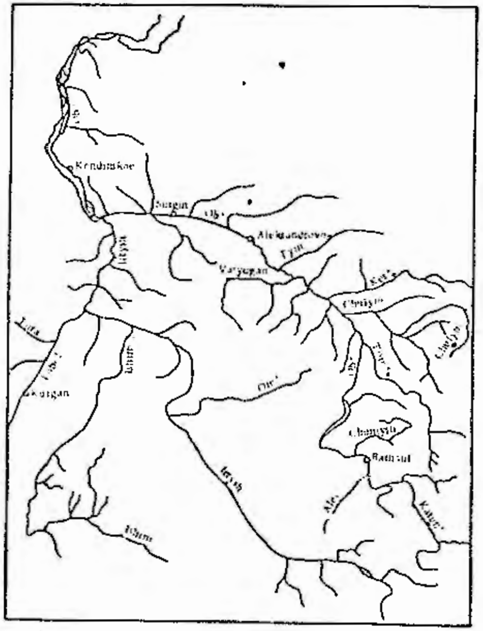

FIGURE 56. Drainage net of the Ob' River

The time of ice breakup on these rivers is determined mainly by the time of the beginning and the intensity of the snow melting in the headwaters, as well as by the rate of propagation of the thawing front downstream the river.

The supply of water, sufficient to form a high-water wave that breaks up the ice cover, is caused by the arrival, on the upstream part of the river basin, of a definite amount of heat which can be approximately expressed by the equivalent sum $\Sigma\theta_{+}$ of positive air temperatures. For some rivers it is assumed constant, for others it is assumed to depend on the water yield of a given river basin. The recorded date of this sum is the main term in the expression for the determination of the ice breakup date for a downstream river stretch. The lower along the stream the point is situated for which a forecast of ice breakup is prepared, the longer the forewarning period.

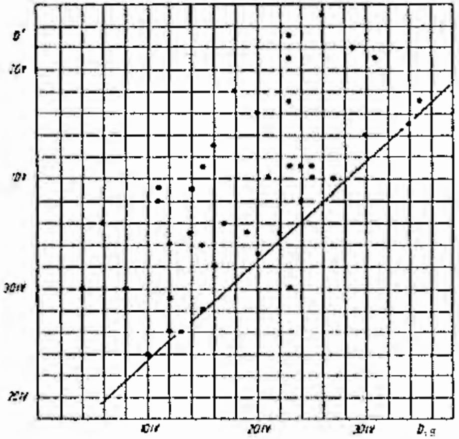

FIGURE 57. Correlation between early possible date of ice breakup on the Ob' River at Aleksandrovo, D', and the date of accumulation of $\Sigma\theta_{+} =$ [illegible], D_g at Barnaul

In many cases, ice breakup can be predicted on the basis of actual air-temperature data without using the meteorological forecast.

The factors which determine the beginning of the local runoff and of the degree of destruction of the ice cover in a given stretch are allowed for in different ways, depending on the distance of the stretch from the region where high water begins.

As examples we consider forecasts of ice breakup for the Ob' River at Aleksandrovo and for the Northern Dvina and Bereznik.

Example 1. The time of the ice breakup on the Ob' at Aleksandrovo (Figure 56) depends on the time of the beginning of snow melting, the intensity of high-water wave in the headwaters of the river and on the rapidity of its propagation on all the remaining parts of the basin upstream from Aleksandrovo.

As the main terms in the expression for the determination of the ice-breakup date D we take: (1) the recorded date of a sum of positive air temperatures equal 30° (D_{B}) (measured at Barnaul); and (2) the length in days of the period from the date of accumulation of $\Sigma\theta_+ = 30°$ at Barnaul to the date of accumulation of $\Sigma\theta_+ = 15°$ at Surgut (D_{S}), i.e., ($D_{\text{S}} - D_{\text{B}}$).

At both stations $\Sigma\theta_+$ is calculated from the mean-diurnal data. The following dates are used as the dates for which the air temperature passes through 0°: at Barnaul the date taken is that after which there were coolings shorter but no longer than 3 days, but with a sum of negative temperatures exceeding the already accumulated sum of positive temperatures; at Surgut the date taken is that after which there was not more than one day with a negative temperature (not lower than −3.0°).

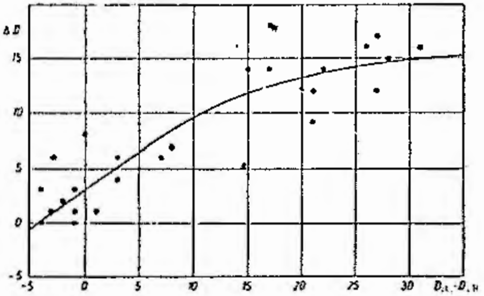

FIGURE 57. Relationship between correction ΔD to the early possible date of ice breakup D' on the Ob' River at Aleksandrovo and the factor of rapidity of heat propagation over the basin $D_{\text{S}} - D_{\text{B}}$.

The line of the relationship $D' = f(D_{\text{B}})$ was drawn in Figure 57 along the lower edge of the field of the points (D', D_{B}) and gives the earliest possible ice-breakup date D' for a given value of D_{B}. The earliest possible ice breakups are observed during particularly early and rapidly developing springs.

The latter are the cases when towards the date D_{B} thawing periods of a duration more or equal to 6 days, during $\Sigma\theta_+ \geqslant 9°$, have already been observed at Surgut. In these cases ice breakup begins on the average on the next day after the early possible date, i.e., $D = D' + 1$.

In all other cases, a correction of ΔD in days, depending on the rapidity of the heat propagation over the river basin, i.e., depending on the value of $D_{\text{S}} - D_{\text{B}}$, is introduced in the early possible date D' for determining the ice-breakup date D (Figure 58).

If at Surgut the day after $\Sigma\theta_+ = 15°$ the air temperature drops below 0°, ice breakup at Aleksandrovo is delayed. The length ΔD_1 of this delay is determined from Figure 59 as dependent on the duration of the cooling period.

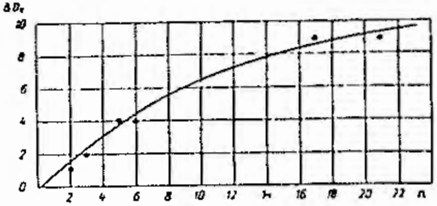

FIGURE 59. Variation of correction for cooling ΔD_1 with the number of days n of negative air temperature at Surgut.

In those cases when the forecast is prepared for a point on a river downstream from the mouth of a large tributary, the influence of the latter should be taken into consideration.

Thus, for example, the ice breakup on the Ob' River downstream from the mouth of the Irtysh is mainly affected by the arrival of the flood wave of the Tobol tributary. Therefore, the date of accumulation of $\Sigma\theta_+ = 30°$ at (D_{K}) Kurgan and the difference $D_{\text{S}} - D_{\text{K}}$ are taken as the main terms in the expression for forecasting ice breakup on the Ob' at the village of Kondinskoe.

Example 2. Ice breakup on the Northern Dvina at Bereznik is caused by the rise in the water stage as a result of the arrival of water from the Vaga River, as well as of the advance of the flood wave from the headwaters of the Northern Dvina.

The amount of heat necessary to cause a rise in the water stage sufficient for ice breakup depends on the degree of destruction of the ice cover and on the water-yielding capacity of the snow.

This amount of heat is expressed by the sum $\Sigma\theta_+$ of positive air temperatures, and the preceding conditions by the mean air temperature during the 10 days until they take on positive values, $\left(\frac{\sum_{1}^{10} t}{10}\right)$.

All the temperature characteristics are determined from the data of the Shenkursk meteorological station, which is situated at the lower course of the Vaga River. The quantity $\Sigma\theta_+$ is calculated for the period from when air temperature takes on positive values to ice breakup, except the last 5 days $(\overset{i-5}{\Sigma\theta_+})$. As transition period in the calculation, we use the passage of the mean-diurnal air temperature to positive values, after which a mean-diurnal negative temperature is observed not more than 3 days. In the calculation of $\Sigma\theta_+$, thawing periods in March and April are also included with a coefficient of 0.5

Thus, the forecast is prepared on the basis of the graph shown in Figure 60

$$\sum^{t-5}\theta_+ = f\left(\frac{\sum_{1}^{10}\theta}{10}\right).$$

Ice breakup, as follows from the definition of the necessary $\Sigma\theta_+$, starts 5 days after accumulation.

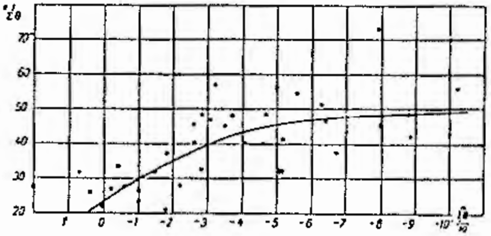

FIGURE 60. Sum $\sum^{t-5}\theta_+$ of mean-diurnal positive air temperatures (without the temperatures during the 5 days before the breakup) necessary for the breakup of the ice on the Northern Dvina at Bereznik as a function of the mean air temperatures $\frac{\sum_{1}^{10}\theta}{10}$ during the 10 days before they take on positive values.

If the flood develops simultaneously on the Vaga and on the Northern Dvina rivers, ice breakup at Bereznik will be accelerated. If, during the 3 days until the accumulation of the necessary sum $\Sigma^{t-5}\theta_+$, the water stage in the upstream part of the river basin (the Ust'-Kur'e gaging site) rises over the winter stage by 1 m and more, ice breakup at Bereznik occurs a day earlier on the average.

With a forewarning period of up to 5 days, ice breakup forecasts can be prepared without using the air temperature forecast. When the air-temperature forecast is used, the forewarning period of ice break-up forecasts can be increased to 9–10 days.

Besides rivers which flow from the south to the north, on many small and medium rivers and on the headwaters of large rivers ice breaks up due to the rise in the water stage and if the rate of high-water travel is high. Since the time of flow there is small and the local runoff plays a great role, ice-breakup forecasts for these rivers are prepared by using the air temperature forecast, with a forewarning period of about 5 days.

The stage rise necessary for ice breakup depends on the thickness and strength of the ice cover. The thicker and stronger the ice cover, the larger the rise necessary for its destruction.

The rise of water stage before ice breakup is either predicted or, more often, is allowed for indirectly by means of various heat-inflow characteristics. These characteristics also take into account the thermal destruction of the ice, which takes place on most of these rivers.

Sometimes it is sufficient to use only a qualitative characteristic of stage rise, for example, the rise of water stage above a definite datum line (often the datum line of the water overflow to floodplain), or the date at which the stage rise reached a certain value.

In the absence of data on the thickness of the ice cover over many years, the sum of the negative air temperatures during the stable ice period or during a part of the stable ice period, in the course of which the main growth of the ice takes place, is introduced in the relationship used for ice breakup forecasting.

In order to characterize the strength of the ice sheet, often the mean air temperature during some period until the passage through 0° which is used in the calculation (during 10–20 days, sometimes more) is introduced in the relationship. This serves, at the same time, to characterize the water-yielding capacity of the snow cover on the given river basin.

In rivers flowing in regions with a severe winter, the thickness of the ice sheet is always large and varies only relatively little from year to year. Therefore, in forecasts of ice breakup on these rivers, the thickness of the ice cover can be neglected.

Let us consider some examples.

To forecast ice breakup on the Oka River at the town of Kaluga (Figure 61) the following relationship is used

$$\Delta H_b = f(\Sigma\theta_-, \Sigma\theta_+),$$

where ΔH_b is the rise of the water stage during breakup over the minimum winter stage (the value of ΔH_b is predicted by any of the existing methods),* $\Sigma\theta_-$ is the sum of the mean-diurnal negative air temperatures from the date of the beginning of the stable ice period to the passage of the air temperatures through 0°, $\Sigma\theta_+$ is the sum of the mean-diurnal positive air temperatures until ice breakup. It includes the sum of the positive temperatures from the last passage through 0° (used in the calculation) before ice breakup, as well as the sum of the positive temperatures during thawing periods with some coefficient k. If from the end of the thaw till the passage (used in the calculation) through 0° not more than 10 days passed, then $k = 0.5$, if 11–20 days passed, then $k = 0.2$. Further thaws are disregarded.

The forecast is prepared by successive approximations as follows. Knowing $\Sigma\theta_-$ for the stable ice period and with forecasts of the water stage and air temperature on hand, we predict the breakup date. We determine from the forecast for this date the values of ΔH and $\Sigma\theta_+$. If the point $(\Sigma\theta_-, \Delta H_b)$ lies on the graph in accordance with the value of $\Sigma\theta_+$, the chosen date will be the date of ice breakup. If the point $(\Sigma\theta_-, \Delta H_b)$ lies higher than the place where it should be according to the value of $\Sigma\theta_+$, then breakup may occur earlier than the chosen date, if it lies lower, ice breakup occurs later. In these cases the calculation is repeated.

Ice breakup on the Ob' River in its middle and upper course is always due to the rise of the water stage. This rise is caused both by the arrival of high water wave from the upper reaches of the river and by the local inflow [from tributaries].

---

* See Manual, No. 1

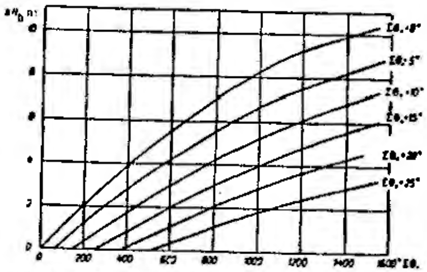

FIGURE 61. Rise of water stage above the winter minimum, necessary for ice breakup on the Ob' River at the town of Kaluga, ΔH_b, as a function of the sum of the mean-diurnal negative air temperatures during the stable ice period, $\Sigma\Theta_-$, for various values of the sum of the mean-diurnal positive air temperatures until ice breakup $\Sigma\Theta_+$.

Ice breakup on the Ob' River at the village of Polovskoe was found to occur as a result of a rise in the water stage above the winter minimum of not less than 4.5 m. This is the mean rise at which bankful stage develops on the Ryazan'-Polovskoe river stretch. In order to increase the forewarning period of the forecast, the rise is determined according to the Ryazan' gage. The time interval between a 4.5 m rise in the water stage at Ryazan' and ice breakup at Polovskoe varies from 1 to 12 days and depends on the thickness of the ice cover and on the meteorological conditions.

The ice-breakup date is determined by means of the relationship (Figure 62)

$$\sum_{\Delta H=4.5} q_0 = f(h_{ic}),$$

where $\sum_{\Delta H=4.5} q_0$ is the amount of heat input per unit outer surface of the snow-ice cover during the period from the 4.5 m rise date to the date of ice breakup (calculated from a nomograph similar to that described in § 1 and based on data from the Ryazan' gage and meteorological station), h_{ic} is the maximum ice thickness.

In cases when the use of the actual date of the 4.5 m level rise does not provide the necessary forewarning period, it is possible to use the forecast of the water stage prepared on the basis of the stage rise tendency.

Ice breakup is predicted as follows. Knowing the value of h_{ic}, we determine from Figure 62 the value $\sum_{\Delta H=4.5} q_0$ necessary for ice breakup. Knowing the date of the 4.5 m rise, or determining it from the forecast, we find from the air-temperature forecast the date of accumulation of the necessary value of $\sum_{\Delta H=4.5} q_0$. This will be the date of the ice breakup on the river.

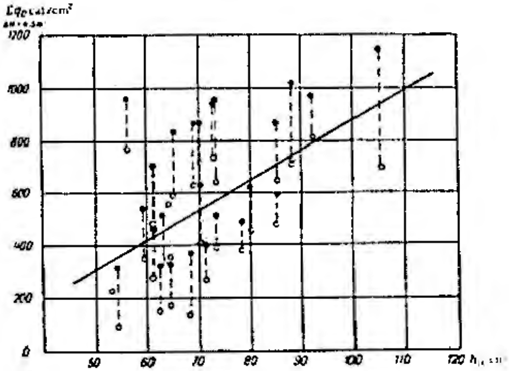

FIGURE 62. Amount of heat input during the time interval between a 4.5 m rise in the water stage at the town of Ryazan' and ice breakup on the Ob' River at the village of Polovskoe, $\sum_{\Delta H=4.5} q_0$, as a function of the maximum ice thickness at Ryazan', h_{ic}.

● – $\sum_{\Delta H=4.5} q_0$ includes the value of q_0 during the day of ice breakup, ○ – $\sum_{\Delta H=4.5} q_0$ without the value of q_0 for the day of ice breakup.

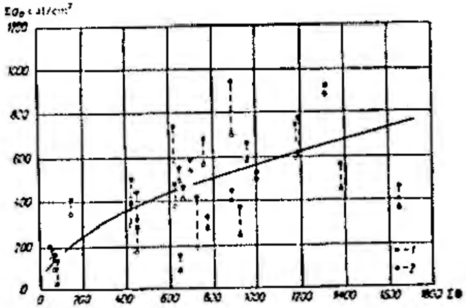

FIGURE 63. Amount of heat Σq_0, necessary for ice breakup on the [illegible] River at the village of [illegible], as a function of the sum $\Sigma\Theta_-$ of [illegible] negative temperatures during the stable-ice period.

1 – Σq_0 includes the value of q_0 during ice breakup day, 2 – Σq_0 without the value of q_0 of ice breakup day.

The relationship for the forecasting of the ice breakup on the Oskol River at Ninovka (Figure 63) is

$$\Sigma q_0 = f(\Sigma \theta_-),$$

where Σq_0 is the amount of heat input to the outer surface of the ice cover starting at the date after which periods of cold either did not return at all, or were so weak and short that they did not substantially affect the formation of the flood; $\Sigma\theta_-$ is the sum of the mean-diurnal negative air temperatures during the stable-ice period.

The values of Σq_0 are calculated from a nomograph similar to that described in § 1.

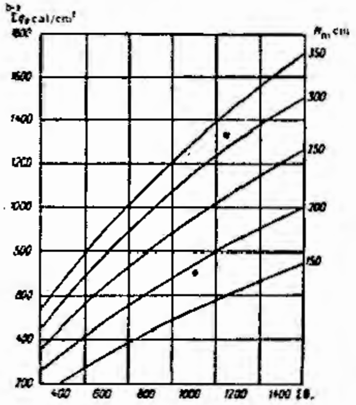

FIGURE 64. Amount of heat necessary for ice breakup on the Western Dvina River at the town of Surazh (without the three days before ice breakup, $\overset{b-3}{\Sigma q_0}$) as a function of the sum of the mean-diurnal negative air temperatures during the stable-ice period, $\Sigma\theta_-$, for several values of the maximum winter water stage H_m.

Relationships of this kind are used to forecast ice breakup on many small rivers. In some relationships the values of Σq_0 are calculated from the date of the beginning of a stable rise in the water stage.

On rivers where the water stage and the flow velocity in the period of the autumn ice drift vary from year to year within wide limits, the degree of winter frazil-ice deposition on river bed and the thickness of the ice cover considerably vary. In the relationships used to forecast ice breakup on such rivers, the absence of long-time data on the ice-cover thickness, it is therefore expedient to introduce, in addition to the sum of the negative air temperatures during the stable ice period ($\Sigma\theta_-$), the height of the water stage at the beginning of the stable-ice period. As an additional characteristic of the ice thickness, instead of the water stage at the beginning of the stable ice period, we may use the medium or maximum (H_m) water stage during the stable-ice period (until the beginning of the spring rise).

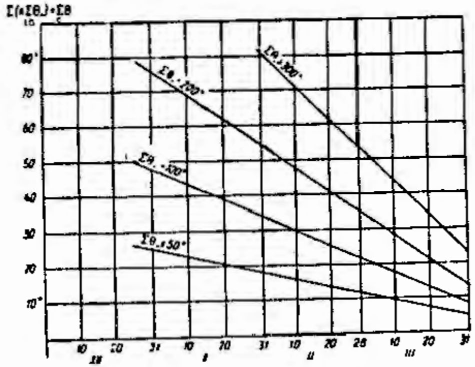

FIGURE 65. Graph used to forecast ice breakup on the Dnieper at the town of Kherson before the runoff control works were carried out (the air temperature is taken as measured at 13 hours).

The relationship $\Sigma q_0 = f(\Sigma\theta_-, H_m)$ has been worked out for forecasting ice breakup on the Lower Volga and successfully used until the construction of the Volga Hydroelectric Plant im. XXII Congress of the CPSU. At the present time such relationships are used, in particular, to forecast ice breakup on the headwaters of the Western Dvina.

As an example we give in Figure 64 the relationship for forecasting ice breakup on the Western Dvina at the town of Surazh. In this case the quantity $\overset{b-3}{\Sigma q_0}$ also includes the heat input during thaws, but does not include the heat input during the last 3 days before ice breakup. Ice breakup on the upper course of the Western Dvina is associated with a rise in the water stage. However, the magnitude of the stage rise varies only little and therefore in forecasting ice breakup, it may be neglected.

To forecast the ice breakup on rivers which flow in regions with a soft winter poor in snow and with frequent thaws graphs are used (Figure 65)[*]

---

[*] The graph in Figure 65 was based on data of observations on the Dnieper at the town of Kherson during the years before runoff control by the Dneprostroi reservoir. As a result of this runoff control the ice regime of the Dnieper on this stretch changed.

which can be represented by the equation

$$\sum_{c}\theta_{+}+\sum\Big(k\sum_{th}\theta_{+}\Big)=f(D,\ \Sigma\theta_{-}),\qquad (7.\mathrm{V})$$

where $\sum_{c}\theta_{+}$ is the sum of the daily positive air temperatures during the period from the theoretical passage through 0° until ice breakup, (the theoretical transition date is the date of the beginning of the warming (up to a positive temperature) which causes ice breakup); $\sum_{th}\theta_{+}$ is the sum of the daily positive temperatures of each thaw, k is a factor (smaller than unity) which is determined for each thaw; $\Sigma(k\sum_{th}\theta_{+})$ is the sum of the quantities $k\sum_{th}\theta_{+}$ during the stable ice period; D is the theoretical date for which the air temperature passes through 0°; $\Sigma\theta_{-}$ is the sum of the mean-diurnal negative air temperatures during the stable ice period.

It is recommended to determine the values of $\sum_{c}\theta_{+}$ and $\sum_{th}\theta_{+}$ from the daytime temperatures (for example as measured at 13 hours).

The values of $[\sum_{c}\theta_{+}+\Sigma(k\sum_{th}\theta_{+})]$ are plotted on the ordinate* and the values of D on the abscissa; $\Sigma\theta_{-}$ are the parameters of the curves. The factor k for each thaw represents the ratio of the value of $f(D,\ \Sigma\theta_{-})$, corresponding to the date D of the theoretical date of transition of the air temperature through 0° (see Figure 65), to the value of $f(D,\ \Sigma\theta_{-})$, corresponding to the date of the beginning of the given thaw for the same value of $\Sigma\theta_{-}$ (for the date of the theoretical transition).

TABLE 33. Example of calculating the sum of positive air temperatures necessary for ice breakup, using the date of theoretical transition $\Big(\sum_{c}\theta_{+}\Big)$

Year	Date of beginning of stable ice	Date of theoretical transition	$\Sigma\theta_{-}$ deg.	Date of beginning of the thaw	$\Sigma\theta_{+}$ during thaw, deg.	$f(D,\ \Sigma\theta_{-})$ deg.	k	$k\sum_{th}\theta_{+}$ deg.
1	2	3	4	5	6	7	8	9
1933	12 I	14 III	251			32.0		
				18/I	1.2	80.0	0.40	0.5
				29/I	16.1	70.0	0.46	7.4
				11/II	1.2	59.0	0.54	0.6
				14/II	6.8	56.5	0.57	3.9
				23/II	4.5	48.0	0.67	3.0
				4/III	7.4	41.5	0.77	5.7

$$\sum\Big(k\sum_{th}\theta_{+}\Big)=21.1^\circ\approx 21^\circ$$

The sum of the positive air temperatures, necessary for ice breakup, calculated from the transition date, is determined from equation (7.V)

$$\sum_{c}\theta_{+}=f(D,\ \Sigma\theta_{-})-\sum\Big(k\sum_{th}\theta_{+}\Big).\qquad (8.\mathrm{V})$$

---

* Two values, one including the value of θ_{+} of the breakup day and the other without it.

Let us consider the example of calculation of $\sum_{c}\theta_{+}$, made in connection with the ice breakup forecast for 1933 at the town Kherson on the Dneper (Table 33).

Knowing the date of the beginning of the stable ice period and the predicted date of the transition of the air temperature through 0°, we determine the quantity $\Sigma\theta_{-}$ during the stable ice period (during the period between the indicated dates); it is equal to 251°. We record the dates of the beginning of thaws observed in the stable ice period. For each thaw from the observation data at 13 hours we determine the sum of the daily positive air temperatures. Further, for the value 251° of $\Sigma\theta_{-}$ we find on the ordinate of Figure 65 the value of $f(D,\ \Sigma\theta_{-})$ for the predicted date of the transition (the 1st figure in column 7) and for the dates of each thaw (the following figures in column 7). We determine the values of k; for this purpose we divide the value of $f(D,\ \Sigma\theta_{-})$ for the date of the transition (32°) by the value of $f(D,\ \Sigma\theta_{-})$ for each thaw. For example, in order to obtain the factor for the thaw which began on 18 January, we divide 32° by 80°, obtaining $k=0.40$. Then we find the values of $k\sum_{th}\theta_{+}$ for each thaw and, summing, obtain $\Sigma(k\sum_{th}\theta_{+})=21°$. Substituting in equation (8.V) the value of $f(D,\ \Sigma\theta_{-})$ for the date of the transition and the value of $\Sigma(k\sum_{th}\theta_{+})$, we obtain for the required value of $\sum_{c}\theta_{+}$

$$\sum_{c}\theta_{+}=32^\circ-21^\circ=11^\circ.^*$$

In order to determine the date of ice breakup we have to find the date of accumulation of the sum of the 13 hours positive air temperatures, equal to 11°.

To obtain the calculation graph (Figure 65), a similar graph is initially plotted for cases when, in the stable ice period until the theoretical transition, there were insignificant thaws or no thaws at all. This graph serves to determine the factors k to a first approximation. We determine the values of k in the same way as in the calculation of the breakup date (see above). Knowing the approximate values of k, we calculate the values of $\Sigma(k\sum_{th}\theta_{+})$. Adding to the latter the values of $\sum_{c}\theta_{+}$ from the actual data, we obtain the values of $[\sum_{c}\theta_{+}+\Sigma(k\sum_{th}\theta_{+})]$ necessary for plotting the calculation graph. From these values, as well as from the dates of the transition and from the sums of the negative air temperatures during the stable ice period, we plot the first-approximation graph. From it we correct the values of the factors k and repeat the calculation of the quantities $\Sigma(k\sum_{th}\theta_{+})$.

Using the latter, we plot the second-approximation graph similarly to the first-approximation graph. The second graph is used for calculation.

If rivers for which the above forecasting method is used have a high water-stage rise with ice breakup occurring before $\sum_{c}\theta_{+}$ is recorded, the breakup forecast is prepared in accordance with the forecast of the water-stage rise up to the critical stage for ice breakup (for the given conditions).

The critical stage rise for ice breakup is connected with the form of the river bed. For a given river stretch it depends mainly on the thickness of the ice cover and its strength, as well as on the water stage before its critical rise and in general on the water stage in the stable ice period. Among the methods for determining the critical water stage rise we mention the following. On a graph, whose abscissa gives the ice thickness h_{ic} or the value of $\Sigma\theta_-$ during the stable ice period, and whose ordinate gives the stage rise before ice breakup (over the minimum stable stage), ΔH, the points $(h_{ic}, \Delta H)$ or $(\Sigma\theta_-, \Delta H)$ are plotted for all the breakups whose data have been used in setting up the relationship (7.V). On this graph we distinguish between cases of ice breakup before recording of the value of $\Sigma\theta_c$ determined from Figure 65. The points representing these cases usually lie in the upper part of the field. These points are connected by a line by the following relationship

$$\Delta H = f(h_{ic})$$

or

$$\Delta H = f(\Sigma\theta_-).$$

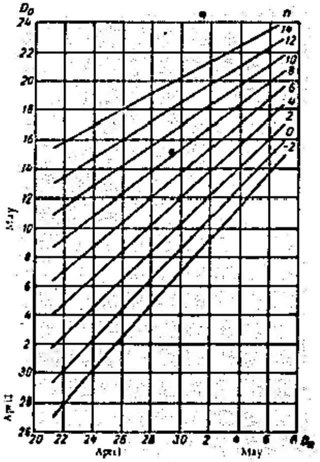

FIGURE 66. Date of ice clearing of the Zeya River at the village of Mazanovo D_o, as a function of the time of the beginning of ice pushes at Mazanovo D_p, for several values of the number of days from the beginning of ice pushes at Zeiskie Vorota to the beginning of ice pushes at Mazanovo, n.

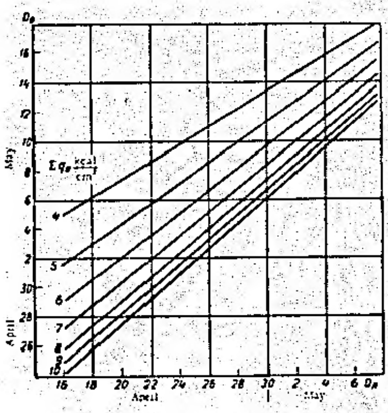

FIGURE 67. Times of ice clearing of the Amur at Ekaterino-Nikol'skoe, D_o, as a function of the time of the beginning of ice drift at the same point, D_d, for various values of the total heat input to the ice cover through its upper surface, Σq_s.

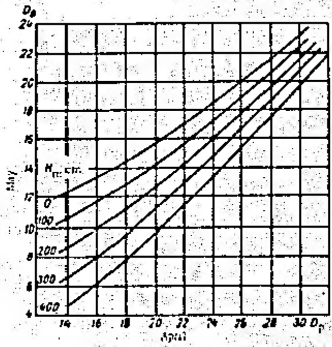

FIGURE 68. Time of ice breakup on the Amur at the village of Bogorodskoe, D_o, as a function of the time of the beginning of ice push, D_p, for several values of the maximum water stage of the spring high water on the Amur at Khabarovsk, H_{max}.

§ 4. Forecasting ice clearing (freeing)

The duration of ice drift on rivers (after ice breakup) is wholly determined by the climatic peculiarities of the different parts of the basin, the direction and velocity of the stream and its tributaries, and the presence of lakes in the river system. On rivers where ice breakup advances downstream, the spring ice drift is, as a rule, shorter, other conditions being equal, than on rivers whose ice breakup advances upstream.

The yearly variation in the duration of the spring ice drift on each given river stretch is determined by the thickness of the ice cover and by the extent to which it is destroyed toward the beginning of ice drift (toward the date of ice breakup), the character of the breakup, the amount of water in the river and, finally, the meteorological conditions in the period of ice drift.

We give below examples of methods of forecasting ice clearing of rivers.

The time of ice clearing on the Zeya River at Mazanovo depends on the time of appearance of the first ice pushes at Mazanovo and at Zeiskie Vorota (380 km upstream from Mazanovo) (Figure 66).

The time of ice clearing on the Amur River at Ekaterino-Nikol'skii depends on the date of the beginning of ice drift and on the total heat input to the ice cover through its outer surface, $\Sigma\varphi_n$, at a date preceding the date of the beginning of ice drift (Figure 67).

The time of ice clearing on the Amur River at the village of Bogorodskoe (in its lower course) depends on the date of ice push and on the maximum level of the spring high water at the town of Khabarovsk (Figure 68).

C. FORECASTS TAKING INTO ACCOUNT THE DEVELOPMENT OF THE ATMOSPHERIC PROCESSES (LONG-RANGE FORECASTS)

For a number of years long-range forecasts of ice breakup on rivers were prepared by a technique according to which the breakup time was determined as dependent on the type of the atmospheric circulation (see Chapter I, Part C, § 7), and on the water temperature in the northern part of the Gulf Stream. The physical basis for the use of the latter characteristic lies in the fact that the high water temperature in the northern part of the Gulf Stream, where the maximum heat transfer from the water to the air in the winter months occurs, contributes to the appearance of a stable positive air-temperature anomaly over this region and of a negative anomaly over the ETS. The latter is connected with the formation of a high-altitude pressure ridge over warm waters of the Atlantic; along the eastern periphery of this ridge cold air masses from the north arrive at the ETS. If the water temperature of the North Atlantic is low, the inverse situation arises. This relationship between the temperature anomalies produces a late or early ice breakup on the rivers of the ETS.

In forecasts of ice breakup on rivers use was made of the fact that the alternation of the prevailing circulation types during the months of January and February determines the subsequent development of atmospheric processes in the spring months.

In practice, due to the absence or incompleteness of the water-temperature data for the North Atlantic, this temperature was replaced by its equivalent air temperature anomaly averaged over the ETS. This reduced the accuracy of the forecasting relationships and of the forecasts themselves. Despite the general satisfactory accuracy of the forecasts (about 80%, in a number of cases the forecasts by this method were unsuccessful.

The principal shortcoming of the method is the fact that the atmospheric processes are qualitatively estimated by means of their classification. The use of the same estimates of the atmospheric processes and conditions on the underlying ground that influence them for rivers of different geographical regions of the ETS is also only a very rough approximation. Finally, the adopted schemes of alternation of the atmospheric processes from winter to spring almost always do not correctly reflect the true development of these processes. At the present time therefore this method, despite its general correctness, cannot be recommended as a basis for routine long-range forecasting of ice breakup on rivers.

The methods used today for long-range forecasting of ice breakup on rivers are based on an analysis and quantitative estimation of the atmospheric processes causing breakup, with due allowance for other factors, as applied to rivers of different geographical regions which influence breakup.

In working out methods for long-range forecasting of ice breakup on rivers, it is necessary to find a possibility of estimating, with a sufficient forewarning period, the time of the beginning and the intensity of the heat input to the ice cover and to the snow cover in the given river basin. This is the basic and most difficult part of the problem. An estimate of the thickness and strength of the ice cover can, usually, be made directly from observation data available at the moment the forecast is being prepared.

The time of the beginning and the intensity of the heat input are connected with the development of the atmospheric processes during the spring, with the appearance and duration of so-called heat waves. The forecasting of the ice breakup on rivers would be more accurate if it were based on an early estimation of such heat waves. However, the current state of knowledge of the development of atmospheric processes permits such an estimate only with a short forewarning period. Only generalized averaged characteristics of the intensity of the warming-up periods during the time interval when thaw of ice and snow may start and ice breakup on rivers may occur can be estimated with a large forewarning period (about a month or more). Thus, for example, the Kama, Northern Dvina, Pechora and Ob' rivers with their tributaries have their ice broken up in the second half of April or in May. In the case of frequent and intensive warming-up periods in April, the heat input necessary for ice breakup on these rivers may exist already by the middle of April; in the case of rare and weak warming periods, ice breaks up only later (May). Thus, dates of the ice breakup for these rivers can, obviously, be determined as dependent on the total or averaged characteristic of warming-up periods in April.

Warming-up periods in other months are typical of other regions.

Of course, a particular distribution of the time of the beginning and of the intensity of individual warming-up intervals may appreciably affect the dates of ice breakup on rivers.

When the period for which the generalized heat-input characteristics have to be obtained is determined, it is necessary to clarify which are the basic atmospheric processes with which the arrival of warm air masses to the given basin or region is connected.

The analysis of these processes should first be carried out qualitatively. Sometimes it is possible to use investigations on the regional synoptic factors of the given region for this purpose. Often such investigations do not exist or they do not cover the processes which cause the warming-up periods in spring. In the latter case such processes have to be characterized independently.

Spring warming-up periods are usually connected with the transport of heat in cyclonic systems which move to the given region from the west or southwest. However, under different geographical conditions the influence of the direction of transport on its intensity may be different. Thus, for example, for the Kama River system heat transport from the west and southwest has, on the average, the same intensity, whereas in the upstream part of the Ob' system considerable snow melting is usually only caused by heat transport from the southwest.

Considering the process that leads to warming-up periods, attention should also be given to the state of the underlying ground on the path along which the warm air masses move. It has the largest effect on warming-up in steppe regions, where in some years huge areas are completely covered with snow and free of snow in other years.

Over the snow surface the air cools down, over bare soil it warms up. This difference is particularly strong when clear weather prevails.

We note that in regions where the snow cover toward the beginning of the spring is always stable, some influence of its thickness on ice breakup can sometimes be noted. This is due to the fact that if the snow reserves are large, a large amount of heat is required for snow-melt water to begin to flow to the drainage net. In such cases the depth of the snow pack on the ice is also larger, which delays the thawing of snow.

Having revealed the basic processes causing the arrival of heat to the river basin or region under consideration, it is necessary to investigate further the possibilities and methods of an early estimation of the development of these processes. In this case, it is necessary to resort to long-range weather forecasts, from which it is possible to form an idea on the laws governing the development of the atmospheric processes.

In this case it should be borne in mind that for hydrologic forecasting it is sufficient to use the development laws for a definite type of processes at a definite time of the year and in a definite region, by using the total or averaged characteristics of these processes. In particular, for example, for long-range forecasting of the ice breakup on many rivers the uniformity of the atmospheric processes prevailing during the synoptic spring season is successfully used.

An important stage in working out a long-range forecasting technique is to find quantitative, objective characteristics of atmospheric processes. Although the analysis of these processes and of the laws governing their development usually begins qualitatively, it is not applicable to a given forecasting method.

A qualitative estimation of processes inevitably introduces into the technique an element of subjectiveness, even if its result is expressed by a number (for example, the number of days with processes of a given type, etc.). Experience shows that when using forecasting methods which contain qualitative estimates of the atmospheric processes, the accuracy of forecasts for a number of years is, as a rule, appreciably lower than the confidence limit of the method, calculated from data of check forecasts for past years.

The type of the quantitative characteristic of the atmospheric processes depends on the peculiarities of the processes which it should reflect. Thus, if the direction of air-mass transport plays the main role for the development of warming-up periods, circulation indices, reflecting the direction of the leading current in the troposphere, can be used. In a number of cases the peculiarities of the processes are reflected by a combination of fluctuations of the meteorological elements characteristic of them.

When the conditions which predetermine the intensity of heat arrival to a given river basin or region are expressed by objective quantitative characteristics, we can represent, also quantitatively, the dependence of the dates of ice breakup on rivers on these conditions and on other factors (ice-cover thickness, the snow reserves, the water-stage or discharge characteristics, and others).

The methods used at the present time can be divided into two basic groups, depending on the laws governing the development of the atmospheric processes used in the forecasting. Some of them are based on the uniformity of the atmospheric processes during the synoptic spring season (§ 1); others take into account the development and transformation of the atmospheric processes from one season to another (§ 2).

§ 1. Forecasting based on the uniformity of the atmospheric processes during the spring synoptic season

Ice breakup on most rivers of Siberia and of the northern half of the ETS occurs usually in the second half of April and in May. Their breakup dates therefore depend on the frequency and intensity of the warming-up periods during this period and that directly preceding it, i.e., during the spring synoptic season.

The spring synoptic season begins on the average on 13 March and ends on 5 May. The earliest beginning of spring was observed on 19 February, the latest on 31 March.

The nature of the synoptic processes, developing with the onset of the spring season, i.e., usually from the middle of March to the beginning of April, makes it possible to describe the prevailing synoptic processes in the later part of the season, i.e., in April and at the beginning of May, which directly determine the time of ice breakup on rivers. This is possible because of the assumption that uniform atmospheric processes prevail during one synoptic season.

If in March and at the beginning of April synoptic processes which give rise to transport of warm air masses to the given region prevail, ice breakup on the rivers is early. If, on the other hand, at this time processes which are connected with the penetration of cold air masses prevail, the breakup is delayed to later dates, in May. Since a qualitative visual determination of the date of the beginning of the spring synoptic season from synoptic maps inevitably leads to inaccurate conclusions, it is advisable to estimate the synoptic processes for the whole month of March. This is possible since, usually, the location of the principal ridges and troughs on the mean H_{500} maps for March and for the spring season coincides and, consequently, the prevailing direction of transport of the air masses also coincides. The form in which this regularity can be used in working out a forecasting technique depends on the peculiarities and conditions of the development of the atmospheric processes with which the arrival of heat to the given river basin is connected.

Thus, for example, the principal condition for ice breakup on rivers of West Siberia are periods of intensive warming-up, extending both over the mountainous regions of Altai, where the high-water forms, and over the lowland part of the basin. Examination of aerological data on intensive warming-up near the ground and at an altitude of 1 km, showed that such periods of warming-up are caused by heat transport from the southwest, taking place when cyclones move to West Siberia from the Black and Caspian seas or from Central Asia (processes of the southwestern type).

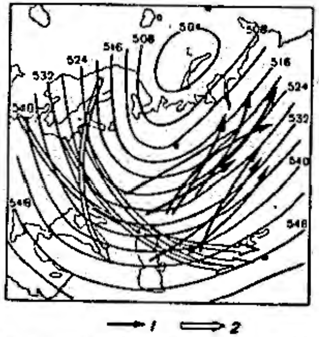

FIGURE 69. Chart of atmospheric processes of the southwestern type, causing heat transport to West Siberia.

1—cyclone trajectories; 2—anticyclone trajectories.

The formation of a deep high-altitude barometric trough over the ETS and of a high-pressure ridge over Siberia is characteristic of processes of the southwestern type (Figure 69).

In this case heat is advected along the eastern periphery of the trough and cold air masses penetrate along the western periphery of the trough to the northwestern and the central regions of the ETS. Consequently, by comparing the air temperature fluctuation in West Siberia and in the indicated regions of the ETS, it is possible to objectively determine the days with processes of the southwestern type, without a visual estimation by synoptical maps. The following method is used for this: for each day of March the average of the mean diurnal air temperatures at three meteorological stations in West Siberia (Barnaul, Taiga and Surgut), as well as the average value from two meteorological stations on the ETS (Moscow and Leningrad) is calculated. Days when the rise in the mean air temperature in West Siberia was associated with a drop in the mean air temperature in the northwest and center of the ETS are considered as days with southwestern type processes.

However, the days of ice breakup on rivers are affected not only by the frequency, but also by the intensity of the processes which cause heat transport. This can be taken into account by the total characteristic of the warming-up in days with atmospheric processes of the southwestern type during March (by the sum of temperature rises). The sum of the warming-up temperatures is calculated as follows. For each day, singled out as described above, the excess over −15° of the air temperature, averaged over three West-Siberian meteorological stations, ($\Delta\theta = \theta + 15°$) is calculated, and then the values of $\Delta\theta$ are summed over all such days in March ($\Sigma\Delta\theta_{III}$).

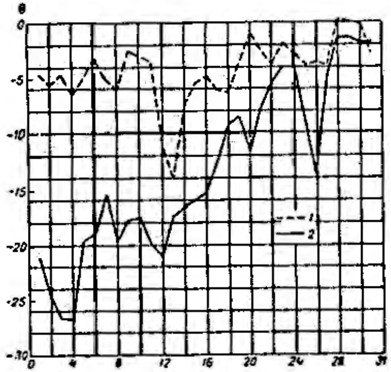

FIGURE 70. Graph of the mean-diurnal air temperature fluctuations in March 1946.

1—mean value from the meteorological stations Moskva and Leningrad
2—mean value from the meteorological stations Barnaul, Taiga and Surgut.

Let us follow the technique of calculating the sum $\Sigma\Delta\theta_{III}$ of temperature rises in the example for March 1946. The graphs of the mean-diurnal air temperatures during this month in West Siberia (mean values of the meteorological stations Barnaul, Taiga and Surgut) and on the ETS (mean values for Moskva and Leningrad) are given in Figure 70. As follows from this figure, the air temperature over West Siberia was below −15° until

16 March. Consequently, the first half of March drops out of our considerations. The first warming-up over West Siberia with a simultaneous cooling on the ETS* was observed on 17 March. In this case the mean-diurnal air temperature for the stations Barnaul, Taiga and Surgut was $\theta=-12.7^\circ$. Consequently, the excess of the air temperature over -15° was $\Delta\theta=\theta+15^\circ=+2.3^\circ$.

On 18 March warming-up in West Siberia and cooling on the ETS continues. The mean temperature of the West Siberian stations on this day was -9.2°, and $\Delta\theta=5.8^\circ$. On 18 March warming-up began on the ETS, and this day is not taken into account in the calculation. The warming-up in West Siberia and the temperature drop in the ETS was renewed on 21 March and continued on 22 March. The temperature on these days was respectively -7.9 and -5.5°, and the value of $\Delta\theta$ was 7.1 and 9.5°. On 23 and 24 March the air temperature in West Siberia was -4.2°, but on 23 March it rose on the ETS, and therefore only 24 March is included in the calculation ($\Delta\theta=10.8^\circ$) when the temperature on the ETS began to drop. We should be more precise by specifying that days when the air temperature in West Siberia is maintained stable after rising (to within 0.5°) are included in the calculation. The calculation therefore involved not only 27 March, when in West Siberia a sharp temperature rise (up to -5.9°) began, but also 29, 30 and 31 March, when the air temperature was maintained from -2 to -2.5°. The value of $\Delta\theta$ in these days was respectively 9.1, 13.0, 13.2, 13.5°. The total sum of temperature rises during March 1946 was $\Sigma\Delta\theta=84.7^\circ$.

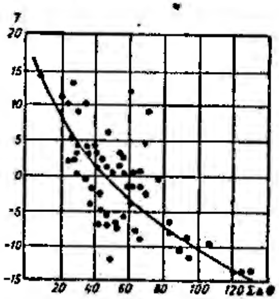

FIGURE 71. Deviations from the rated value of the time of ice breakup T on the middle course of Ob' as a function of the sum of the temperature rises (warming-up period) in March $\Sigma\Delta\theta$.

The thus-calculated characteristics of the sum of temperature rises are fairly closely related to the dates of the ice breakup on the basins of the Ob', Irtysh and Middle Yenisei rivers. As an example we give in Figure 71 the relationship between the deviations from the rated value of the dates of ice breakup on rivers of the Ob' Basin from Novosibirsk to Surgut (T) and the sum $\Sigma\Delta\theta$ of the temperature rises in March. Despite some large errors, the relationship has a satisfactory accuracy ($\frac{s}{\sigma}=0.67$).

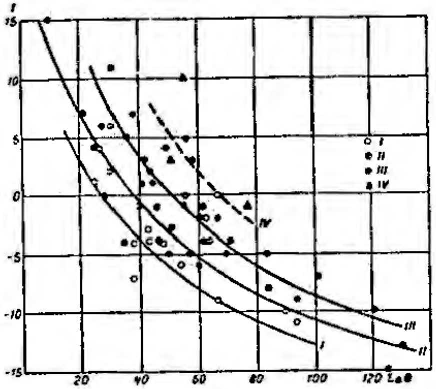

FIGURE 72. Deviations from the rated value of the time of ice breakup on rivers of the basin of the Upper Ob' as a function of the sum $\Sigma\Delta\theta$ of the temperature rises in March taking into account the depth of the snow cover and the pressure anomaly in March in North Kazakhstan and in Altai.

I=mean depth of the snow cover by about 10 cm below the rated value; II=mean depth of the snow cover 3–5 cm lower than the rated value; III=mean depth of the snow cover close to the rated value or higher than it; IV=negative pressure anomaly with the air current directed from the north.

When using this method for forecasting ice breakup on rivers of southern West Siberia it is taken into account that intensity of warming-up in this region under the same atmospheric processes considerably rises if there is no snow or if the depth of the snow cover is small on the path of the warm air masses in the steppes of North Kazakhstan and on the foothills of Altai. The reason for this influence of the snow-cover depth is that over a continuous snow surface the air cools down, and over a snow-free soil surface it warms up. If the depth of the snow cover is small, thawed patches form rapidly, the melting of the snow is accelerated, and warming-up begins to prevail over cooling. If the snow cover is thick, the cooling continues a long time. It is clear that this difference is particularly strongly manifested when clear anticyclonic weather prevails (when the direction of the air current is from the south).

Figure 72 gives the relationship between the deviations from the rated values of the dates of ice breakup on rivers of the basin of the Upper Ob' and the sum of temperature rises in March, the depth of the snow cover, and the atmospheric-pressure characteristics in North Kazakhstan and in Altai during the month of March. The data on the snow depth on 10 March (before the beginning of thawing) are averaged from five stations in the Irtysh River basin (Pavlodar, Semiyarsk, Semipalatinsk, Shemonaikha and Charskaya), and from three stations in the Ob' basin (Barnaul, Biisk and Aleiskaya) and their average deviations from the rated value are found.

---

* Further on in this section the mean air temperature for the meteorological stations of Moscow and Leningrad is called the temperature on the ETS.

Anticyclonic weather conditions prevail if a positive pressure anomaly in Barnaul exists; the direction of the air current is evaluated from the sign of the difference in the pressure anomalies in regions to the southwest (Kazalinsk) and northeast (Yeniseisk) of the region under consideration. If the difference in the pressure anomalies between Kazalinsk and Yeniseisk is negative, we have conditions for heat transport from the south and if positive conditions, for inflow of cold from the north and northwest prevail.

Taking all these factors into account, the accuracy of the dependence is given by $\frac{s}{\sigma} = 0.56$.

The method of forecasting ice breakup for the Kama and Tobol river basins also makes use of the uniformity of the atmospheric processes in the spring season. The development of atmospheric processes causing ice breakup on rivers, heat transport from the west and southwest, is also estimated there from the characteristics of total warming-up periods at the end of February and in March. The inclusion, in the calculation, of data for the last ten-day period of February is due to the earlier beginning of spring processes on the ETS. Warming-up periods are estimated from the fluctuations in the mean daily air temperatures from data of three meteorological stations (Perm', Cherdyn' and Ufa). The peculiarity of the estimation of the warming-up periods in this method consists in that we take into account not each of the warming, but the warming-up period as a whole, from the beginning to the end of the air temperature rise. The basic warming-up characteristic is the highest temperature excess over $-10°$ $(\theta_m + 0°)$ during the warming-up period. Other indices, mainly the duration and intensity of the warming-up, are taken into account by a factor β, which for a warming-up of short duration but of high intensity is equal to 0, for a very large duration is 2, and in most cases is equal to 1. Thus, the characteristics of each warming-up is $\Delta\theta = \beta(\theta_m + 10°)$. These quantities are summed over the whole period from 20 February to 31 March. The total characteristics $\Sigma\Delta\theta$ obtained are connected by fairly reliable relationships with the dates of ice breakup on the Kama and Tobol river basin. An example of such a relationship for the Belaya river basin is given in Figure 73.

To increase the forewarning period it is possible to restrict the period of calculation of $\Sigma\Delta\theta$, for example, to the day of 20 March. The accuracy of the relationships in this case of course decreases, but for southern rivers of the Kama and Tobol basins, where an earlier issuing of forecasts is necessary, it remains satisfactory.

The methods described as examples of forecasting ice breakup on rivers, based on estimation of the character of the warming-up periods at the beginning of the spring synoptical season, have been successfully used in routine practice for over 10 years. Experience shows sufficient reliability of the principles of these methods and the possibility of applying them to forecast of ice breakup on other rivers, when this phenomenon occurs in the second half of the spring synoptic season.

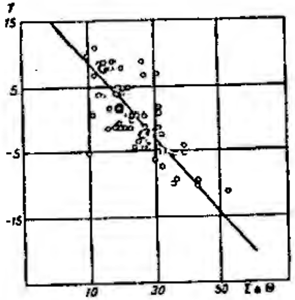

FIGURE 73. Deviation from the rated value of the term of ice breakup on rivers of the Belaya basin as a function of the sum $\Sigma\Delta\theta$ of the temperature rises in the last ten-day period of February and in March.

However, this method of estimating the development of spring processes is not the only one. In regions where the arrival of warm or cold air masses depends mainly on the direction of their transport, the technique of forecasting ice breakup on rivers can be based on the characteristics of the prevailing direction of air masses transport at the beginning of the spring synoptic season. Technique of forecasting ice breakup on rivers of the [illegible]

TABLE [illegible]. Values of the atmospheric circulation index I and of the pressure anomaly at Murmansk during March (Δp) (the rated value I [illegible])

Year	Circulation index I	Pressure anomaly in Murmansk (Δp)	Year	Circulation index I	Pressure anomaly in Murmansk (Δp)
1938	−6	−2	1950	−6	−5
1939	−3	+7	1951	−10	0
1940	+3	+4	1952	+17	+9
1941	+9	+5	1953	+16	−6
1942	+12	0	1954	+8	−1
1943	−4	−4	1955	+7	+1
1944	−5	−1	1956	+5	+5
1945	+14	+1	1957	+10	+5
1946	+9	+5	1958	+9	+8
1947	−1	−3	1959	+12	−1
1948	+2	−2	1960	+21	+13
1949	+5	+9			

of the ETS serves as an example. Ice on these rivers starts to break up at the end of April and continues to the middle of May; consequently, its dates are determined by the prevailing direction of transport of air masses during the spring season. An idea of the direction of transport can be formed, in accordance with the abovesaid, from the direction of the leading current on the mean H_{500} isobaric surface contour maps for March. As in a number of other methods, the meridionality index I, calculated as the difference between the mean values of the geopotential over western and eastern spherical rectangles, whose boundary passes along the meridian 42° E. long., is taken as the characteristic of this direction. A description of the calculation of I is given in Chapter I, Part C, § 1. The value of the circulation index I for March (Table 34) is the basic element in the expression used to forecast ice breakup on rivers of the northeast of the ETS.

If the circulation index for a given month is positive and relatively large in terms of its absolute magnitude, this indicates that a well-pronounced ridge is situated over the western rectangle, a trough over the eastern rectangle, and cold air masses arrive on the given ETS northeastern region from the northwest, north or northeast, which leads to late ice breakup on the rivers. Negative values of the circulation index indicate the transport to the northeast of air masses from the southwest, which also causes early ice breakup dates. Figure 74a gives the dependence of the ice breakup dates for the Pechora River on the atmospheric circulation index I for March.

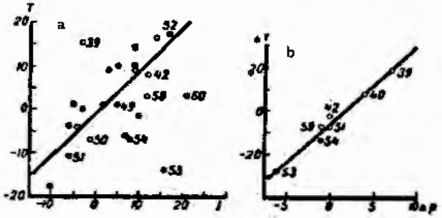

FIGURE 74. a—Deviations of the time of ice breakup on rivers of the Pechora and Mezen' basins from the rated value, T, as a function of the atmospheric circulation index in March, I; b—corrections to the values obtained by means of graph a, as a function of the pressure anomaly in Murmansk in March, Δp.

It is seen from this graph that in a number of cases very large deviations from the general law, represented by the dependence shown on it, occur. These are due to the fact that the value of I reflects only the prevailing direction of air mass transport, but does not indicate over what ground-based barometric formations this transport takes place. Usually, in the case of a meridional direction of current, anticyclones penetrate from the north or northwest and cause stable cold weather, but in some cases so-called "diving" cyclones move at the surface in the direction of the leading current. In such cases the cold weather is unstable since, upon the passage of the cyclones, the high-altitude trough in the region of the eastern rectangle is gradually filled up. This process develops faster, the stronger the cyclonic activity in March. When the air current is directed from the southwest, cyclonic systems usually pass considerably to the west of the regions under consideration. It occurs, however, that the paths of near-the-ground cyclones under the same general direction of the current pass to the east, and over close western regions in the rear of these cyclones strong anticyclonic penetrations occur. In these cases, the further displacement of the cyclone path to the east and the propagation of cold air masses to the northeastern regions of the ETS is most likely.

These peculiarities may be taken into account by means of data on the pressure anomaly in Murmansk. For the usual character of the atmospheric processes, the sign of the pressure anomaly at this point agrees with the sign of ΔI — the deviation of the index I from the norm. In the special cases described above, the pressure anomaly Δp in Murmansk has an opposite sign, or in the case of a highly meridional current is equal to zero. For such cases, the difference between the actual date of ice breakup on the Pechora, T, and that expected from relationship (74a), T', $(\Delta T = T - T')$ is connected with the value of Δp (Figure 74b).

Taking into account the corrections to the expected ice breakup dates, obtained by means of this relationship, the forecasting method acquires satisfactory accuracy, expressed by the ratio $\frac{s}{\sigma} = 0.62$. In preparing a forecast one should first calculate the value of A for March, its deviation from the rated value and the pressure anomaly Δp for March in Murmansk. If ΔI and Δp have the same sign, the expected breakup date for the Pechora River is determined directly from Figure 74a. If the signs are different, then first the expected date corresponding to the value of I is determined from Figure 74a, and then a correction ΔT, obtained from Figure 74b in accordance with the value of Δp, is introduced. The forecast of ice breakup on the Pechora in 1959 is an example. For this case $I = +12$ dkm, $\Delta I = +7$ dkm, $\Delta p = -1$ mb; the expected deviation of the time of ice breakup from the rated value is, according to the relationship, shown in Figure 74a, $T' = +10$ (i.e., 10 days later than the rated value). Since the signs of ΔI and Δp are different, we introduce a correction according to Figure 74b which is $\Delta T = -9$ days. The expected day $T = T' + \Delta T = +10 - 9 = +1$. Consequently, ice breakup on the Pechora should be expected 1 day later than the rated date. The breakup in 1959 actually occurred 3 days later than expected.

In order to examine the dependence of the dates of ice breakup on rivers on the prevailing direction of air mass transport in March over a number of years, it is also possible to use maps of the monthly mean pressure at sea level. The method of estimating the direction of the isobars on these maps by measuring their angle of inclination to the parallel has already been described in Chapter I, Part C, § 1. In forecasting ice breakup on rivers of the north-east of the ETS, the angle α is measured at a point with the coordinates 60° N. lat. and 55° E. long.

The development of atmospheric processes in March determines to a large extent also the time of ice breakup on rivers of East Siberia. The inflow of warm air masses to this region begins with the decay of the Siberian anticyclone and with the passage over the Lena River basin of cyclonic series, from the west. The time of the beginning of the western transport affects the ice breakup dates on the Lena and can serve as a forecasting argument, since this process begins more than a month before ice breakup. However, direct determination of the dates of the beginning of the west-east transport is connected with a visual estimation of synoptic maps and, consequently, is not sufficiently objective.

An objective characteristic of the process of decay of the Siberian anticyclone is given by the meridionality index I, calculated from the mean H_{500} isobaric surface-contour map for March. The western spherical rectangle is bounded by 70° and 125° E. long., the eastern by 125° and 180° E. long., the southern by 50° N. lat. and the northern by 70° N. lat. The reference points are taken through intervals of 10° in longitude and in latitude. The index I is calculated by determining the deviations of the mean-monthly geopotential at each point from their rated value, averaging these deviations over each spherical rectangle and subtracting the mean over the eastern from the mean over the western rectangle. If the decay of the Siberian anticyclone begins late, in March over the western rectangle a stable high-altitude ridge is maintained, the geopotential exceeds the rated value and the index has a positive value. If west-east transport develops in March, the high-altitude ridge in the western zone decays and the index becomes negative.

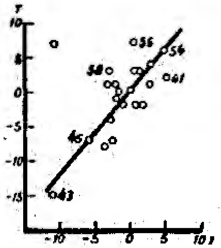

FIGURE 75. Deviations of the date of ice breakup on the Lena at Olekminsk, T, from the rated value as a function of the atmospheric circulation index in March, I.

This makes it possible to use the values of I for forecasting ice breakup on rivers of East Siberia. Figure 75 gives as an example the relationship between ice breakup on the Lena at Olekminsk and the index I in March. It follows from the graph that the dependence is fairly well defined and only in one case, in 1960, it was sharply upset. In the spring of 1960 the decay of the Siberian anticyclone began very early; on 17 March the first cyclones were observed to pass from the west through the Lena River basin. The index I had, therefore, in March a very large negative value. However, in April this process was discontinued.

As a result, ice breakup on the Lena was delayed to extremely late dates. The possibility of such a large forecasting error reduces, of course, the reliability of the method, but on the whole the dependence remains satisfactory, since the confidence limit of the permissible error ($\delta_в = 0{,}674\,\sigma = 4$ days) is 89%.

It should be noted that such interruptions in the decay of the Siberian anticyclone have a particularly significant effect on ice breakup on the upper course of the Lena, for which the method described was found to be unreliable.

On the whole, methods in which use is made of the uniformity of the atmospheric processes of the spring season are relatively reliable. However, in individual cases forecasts prepared by means of them contain large errors. Such errors, in addition to those connected with the extreme intensity and nonuniformity of the alternation of individual heat and cold waves, are due either to a very late onset of the spring synoptical season, sharply differing in the nature of the processes from the preceding season, or to a partial change in the processes during the spring season, which was found to be most important in the given region.

The possibility of such errors is the main shortcoming of the whole technique described in this section.

§ 2. Forecasting based on allowance for the character of the rearrangement of the atmospheric processes from winter to spring

Many rivers most important for the national economy, such as the Volga and its right tributaries, the Don, Dneper, as well as rivers of the northwestern basins, have their ice broken up not at the end of the spring synoptical season, but at the beginning — at the end of March and in the first half of April. Long-range forecasting of ice breakup on these rivers cannot be based on the uniformity of the atmospheric processes of the season, since to provide the necessary forewarning period it should be prepared at the beginning or middle of March, i.e., usually before the beginning or at the very beginning of the spring synoptical season. The corresponding forecasting methods should, therefore, in some way take into account the laws governing the rearrangement of the atmospheric processes from winter to spring.

These laws can be taken into account relatively simply for regions and rivers where the transformations of the atmospheric processes take place more or less smoothly and winter conditions preserve their influence on the spring processes. In such cases, it is sufficient to take into account, along with the character of the winter processes, the tendency of new spring processes sharply differing from the winter ones, to appear early. The method of forecasting ice breakup on rivers of the northwestern regions of the ETS may serve as an example. The inflow of warm air to this region in winter and spring depends mainly on the higher or lower intensity of the western transport of air masses. Strong development of this transport is usually connected with the intensification and displacement of the Icelandian pressure minimum during January–February toward the coasts of Europe and a gradual development, in March–April, of a high-pressure ridge or anticyclone over the southeastern regions of the ETS. The latter process also causes the inflow of heat to the given regions. In the case of weakened western transport, these processes are less stable. However, in this case too, the influence of winter conditions also prevails, particularly if the ice breakup on the rivers of these regions is due mainly to the thermal destruction of the ice and to the local runoff, so that a severe winter particularly at the end considerably affects the delay in ice breakup.

The intensity of the western transport can be characterized by the pressure gradient or difference between the zones of the subtropical maximum and of the Icelandian minimum. The larger this difference, the higher the intensity of the air current. Differences (in terms of deviations from the rated value) are calculated for February. The subtropical maximum is determined from observation data at the Saint George meteorological station, and that of the zone of the Icelandian minimum from observation data at the Jan-Mayen and Murmansk stations.

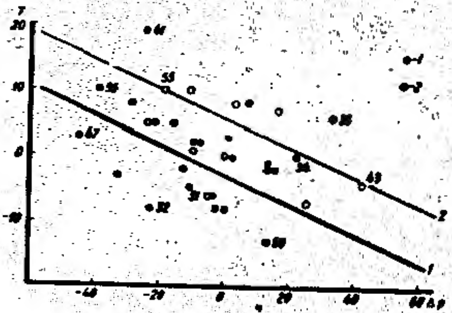

FIGURE 76. Deviations of the time of ice breakup on rivers of Karelia from the rated value, T, as a function of the deviations from the rated value of the pressure difference according to the meteorological station Saint George and from the mean according to the meteorological stations Jan-Mayen and Murmansk, in February, Δp.

1—cases of increase in the air temperature anomaly in Petrozavodsk starting in February and continuing until the first two ten-day periods of March; 2—cases of decrease in the air pressure anomaly.

The course of the transformation of the processes from winter to spring is taken into account by the variation in the air temperature anomaly from February to the first two ten-day periods of March.

When the dependence of the breakup dates on rivers, for example, of Karelia (Figure 76) on the pressure difference in February is given graphically, all cases are seen to fall into two groups. If the variation to the temperature anomaly in Petrozavodsk from February to the two ten-day periods of March is positive, ice breakup occurs relatively early and, if negative, relatively late. Even such a highly simplified way of allowing for the variation tendency of the character of the atmospheric processes is found to be sufficient to obtain a satisfactory forecasting method.

Considerable errors when using this dependence, as well as other dependences which take into account the character of the transition to the spring from data only during the first one or two ten-day periods of March, arise in those, relatively rare cases, when the spring synoptical season begins late – at the end of March or at the beginning of April, and the atmospheric processes characterizing it differ sharply from those prevailing during the preceding months.

Keeping such a possibility in mind, which though rare are very dangerous in routine forecasting, it is necessary also to work out a technique for correcting a long-range forecast with smaller forewarning period, but taking into account the development of the atmospheric processes at the beginning of the spring, i.e., at least throughout March.

The estimation of the heat input in spring, required for forecasting ice breakup on rivers of those regions characterized by sharp changes in the prevailing atmospheric processes from season to season, is more complicated. Such rivers are the Dnieper Don, Lower Volga and the right-hand tributaries of the Volga. The matter is still more complicated by the fact that ice breakup on most of these rivers usually occurs already in March and the requirements for a forewarning period make it impossible to use even data for the first half of March in order to estimate the tendency of the spring season. It is necessary, consequently, to find the conditions for the transformation of the atmospheric processes and, for purposes of forecasting ice breakup on rivers, the conditions of intensification or attenuation of warming-up periods from season to season. These conditions can be determined by an analysis of relative H_{1000}^{500} isobaric surface-contour maps which reflect, as in known, the mean air temperature in the 5-km high tropospheric layer.

A peculiarity of the distribution of the values of H_{1000}^{500} in months of the cold season of the year, from November to March, is the existence of a stable horizontal gradient, directed to the southern and central regions

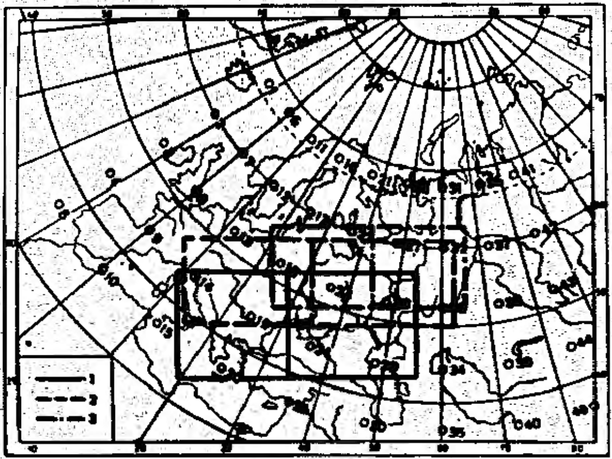

FIGURE 77. Reference points for calculating the deviations of the values of H_{1000}^{500} from the rated values.

1—boundaries of the regions for calculating the quantity C used in forecasting ice breakup on the Don and Lower Volga rivers; 2—the same for the Oka River basin; 3—the same for the Kuibyshev storage reservoir (see Chapter VI, Part C).

of the ETS from the southwest. Only the magnitude of this gradient varies. An increase in the gradient causes subsequent intensification of warming-up, and a decrease causes attenuation. Therefore, from the variation in the gradient of H_{1000}^{500} from the pre-winter season (November) to the first half of the winter (December–January) it is possible to estimate the intensity of warming-up in the second half of the winter (February and the first half of March). The intensity of these warming-up periods is important in ice breakup on southern rivers, particularly in cases of an early breakup. From the variation in the gradient of H_{1000}^{500} from the first to the second half of the winter (which in this case can be determined from data during February), it is possible to form an idea of the intensity of the warming-up intervals during the spring synoptical season, i.e., in the second half of March and in April, when ice breaks up on the rivers of the central regions.

The magnitudes of these gradients are characterized by the difference in the mean deviations of the relative geopotential H_{1000}^{500} from the rated value from two groups of points uniformly distributed over the territory. The first group is taken southwest of the region for which the technique is being worked out and the second group in this region itself and somewhat northeast of it. Figure 77 gives examples of point groups used in determining the gradients for different regions of the ETS.

TABLE 35. Mean values of H_{1000}^{500} in months of the cold season of the year in dkm (1938–1954)

No. of points	I	II	III	XI	XII	No. of points	I	II	III	XI	XII
1	521	519	521	527	522	24	537	533	535	545	538
2	530	530	533	535	530	25	542	543	544	554	546
3	538	538	540	543	537	26	511	512	512	522	516
4	544	544	545	550	541	27	515	516	519	527	520
5	547	548	550	555	545	28	521	522	525	533	526
6	521	521	523	527	523	29	530	531	533	543	535
7	529	529	533	535	531	30	541	542	544	553	544
8	535	535	538	542	535	31	508	509	509	519	513
9	540	540	543	548	538	32	513	514	516	524	517
10	545	545	549	555	543	33	520	520	524	531	523
11	520	519	521	527	524	34	531	531	535	541	532
12	524	524	527	533	530	35	541	542	545	551	543
13	529	530	534	539	534	36	507	505	507	514	509
14	536	537	540	546	539	37	511	511	515	519	513
15	544	545	545	554	548	38	519	518	525	527	521
16	517	517	519	526	523	39	531	530	539	538	531
17	521	521	524	532	528	40	542	543	547	551	543
18	525	527	530	538	532	41	503	503	505	510	504
19	533	534	535	544	537	42	508	509	513	516	511
20	542	544	545	554	546	43	518	515	523	524	517
21	514	516	516	525	520	44	527	526	536	536	529
22	518	519	521	530	524	45	540	540	547	549	542
23	523	524	527	536	529						

For each point of the group the mean-monthly value of the geopotential H_{1000}^{500} for November, December, January and February of each year and its deviation from the rated value for the given month are calculated from relative isobaric surface-contour maps. The norms of H_{1000}^{500} are given in Table 35.

The values of H_{1000}^{500} (particularly monthly-average) and their deviations ΔH_{1000}^{500} from the rated value vary smoothly over the territory. This makes it possible to use, as the gradient characteristic, the difference between the mean values of ΔH_{1000}^{500} over the southwestern and the northeastern group of points. Subtracting from the deviation averaged over the southwestern group the deviations averaged over the northeastern group, we obtain the characteristic of the gradient of H_{1000}^{500}, which is denoted by Γ. The values of Γ are calculated separately for each month.

The value of Γ for November (Γ_{XI}) characterizes the heat flow in the pre-winter synoptical season. The values of Γ for December (Γ_{XII}) and January (Γ_{I}) are averaged and reflect the conditions of the first half of the winter. The value of Γ for February (Γ_{II}) reflects the conditions of the second half of the winter.

The differences $\delta\Gamma$ of these quantities reflect seasonal fluctuations in the heat flow intensity, namely: from the pre-winter to the first half of the winter $\delta\Gamma_1 = \frac{\Gamma_{XII} + \Gamma_{I}}{2} - \Gamma_{XI}$, from the first to the second half of the winter $\delta\Gamma_2 = \Gamma_{II} - \frac{\Gamma_{XII} + \Gamma_{I}}{2}$.

An increase in the gradient from the preceding to the current season ($\delta\Gamma > 0$) causes a rearrangement of the conditions for warming up in the next season and, conversely, a decrease in the gradient ($\delta\Gamma < 0$) causes a rearrangement to cold periods. Here we have in view relative warming and cooling periods with respect to the normal annual fluctuations in the air temperature.

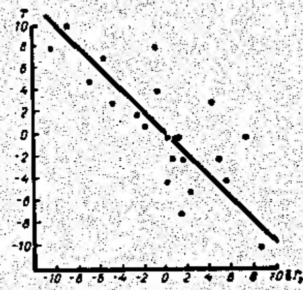

FIGURE 78. Deviations from the rated value of the time of ice breakup on the Oka River below the mouth of the Moskva River, T, as a function of the variation in the characteristics of the relative geopotential gradient from the first to the second half of the winter, $\delta\Gamma_2$

Let us consider examples of the use of the characteristics of the relative potential gradient ($\delta\Gamma_1$ and $\delta\Gamma_2$) in the technique of forecasting ice breakup on rivers.

The ice on the Oka River breaks up under the influence of the heat input in the period of snow melting in the river basin (its breakup date depends only slightly on the thickness of the ice cover). Considerable warming-up begins with rare exceptions, there in the second half of March or at the beginning of April, i.e., in the spring season. The breakup dates for the Oka River therefore depend on the variation in Γ from the first to the second half of the winter ($\delta\Gamma_2$). The values of Γ are determined from the groups of points shown in Figure 77.

A dependence of the type $T = f(\delta\Gamma_2)$ for forecasting ice breakup on the middle and lower course of the Oka River is given in Figure 78. The values of $\delta\Gamma$ are given in Table 36.

TABLE 36. Seasonal fluctuations in the characteristics of the relative geopotential gradients

Year	For basin of Don and of Lower Volga rivers		For basin of Oka River	For the Kuibyshev storage reservoir	Year	For basin of Don and of Lower Volga rivers		For basin of Oka River	For the Kuibyshev storage reservoir
	$\delta\Gamma_1$	$\delta\Gamma_2$	$\delta\Gamma_2$	$\delta\Gamma_2$		$\delta\Gamma_1$	$\delta\Gamma_2$	$\delta\Gamma_2$	$\delta\Gamma_2$
1939	0.4	−1.5	−1.8	7.0	1950	7.5	−3.0	0.7	3.0
1940	−0.9	1.0	1.2	1.3	1951	0.5	4.0	8.7	8.2
1941	1.8	0.5	−0.7	0.3	1952	−4.6	−3.0	−5.5	−5.4
1942	−1.7	−7.5	−8.7	−3.0	1953	0.0	3.5	2.3	1.3
1943	—	—	0.2	0.8	1954	−3.1	0.5	5.5	2.5
1944	3.3	−7.5	−6.7	−0.9	1955	2.3	−1.3	−0.5	0.3
1945	−0.7	7.0	7.4	3.6	1956	1.6	−6.4	−10.2	−5.3
1946	2.4	−2.5	−4.6	−6.3	1957	−4.7	−4.1	−2.5	0.4
1947	1.4	−2.5	1.5	−0.5	1958	−4.2	6.2	4.4	0.5
1948	−2.0	5.0	0.3	−1.8	1959	−5.0	6.7	5.0	6.6
1949	−1.6	3.5	1.7	0.9	1960	−2.4	−1.9	1.0	−2.3

The forecast can be prepared at the beginning of March.

Similar dependences have been obtained for the upper course of the Oka and for other rivers of the central region of the ETS.

It should be noted, however, that in some cases ice breakup occurs already in the middle of March, particularly on the upper Oka. It is connected with a considerable development of heat transport already in the second half of the winter. Such cases did not exist in the series of years considered when working out the method (from 1939 to 1960). For this period there are OT^{100}_{1000} maps.

At the time of preparation of the forecast, the conditions for such an early ice breakup can be estimated from the prevailing direction of transport of air masses and from the intensity of warming up in February.

A characteristic of the transport direction can be the angle α, formed in the direction of the air currents between the isobars and the parallel in the region of Moscow on the mean-monthly pressure map (see Chapter I, Part C, § 1).

The characteristic of warming-up intensity is determined from data on the mean-diurnal temperature (observatory im. Mikhel'son, Moscow). Days are chosen when this temperature was higher than the day before and exceeded −10°, as well as all days with a temperature above 0°. The extent of temperature rise during each of these days is determined as $\Delta\theta = \theta + 10°$. The sum of the temperature rises during all such days, observed during February ($\Sigma\Delta\theta$), serves as a total generalized characteristic of heat-transport intensity during this month.

The ice on the Oka River breaks up earlier than the time determined from the relationship $T = f(\delta\Gamma_2)$ in cases when the air current in February is flowing in from the southwest (the angle α is within 320° and 10°) and the sum $\Sigma\Delta\theta$ of the temperature rises exceeds 70°. Breakup usually occurs earlier, the larger the sum $\Sigma\Delta\theta$. For $\Sigma\Delta\theta$ above 150° ice breakup on the middle and lower course of the Oka is possible 5–10 days earlier than the rated value and on the upper course 15–20 days earlier. This should be borne in mind when preparing a forecast.

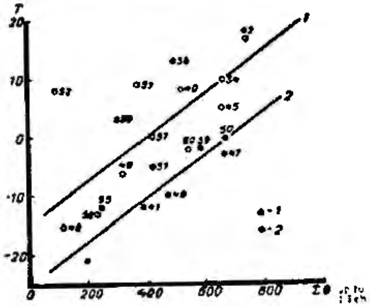

FIGURE 79. Deviations from the rated value of the time of ice breakup on the Volga downstream from Volgograd, T, as a function of the sum of the mean-diurnal negative air temperatures in Volgograd during the stable ice period until 1 February, $\Sigma\theta_-$, and the variation in the characteristic of the relative geopotential gradient from the pre-winter season to the first half of the winter, $\delta\Gamma_1$.

1 – $\delta\Gamma_1 \leq 0$; 2 – $\delta\Gamma_1 > 0$.

An early ice breakup on the Don and Lower Volga occurs in the first half of March, and sometimes also at the end of February. Therefore, the first forecast should be prepared already at the beginning of February. In this case, it is necessary to take into account the conditions of heat input in the second half of the winter, as well as the thickness of the ice cover, on which the time of ice breakup on these rivers depends to a larger extent than the time of breakup on the Oka.

As a characteristic of the thickness and strength of the ice cover the sum of the mean-diurnal negative air temperatures from the beginning of the stable ice period to 1 February is taken. To estimate the heat input in the second half of the winter the variation in the relative geopotential gradient from the pre-winter to the first half of the winter, $\delta\Gamma_1$, is used. An example of such a relationship is shown in Figure 79 for the Volga below Volgograd. The sum $\Sigma\theta_-$ of negative temperatures is calculated for Volgograd, the value of $\delta\Gamma_1$ is calculated for the points shown in Figure 77. $\delta\Gamma_1$ is introduced on the graph by separating all the cases into two groups. The first group includes cases with positive values of $\delta\Gamma_1$, i.e., cases when intensification of the heat input in the second half of the winter should be expected. In these years ice breakup occurs relatively early, the breakup days being fairly closely correlated with $\Sigma\theta_-$ until 1 February. The second group is made up of cases when $\delta\Gamma_1 \leqslant 0$, i.e., when conditions exist for the attenuation of the heat input. In this case, the dependence of the breakup dates on $\Sigma\theta_-$ is somewhat less clearly defined than in the first group. This is regular; the breakup in such cases occurs later and is more influenced by the conditions of the ensuing season, which are not taken into account by the given relationship.

The total accuracy of the relationship is low ($\frac{s}{\sigma} = 0.77$). However, when issuing a forecast with such a long forewarning period (a month before the earliest dates), most important is the possibility to correctly predict an early ice breakup, which can be done well with this relationship.

At the end of February, it is possible to introduce a correction in the forecast. For this purpose the following are taken into account: (a) the variation of the sum of the negative temperatures, which determines the state of the ice cover; (b) the variation in the characteristics of the relative geopotential gradient from December–Janaury to February $\delta\Gamma_2$, which indicates the intensification or attenuation of the heat input in the following season, spring.

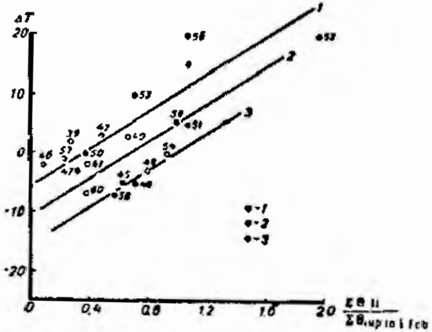

FIGURE 80. Deviations of ice-breakup dates on the Volga downstream of Volgograd from those obtained from Figure 79, ΔT, as a function of the ratio of the sum of the mean-diurnal negative air temperatures during February to the sum during the preceding stable ice period, $\frac{\Sigma\theta_{-II}}{\Sigma\theta_{-\text{up to 1 Feb}}}$, and the variation in the characteristics of the relative geopotential gradient from the first to the second half of the winter, $\delta\Gamma_2$.

1 – $\delta\Gamma_2 < -2$; 2 – $-2 < \delta\Gamma_2 < +2$; 3 – $\delta\Gamma_2 > +2$.

To increase the forecast accuracy it is possible to use the expression described in Figure 80. It connects the deviations in the dates of ice breakup on the Volga from the dates expected, according to the relationship given in Figure 70, with the ratio of the sum $\Sigma\theta_{-II}$ of the mean-diurnal negative air temperatures during February to the sum $\Sigma\theta_-$ accumulated until 1 February. Using in the first forecast the value $\Sigma\theta_-$ calculated until 1 February, as a characteristic of the ice thickness and strength, we base our consideration on the corresponding conditions actually remaining the same in February as well, i.e., on the mean ratio of $\Sigma\theta_{-II}$ to $\Sigma\theta_-$ of the preceding period. However, if in the given year the ratio $\frac{\Sigma\theta_{-II}}{\Sigma\theta_-}$ is considerably larger than the mean, the ice grows in February more intensely than was expected, and this delays ice breakup on the river.

All the points on the graph (Figure 80) were divided, in accordance with the value of $\delta\Gamma_2$, into three groups: cases of large negative values of $\delta\Gamma_2$, cases of large positive values and cases close to the rated value (± 2 dkm).

In cases when ice breakup on the Volga downstream from Volgograd, according to the first forecast, is expected earlier than 20 March, the value of $\delta\Gamma_2$ should not be taken into account when correcting the forecast, since the conditions of the spring season do not have time to affect the breakup dates. The technique of improving the forecast, i.e., of using successively two relationships, gives a higher accuracy ($\frac{s}{\sigma} = 0.54$). It should be borne in mind, however, that for a small total number of cases (about 20) the ice-breakup date is determined as dependent on four variables.

Experience gained in routine work by using such relationships for forecasting ice breakup on rivers, which take into account the characteristics of the variation in the heat input conditions from season to season, shows that considerable forecasting errors are due, as a rule, to an unusual duration of the synoptical season or in general to a sharp deviation of the dates of the beginning or end of the season from the mean dates used in the method. In this connection it is useful to work out correction methods taking into account the processes at the beginning of the spring season, i.e., in March, if in this case a sufficient forecasting forewarning period is provided, at least in cases of a normal or late ice breakup.

Chapter VI

FORECASTING OF ICE BREAKUP AND ICE CLEARING ON LAKES AND STORAGE RESERVOIRS

A. ICE BREAKUP AND ICE CLEARING ON LAKES AND STORAGE RESERVOIRS

Spring ice breakup of lakes and storage reservoirs differs from that on rivers. Before ice breaks up and wind ice drift begins on a lake or reservoir the ice cover has been melting for a long time under the influence of the increasing spring heat input from the air and by solar radiation. The beginning of the thawing period on most reservoirs coincides with the time of maximum reservoir drawdown. Warm underground water, particularly that stored in shores, arriving in low-water reservoirs, increases the rate of thaw, much more than in high-water reservoirs.

As the melting of the snow on the ice cover progresses, an increasing amount of solar radiation penetrates through the ice to the water. This heat, together with the groundwater heat, proceeds at a higher or lower rate (depending on the rate of mixing of the water masses), to the ice cover, causing thawing of its under surface.

Differences in the thickness of the ice cover and in the depth of snow on it in different parts of the reservoir and the different stream velocities cause nonuniform melting of the ice cover both at the outer and inner (under) surface. First ice flanges appear, and then cracks in the ice made by the flow of currents in former river beds or in places of concentrated outflow of groundwater. Due to the arrival of snow-melt water and to the rise in the water level the ice flanges expand. A further rise in the water level increases the water surface of the reservoir. The role of wind and wave action increases. Under the influence of the wind ice pushes begin. Leads appear, i.e., ice breaks up.

The mechanical destruction of the ice cover, already weakened by the thermal effect, gradually extends over newer parts of the reservoir or lake.

As the area of the open water surface increases, the heating of the water body intensifies. Wind mixing of the water masses and ice drift contribute to intensive heat transfer from the water to the ice.

On lakes and storage reservoirs ice drift usually does not occur, but wind ice drift takes place in such cases. Ice drift on reservoirs is usually near their river zones and in contractions, where sufficient flow velocity exists.

The ice on reservoirs is usually not discharged into the tailwater, but is stopped upstream from the dam and thaws on the spot. Only from small water reservoirs, when an increased discharge for power purposes coincides with ice drift, is ice sometimes discharged into tailwater.

Wind ice drift contributes to melting and to further destruction of the ice cover. If the wind direction is stable, the ice accumulates in individual coastal zones or inlets. Often the wind contributes to clearing of bays and reservoir zones important for navigation, carrying the ice out of them. But, the wind may drive the ice into these bays and zones, delaying the beginning of navigation.

As a result of the autumn–winter drawdown of a storage reservoir, part of the ice cover melted since the ice cover settles to the ground and freezes there. Depending on the amount of drawdown and shape of the water reservoir, the area of the ice settled on the ground varies within wide limits. The thickness of the settled ice is nonuniform and depends mainly on the settling time.

The settled ice, frozen to the ground and covered with snow, lies until it is flooded by the spring filling of the reservoir. Sometimes it remains under the water and then when it begins to thaw it detaches itself from the bottom and floats up to form ice blocks.

The lower the winter drawdown level of the reservoir and the higher the rate of rise of the level during spring, the larger the area of open water surface formed toward the beginning of the floating up of the ice frozen on the ground. In other words, the more completely is the water reservoir emptied for the winter and the faster is it refilled in spring, the more favorable are the conditions for the destruction and melting of the ice cover.

The role of the variation in the water level during the autumn-winter drawdown of the reservoir and its subsequent recharge is particularly noticeable in cases of the destruction of the ice cover on reservoirs or lake-like formations and on bays of reservoirs having large shallow water areas.

The lowering of the water level as a result of drawdown and its rise during the spring recharge also affect the destruction of the ice cover in river zones and in contractions (river-channel sections) of reservoirs.

The flow velocities in the river zones of reservoirs depend on the degree of filling of the reservoir, but they are always lower than on the river upstream from the backwater zone. Ice breakup in the backwater zone, therefore, occurs later than on the more upstream-lying nonregulated stretch of the river, as a result of which at the terminal zone of the back-water area ice jam may form. Jam phenomena may be observed also on tributaries.

The effect of wind blowing from a definite direction on the destruction of the ice cover on river zones of water reservoirs is manifested in delaying ice drift or, on the contrary, in intensifying ice drift to the main, lake-like part of the reservoir.

The disappearance of ice on lakes and reservoirs is completed by ice breaking into individual needles and their rapid thawing on the surface water layers.

Thus, the destruction of the ice cover on lakes and reservoirs and their complete or partial clearing from ice is determined mainly by the following factors: (1) the heat input to the upper and lower surface of the ice cover, (2) the velocity and direction of the wind, (3) the variation in the water discharges and stages.

We still do not have at our disposal reliable methods for taking into account all the above-listed factors that determine the destruction and thawing of the ice cover. For example, the mechanical effects of the wind, not manifested to full extent every year, are not at all or only approximately taken into account in the form of a correction to the obtained results of calculation or forecasting.

B. CALCULATIONS OF ICE CLEARING USING THE WEATHER FORECAST

§ 1. Calculation of ice clearing

Calculation of the melting of the ice cover on reservoirs is based on the heat-balance equation

$$\sum q = L_{ic}(h_{cr.ic}\rho_{cr.ic} + h_{sn.ic}\rho_{sn.ic} + h_{sn}\rho_{sn}), \qquad (1.VI)$$

where Σq is the amount of heat (per unit surface) required for complete melting of the ice cover,* L_{ic} is the heat of ice melting (80 cal/g), $h_{cr.ic}$, $h_{sn.ic}$, h_{sn} and $\rho_{cr.ic}$, $\rho_{sn.ic}$, ρ_{sn} are, respectively, the thickness and density of crystalline ice, snow ice and snow on the ice.

The following values can be used in the calculations: $\rho_{cr.ic} = 0.91$ g/cm^3, $\rho_{sn.ic} = 0.88$ g/cm^3, $\rho_{sn} = 0.25$ g/cm^3. Then

$$\sum q = 73h_{cr.ic} + 70h_{sn.ic} + 20h_{sn}\ \text{cal/cm}^2. \qquad (2.VI)$$

Σq is the amount of heat necessary for melting a column of the ice cover and the snow on it, the column having a cross section of 1 cm^2.

As is known, at water gaging sites, only the total ice thickness h_{ic} and the depth of the snow on the ice are measured. The thickness of the snow and of the crystalline ice for a known total thickness therefore has, thus, to be calculated.

The approximate value of the mean thickness of the snow ice for the water-body area under consideration can be determined by

$$h_{sn.ic} = a(0.1h_{so.pr} - 0.25h_{sn})\ \text{cm}. \qquad (3.VI)$$

From observation data for the Klyaz'ma storage reservoir of the Moskva-Volga Canal, $a = 1.66$. This value can be used to calculate the value of $h_{sn.ic}$ in cases when traversing cracks, polynias and ice holes exist on the given stretch. It can be used in practice for small and shore zones of large water bodies.

As to large bodies of water on the whole, the coefficient a for them should apparently be smaller (see Chapter IV).

In (3.VI), $h_{so.pr}$ is the depth of solid precipitation during the stable ice period, in millimeter of water. The depth of solid precipitation is taken from observations at the meteorological station nearest to the water-body stretch under consideration. If there are several meteorological stations closely situated to the reservoirs, the mean of the observed values from data of these meteorological stations should be taken to determine the depth of precipitation.

The depth of the snow pack on the ice is determined for the date nearest to the date of the beginning of melting, averaged over all the gaging sites of the section.

The thickness of the crystalline ice is equal to

$$h_{cr.ic} = h_{ic} - h_{sn.ic}. \qquad (4.VI)$$

The total ice thickness on the given reservoir section before the beginning of melting (h_{ic}) is determined from observations at all the gaging sites of the section. The method of determining this quantity depends on the purpose of the calculation, i.e., on whether the calculation is for the date of complete ice clearing or for the date of ice clearing on most of the given area (see Part A).

If the date is calculated for complete ice clearing, the maximum thickness, chosen from observations at all the gaging sites of the section, is taken as the ice thickness h_{ic} on the section, i.e., the largest peak thicknesses observed at the sites in measurements both far from the shore and at the shore (h_m).

If we calculate the date of ice clearing for most of the given area, the arithmetic mean of the maximum thicknesses observed at all the sites ($\bar{h}_m$) is taken as the total thickness h_{ic} of the ice on the given section.

When calculating the thickness of crystalline ice, the value of h_{ic} is substituted for h_m in (4.VI) (if the date of complete ice clearing is being determined) or $\bar{h}_m$ is substituted for h_{ic} (if the date of ice clearing of most of the given area is being determined).

To find the time of accumulation of the amount of heat input, Σq, necessary for ice clearing of the reservoir, the magnitude of q per unit time should be known. The unit time in the method described is 24 hours. The quantity q consists of the specific heat input due to solar radiation Q, evaporation or condensation heat exchange LE, heat exchange with the air P, effective radiation I_{eff} and heat input from the water q_w

$$q = Q + LE + P + I_{eff} + q_w. \qquad (5.VI)$$

The values of Q, LE, P, I_{eff} can be calculated by existing formulas (see Manual, No. 1), in particular, by the formulas (and methods) given below. All the heat-exchange components are given in cal/cm^2·day.

a) The specific heat input from solar radiation can be determined from

$$Q = 0.55Q'_r k_N, \qquad (6.VI)$$

where Q'_r is the maximum density of the heat flux from total solar radiation incident on the ice, taking into account its multiple reflection by the atmosphere; k_N is the coefficient of radiation attenuation by the clouds.

The value of Q'_r is determined from Figure 81 as dependent on the geographical latitude and on the particular date. The coefficient k_N is found from Table 37 for equivalent cloudiness N.

TABLE 37. Coefficient of solar radiation attenuation k_N for various values of equivalent cloudiness N.

N	0	1	2	3	4	5	6	7	8	9	10
k_N	0.98	0.96	0.94	0.88	0.79	0.68	0.59	0.50	0.42	0.35	0.28

The equivalent cloudiness is calculated from

$$N = \frac{N_t + N_l}{2}, \qquad (7.VI)$$

---

* We are considering conditions when the ice cover melts completely without drifts.

where N_t is the total cloudiness, N_l is the low-level cloudiness (given in the [Soviet] decimal scale).

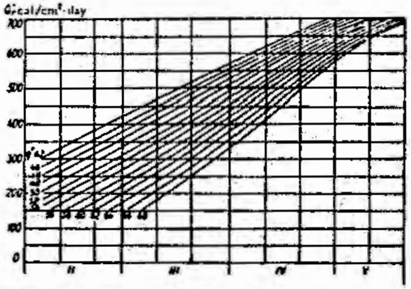

FIGURE 81. Maximum density of heat flux of total solar radiation incident on the ice, taking into account its multiple reflection by the atmosphere for an albedo of 0.4 of the surrounding terrain, for different latitudes.

b) The amount of heat received by the ice from the air (or given by the ice) and the heat input due to condensation of water vapor (or heat loss on evaporation) on the ice cover can be calculated from

$$LE + P = 6(\theta + 1.5e - 9.2)(1 + 0.72w) \text{ cal/cm}^2\cdot\text{day}. \qquad (8.\text{VI})$$

In this formula w, θ, e are the mean-diurnal values of the wind velocity (m/sec), air temperature and water-vapor pressure (mb) at a height of 2 m above the reservoir.

A working nomograph (Figure 82) was plotted on the basis of this formula. This nomograph is suitable for calculations for any type of reservoir.

The meteorological elements appearing in (8.VI), whose values must be known when using the above nomograph, are taken from observations at the nearest meteorological station and are reduced to the conditions of the given reservoir. This is done from corresponding correction graphs or tables.

Figure 83 gives a graph of the ratio of the wind velocity at an altitude of 2 m above the reservoir to the wind velocity at the altitude of the anemometer at the meteorological station ($\frac{w}{w_1} = k_w$) versus the mean-diurnal air temperature (from observations at the meteorological station) θ_1, for various values of the mean width of the given reservoir section, b. It is best to determine the latter as the ratio of the water area of the reservoir section to its length. The areas of bays and widened sections of tributary mouths should be included in the water area of the section. In the case of a negative air temperature, the coefficient k_w is taken constant, equal to 0.8 (reduction of the wind velocity to an altitude of 2 m).

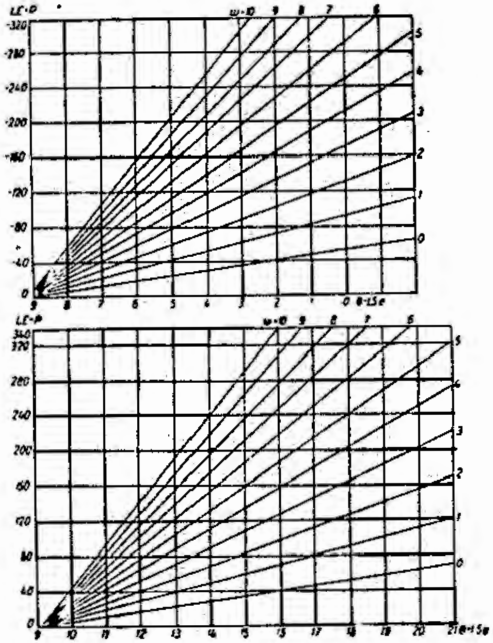

FIGURE 82. Nomographs for determining the heat-exchange components $LE + P$ (cal/cm²·day) as dependent on the mean-diurnal values of the air temperature θ, vapor pressure e (mb) and wind velocity w (m/sec) at a height of 2 m above the surface of the reservoir ice cover.

The unknown variation in the wind velocity is determined as the product of the wind velocity w_1, measured by the anemometer of a shore meteorological station, and the coefficient k_w

$$w = k_w w_1.$$

The air temperature and water-vapor pressure in the air over the ice cover (θ and e) are determined as dependent on the values of θ_1 and e_1 measured at meteorological stations and on the width b of the reservoir section (Figures 84 and 85).

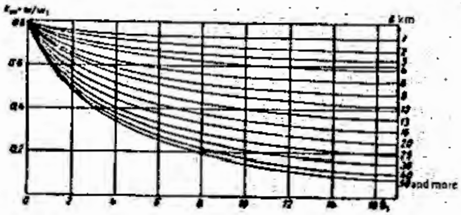

FIGURE 83. Ratio $k_w = \frac{w}{w_s}$ of the wind velocity at an altitude of 2 m above the ice cover to the wind velocity at the height of the anemometer at the meteorological station versus the air temperature θ_s at the meteorological station for various values of the mean width b of the given reservoir section.

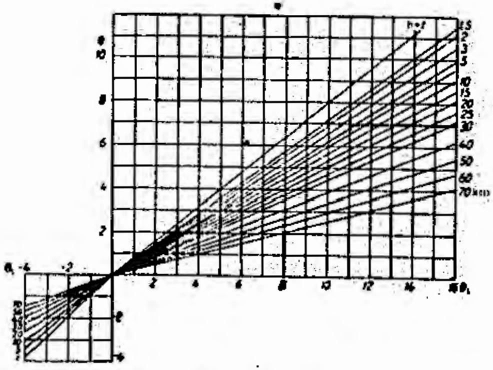

FIGURE 84. Air temperature θ at a height of 2 m above the reservoir versus the air temperature θ_s at the meteorological station for various widths b of the reservoir.

c) The effective radiation can be determined from the nomograph given in Figure 86, as dependent on the air temperature θ_s at the meteorological station and equivalent cloudiness N.

The heat input to the under surface of the ice cover, in contrast to the components of the heat balance on the upper surface, which are determined on a 24 hour basis, is taken into account, in the calculation method described, for the whole thawing period. The heat input to the under

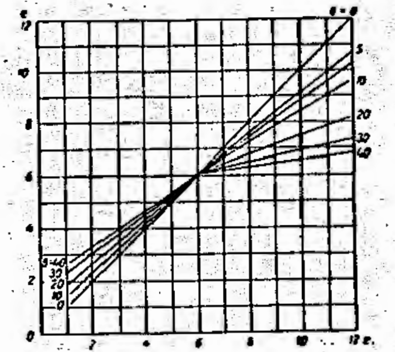

FIGURE 85. Pressure of water vapor in the air at a height of 2 m above the reservoir, e, versus the vapor pressure at the meteorological station e_s, for various width of the reservoir, b.

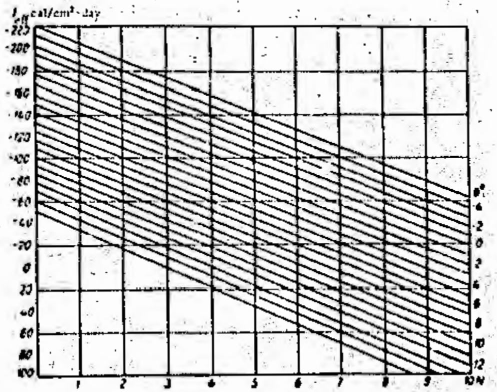

FIGURE 86. Nomograph for determining the effective radiation I_{eff} in cal/cm²·day versus the air temperature θ_s at the meteorological station and the equivalent cloudiness N (measured in the decimal scale).

surface of the ice cover is taken into account in two stages: first stage the heat arriving to the water and second the heat arriving from the water to the ice.

Heat arrives to the water body (basin) mainly from two sources: (1) the soil of the basin bottom and from the groundwater and (2) solar radiation penetrating through the ice. At the end of the melting period heat arrives also together with water of tributaries which are ice free and during the period of ice drift over the reservoir also as a result of heat exchange at ice-free water surfaces.

The heat input from the bottom soil of low water-inflow reservoirs amounts, on the average during the melting period, to about 5 cal/cm²·day.

The rate of the joint input of heat in the reservoir from both the bottom of the basin and groundwater during the melting of the ice cover, q_g, usually exceeds by several times the above-given rate of heat input from the soil of the basin bottom.

The heat input with the groundwater in spring time apparently depends, other conditions being equal, mainly on the extent of the preflood drawdown of the reservoir. The more the reservoir is drained, the higher the pressure head and, consequently, also the input of groundwater from aquifers and of water accumulated by the reservoir shores.

TABLE 38. Specific magnitudes of heat input from the soil of the basin bottom and from groundwater, for several reservoirs during spring in the period of the melting, q_g cal/cm²·day

No.	Storage reservoirs	q_g
1	Akulovskoe	6–7
2	Ivan'kovo	11–12
3	Klyaz'ma	12–14
4	Kama	18–20
5	Tsimlyanskoe	22–24

Table 38 gives data on the daily input of heat to the water from the soil of the bottom and with the groundwater, for several reservoirs.

The arrival of heat in the water due to solar radiation penetrating through the ice during the melting period, ΣQ_{pen}, for a thickness not less than 25 cm of the crystalline ice before the beginning of melting can be determined from Figure 87 as dependent on the thickness of the crystalline ice, $h_{cr.ic}$, before the beginning of melting and on the ratio of the amount of solar radiation absorbed by the ice from the upper surface during the melting period, ΣQ, to the total heat input from upper layers during the same period, Σq_0, equal to $\Sigma Q + \Sigma LE + \Sigma P + \Sigma L_{fl}$, i.e.,

$$\Sigma Q_{pen} = f\left(h_{cr.ic}, \frac{\Sigma Q}{\Sigma q_0}\right). \qquad (9.VI)$$

The heat input to the water during the melting period is given by the sum $\Sigma q_g + \Sigma Q_{pen}$.

The amount of heat input from the water to the ice during the melting period, Σq_w, can be determined from (by the means of Figure 88)

$$\frac{\Sigma q_w}{\Sigma q_g + \Sigma Q_{pen}} = f\left(\frac{vt}{h}\right). \qquad (10.VI)$$

whence

$$\Sigma q_w = (\Sigma q_g + \Sigma Q_{pen})\, f\left(\frac{vt}{h}\right),$$

where v is the mean flow velocity on the section, in m/sec; h is the mean depth (in m) during the melting period; t is the duration of the melting period in days.

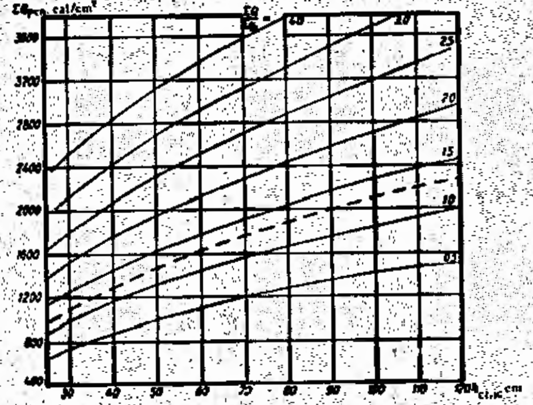

FIGURE 87. Amount ΣQ_{pen} (cal/cm²) of radiant heat penetrating through the ice cover to the water versus the thickness $h_{cr.ic}$ (cm) of crystalline ice for various ratios $\frac{\Sigma Q}{\Sigma q_0}$ of the amount of radiant heat absorbed by the ice from the outer ice surface during the thawing period to the total heat input from upper layers during the same period.

The flow velocity can be determined approximately as the ratio of the mean water discharge to the mean cross-sectional area for the mean water level on the stretch during the thawing period.

With values $\frac{vt}{h}10^3 > 200$ it is not necessary to determine the fraction of the heat spent on thawing, since almost all the heat arriving in the water is spent on thawing.

It should be borne in mind that Figure 88 can be used only when the water temperature of the upstream section of the reservoir, from where the water arrives at the given section, does not differ from the water temperature of the latter.

In some cases, for example, when preparing long-range forecasts of ice clearing of the reservoir, it is impossible to determine in advance the

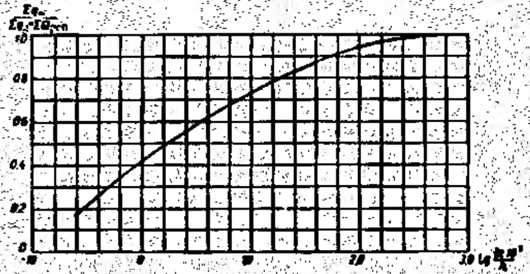

FIGURE 88. Relationship between $\frac{\Sigma q_w}{\Sigma Q_{pen}+\Sigma q_2}$ and lg $\frac{\omega f\cdot 10^3}{h}$.

ratio $\frac{\Sigma Q}{\Sigma q_0}$ necessary for finding the radiant heat input to the water. In such cases, the value of ΣQ_{pen} can be determined from the broken curve in Figure 87.

§ 2. Example of ice-clearing calculations

The procedure of the calculation of the date of ice clearing is shown in the example of the Tsimlyanskii storage reservoir for 1957.

The calculation is made for the downstream (wider) part of the reservoir, near the village of Suvorovo up to the dam (Figure 89). The mean width of this part is 14.5 km. The meteorological elements are taken from the meteorological station of Tsimlyanskii.

The following six gaging sites are situated on this part of the reservoir: Suvorovskoe, Krasnoyarskii, Krivskoi, Primorskii, Tsimlyanskii port, and Tsimlyanskii.

The data of the Krasnoyarskii gaging site were not used to determine the ice thickness, since the site is situated deep in a bay of the reservoir and the ice thickness measured near it is not characteristic of the water reservoir; the data of the Tsimlyanskii-port gaging site, situated at a mooring pier, were not used in the calculation of the mean depth of the snow on the ice, since in many cases the snow depth there is most uneven due to wind snow drifting.

Table 39 gives data on the maximum ice thickness, snow depth on the ice and dates of ice clearing for gaging sites located on the wide section of the reservoir, as well as data on solid precipitation during the stable ice period (until the first warming-up) for the Tsimlyanskii meteorological station.

TABLE 39. Peak ice thickness $h_{ic.m}$, snow depth h_{sn} on the ice before the beginning of melting, amount of solid precipitation $h_{so.pr}$ during the stable ice period and ice clearing along the lower part of the Tsimlyanskii reservoir

	Suvorovskoe	Krasnoyarskii	Krivskoi	Primorskii	Tsimlyanskii port	Tsimlyanskii
$h_{ic.m}$, cm	52	—	49	54	60	54
h_{sn}, cm	7	8	9	9	—	3
$h_{so.pr}$ (precipitation, mm)	—	—	—	—	—	37
Ice clearing date	7 IV	4 IV	6 IV	6 IV	29 III	7 IV

From Table 39 it follows that the largest of the peak ice thicknesses is 60 cm, the mean of the peak ice thicknesses is 54 cm, and the mean snow depth is 6 cm. The date of complete ice clearing is 7 April, the date of ice clearing at more than half of all the gaging sites is 6 April.

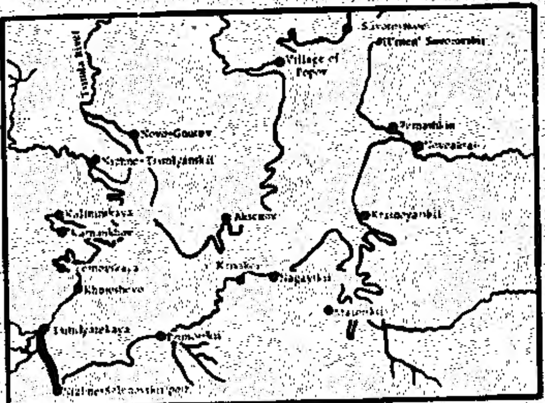

FIGURE 89. The downstream part of the Tsimlyanskii water reservoir.

From (3.VI)

$$h_{sn.ic}=a(0.1h_{so.pr}-0.25h_{sn})$$

we determine the thickness of the snow ice

$$h_{sn.ic}=1.66(0.1\cdot 37-0.25\cdot 6)=3.6\text{ cm}.$$

According to (4.VI)

$$h_{cr.ic} = h_{ic} - h_{m.ic}$$

the thickness of the crystalline ice will be: (a) for the calculation of the date of ice clearing of most part of the reservoir water area under consideration

$$h'_{cr.ic} = 54 - 3.6 = 50.4 \text{ cm},$$

(b) for the calculation of the date of complete ice clearing

$$h_{cr.ic} = 60 - 3.6 = 56.4 \text{ cm}.$$

By means of (2.VI) we determine the amount of heat necessary for ice clearing on most of the area under consideration

$$\sum^{m.p} q = \sum q_0 + \sum q_w = 73\cdot 50.4 + 70\cdot 3.6 + 20\cdot 6 = 5145 \text{ cal/cm}^2$$

and for complete ice clearing

$$\sum^{c} q = \sum q_0 + \sum q_w = 73\cdot 56.4 + 70\cdot 3.6 + 20\cdot 6 = 5580 \text{ cal/cm}^2.$$

The dates of the accumulation of these heat amounts and, thus, the dates of the corresponding ice clearing we calculate by computing the daily amounts of the heat-exchange components at the outer surface ($Q + I_{ef} + LE + P = q_0$) and of the total heat input to the under surface of the ice cover for the given date, $\sum q_w$.

We determine that a positive mean-diurnal air temperature sets in on 8 February, but a day before (on 7 February) it was still negative (−0.1°).

We calculate the heat exchange on the outer surface of the ice cover for 7 February.

From Figure 81 for the latitude 48° we obtain for 7 February $Q'_c = 245$ cal/cm²·day.

From (7.VI) we obtain for the equivalent cloudiness the value of 10. From Table 37 we have $k_N = 0.28$.

Substituting in (6.VI)

$$Q = 0.55 Q'_c k_N$$

the values for Q'_c and k_N, we obtain for the amount of radiant heat input

$$Q = 0.55\cdot 245\cdot 0.28 = 38 \text{ cal/cm}^2\cdot\text{day}.$$

For a equivalent cloudiness of $N = 10$ and a mean-diurnal air temperature of −0.1° (from the Tsimlyanskii meteorological station) we find from Figure 86 for the effective radiation

$$I_{ef} = -19 \text{ cal/cm}^2\cdot\text{day}.$$

For an air temperature at the meteorological station $\theta_1 = -0.1°$ and a reservoir width of 14.5 km we obtain, from Figure 84, for the air temperature θ over the reservoir a value of −0.1°. The vapor pressure, according to the data of the meteorological station, $e_1 = 6.0$ mb and the reservoir width is 14.5 km. For these values we obtain, from Figure 85, for the vapor pressure at a height of 2 m over the reservoir, $e = 5.8$ mb. From Figure 83 for $\theta_1 = -0.1°$ and $b = 14.5$ km we obtain for the coefficient of reduction of the wind velocity at the meteorological station (according to the anemometer) to the wind velocity at a height of 2 m over the reservoir, $k_w = 0.8$. With a wind velocity over the meteorological station $w_1 = 10.8$ m/sec, we obtain for the wind velocity over the reservoir $w = 10.8\cdot 0.8 = 8.6$ m/sec. Further, with $\theta = -0.1°$, $e = 5.8$ mb and $w = 8.6$ m/sec, from Figure 82, we find the total values of the heat exchange due to evaporation or condensation, LE, and heat exchange with the air, P

$$LE + P = -20 \text{ cal/cm}^2\cdot\text{day}.$$

For the heat exchange at the outer surface of the ice cover on 7 February we obtain

$$q_0 = Q + I_{ef} + LE + P = 38 - 19 - 20 = -1 \text{ cal/cm}^2\cdot\text{day}.$$

Thus, the calculation shows that there will be no melting on 7 February.

A similar calculation of the heat-exchange components at the outer surface of the ice cover on 8 February for $N = 10$, $\theta_1 = 1.2$, $e_1 = 6.6$ mb, $w_1 = 1.5$ m/sec, gives $Q = 38$, $I_{ef} = -8$, $LE + P = 22$ and $q_0 = 52$ cal/cm²·day.

Maximum heat necessary for ice clearing accumulates on 8 February. It is convenient to tabulate the initial data and the calculation results (Table 40).

In the same way we calculate the heat input (the values of q_0) for the following days and obtain the values of $\sum_{t=1}^{t} q_0$ at the end of each day.

For cases when the heat exchange q_0 during individual days or during a series of successive days is negative, i.e., if there is heat transfer, it is agreed, on the basis of considerations concerning the processes which take place when frosty weather sets in during the thawing period, to use the following order of summation of q_0. To obtain the values of $\sum_{t=1}^{t} q_0$ for these days, the negative quantity (or the negative quantities) obtained for q_0 are subtracted from the values $\sum_{t=1}^{t} q_0$ for the last days with positive values of q_0, in such a way, however, that the subtracted value does not exceed the amount of heat input during the two days before q_0 takes on negative values.

For example, in the thawing period of 1957 negative values of q_0 occurred, in particular, from 7 to 13 March, amounting to −700 cal/cm². But the sum q_0 during 5 and 6 March was only 12 + 12 = 24 cal/cm². Therefore, to determine $\sum_{t=1}^{t} q_0$ for the end of the 24 hours of 7 March ($q_0 = -3$ cal/cm²), we subtract 3 cal/cm² from $\sum_{t=1}^{t} q_0$ for the end of 6 March, equal to 897 cal/cm²; for 8 March ($q_0 = -42$ cal/cm²) we do not subtract 45 cal/cm² but only 24 cal/cm² from 897 cal/cm² already obtaining $\sum_{t=1}^{t} q_0 = 873$ cal/cm². This is the value we adopt for 9 to 13 March.

Parallel with the calculation of the heat input from upper layers we calculate the total sum of heat input to the under surface on a given date ($\sum_{t=t_1}^{t} q_w$). There is no need to carry out the calculation for each day from the beginning of the thawing period.

In the given example the first calculation of $\sum_{t=t_1}^{t} q_w$ is made for 24 March.

As indicated above, the first stage of the calculation of this quantity is to determine the total heat input to the water during the thawing period. To determine the total heat input to the water due to the penetration of

Table 39. Table used in the calculation of the date of complete ice clearing on the [illegible] reservoir

[illegible]	Date	Q_0', cal/cm²·day	Degree of cloudiness			A_s	Q, cal/cm²·day	θ_c	I_{eff}, cal/cm²·day	θ	[illegible]		w, m/sec	k_0	v, m/sec	$LE+P$, cal/cm²·day	q_0, cal/cm²·day	$\sum_{i=1}^{t} q_0$, cal/cm²	$\sum_{i=1}^{t} Q$, cal/cm²	$\frac{\sum_{i=1}^{t} Q}{\sum_{i=1}^{t} q_0}$	$\sum_{i=1}^{t} Q_{pen}$, cal/cm²	$\sum_{i=1}^{t} q_c$, cal/cm²	$\Sigma Q_{pen}+\Sigma q_c$, cal/cm²	$\sum_{i=1}^{t} q_w$, cal/cm²	$\sum_{i=1}^{t} q$, cal/cm²
			N_0	N_n	N						e_s	e													
1	2	3	4	5	6	7	8	9	10	11	12	13	14	15	16	17	18	19	20	21	22	23	24	25	26
													1957												
1	8/II	250	10	10	10	0.28	38	1.2	−8	0.5	6.6	6.3	7.5	0.65	4.9	22	52	52							
25	4/III	378	10	10	10	0.28	58	0.6	−13	0.3	6.1	6.1	2.9	0.71	2.0	5	50	873							
26	5/III	384	10	9.5	9.9	0.29	61	−0.2	−22	−0.1	5.2	5.3	3.5	0.80	3.0	−27	12	885							
27	6/III	390	10	10	10	0.29	60	−0.3	−21	−0.2	5.2	5.3	3.5	0.99	2.8	−27	12	897							
28	7/III	396	10	10	10	0.28	61	−0.9	−25	−0.7	5.2	5.3	3.3	0.80	3.0	−34	−3	894							
29	8/III	401	7.5	7.5	7.5	0.46	102	−1.8	−74	−1.3	4.8	4.9	4.8	0.89	3.8	−70	−42	873							
30	9/III	406	10	9.8	9.9	0.29	65	−3.0	−46	−2.2	4.4	4.6	7.2	0.60	5.4	−64	−49	873							
34	13/III	427	10	5	7.5	0.46	108	−1.6	−71	−1.1	5.0	5.1	4.5	0.60	3.6	−54	−17	873							
35	14/III	433	10	7.5	6.8	0.36	86	2.0	−19	1.0	6.1	6.1	4.0	0.50	2.3	17	84	957							
45	24/III	488	10	10	10	0.28	75	1.2	−8	0.5	6.4	6.2	1.0	0.65	0.6	4	71	1375	3776	2.75	2620	1035	3655	3070	4445
58	6/IV	570	5.0	1.2	3.1	0.87	274	7.9	−59	4.2	7.0	6.5	0.5	0.40	0.2	33	242	2310	5419	2.52	2440	1334	3774	3169	5479
59	7/IV	575	0.8	0.8	0.8	0.94	292	10.6	−75	5.7	6.6	6.3	1.5	0.37	0.7	53	270	2580	6111	2.37	2330	1357	3687	3097	5677

radiant heat through the ice by summing the daily values of Q (column 8), we find the value of $\sum_{i=1}^{45} Q$ (column 20) for 24 March (during 45 days before the beginning of melting). Next we determine the ratio $\frac{\Sigma Q}{\Sigma q_0}=\frac{\sum_{i=1}^{45} Q}{\sum_{i=1}^{45} q_0}=2.75$ (column 21).

From Figure 87 we determine the input of radiant heat through the ice to the water during the period from the beginning of thawing to 24 March (ΣQ_{pen}), corresponding to the value $\frac{\Sigma Q}{\Sigma q_0}=2.75$ and to the above-obtained thickness of the crystalline ice, $h_{cr.ic}=56.4$ cm, for the calculation of the complete ice clearing. We obtain ΣQ_{pen} 2640 cal/cm²·day. The specific heat input to the water from the bottom and groundwater, q_c, we take according to Table 38 equal to 23 cal/cm²·day. We have $\sum_{i=1}^{45} q_c=1035$ cal/cm² (graph 1°).

The total heat input to the water from the beginning of thawing to 24 March is $(\Sigma Q_{pen}+\Sigma q_c)=2620+1035=3655$ cal/cm² (column 24).

The second stage, determination of the total heat input from the water to the under surface, Σq_w, is calculated by means of Figure 88. We calculate the mean flow velocity v and the mean depth h necessary for this, as indicated above, from data on the water stages and discharges. We obtain $v=0.005$ m/sec and $h=7.9$ m.

We have $\lg\frac{vt\cdot 10^3}{h}=\lg\frac{0.005\cdot 45\cdot 10^3}{7.9}=1.45$.

From Figure 88 we have $\frac{\Sigma q}{\Sigma Q_{pen}+\Sigma q_c}=0.84$, hence

$$\Sigma q_w=0.84(\Sigma Q_{pen}+\Sigma q_c)=0.84\cdot 3655=3070\ \text{cal/cm}^2\ \text{(column 25)}$$

The value of Σq_0 at the end of 24 March was 1375 cal/cm² (column 19).

Thus, the total heat input to the ice cover during the period from the beginning of thawing until 24 March was (column 26)

$$\Sigma q=1375+3070=4445\ \text{cal/cm}^2.$$

For complete ice clearing $\Sigma q=5580$ cal/cm² is required.

The calculation is continued until the total amount of heat inflow from above and from below ($\Sigma q=\Sigma q_0+\Sigma q_w$) becomes equal or larger than the amount of heat necessary for ice clearing (5580 cal/cm²). This amount is accumulated on 7 April. For the date of ice clearing the next day after the accumulation of the necessary amount of heat, in the present case 8 April, is taken.

The calculation method described can be used not only for calculating long-time series of dates of ice clearing on new water reservoirs, but also for short-range ice clearing forecasts. When preparing a short-range ice-clearing forecast, the heat input from above to the ice cover during the period from the beginning of melting till the day of issuing the forecast is calculated on the basis of the actual meteorological data, as described above, and for the forewarning period of the forecast, on the basis of data from the meteorological forecast. In the absence of a forecast for wind velocity w_z, cloudiness N, and air humidity e_z, the mean values for the thawing periods of w_z and N are taken over a long-time period, and the value of e_z is taken from its relationship with the air temperature.

The calculation of the heat input from the water has no peculiarities compared with that described above.

§ 3. Forecasting the dates of beginning of ice drift and ice clearing from empirical relationships

Computations of ice clearing on the basis of the calculation of thawing, described in the previous sections, are used to prepare forecasts mainly in cases when the observation data are not sufficient to set-up empirical relationships.

a) **Forecasting of the date of ice clearing on most parts of a given reservoir from its relationship with the date of accumulation of the amount of heat corresponding to a given thickness of the ice cover.** The amount of heat necessary for ice clearing Σq, is determined from the mean of the maximum values of the ice cover thickness h_{ic}, measured at all the gaging sites of the given reservoir section (the original ice thickness)

$$\sum q = \rho_{ic} L h_{ic} = 73 h_{ic} \quad \text{cal/cm}^2,$$

where h_{ic} is the thickness of the ice cover in cm, ρ_{ic} and L_{ic} are the ice density and ice-thawing heat.

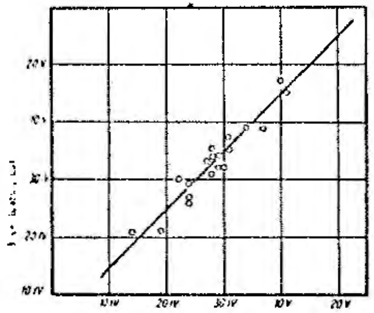

FIGURE 90. Date of ice clearing on the Perebory Bay of the Rybinsk reservoir [illegible] as a function of the date of accumulation of the necessary amount of heat

The dates of annual accumulation of this amount of heat in the given examples are determined by means of a nomograph for the particular region similar to that given in Chapter V, Part B, § 1 (Figure 52). Also described there is the technique of plotting such nomographs.

In the examples given here the heat inflow is summed from the day after which a mean-diurnal negative air temperature is observed for not more than three successive days.

The relationship for forecasting the date of ice clearing is prepared as follows.

In accordance with the values of the original ice thickness during the several years the reservoir exists, the amount of heat necessary for complete ice clearing is determined for each year. From the air temperature the daily heat input is determined by means of a nomograph. In this way, the date of accumulation of the necessary amount of heat, Σq, for each year is determined. The obtained dates for the accumulation of Σq are graphically related to the actual dates of ice clearing on most of the given reservoir. An example of such a relationship (for forecasting the dates of ice clearing on the Perebory Bay of the Rybinsk reservoir) is shown in Figure 90. Actual ice clearing is observed later than at the calculated dates of accumulation of the necessary heat, in the given example 5 days later on the average.

An earlier accumulation of the necessary amount of heat as compared with the actual dates of ice clearing makes it possible to prepare forecasts of ice-clearing dates with a mean forewarning period of 5 days (in the

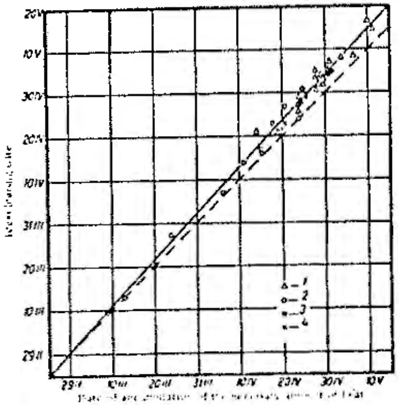

FIGURE 91. [illegible] date of ice clearing [illegible] date of accumulation of the necessary amount of heat

1—[illegible]

present example without using air-temperature forecast. When using the latter, the forewarning period of the ice-clearing forecast can be accordingly increased.

Figure 91 gives a generalized relationship for forecasting the ice clearing on most of the open regions of the reservoir, obtained from data of observations on the Rybinsk, Tsimlyansku, Gor'kii and Kuibyshev water reservoirs. The use of this relationship without air-temperature forecasts does not always provide the necessary forewarning period.

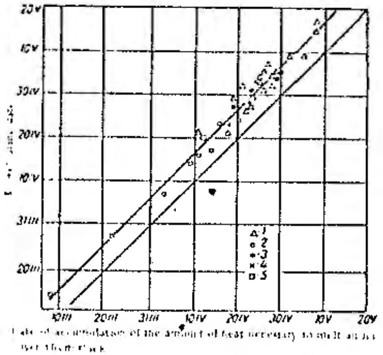

FIGURE 92. [illegible] graph relating the date of ice clearing on most of [illegible] the open regions of the reservoir to the date of accumulation of the amount of heat necessary to melt an ice cover 10 cm thick.

[illegible], 2—Tsimlyanskii, 3—Gor'kii, 4—Kuibyshev, 5—Volgograd

In order to increase the forewarning period (without using the air-temperature forecasts), it is possible to use the relationship shown in Figure 92, where the date of ice clearing on most of the open region of the reservoir is determined as dependent on the date of the accumulation of the heat, Σq, necessary for melting an ice cover 10cm thick. The forewarning period of the forecast not using air-temperature forecasts varies from 4 to 11 days and is on the average 6 days. When using the weather forecast, the forewarning period accordingly increases.

b) Forecasting date of the beginning of ice drift (breakup) from its relation to the date of the accumulation of the heat amount necessary for melting an ice cover 15 cm thick. The beginning of ice drift can be predicted similarly in the same way as shown in a subsection of this part. For the beginning of the drift (breakup) the earliest date of ice drift on a given stretch is taken. In this connection, local ice breakup or local ice drift is not taken into account.

Figure 93 gives a generalized relationship between the date of the beginning of ice drift (or breakup) and the date of the accumulation of the heat amount necessary for melting an ice cover 15 cm thick. The graph gives two lines (plotted on the basis of two groups of points). The lower line corresponds to the beginning of ice drift in open sections, the upper line to closed sections of water reservoirs.

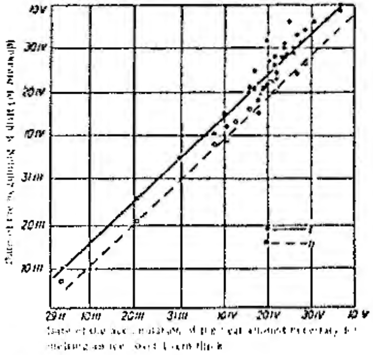

FIGURE 93. Generalized graph relating the date of the beginning of ice drift (or breakup) to the date of the accumulation of the heat amount necessary for melting of ice cover [illegible]

[illegible]

The beginning of ice drift in bays is determined from observations at the following gaging sites: Pereboiy (Pereboiy Bay) on the Rybinsk, Zheltukhino on the Gor'kii and Yablonovyi Ovrag on the Kuibyshev water reservoirs. On the Tsimlyansku storage reservoir observations were not conducted in special parts; use was made of observations on ice breakup on the small Bereslavskoe storage reservoir of the Volga-Don canal. The forecasting accuracy by the indicated relationship is satisfactory. The forewarning period of the beginning of ice drift on open water areas is on the average equal to the forewarning period of the air-temperature forecast, and the forewarning period of the beginning of ice drift in bays (closed water area) is on the average 3 days longer.

Forecasting of the beginning of ice drift in isolated parts of water reservoirs by means of the generalized relationship given in Figure 93 is less accurate than for forecasts in open parts. This is due to the considerable influence of the difference in the hydraulic and morphometric factors, which are not taken into account by the described technique.

c) Forecasting local ice breakups and ice clearing on river zones and bays of water reservoirs. The accuracy of forecasts for relatively small isolated regions (bays) of water reservoirs by the above given generalized relationships is reduced mainly due to the fact that, in this case, the lowering of the water level during the winter and preflood drawdown and subsequent level rise during the spring recharge contributes considerably to the destruction of the ice cover. This influence is particularly strong in places where, in accordance with the morphometric features of the given reservoir, the ice during the winter drawdown freezes to the bottom over large areas.

In such cases, taking these conditions into account may considerably increase the accuracy of the determination of the amount of heat necessary for ice breakup or ice clearing. The thickness of the ice cover h_{ic} before the beginning of thawing, the level H_0 of the preflood drawdown and the rise in the water level before ice breakup or the first ice push

$$\Sigma q_0 = f(h_{ic}, H_0, \Delta H), \tag{11.VI}$$

are factors which determine the amount of heat Σq_0 necessary for ice clearing (or breakup).

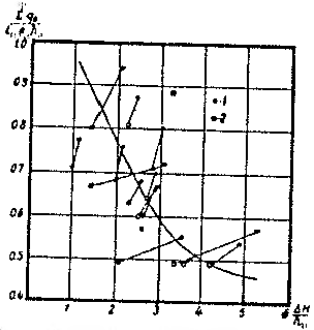

FIGURE 94. Graph of (13.VI), used to determine the total heat inflow per unit outer surface of the ice cover necessary for ice breakup on the Rybinsk reservoir in the region of the Koprino station. $\overset{\text{up}}{\Sigma} q_0$ is dependent on the thickness of the ice cover before the beginning of thawing h_{ic}, and on the water-level rise above the lowest preflood drawdown level.

1—values of $\overset{\text{up}}{\Sigma} q_0$ and ΔH at the day of ice breakup; 2—values of $\overset{\text{up}}{\Sigma} q_0$ and ΔH on the previous day

To forecast local ice breakups on river zones of water reservoirs, as well as to forecast ice breakup on rivers, it is possible, with observation data on hand, to use relationships similar to (2.V)

$$\overset{\text{up}}{\Sigma} q_0 = f(h_{ic}, \Delta H), \tag{12.VI}$$

where $\overset{\text{up}}{\Sigma} q_0$ is the total heat inflow per unit outer surface of the ice cover, which is necessary for ice breakup; h_{ic} is the thickness of the ice cover before the beginning of thawing; ΔH is the water-level rise above the lowest preflood drawdown level.

The quantity ΔH directly also characterizes the flow velocity, to which it is closely related.

Using dimensional analysis the relationship for determining the quantity $\overset{\text{up}}{\Sigma} q_0$, in this case, may be represented as

$$\frac{\overset{\text{up}}{\Sigma} q_0}{L_{ic}\rho_{ic}h_{ic}} = f\left(\frac{\Delta H}{h_{ic}}\right), \tag{13.VI}$$

where L_{ic} and ρ_{ic} are the thawing heat and the ice density.

Figure 94 gives such a relationship for the Rybinsk storage reservoir in the region of the Koprino station. The values of $\overset{\text{up}}{\Sigma} q_0$ are determined from the air temperature (at the Rybinsk meteorological station) by means of a nomograph similar to that described in Chapter V, Part B, § 1, but plotted for the region under consideration.

When plotting the graphs of (13.VI) it is convenient to represent each case by two points, corresponding to the values of $\overset{\text{up}}{\Sigma} q_0$ and ΔH on the breakup day (including q_0 during the breakup day) and on the previous day.

The values of $\overset{\text{up}}{\Sigma} q_0$ are calculated by means of the graph of (13.VI) using the method of successive approximation.

The accuracy of the calculation of the time of ice breakup by means of the relationship shown in Figure 94 is very high (in 11 cases the calculation error is equal to 0 days, in two cases to 1 day, and in 1 case to two days). However, a shortcoming in the preparation of an ice breakup forecast is the necessity to forecast the values of ΔH.

C. FORECASTING USING THE CHARACTERISTICS OF THE ATMOSPHERIC PROCESSES (LONG-RANGE FORECASTING)

The main peculiarity of the spring ice breakup over the widened areas of water reservoirs is ice melting in still-water zones due to the very low flow velocities. Under such conditions, provided the ice cover is thicker than on rivers, the period of ice melting is very long (a month and more). In this case, the dates of ice clearing of the reservoirs is more or less independent of individual air-temperature fluctuations in the course of this period. The time of ice clearing for a given thickness of the ice cover can therefore be determined as dependent on large air-temperature anomalies, caused by those atmospheric processes which prevail during a long period. These peculiarities facilitate long-range forecasting of the ice clearing of water reservoirs.

As an example we present the method of forecasting ice breakup and clearing on the Rybinsk reservoir. The method is based on the dependence of the dates of ice clearing of the reservoir on the maximum ice thickness and the date of the final transition of the mean daily air temperature through 0 (Figure 95). The forecast is prepared at the beginning of April with a mean forewarning period of more than a month. [illegible] ratio $\frac{s}{\sigma}$ for the relationship, calculated for all the 19 years the reservoir exists, is 0.47; during 9 years of routine use of the relationship (1952–1960), this dependence was found to be very stable,* although in the last years sharp rearrangements in the atmospheric processes, in no way taken into account by the arguments of the dependence, were rather frequent.

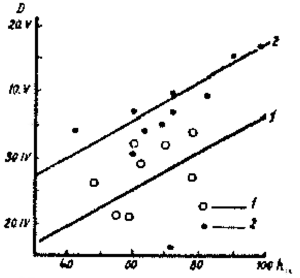

FIGURE 90. Dates of ice clearing of the [illegible] Bay of the Rybinsk reservoir, D, as a function of the ice thickness on 15 March, h_{ic}, and of the date the mean-diurnal air temperature takes on positive values.

1—transition of mean air temperature through 0° earlier than 5 April; 2—transition through 0° later than 5 April.

The forecast of ice clearing on the Rybinsk reservoir is corrected by taking into account the observed sum of temperature rises, $\Sigma\Delta\theta$, during the period from 6 March to 15 April. The calculation of $\Sigma\Delta\theta$ from the mean-diurnal air-temperature data at the Rybinsk meteorological station is carried out as indicated in Chapter V, Part C. The quantity $\Sigma\Delta\theta$ characterizes the degree of development of the atmospheric processes which are connected with warming-up periods, at the beginning of the spring synoptical season throughout which ice melting takes place, and, in the case of a high intensity of warming-up, with the melting conditions themselves. The correction for the ice clearing forecast from the dependence of the ice clearing dates for the Rybinsk reservoir and of the value of $\Sigma\Delta\theta$ on the maximum ice thickness on it is made on 16 April with a mean forewarning period of about 20 days.

With long-time observation data on the thickness of the ice cover and on the ice clearing on the reservoir, it is not particularly difficult to work out a technique of long-range forecasting ice clearing. However, most water reservoirs are of more recent existence, and the methods of forecasting their ice clearing have to be prepared, as a rule, before they are filled. The problem arises of being able to prepare forecasts in the absence of observation data.

This problem was solved in two ways.

The first consists in obtaining a long-time series of data on ice cover thicknesses and ice clearing dates for the conditions of the given reservoir, by calculating from meteorological data for past years. To obtain the dates, a technique of long-range forecasting is worked out.

The thickness of the ice cover before the beginning of melting can be calculated for each year with sufficient accuracy for long-range forecasting of ice clearing from meteorological data for the stable ice period (see Chapter IV). Of course, the beginning of the stable ice period is also determined in this case by calculation (see Chapter III).

Ice clearing dates can be calculated by the method described in Part B § 1, of this chapter (for a thickness of the ice cover before the beginning of melting not smaller than 25 cm). In working out methods for long-range forecasting of ice clearing in widened areas of the Tsimlyanskii, Kuibyshev and some other reservoirs, the series of ice-clearing dates were calculated by a somewhat different method. In this method the following equation is used

$$1.1L_{i}\rho_{i}h_{t} = Q + I_{ef} + LE + P. \qquad (14.VI)$$

The left-hand side of this equation represents the amount of heat necessary to melt completely the theoretical ice thickness h_{t}. The right-hand side of the equation is the sum of the heat exchange components on the outer surface of the ice cover. The heat input to the under surface of the ice cover is not introduced in the equation. In calculating LE and P, the wind velocity is taken at the height of the anemometer without corrections for the influence of the reservoir.

The heat-exchange components (besides the radiant-heat input) are calculated from the data of each of the four standard hours of observation of the meteorological elements. Both positive and negative values of the heat-exchange components are summed.

In the absence of a considerable stream flow and of climatic conditions close to those at water reservoirs whose data are used to obtain the graphs given in Figures 91 and 92, the dates of ice clearing of a large part of the given reservoir region can be calculated to a first approximation by means of these graphs.

The second way consists in determining, from meteorological observations during past years, the dates of the accumulation of definite heat amounts and in finding out the relationships between these dates and the characteristics of development of the atmospheric processes. In forecasting, the ice clearing date is determined as the expected date of accumulation of the amount of heat necessary for melting the ice existing on the reservoir in the given year. This approach makes it possible to dispense with the calculation of the ice thickness during years before the reservoir existed. This is particularly important for water reservoirs with considerable water inflow and discharge, important winter drawdowns, other peculiarities of the hydraulic conditions, which affect ice growth, or with special conditions of heat input from groundwater. An advantage of this way is also the possibility of preparing an ice clearing forecast for individual sections of the water reservoir taking into account the difference in the ice thickness on them.*

---

* In methods in which the date of the final transition of the air temperature through 0° is used as argument, this date should be determined diagnostically. In the method given this has been done.

The first way also has advantages. First of all, as a result of the calculation of the ice clearing dates for a number of years, we obtain the characteristics of the future ice regime of the reservoir, which have a practical value. Working out the technique on the basis of the calculated ice clearing dates, we are not bound by the necessity to use data on the maximum ice thickness in order to issue the forecast. This makes it possible to increase the forewarning period of the forecast and to issue it at definite calendar dates.

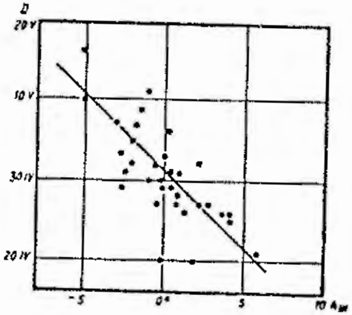

FIGURE 96. Dates of ice clearing of the widened area of the Kuybyshev storage reservoir at Ul'yanovsk, *D*, as a function of the air-temperature anomaly at Ul'yanovsk in March A_{III}.

Let us give examples. The method of forecasting ice clearing on the Kuibyshev storage reservoir is based on the calculated dates of this phenomenon for a series of past years (from 1925 to 1957). The reservoir in the region of the widened area at Ul'yanovsk clears up on the average (according to calculation) on 1 May. The ice clearing in this region occurs later than in other regions of the Volga stretch. Ice melting usually begins on it in March. The conditions in the period of the beginning of ice melting therefore can be characterized by the mean air-temperature anomaly in March. If in this month there are low temperatures, ice melting begins late, and the ice itself, although its thickness does not considerably increase in March, preserves its structure and strength toward the beginning of melting. Such conditions contribute to late ice clearing of the reservoir. A high air temperature in March, on the other hand, causes in this month melting of the snow on the ice cover, break down and weakening of the ice cover, and in some cases also direct melting of the ice. In addition, in March the spring synoptical season begins, which extends over the following period, including the beginning of May. In virtue of the uniformity of the atmospheric processes prevailing during the season, the temperature conditions in March approximately characterize also the conditions of the whole ice-melting period. The air-temperature anomaly in March (bench-mark meteorological station Ul'yanovsk) therefore determines, to a large extent, the time of ice clearing of the reservoir (Figure 96). The forewarning period of the forecast, which can be prepared on 1 April, is equal to 30 days on the average. The accuracy of the relationship is characterized by $\frac{s}{\sigma}=0.72$.

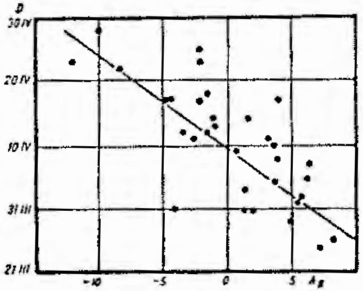

FIGURE 97. Dates of ice clearing of the Tsimlyansk reservoir, *D*, as a function of the air-temperature anomaly at Tsimlyanskaya in February, A_{II}.

Another example. The Tsimlyansk storage reservoir is clear of ice on the average on 10 April (by calculation for the period from 1925 to 1957), ice melting on it usually begins in February. In February the synoptical season of the second half of the winter begins and extends over the first half of March. The dates of ice clearing therefore largely depend on the air-temperature anomaly in February (Figure 97). The forewarning period of the forecast, which can be prepared on 1 March, on the average exceeds a month. The accuracy of the relationship is characterized by $\frac{s}{\sigma}=0.71$.

Such relationships are extremely simple and to a first approximation satisfy practical requirements. However, the forewarning period and accuracy of the forecasts can be considerably improved, if the variation in the air-temperature anomaly from season to season, as dependent on the preceding variation in the characteristics of the heat input from the southwest, Γ (see Chapter V, Part C, §2), is taken into account. In this way it is possible, at the beginning of February, to determine the conditions of heat input in the second half of the winter, i.e., in February–March, and at the beginning of March – the conditions of heat input in the spring synoptical season, i.e., in March–April. The air temperature in these months mainly determines the dates of ice clearing. Thus, for example, the dates of ice clearing on the Kuibyshev reservoir are obviously related with the temperature anomaly in March and April, which can be seen from Figure 98. This figure also shows how the severity of the winter, expressed by the sum of the mean-monthly temperatures from October to March (bench-mark meteorological station Ul'yanovsk), influences these dates.

---

* It should be borne in mind that when using the second way, the accuracy of ice clearing forecasts is essentially not estimated. Only the accuracy of the method of forecasting the accumulation of the amount of heat necessary for complete melting of the definite ice thickness is estimated.

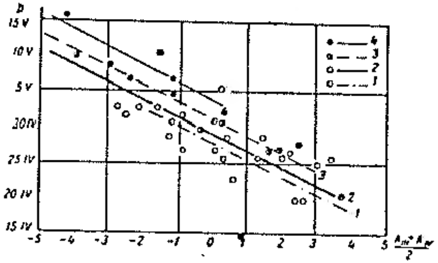

FIGURE 98. Variation in dates of ice clearing on the widened reservoir area at Ul'yanovsk, D, with the air-temperature anomaly during March and April $\frac{A_{III}+A_{IV}}{2}$, for various values of the sum of mean-monthly air temperatures at Ul'yanovsk from October to March, $\Sigma\theta_{-}$.

1 – $\Sigma\theta > -55°$; 2 – $-55° > \Sigma\theta_{-} > -4$[illegible]°; 3 – -4[illegible]° $> \Sigma\theta > -32°$; 4 – $\Sigma\theta_{-} < -32°$.

The basis for the forecasting technique is the relationship between the clearing up dates of the storage reservoir and the variation in the characteristics of the relative geopotential gradient from the first to the second half of the winter, $\delta\Gamma_2$ (Figure 99). Cases of particularly severe winters are marked as a separate group. Particularly severe are cases when the sum of the mean-monthly air temperatures from October to February was below −48°.

The values of $\delta\Gamma_2$ (Table 36) were determined, as described in Chapter V, Part C, § 2, from the deviations of the mean-monthly values of ΔH_{1000}^{500} at the points shown in Figure 77, during December, January and February from the rated values. The accuracy of the method is characterized by $\frac{s}{\sigma} = 0.54$. It should be noted that the relationship lines drawn for years with a particularly severe winter are arbitrary due to the small number of such points. However, even if these cases are not put into a separate group, the relationship (Figure 99) remains satisfactory (the confidence limit of the permissible errors $\delta = 0.674\sigma$ is 93%).

The forecast of ice clearing on the Ul'yanovsk section of the Kuibyshev reservoir by this method can be prepared at the beginning of March with a mean forewarning period of about two months.

The forewarning period makes it possible to refine the forecast in the middle of April, using the expression described above, for the Rybinsk reservoir, i.e., the dependence of the dates of ice clearing and ice thickness on the sum of temperature rises $\Sigma\Delta\theta$ during the period from 16 March to 15 April. The peculiarity of this relationship (Figure 100) for the Kuibyshev storage reservoir (as also for others, recently created) consists in that the maximum ice thickness and the dates of ice clearing in past years, used to set it up, are not observed, but calculated. The ratio

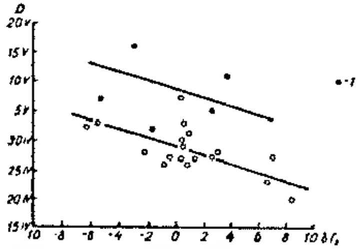

FIGURE 99. Dates of ice clearing of the widened area [illegible] D as a function of the variation [illegible] geopotential gradient from the first to the second half [illegible] $\delta\Gamma_2$

● – cases of particularly severe winters

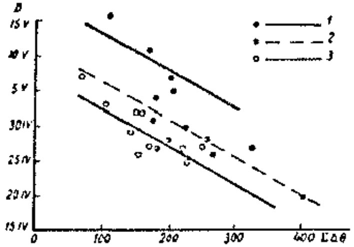

FIGURE 100. [illegible] D [illegible] $\Sigma\Delta\theta$ [illegible] h,

1 – h [illegible] > [illegible] > h [illegible] h < [illegible]

$\frac{s}{\sigma}$ for this relationship is 0.46. The root-mean-square error, $\delta = 2.7$ days, is close to the error of the ice clearing calculations themselves. The forewarning period for the corrected forecast is 15 days on the average

We turn to another example — the Tsimlyanskii water reservoir. Here, as already mentioned, the time of ice clearing depends largely on the conditions of the second half of the winter, but in cases of normal and late ice-clearing spring conditions (of the second half of March and of April) become most important. The thickness and strength of the ice cover considerably influence the dates of ice clearing on the reservoir. Thus, all the conditions here are similar to those considered in Chapter V, Part C, § 2 for the ice breakup on the Lower Volga. Therefore, the technique of forecasting ice clearing on the Tsimlyanskii reservoir resembles that described for forecasting ice breakup on the Lower Volga. The difference lies only in that to calculate the sum of the negative temperatures data of the meteorological station Boguchar are used.

A similar technique of long-range forecasting of ice clearing has been worked out for a number of reservoirs — Gor'kii, Kuibyshev, Volgograd, Tsimlyanskii and Kakhovka.

A technique for forecasting ice clearing on the Kama reservoir has been worked out differently. Instead of the dates of ice clearing during past years the dates of accumulation of definite amounts of heat, Σq_0, arriving through the outer surface of the ice cover, were calculated.

For each year (from 1940 to 1959) the dates of the accumulation of the sum Σq_0, equal to 2000, 2500, 3000 and so on up to 5500 cal/cm^2 were calculated by means of nomographs similar to that given in Part B, (Figure 52) and based on the data of the meteorological stations Chermoz (for the central part of the reservoir) and Perm' (for the part near the dam). In this way the long-time series of dates of accumulation of each value of Σq_0 were calculated. These dates can be related to the atmospheric-circulation characteristics by means of which an early estimate is made of the conditions of heat input in the period of ice melting.

Such characteristics for the Kama reservoir may be the indices of development of the atmospheric processes at the beginning of the spring synoptical season (in March), since ice clearing of the reservoir usually occurs at the end of this season. To forecast ice breakup on rivers of this region two types of such characteristics are used.

The first characteristic, the prevailing direction of transport of air masses relative to the northeastern regions of the ETS (Chapter V, Part C, § 1), is expressed by the angle between the isobars on the mean-monthly pressure map for March and the parallel in the region of the station Troitsko-Pechorskoe (α). The current in March is usually directed from the west, northwest or north ($0° < \alpha < 100°$), or from the southwest or south ($250° < \alpha < 360°$). Eastern current direction is very rarely observed.

The second characteristic, the number n of days in March with processes of the western or southwestern type, reflects the intensity of processes causing warming-up periods in the basin of the Kama River. To these processes belong all cases when cyclones emerge in the basin of the Kama River from the west or southwest. These characteristics are related since they reflect different features of the same atmospheric processes in March.

The date of the accumulation of the heat amount Σq_0 necessary for ice clearing is determined from the graph (Figure 101) plotted for the middle part of the Kama reservoir. For $\alpha > 150°$ and $n < (0.076\alpha - 7.8)$, and also for $\alpha < 150°$ and $n < (15 - 0.076\alpha)$, the system of lines 1 should be used; in other cases, the system of lines 2. For $\alpha > 180°$ the required date is determined from the difference $360° - \alpha$.

Let us follow the order of preparation of the forecast in the example of 1958. In March of this year the angle of the isobars of the mean pressure was $\alpha = 340°$, $n = 11$ days. In this case $\alpha > 150$ $(0.076\alpha - 7.8) = 0.076 \cdot 340 - 7.8 = 18$, the number n is smaller than 18. Therefore, we determine the required date from the system of lines 1 (Figure 101).

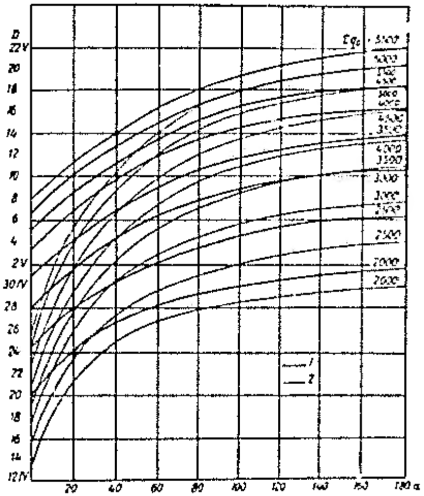

FIGURE 101. Variation of the dates of accumulation [illegible] amounts, D, with the angle between the [illegible] air current and the parallel, α, and [illegible] α and the number n of western and southwestern [illegible]

1 — for $\alpha > 150°$ and $n <$ [illegible], and also for $\alpha <$ [illegible] and $n <$ [illegible]; 2 — for other relations between α and n

The ice thickness in 1958 in the central part of the reservoir reached 83 cm, the mean snow depth, 25 cm and the depth of solid precipitation during the stable ice period was 13.2 cm. According to these initial data, the amount of heat necessary for ice clearing in the central part of the reservoir, calculated by the method described in Part B, was in this year 4700 cal/cm^2. Such an amount for $\alpha = 340°$, or for its corresponding value of the argument $360 - \alpha = 20°$ should accumulate on 9 May (Figure 101), and the reservoir should become free of ice on 10 May. Actually in this year the central part of the Kama reservoir was cleared on 13 May.

Chapter VII

FORECASTING OF ICE JAMS AND RISE OF WATER STAGE DUE TO JAMMING

§ 1. Conditions for the formation of jams. Factors determining ice-jam stage rise

Ice breakup on a river is not a process which advances along the river strictly successively. The nonuniform thickness of the ice cover and the nonuniform resistance of the river channel on its various stretches exclude such a strict succession even when ice breakup begins in the lower reaches of the river. Even in the case of ice breakup which advances upstream, the moving ice encounters individual sections of stable ice. However, the ice in this case is already so weakened that usually considerable ice jams do not form under these conditions. The fact that ice breakup usually occurs there before the arrival of the flood wave is important. If, in accordance with the physiographical features of the river basin and the meteorological conditions, the flood wave and ice breakup on the river travel downstream, then the ice moving downstream usually bars the path of the ice cover on a stretch where conditions for ice breakup have not yet set in. Ice jamming with destruction of adjacent parts of the ice cover begins, while piling of ice blocks continues and a considerable part of the cross section of the stream becomes obstructed.

Ice jams form preferably in sections where the longitudinal slope of the river considerably decreases, in places with islands, sharp bends or contractions of the bed and in zones of the backwater area in water reservoirs, etc.

Ice jams may form in places with favorable bed conditions also in the absence of an ice cover or continuous ice fields. Such jams are, however, less stable and do not result in a large rise of the water stage.

Before ice breakup, the ice cover is usually preserved for longer time in places of reduced slope and flow velocity. During the freezing of rivers in such places the first stable ice bridges and, in the case of sufficiently high rate of ice approach to the bridge, accumulations and pilings of ice (jams) may form. Ice accumulations in such places are larger, the higher the flow velocity of ice blocks approaching the bridge and the larger in this period the air-temperature fluctuations (see Chapter II). Owing to the presence of various ice forms under the ice cover, its thickness in such places increases at a higher rate than on neighboring sections. Toward spring the thickness of the ice cover there is larger than on the more upstream located stretch.

Besides the preservation of the ice cover downstream of a river stretch where ice drift began, an intensive ice drift with a flow velocity sufficient for the piling of ice blocks is necessary for the formation of a considerable ice jam.

An ice jam may form if at the time of the approach of the flood wave and ice drift the rise in the water stage (and in the ice cover), due to local runoff and also to the weakening of the ice cover, is still small and insufficient for breakup.

Decrease in the air temperatures to negative values during ice breakup period also contributes to the formation of ice jams.

Most often ice jams tend to form in the same place with a general decrease in the river slope, meaning a decrease in the slope over a considerable river stretch due to the topographical and geological features of the river basin, in contrast to local decreases in the slope on some isolated river stretches. In such places ice jams are most stable. It is much more difficult to combat such ice jams than those forming in other places under conditions favorable for ice-jam formation.

It should be borne in mind that particularly favorable conditions for ice jamming during spring breakup are created in places when it was preceded by ice breakup during the winter flood, which stopped on the given river stretch, with ice-jamming and gorging in the next cooling.

A general decrease in the slope is the cause of frequent ice jamming also in upper parts of water reservoirs. However, in this case the conditions of ice jamming are greatly influenced by the nature of the runoff control (winter and spring drawdown or spring recharge).

Owing to the considerable filling of the bed by disorderly piled-up ice blocks, the resistance to the streamflow increases sharply, the slope of the water surface on the ice-jam section accordingly also increases sharply, and upstream from the ice jam backwater thus formed increases, the larger the increase in the resistance to water motion on the stretch of the ice jam. The increase in the flow resistance on the ice-jam stretch is, in the final analysis, larger the larger the amount of ice, the higher its strength and the higher the velocities at which it approaches the place of ice jamming.

The maximum rise in the water stage during ice jamming depends on the amount of ice piling up to form a gorge until its break-through. The time of break-through of a jam depends on the strength of the ice cover and on the resistance of the shores to the drift of the ice cover or, if we are talking of the break-through of a jam which forms in a definite place of a river, then it depends on the ice strength and in the rise in the water stage below the ice cover downstream from the ice jam.

Depending on the local conditions, when a sufficiently low negative air temperature sets in during ice jamming, the rise in the water stage is higher than in cases when a positive air temperature is maintained.

In cases when winter ice breakups with subsequent ice jamming have been observed before ice jamming, the ice-jam water stage is higher than under usual conditions. The maximum ice-jam level is higher than under usual conditions also generally in cases of a stable ice associated with a high water stage.

The height of maximum ice-jam water stage depends, of course, also on the form of the river bed on the ice-jam stretch.

In cases when, under the existing river-bed conditions, the water (together with the ice) reaches a certain ice-jam level and floods the river banks, bypassing the jam, the maximum ice-jam water stage is limited by the indicated river-bed features.

The water-stage rise due to ice jamming also depends on ice jamming in upstream stretches of the river. The magnitude of the backwater effect and the ice-jam water stage at a given point of a river also depend on the distance to the place where the jam forms which, unfortunately, is not strictly fixed, particularly on stretches on which there is no general decrease in the river slope.

Finally, when analyzing observations on ice-jam stage rises it should be borne in mind that the maximum ice-jam stages can be lowered by explosives and other measures whereby the ice blocks are broken and the strength of the ice cover before the formation of the jam is reduced. On small stretches favorable for jam formation such measures may, in some cases, avert the formation of a jam.

Explosions, carried out to destroy ice jam, may apparently have some influence on the ice-jam water stage.

In general, however, the maximum rise in the water stage upstream from a jam over the pre-jam stage is mainly due to the following conditions: (1) the character of the river bed and river valley on the particular ice-jam stretch, (2) the character of the ice cover on the ice jam stretch, (3) the amount of ice on the river and, in the case of a continuous ice cover, its thickness, (4) the ice strength; (5) the intensity of ice drift; (6) the velocity at which the ice approaches the place of ice jam; (7) the water stage downstream from the jam; (8) the rate of growth of the flood before and after the formation of the jam, (9) the difference between the time of ice breakup on the main river and its large tributaries on the stretch under consideration; (10) the weather conditions in the period of the ice jamming; (11) the distance from the place of formation of the ice jam and the stage rise.

§ 2. Forecasting ice jamming

The principal conditions for ice jamming are (see § 1): (1) the preservation of the ice cover downstream of the part of the river on which ice breakup occurred and ice drift began and (2) sufficient steepness and velocity of the flood wave. The first condition to some extent depends on the second.

As a characteristic of the second condition the rate of rise of the water stage before the beginning of ice breakup is usually taken. On some rivers the second condition exists every year or almost every year, in accordance with the climatic and orographic conditions of the given river basin. Such, for example, are the large rivers of Siberia, which flow from south to north, where ice breakup is caused mainly by snow-melt floods forming in the upper (southern) parts of the basins. In this case, in order to forecast the possibility of an ice jamming it is sufficient to know whether the first condition (preservation of the ice cover, absence of conditions for breakup at the time of the approach of the flood wave) is satisfied on the particular river stretch. The first condition is fulfilled every year when the river slope and the flow velocities over a long stretch decrease generally. This is particularly true in the case of successive decrease in the slope. Therefore, ice jams always form there during spring breakup on the river, and it is not necessary to forecast the probability of an ice jam. Such a stretch, for example is the stretch of the Tom River downstream from the town of Tomsk.

If, however, there is no general decrease in the slope over a large stretch of a given river, and ice jams form in places where the flow velocities decrease when the stream passes from a shallow stretch to a deep pool, or where the river bed is constrained, or where there are islands, then the first condition (preservation of the ice cover) is not always fulfilled and ice jams do not form every year. This is connected with the ice-cover characteristics and their distribution along the river.

As yet there are no sufficiently accurate methods of forecasting ice jamming which take into account direct characteristics of the ice cover on the given river stretch (thickness, strength of cohesion to the shores or to the shore ice, depth of the snow cover on the ice, roughness of the under surface). Field investigations necessary for this are very laborious, and data of a fairly long series of preceding years and for each current year are necessary in the preparation of a forecast.

Ice jams during breakup form, as a rule, when freezing takes place with considerable ice gorges. A forecast of a considerable ice jamming may, therefore, be prepared from the relationship with one or another ice-jam characteristic. The rise ΔH_3 in the stage during the formation of the ice cover can be taken as a characteristic of ice jamming. On rivers where the long-time amplitude of the water-stage fluctuation before the beginning of ice formation is negligible, the maximum water stage H_3 during the initial stable ice period may be taken. The determination of the probability of ice jamming (at the time of breakup) from the value of H_3 is shown below in the example of the Yenisei River near Krasnoyarsk, from observation data for 1903–1960.

The Yenisei stretch not far downstream of the town of Krasnoyarsk along 19 km is a series of shallows (Ladeinye shallows) with islands. Farther downstream, between the villages of Berezovskoe (19 km downstream of the town) and Kubekovo (35 km still farther down) a deep pool is found. During formation of the ice cover, the advance of the ice edge toward the town is connected with a rise in the water stage, which continues for some time after the formation of stable ice within the town boundaries. At the time of the formation of the ice cover, ice pushes are observed fairly frequently.

Two centers of ice jamming at the time of ice breakup of the river are observed here. The first center is near the islands on Ladeinye shallows. However, strong ice jams do not form there; as a rule, the break-through of the ice jam continues until all the ice from upstream approaches the jam. The second, main ice-jam center is a deep pool downstream from the village of Berezovskoe. An ice jam usually forms in the upper part of the stretch, on the transition from a shallow to a pool, i.e., on an abrupt change in the river slope. There ice drift encounters a stable-ice stretch with a thick and strong ice cover and a strong ice jam forms. In individual cases ice jams are also formed in other places. Figure 102 gives a clear idea of the probability of ice jamming for different water stages H_3 at the beginning of the stable ice period. The shaded columns in the graph correspond to cases of ice jamming of the ensuing spring. From the figure we see that for H_0 (according to the Krasnoyarsk water gage) at a water stage below 240 cm an ice jam formed only in one case out of 31. For H_0 for stages from 240 to 280 cm ice jams formed in half the cases. For H_0 with a stage above 280 cm ice jams formed in 88% of the cases. For H_0 above 310 cm ice jams formed in 7 cases.

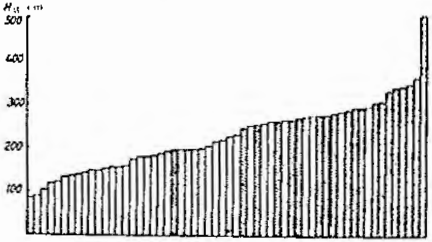

FIGURE 102. Relationship between the formation of an ice jam on the [illegible] River downstream of the town of Krasnoyarsk and the maximum water stage in the initial stable-ice period (H_0 in cm above the datum line of the graph of the Krasnoyarsk water gage)

Thus, on rivers on which there is always sufficient flood intensity (the second condition) it is possible, at the beginning of the stable ice period, to forecast from the value of the maximum water stage of this period the probability of ice jamming at the time of ice breakup. In this case, analysis can be graphical (Figure 102) or in tabular form.

It should be noted, however, that although ice jams form, as a rule, on a definite stretch of the river, their formation in other places also is not excluded. In particular, if ice jamming occurs downstream of the town Krasnoyarsk, then the probability of ice jamming downstream of the town of decreases, since at the moment of the break through of upper ice jam the ice cover on the lower stretch has already had time to disintegrate. For a more reliable forecast of the probability of ice jamming, it is necessary to have observations not for a single isolated gaging site, but for a series of closely-situated sites on the stretch above and below the main site. In important cases the probable places of ice jams can be determined from ice courses at the end of the winter.

For not very high stages H_0, the probability of ice jamming on such a stretch apparently also depends on the preliminary measures taken to break up the ice cover, in particular by explosions.

On other rivers, in particular on rivers of the west of the ETS, the principal index of the possibility of the formation of an ice jam is the rate of the water-stage rise before ice breakup. A certain dependence of the probability of ice-jam water-stage rise on the negative air temperature at the time of ice breakup is also observed. Figure 103 shows the relationship between the probability of ice jamming on the Neman River downstream from Kaunas (before the construction [illegible] electric plant) and the rate of the water-stage [illegible] temperature.

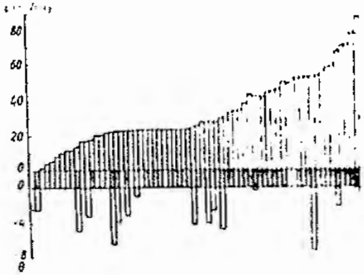

FIGURE 103. [illegible] Kaunas (before the construction of [illegible]) as a function of the rate of [illegible] and of the negative [illegible] of [illegible]

In this figure, for each case of ice breakup [illegible] (in cm/day) at the water gage of Kaunas, during [illegible] of a rise at a rate of not less than 10 cm/day to the [illegible] ice push, is plotted above the abscissa and the [illegible] temperature, the lowest of those observed in [illegible] next day, is plotted below it. The shaded areas [illegible] of the breakup an ice-jam stage rise was observed.

It follows from Figure 103 that if the air temperature at the time of ice breakup is positive, ice jams form when the mean rate of water-stage rise is not lower than 24 cm/day. If the air temperature [illegible] at the time of breakup below −2.5°, ice-jam stage rises [illegible] water gage also for lower rates of stage rise.

The probability of ice jamming for a mean rate of stage rise [illegible] than 24 cm/day is 93%. The total confidence [illegible] of forecasting ice jamming, taking into account the rate of stage rise and the air temperature at the time of ice breakup, is [illegible]

The rate of stage rise can be determined from [illegible] with a mean forewarning period of 2–3 days.

To forecast ice jamming in the case of a rate of stage rise [illegible] than 24 cm/day the air temperature forecast is necessary.

The method of forecasting ice jamming from the rate of stage rise before ice breakup and from the air temperature of the [illegible] days, originally developed for the Neman River in the region of the town of Kaunas, also gave good results for rivers of the west [illegible]

Forecasting of ice jamming from spring characteristics – rate of stage rise and air temperature – does not exclude, in principle, the possibility of forecasting the probability of ice jamming from autumn characteristics – the rise of stage at the beginning of the stable ice period, autumn ice pushes, etc.

The forewarning period of forecasting on the basis of the rate of stage rise can be increased by analyzing (from observation data) the dependence of the rate of stage rise on its determining factors.

§ 3. Forecasting the maximum water stage caused by ice jamming

It should be noted that a technique of forecasting maximum ice-jam water stages has been successfully obtained, till now, only for river stretches where ice jamming is due to a general decrease in the river slope.

For such conditions the main factors determining the maximum stage rise, ΔH_m, over the pre-jamming stage at a given point upstream from the ice jam (§ 1) can, for the purpose of obtaining a forecasting technique, be summarized as follows:

1) the thickness of the ice cover on some river stretch from which ice arrives to the given ice-jam stretch, h_{ice};

2) the depth of the snow cover on the ice (and in the basin), h_{sn};

3) the rate of water stage rise before the beginning of ice pushes or before the beginning of the ice-jam stage rise, i;

4) the ratio of the total heat input per unit surface of the snow-ice cover in the region of ice jamming (Σq_{ice}) to the total heat input per unit surface of the snow cover in the region of flood formation during ice jamming (Σq_{sn});

5) the onset of a negative air temperature in the ice-breakup period (θ_-).

In general, the following should also obviously be taken into account:

6) the character of the ice cover on the expected ice-jamming stretch (I).

If large tributaries flow into the ice-jam stretch of a river it is necessary to introduce in the calculation also:

7) the difference between the time of breakup on the main river and of its large tributaries, which flow into the given river stretch (Δt).

Thus, it is possible to assume that

$$\Delta H_m = f\left(h_{ice},\ h_{sn},\ i,\ \frac{\Sigma q_{ice}}{\Sigma q_{sn}},\ \theta_-,\ I,\ \Delta t\right). \qquad (1.\mathrm{VII})$$

However, it is not always necessary to introduce all the factors appearing in equation (1.VII). It is obvious that if there are no large tributaries on the given river stretch Δt may be excluded.

In methods of forecasting for stretches with a general slope decrease the ice-cover characteristic on the expected ice-jamming stretch (I) has to be introduced only in the rare cases which were preceded by winter breakups with subsequent formation of ice jams and gorges.

In some rivers a negative air temperature θ_- in the period of ice breakup is extremely rare.

With a small difference between the amounts of heat input during the melting period in the region of ice formation and the region of flood formation, which determines (among other factors) the process of ice jamming, $\frac{\sum q}{\sum q_{sn}}$ may be excluded from the calculation.

In some cases the effect of the rate of water-stage rise i is insignificant. Even h_{sn}, which, for example, in western regions where it strongly varies, has a decisive influence on the value of ΔH_m, has little effect on ΔH_m on rivers of East Siberia.

To forecast maximum ice-jam water stage for the Tom River at the town of Tomsk, it turns out expedient to include only h_{ice}, h_{sn}, i, $\frac{\sum q}{\sum q}$ and θ_-; for the Neman River at the town of Kaunas only h_{sn}, θ_-, I, Δt; for the Lena River at the town of Olekminsk, where the backwater effect from the ice jamming downstream of the mouth of the Olekma River extends, i, h, Δt.

It is not always possible to say beforehand which factors, for example of those involved in equation (1.VII), are the determining ones for a given stretch and should be introduced in the forecasting graph [illegible] those whose influence can be neglected. This should be checked by analyzing the corresponding observation data.

We give below, as an example, the technique of forecasting the maximum ice-jam water stage of the Tom River at the town of Tomsk.

Ice jams at the time of breakup of the Tom [illegible] downstream from the town of Tomsk are observed every year, but the maximum ice-jam water stages vary within wide limits – from 497 cm (1944) to 1103 cm (1947) above the zero of the graph plotted at the gaging site near the town of Tomsk.

Here, ice jamming is due to climatic conditions [illegible] formation and propagation of the flood wave from the upper and middle to downstream parts of the basin and to the morphological properties of the river bed which favor ice jamming. The basin of the Tom River extends from the south-southeast to the north-northwest. This is also the general direction of river flow. All the upper part of the basin, approximately to the town of Novokuznetsk, and the right-hand bank, further downstream [illegible] to the town of Kemerovo, is mountainous in character. The catchment basin up to the town of Tomsk has an area of 57 200 km². Islands are located on the Tom River below the town of Tomsk; somewhat more downstream, in the region of the village of Beloborodovo, the general slope of the river considerably decreases.

There are no large tributaries on the given stretch, thus Δt is not one of the determining factors.

Since there is a considerable general decrease in the slope on the given river stretch and no winter ice breakups occur there, the ice-cover characteristic on the ice-jamming stretch, I, need not be included amongst the determining factors. This is confirmed by a joint analysis of the observations data for the water stage during freezing and ice jamming in the period of ice breakup and data on the character of the freezing and measurements of the ice thickness on this stretch.

The remaining factors in equation (1.VII) should, as aforesaid, [illegible] physiographical conditions, considerably influence the value of ΔH_m. Let us verify this by comparing the plotting graphs of the annual values of ΔH_m with the annual values of each of these factors. Such a verification confirms the conclusion

Thus, we assume for the Tom River at the town of Tomsk

$$\Delta H_{m} = f\left(h_{i}, h_{s}, i, \frac{\Sigma q_{1}}{\Sigma q_{2}}, \theta_{-}\right). \qquad (2.VII)$$

A negative air temperature at the time of ice breakup does not occur every year but only in some cases. The influence of θ_- is therefore taken into account in the form of corrections to the values of ΔH_m, obtained from

$$\Delta H_{m} = f\left(h_{i}, h_{s}, i, \frac{\Sigma q_{1}}{\Sigma q_{2}}\right). \qquad (3.VII)$$

Owing to the absence of sufficient data on the ice-cover thickness h for a given river stretch we take it approximately proportional to the square root of the sum of mean-diurnal negative air temperatures, using the well-known formula ($h_i = m\sqrt{\Sigma\theta_-}$). In this case we determine the quantities $\Sigma\theta_-$ for the period from the beginning of the stable ice formation to January inclusive, since for the Tom River at the town of Tomsk, according to the laws governing the growth of the ice cover, the values of ΔH_m were found to be somewhat more closely related to $\Sigma\theta_-$ during this period than to $\Sigma\theta_-$ during other periods, also during the whole stable-ice period.

From the values of H_i, obtained from ice courses taken by the West Siberian branch of UGMS on the Tom River from the village of [illegible] to the town of Tomsk (during 9 years), the mean value of the coefficient m of $\sqrt{\Sigma\theta_-}$ was found to be 1.1 cm · degrees$^{-0.5}$.

The mean rate of the stage rise at the Tomsk gaging site, during a period from the beginning of a rise of approximately 10 cm per day to the beginning of a sharp stage rise due to ice jamming ($i = \frac{\Delta H_i}{t}$), was taken as a characteristic of the rate of rise of flood intensity before breakup i.

We express the relationship between the amounts of total heat input per unit surface of the snow-ice cover approximately by the ratio between the corresponding sums of positive (mean-diurnal) air temperatures at the meteorological stations Tomsk ($\Sigma\theta_1$) and Kondoma ($\Sigma\theta_2$), situated in the upper part of the basin, during the period from the beginning of melting until ice breakup.

Thus, we have to find the relationship

$$\Delta H_{m} = f\left(\sqrt{\Sigma\theta_{-}}, h_{s}, i, \frac{\Sigma\theta_{1}}{\Sigma\theta_{2}}\right). \qquad (4.VII)$$

Observation data show that the dependence of ΔH_m for each factor of equation (4.VII), can be taken as a linear function. This makes it possible to solve equation (4.VII) by the least-squares method.

Not having data for a reliable determination of the dependence of the annual values of the factor m on the factors determining it, we assume it constant. In this case, the final result of the calculation of ΔH_m does not depend on the numerical value taken for it.

Analysis of the graphs for ΔH_m and their variables shows that cooling causes an additional rise in the water stage, if it begins before the ice breakup on the Tom River in the region of the main center of ice jamming downstream from the town of Tomsk, and not earlier than one day before ice breakup at the town of Tomsk, and if the mean-diurnal air temperature was lower than −1.5°. Such conditions and, accordingly, an additional stage rise in the period from 1928 to 1958 were observed in 6 years (1935, 1947, 1948, 1950, 1956, and 1958).

Then, from observation data for the period from 1928 to 1958 (25 typical years), excluding data for the above 6 years with temperature drops, we find the numerical expression for equation (4.VII) by the method of least squares:

$$\Delta H_{m} = 12.09\sqrt{\Sigma\theta_{-}} + 5.48i + 2.76h_{s} - 71.4\frac{\Sigma\theta_{1}}{\Sigma\theta_{2}} - 7, \qquad (5.VII)$$

where ΔH_m is the maximum water-stage rise during ice jamming over the prejamming stage (in cm) according to the gaging site near Tomsk, i is the mean rate of stage rise at the town of Tomsk from the beginning of a rise, approximately by 10 cm per day, until the beginning of a sharp rise in the stage due to ice jamming, in cm/day, $\Sigma\theta_-$ is the sum of the mean-diurnal negative air temperatures from the beginning of the stable ice period to 31 January, h_s is the mean of the maximum snow-cover depths on the shore area of the Tom River basin on the stretch [illegible]–Tomsk before the beginning of melting according to snow-course data, in cm, $\Sigma\theta_1$ is the sum of the mean-diurnal positive air temperatures according to the Tomsk meteorological station during the period from the beginning of melting until the ice breakup on the Tom River at the town of Tomsk (without the air temperature on the breakup day and 2 days before ice breakup), $\Sigma\theta_2$ is the sum of the mean-diurnal positive air temperatures during the same period according to the Kondoma meteorological station.

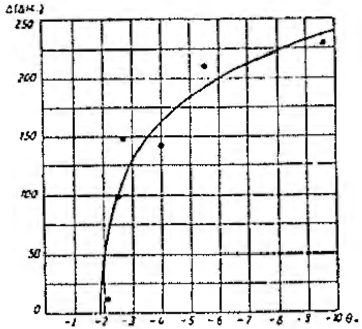

[illegible] $\Delta(\Delta H_m)$ [illegible] θ_-

We use (5.VII) to calculate the values of ΔH_m for the above-mentioned cases when a cooling which caused an additional rise in the water stage was observed. Subtracting the calculated values from the actual figures for ΔH_-, we obtain the values of the additional water-stage rise due to cooling, $\Delta(\Delta H_-)$. For each of these cases we find from the observation data the lowest of the mean-diurnal air temperatures θ_- during the time from the first day before ice breakup on the Tom River at the town of Tomsk until ice breakup on the Tom River in the region of the village of Beloborodovo (in the area of the main center of ice jams).

From the values found we obtain the graph of the relationship (Figure 104):

$$\Delta(\Delta H_-) = f(\theta_-). \qquad (6.VII)$$

When preparing a forecast of the maximum ice-jam water stage H_m, the correction for the cooling during the breakup period $\Delta(\Delta H_-)$ to the maximum ice-jam water-stage rise, ΔH_m, calculated by equation (5.VII), is determined from the graph in Figure 104.

The forewarning period for the Tom River at the town of Tomsk amounts on the average to 4 days, decreasing in a number of cases to 1 day and increasing to 11–12 days.

The forewarning period can be increased by predicting the daily water discharges or by introducing into the calculation instead of the *rate* of water stage rise, its determining factors.

BIBLIOGRAPHY

Apollov, B.A., G.P. Kalinin and V.D. Komarov. Gidrologicheskie prognozy (Hydrologic Forecasting). — Leningrad, Gidrometeoizdat. 1960.

Balashova, I.V. Uchet glubiny reki pri kratkosrochnom prognoze vremeni poyavleniya l'da (Allowance for the River Depth in Short-Range Forecasting of Dates of Ice Appearance). — Trudy TsIP, No. 48 (75). 1956.

Balashova, I.V. Kratkosrochnye prognozy zamerzaniya zaregulirovannykh rek (Short-Range Forecasting of the Freezing of Regulated Rivers). — Trudy TsIP, No. 34 (61). 1954.

Bezuglov, A.A. Ledyanye zatory na reke Nemunas (Ice Jams on the Nemunas River). — Trudy Vil'nyusskogo Gosudarstvennogo Universiteta, Vol. 3, Vil'nyus. 1955.

Braslavskii, A.P. and Z.A. Vikulina. Normy ispareniya s poverkhnosti vodokhranilishch (Rated Amount of Evaporation from the Surface of Water Reservoirs). — Leningrad, Gidrometeoizdat. 1954.

Bregman, G.R. O metodike fonovykh prognozov vskrytiya rek (Technique of Background Forecasting of Ice Breakup on Rivers). — Trudy NIU GUGMS, seriya 4, No. 3. 1941.

Bulatov, S.N. Iz opyta postroeniya zavisimostei dlya prognoza poyavleniya l'da na rekakh Sibiri (An Attempt at Setting Up Forecasting Relationships for Ice Appearance on Siberian Rivers). — Meteorologiya i Gidrologiya, No. 8. 1951.

Bulatov, S.N. Vliyanie zimnei vodnosti na ledovyi rezhim i vskrytie rek (Influence of the Winter Water Amount on the Ice Regime and Ice Breakup on Rivers). — Trudy TsIP, No. 62. 1957.

Bulatov, S.N. Osnovnye faktory, opredelyayushchie nachalo vesennikh podvizhek l'da na rekakh (Main Factors Determining the Beginning of Spring Ice Pushes on Rivers). — Meteorologiya i Gidrologiya, No. 2. 1952.

Bulatov, S.N. Kratkosrochnyi prognoz vskrytiya Volgi v raionakh stroitel'stva Kuibyshevskoi i Volgogradskoi GES (Short-range Forecasting of the Ice Breakup on the Volga in Construction Areas of the Kuibyshev and Volgograd Hydroelectric Stations). — Trudy TsIP, No. 34 (61). 1954.

Bulatov, S.N. Metodika rascheta dat ochishcheniya oto l'da protochnykh vodokhranilishch i prognoz ochishcheniya oto l'da Kamskogo vodokhranilishcha (Methods for Calculating Dates of Ice Clearing of Run-of-River Storage Reservoirs and Forecasting Ice Clearing of the Kama Storage Reservoir). – Trudy TsIP, No. 114, 1961.

Bydin, F.I. Zimnii rezhim rek i metody ego izucheniya (Winter Regime of Rivers and Methods of its Study). – Issledovaniya Rek SSSR, No. 5, 1933.

Chizhov, O.P. Opyt razrabotki prognozov zimnikh urovnei Amu-Dar'i (Developing a Technique of Forecasting the Winter Stages of the Amu-Darya River). – Trudy TsIP, No. 48 (75), 1956.

Efremova, N.D. Zavisimost' intensivnosti osennego ledokhoda na rekakh ot gidrometeorologicheskikh uslovii (Dependence of the Intensity of the Autumn Ice Drift on Hydrometeorological Conditions). – Trudy TsIP, No. 65, 1958.

Efremova, N.D. Metod dolgosrochnogo prognoza nachala ledostava na Novosibirskom vodokhranilishche (Method of Long-Range Forecasting Forecasting of the Beginning of Stable Ice on the Novosibirsk Storage Reservoir). – Trudy TsIP, No. 114, 1961.

Efremova, N.D. Metod dolgosrochnogo prognoza srokov nachala ledostava na Kamskom vodokhranilishche (Method of Long-range Forecasting of the Dates of the Beginning of Stable Ice on the Kama Storage Reservoir). – Trudy TsIP, No. 100, 1960.

Evstratov, F.A. K metodike kratkosrochnykh prognozov vskrytiya rek tsentral'no-chernozemnykh oblastei (Methods of Short-range Forecasting of Ice Breakup on Rivers of the Central Chernozem Regions). – Trudy TsIP, No. 100, 1960.

[illegible], V. Sh. Shuga na rekakh Kavkaza i vozmozhnosti prognoza ee poyavleniya (Forecasting Appearance of Frazil Ice on Caucasian Rivers). – Trudy TsIP, No. 58, 1957.

Ginzburg, B.M. Vozmozhnost' prodleniya srokov navigatsii pered zamerzaniem bol'shikh rek (Possibilities of Prolonging the Navigation Period on Large Rivers Before the Onset of Freezing). – Meteorologiya i Gidrologiya, No. 9, 1951.

Ginzburg, B.M. and B.P. Konovodov. K metodike prognoza vskrytiya Obi i Eniseya (Forecasting Ice Breakup on the Ob' and Yenisei Rivers). – Trudy TsIP, 40 (67), 1955.

Ginzburg, B.M. Osnovy metodiki dolgosrochnogo prognoza vskrytiya rek (Methods for Long-range Forecasting of Ice Breakup on Rivers). – Trudy III Vsesoyuznogo gidrologicheskogo s'ezda, Vol. 3, 1959.

Ginzburg, B.M. K metodike dolgosrochnogo prognoza vskrytiya rek tsentral'nykh raionov Evropeiskoi territorii SSSR (Methods for Long-range Forecasting of Ice Breakup on Rivers of the Central Regions of the ETS). – Trudy TsIP, No. 114, 1961.

Ginzburg, B.M. and I.V. Balashova. [illegible] prognozov razrusheniya l'da na vodokhranilishchakh [illegible] (Calculation and Forecasting of Ice Breakup on Storage Reservoirs). – Trudy TsIP, No. 100, 1960.

Ginzburg, B.M. Kratkii obzor metodov [illegible] vskrytiya i zamerzaniya rek (Short Review of [illegible] Long-range Forecasting of Ice Breakup and [illegible] Rivers). – Trudy TsIP, No. 90, 1959.

Komarov, V.D. Metody kratkosrochnykh [illegible] poyavleniya sala i ustanovleniya ledostava na rekakh [illegible] range Forecasting of Dates of Slush Ice Appearance and [illegible] Formation of Stable Ice on Rivers). – Trudy TsIP, [illegible]

Konovalov, I.M., K.S. Emel'yanov, and [illegible] ledotekhnika rechnogo transporta [illegible] River Navigation). – Leningrad–M[illegible]

Konovodov, B.P. Vliyanie vodokhranilishch [illegible] vozdukha nad nimi pered zamerzaniem [illegible] (Influence of Storage Reservoirs on Air Temperature [illegible] Freezing and Ice Clearing). – Trudy [illegible]

Kravchenko, N.A. Formirovanie zatorov [illegible] metodika ikh izucheniya (Ice Jamming on the [illegible] Methods). – Trudy III Vsesoyuznogo [illegible] Vol. 3, Leningrad, Gidrometeoizdat, [illegible]

Kritskii, S.N., M.F. Menkel', and K.I. R[illegible] termicheskii rezhim vodokhranilishch [illegible] Thermal Regime of Storage Reservoirs [illegible] Moskva–Leningrad, Gosenergoizdat, [illegible]

Kuz'min, P.P. Protsess tayaniya snezhnogo [illegible] Snow Cover). – Leningrad, Gidrometeoizdat, [illegible]

Lebedeva, V.V. Primenenie kharakteristik [illegible] rezhima dlya prognoza [illegible] of Characteristics of the Baron[illegible] Forecasting the Rapidity of the [illegible] Bodies). – Trudy GGO, No. 111, [illegible]

Laser, I.Ya. Vesennie zatory na reke Enisee [illegible] (Spring Ice Jamming on the Yenisei R[illegible] Krasnoyarsk). – Trudy TsIP, N[illegible]

Makarevich, T.N. Metodika dolgosrochn[illegible] severo-zapada SSSR (Methods for L[illegible] Freezing of Rivers of the North[illegible] GGI, No. 58, 1956.

Makarevich, T.N. and N.A. Ant[illegible] osenne-zimnego ledovogo rezhima [illegible] poyavleniya l'da na rekakh Pribaltik[illegible] Formation of the Autumn-Winter Ice [illegible] the Dates of Ice Appearance on Rivers [illegible] GGI, No. 30, 1962.

Savchenkova, E.I. Uluchshenie metodiki dolgosrochnogo prognoza srokov poyavleniya l'da na nekotorykh rekakh Sibiri i Dal'nego Vostoka (Improvement of the Method of Long-range Forecasting of the Dates of Ice Appearance on Some Rivers of Siberia and the Far East). – Trudy TsIP, No. 84. 1959.

Savchenkova, E.I. Metodika dolgosrochnogo prognoza srokov ledostava na reke Lene (Methods for Long-range Forecasting of the Dates of Stable Ice on the Lena River). – Trudy TsIP, No. 114. 1961.

Savchenkova, E.I. Ispol'zovanie indeksa atmosfernoi tsirkulyatsii dlya razrabotki dolgosrochnykh prognozov vskrytiya rek (Application of the Atmospheric Circulation Index in Long-range Forecasts of Ice Breakup on Rivers). – Meteorologiya i Gidrologiya, No. 5. 1957.

Shulyakovskii, L.G. Poyavlenie l'da i nachalo ledostava na rekakh, ozerakh i vodokhranilishchakh. Raschety dlya tselei prognozov (Forecasting of Ice Appearance and Beginning of Stable Ice on Rivers, Lakes and Storage Reservoirs). – Leningrad, Gidrometeoizdat. 1960.

Shulyakovskii, L.G. K metodike kratkosrochnykh prognozov zamerzaniya i vskrytiya rek (Methods for Short-range Forecasting of River Freezing and Ice Breakup on Rivers). – Trudy TsIP, No. 5. 1947

Shulyakovskii, L.G. Ob empiricheskikh zavisimostyakh primenyaemykh dlya kratkosrochnogo prognoza poyavleniya l'da na rekakh (Empirical Relationships in Short-range Forecasting of Ice Appearance on Rivers). – Trudy TsIP, No. 114. 1961.

Shulyakovskii, L.G. O raschete nachala ledostava na rekakh dlya tselei kratkosrochnogo prognoza (Short-range Forecasting of the Beginning of Stable Ice on Rivers). – Trudy TsIP, No. 40 (67). 1955.

Shulyakovskii, L.G. Vskrytie i ochishchenie oto l'da rechnykh zon i zalivov vodokhranilishch v zavisimosti ot gidrometeorologicheskikh uslovii i rezhima ekspluatatsii (Ice Breakup and Ice Clearing on the River Area and Bays of Run-of-River Storage Reservoirs as a Function of the Hydrometeorological Conditions and the Operation Conditions). – Trudy TsIP, No. 34 (61). 1954.

Shulyakovskii, L.G. O zatorakh l'da i zatornykh urovnyakh vody pri vskrytii rek (Ice Jamming and Ice-jam Water Stages at the time of Ice Breakup on Rivers). – Meteorologiya i Gidrologiya, No. 7. 1951.

Shulyakovskii, L.G. and O.I. Ermina. K metodike prognoza maksimal'nykh zatornykh urovnei vody (Contributions to the Methods of Forecasting Maximum Ice-jam water stages). – Meteorologiya i Gidrologiya, No. 1. 1952.

Ulitsina, Z.I. Opyt razrabotki metodom dolgosrochnogo prognoza zamerzaniya rek basseina Verkhnei Volgi (Developing a Technique for Long-range Forecasting the Freezing of Rivers of the Upper-Volga Basin). – Trudy TsIP, No. 23 (50). 1951.

Makarevich, T.N. and N.M. Mytarev. Vskrytie rek severo-zapada SSSR i metodika ego prognoza (Methods for Forecasting Ice Breakup on Rivers of the Northwest of the USSR). – Trudy GGI, No. 67. 1958.

Margolin, L.M. Metod dolgosrochnogo prognoza vskrytiya rek basseina reki Oki (Methods for Long-range Forecasting of Ice Breakup on the Rivers of the Oka River Basin). – Meteorologiya i Gidrologiya, No. 10. 1958.

Mashukov, P.M. Analiz i prognoz ledovykh yavlenii na Amu-Dar'e (Analysis and Forecasting of Ice Phenomena on the Amu Darya River). – Leningrad, Gidrometeoizdat. 1959

Nezhikhovskii, R.A. Gidrologicheskie raschety i prognozy pri ekspluatatsii vodokhranilishch i ozer (Hydrological Calculations and Forecasting for the Operation of Lakes and Storage Reservoirs). Leningrad, Gidrometeoizdat. 1961

Piotrovich, V.V. and N.F. Vinogradova. [illegible] k razrabotke metodiki dolgosrochnogo prognoza srokov [illegible] ocheniya oto l'da sozdovaemykh vodokhranilishch [illegible] Methods for Long-range Forecasting of the Dates of Stable Ice and of the Ice Clearing on Storage Reservoirs [illegible]. – Trudy III Vsesoyuznogo gidrologicheskogo [illegible]

Piotrovich, V.V. O [illegible] l'da [illegible] Evropeiskoi territorii SSSR (Ice Breakup [illegible] Ice on Rivers of the ETS). – Trudy TsIP, [illegible]

Piotrovich, V.V. O pritoke tepla [illegible] pesStova rek (Heat Input to the Under [illegible] Rivers). – Trudy TsIP, No. 2 (29). 1947

Piotrovich, V.V. Obrazovanie i stavanie [illegible] vodokhranilishchakh i raschet srokov ledostava [illegible] and Melting of Ice on Lake-type Storage Reservoirs [illegible] Calculation of the Dates of the Stable [illegible]. – Moskva, Gidrometeoizdat. 1958

Piotrovich, V.V. Metodika dolgosrochnogo [illegible] ocheniya oto l'da vodokhranilishch [illegible] Tsimlyanskoi GES (Methods for Long-range [illegible] of Ice Clearing on the Storage Reservoirs [illegible] and Tsimlyanskii Hydro Power Plants). – Trudy TsIP, [illegible]

Pogosyan, Kh.P. and E.I. Savchenkova. [illegible] atmosfernoi tsirkulyatsii (Numerical [illegible] Atmospheric Circulation). – [illegible] No. [illegible] 1950

Popov, E.G. Gidrologicheskie prognozy (Hydrological [illegible]). – Leningrad, Gidrometeoizdat. 1957

Rozova, A.P. K metodike dolgosrochnogo [illegible] poyavleniya l'da na rekakh Mologe, [illegible] (Long-range Forecasting the Dates of the Appearance [illegible] of Ice on the Mologa, Suda, and Sheksna [illegible]. 1959

Vasil'kov, L.A., Ya.L. Gotlib, F.E. Zaimin, N.I. Smolin, and A.K. Klimenko. Izuchenie zazhorov i raschet maksimal'nykh zazhornykh urovnei pri proektirovanii GES (Study of Ice Jams and Calculation of Maximum Ice Jam River Stages in the Design of Hydro Power Plants). — Gidrotekhnicheskoe Stroitel'stvo, No. 3, 1956

Vinogradova, N.F. Metodika dolgosrochnogo prognoza srokov nachala ledostava na Tsimlyanskom vodokhranilishche i Volgo-Donskom sudokhodnom kanale im. V.I. Lenina (Long-range Forecasting the Dates of the Beginning of Stable Ice on the Tsimlyansk Storage Reservoir and on the Volga-Don Navigation Canal im. V.I. Lenin). — Trudy TsIP, No. 114, 1961.

EXPLANATORY LIST OF ABBREVIATIONS OF USSR INSTITUTIONS APPEARING IN THE BIBLIOGRAPHY

Abbreviation	Full name (transliterated)	[illegible]
GGI	Gosudarstvennyi gidrologicheskii institut	[illegible] Institute
GGO	Glavnaya geofizicheskaya observatoriya	[illegible]
NIU GUGMS	Nauchno-issledovatel'skoe upravlenie Glavnogo upravleniya gidrometeorologicheskoi sluzhby	[illegible]
TsIP	Tsentral'nyi institut prognozov	[illegible]

Values of e^{-x}

x	e^{-x}	x	e^{-x}	x	e^{-x}	x	e^{-x}	x	e^{-x}	x	e^{-x}	x	e^{-x}	x	e^{-x}	x	e^{-x}	x	e^{-x}	x	e^{-x}
0.00	1.000	0.25	0.779	0.50	0.606	0.75	0.472	1.00	0.368	1.25	0.286	1.50	0.223	1.75	0.174	2.00	0.135	2.25	0.105	2.50	0.082
0.01	0.990	0.26	0.771	0.51	0.600	0.76	0.468	1.01	0.364	1.26	0.284	1.51	0.221	1.76	0.172	2.01	0.134	2.26	0.104	2.60	0.074
0.02	0.980	0.27	0.763	0.52	0.594	0.77	0.463	1.02	0.361	1.27	0.281	1.52	0.219	1.77	0.170	2.02	0.133	2.27	0.103	2.70	0.067
0.03	0.970	0.28	0.756	0.53	0.589	0.78	0.458	1.03	0.357	1.28	0.278	1.53	0.216	1.78	0.169	2.03	0.131	2.28	0.102	2.80	0.061
0.04	0.961	0.29	0.748	0.54	0.583	0.79	0.454	1.04	0.354	1.29	0.275	1.54	0.214	1.79	0.167	2.04	0.130	2.29	0.101	2.90	0.055
0.05	0.951	0.30	0.741	0.55	0.577	0.80	0.449	1.05	0.350	1.30	0.272	1.55	0.212	1.80	0.165	2.05	0.129	2.30	0.100	3.00	0.050
0.06	0.942	0.31	0.733	0.56	0.571	0.81	0.445	1.06	0.346	1.31	0.270	1.56	0.210	1.81	0.164	2.06	0.128	2.31	0.099	3.10	0.045
0.07	0.932	0.32	0.726	0.57	0.566	0.82	0.440	1.07	0.343	1.32	0.267	1.57	0.208	1.82	0.162	2.07	0.126	2.32	0.098	3.20	0.041
0.08	0.923	0.33	0.719	0.58	0.560	0.83	0.436	1.08	0.340	1.33	0.264	1.58	0.206	1.83	0.160	2.08	0.125	2.33	0.097	3.30	0.037
0.09	0.914	0.34	0.712	0.59	0.554	0.84	0.432	1.09	0.336	1.34	0.262	1.59	0.204	1.84	0.159	2.09	0.124	2.34	0.096	3.40	0.033
0.10	0.905	0.35	0.705	0.60	0.549	0.85	0.427	1.10	0.333	1.35	0.259	1.60	0.202	1.85	0.157	2.10	0.122	2.35	0.095	3.50	0.030
0.11	0.896	0.36	0.698	0.61	0.543	0.86	0.423	1.11	0.330	1.36	0.257	1.61	0.200	1.86	0.156	2.11	0.121	2.36	0.094	3.60	0.027
0.12	0.887	0.37	0.691	0.62	0.538	0.87	0.419	1.12	0.326	1.37	0.254	1.62	0.198	1.87	0.154	2.12	0.120	2.37	0.093	3.70	0.025
0.13	0.878	0.38	0.684	0.63	0.533	0.88	0.415	1.13	0.323	1.38	0.252	1.63	0.196	1.88	0.153	2.13	0.119	2.38	0.093	3.80	0.022
0.14	0.869	0.39	0.677	0.64	0.527	0.89	0.411	1.14	0.320	1.39	0.249	1.64	0.194	1.89	0.151	2.14	0.118	2.39	0.092	3.90	0.020
0.15	0.861	0.40	0.670	0.65	0.522	0.90	0.407	1.15	0.317	1.40	0.247	1.65	0.192	1.90	0.150	2.15	0.116	2.40	0.091	4.00	0.018
0.16	0.852	0.41	0.664	0.66	0.517	0.91	0.402	1.16	0.314	1.41	0.244	1.66	0.190	1.91	0.148	2.16	0.115	2.41	0.090	4.10	0.016
0.17	0.844	0.42	0.657	0.67	0.512	0.92	0.399	1.17	0.310	1.42	0.242	1.67	0.188	1.92	0.147	2.17	0.114	2.42	0.089	4.20	0.015
0.18	0.835	0.43	0.650	0.68	0.507	0.93	0.395	1.18	0.307	1.43	0.239	1.68	0.186	1.93	0.145	2.18	0.113	2.43	0.088	4.30	0.014
0.19	0.827	0.44	0.644	0.69	0.502	0.94	0.391	1.19	0.304	1.44	0.237	1.69	0.184	1.94	0.144	2.19	0.112	2.44	0.087	4.40	0.012
0.20	0.819	0.45	0.638	0.70	0.497	0.95	0.387	1.20	0.301	1.45	0.235	1.70	0.183	1.95	0.142	2.20	0.111	2.45	0.086	4.50	0.011
0.21	0.811	0.46	0.631	0.71	0.492	0.96	0.383	1.21	0.298	1.46	0.232	1.71	0.181	1.96	0.141	2.21	0.110	2.46	0.085	4.60	0.010
0.22	0.802	0.47	0.625	0.72	0.487	0.97	0.379	1.22	0.295	1.47	0.230	1.72	0.179	1.97	0.140	2.22	0.109	2.47	0.085	4.70	0.009
0.23	0.794	0.48	0.619	0.73	0.482	0.98	0.375	1.23	0.292	1.48	0.228	1.73	0.177	1.98	0.138	2.23	0.108	2.48	0.084	4.80	0.008
0.24	0.787	0.49	0.613	0.74	0.477	0.99	0.372	1.24	0.289	1.49	0.225	1.74	0.176	1.99	0.137	2.24	0.106	2.49	0.083	4.90	0.007

APPENDIX 2

Some synoptic terms encountered in the handbook

Absolute topography (AT). The altitudes of some isobaric surface over sea level in geodynamical meters, represented by isohypses on a synoptical map. A more general term: absolute barometric topography.

Advection. The process of transport of air [illegible]. When heat is transported from a region of higher to a region of lower temperature the term heat advection is used. Cold advection is the transport from a region of lower to a region of higher temperature.

Azores anticyclone. Azores high. A region of high pressure in subtropical and tropical northern latitudes of the Atlantic Ocean with its center above the 35th parallel, not far from the Azores. It can be seen on long-time maps of the pressure distribution for any month of the year.

Anticyclone. A region of higher atmospheric pressure with closed isobars. In the northern hemisphere winds blow around the center of an anticyclone in a clockwise sense. The lines of flow in the lower layer of an anticyclone have the form of spirals which diverge from the center, while above the friction level (0.5–1.5 km above sea level) they are, in general, close to the isobars.

Baric topography. The distribution of the altitudes [illegible] in geodynamical meters of some isobaric surface over sea level (the absolute barometric topography) or above the level of another, lower-lying isobaric surface (relative barometric topography).

Baric systems. Regions in the terrestrial atmosphere with a definite, characteristic distribution of the atmospheric pressure [illegible] of the baric field. Baric systems are mainly divided into high- and low-pressure regions.

Baric gradient. The vector characterizing the rate of three-dimensional variation of the atmospheric pressure.

Height chart. aerological chart, synoptic chart referring to some level or to some isobaric surface in the free atmosphere.

Geopotential. The potential energy of a unit mass determined by the position of the latter in the field of gravity. The geopotential at a given point of the atmosphere is numerically equal to the work which has to be performed in order to raise a unit of mass against gravity from sea level to the given point.

Geopotential meter (G.M.) is equal to the work which has to be performed against gravity in order to raise a unit of mass to a height of [illegible]

[illegible]

of 1 m in the case of an acceleration of gravity of 980 cm/sec². Ten geopotential meters are equal to one decameter (dkm).

Ridge. Extension of a high-pressure (anticyclone) region.

Natural synoptic period. The time interval during which such a thermobaric field is maintained in the troposphere, which determines a definite direction of displacement of baric formations at the earth's surface and the preservation of the geographical position of their centers.

Natural synoptic region. A considerable part of the hemisphere for which it is assumed that atmospheric processes above it possess important local regularities. The northern hemisphere is divided into three natural synoptic regions: (1) from Greenland to Taimyr, (2) from Taimyr to the Bering Strait, and (3) from the Bering Strait to Greenland.

Isobaric surface. A surface of equal pressure; an imaginary surface in the atmosphere at which the atmospheric pressure is the same at all points.

Isohypses. Lines of equal altitude. In meteorology the isohypses refer most frequently to the isobaric surfaces on altitude charts in which the altitude does not denote the height but the geopotential, expressed in geopotential meters.

Circulation index. Some numerical quantity characterizing the intensity or other features of the general circulation of the atmosphere over the whole hemisphere or a definite region of it.

Baric topography maps (isobaric-surface contour maps). Synoptical, mean or climatological maps, in which the altitudes (or rather, the geopotentials in geopotential meters) of some isobaric surface over sea level (absolute isobaric surface contour map) or over the level of a lower-lying isobaric surface (relative isobaric surface contour map) are plotted. Isobaric-surface contour maps characterize the two-dimensional pressure and temperature distribution in the troposphere. The notation is: H_{500} — the absolute 500 mb isobaric-surface contour map; H^{500}_{1000} — the relative contour map of the 500 mb isobaric surface above the 1000 mb surface.

Millibar (mb). A unit of atmospheric pressure equal to 1000 dynes per 1 cm². 1 mb = 0.001 bar which represents a pressure of 1 million dynes/cm². To convert a pressure given in mm Hg to millibars it is necessary to multiply the number of millimeters by 4/3.

Relative geopotential. The geopotential of an isobaric surface at a given point, not measured from sea level but above a lower-lying isobaric surface. The magnitude of the relative geopotential at a given point for definite isobaric surfaces depends (to a first approximation) only on the mean temperature of the air column between them.

Surface-boundary map. A synoptic map based on observation data from a network of ground-based meteorological stations.

Composite-kinematic map. A map on which the centers of cyclones and anticyclones as well as their trajectories during some time interval (for example, during a natural synoptic period) are plotted.

Siberian anticyclone. The hibernal Asian anticyclone.

Synoptic conditions. Those synoptic processes which determine some atmospheric or in general geographical phenomena (for example, ice freezing or ice breakup on rivers).

Synoptic season. A time interval during which atmospheric processes, similar in geographical distribution to the main baric systems and the directions of the motion, prevail. Usually six synoptic seasons, beginning and ending in each year at different dates, are distinguished. On the average, the seasons are divided (in the USSR) as follows: winter — from the middle of December to the middle of March, spring — from the middle of March to the middle of May, first half of the summer — from the middle of May to June, the second half of the summer — from July to the first half of August, autumn — from the middle of August to the middle of Octobe., pre-winter — from the middle of October to the middle of December.

Transformation of an air mass. The gradual variation in air properties in a given baric formation.

Cyclone. An atmospheric disturbance with a reduced air pressure (minimum pressure in the center) and with the air circulating around the center (in the northern hemisphere counterclockwise).